DEVELOPMENT AND CHARACTERIZATION OF HYBRID ALUMINIUM METAL MATRIX COMPOSITES FOR FATIGUE/ WEAR RESISTANT APPLICATIONS

A Thesis submitted to Delhi Technological University, Delhi in fulfilment of the requirement for degree of

DOCTOR OF PHILOSOPHY

in

Mechanical Engineering

by

GIRIJA MOONA
(2K15/PhD/ME/05)

Under the Supervisions of

Dr. Vikas Rastogi (Professor, DTU)

Dr. R.S. Walia (Professor, PEC)

Dr. Rina Sharma (Senior Principal Scientist, CSIR-NPL)

DEPARTMENT OF MECHANICAL ENGINEERING
DELHI TECHNOLOGICAL UNIVERSITY

Main Bawana Road, Shahabad Daulatpur, Delhi- 110042, India

DELHI-110042, INDIA

May, 2020

DECLARATION

I hereby declare that the thesis work entitled **"DEVELOPMENT AND CHARACTERIZATION OF HYBRID ALUMINIUM METAL MATRIX COMPOSITES FOR FATIGUE/ WEAR RESISTANT APPLICATIONS"** is an original work carried out by me under the supervision of Dr. Vikas Rastogi (Professor, Department of Mechanical Engineering, Delhi Technological University, Delhi), Dr. R.S. Walia (Professor, Department of Production and Industrial Engineering, Punjab Engineering College, Chandigarh) and Dr. Rina Sharma (Senior Principal Scientist, CSIR-National Physical Laboratory, Delhi). This thesis has been prepared in conformity with the rules and regulations of the Delhi Technological University, Delhi. The research work presented and reported in the thesis have not been submitted either in part or full to any other university or institute for the award of any other degree or diploma.

GIRIJA MOONA

(Registration Number: 2K15/PhD/ME/05)

Department of Mechanical Engineering

Delhi Technological University, Delhi

Date: May 13, 2020

Place: New Delhi

CERTIFICATE

This is to certify that the thesis entitled, "**DEVELOPMENT AND CHARACTERIZATION OF HYBRID ALUMINIUM METAL MATRIX COMPOSITES FOR FATIGUE/WEAR RESISTANT APPLICATIONS**" submitted by **Ms. Girija Moona (Registration Number: 2K15/PhD/ME/05)** to Delhi Technological University, Delhi for award of the degree of **Doctor of Philosophy** in **Mechanical Engineering** is a bonafide record of original research work carried out by her under our supervision in accordance with the rules and regulations of the institute. The matter embodied in this thesis has not been submitted, in part or full, to any University or Institute for the award of any degree or diploma.

Dr. Vikas Rastogi
Professor
Department of Mechanical Engineering
Delhi Technological University
Delhi, India

Dr. R.S. Walia
Professor
Department of Production and Industrial Engineering
Punjab Engineering College
Chandigarh, India

Dr. Rina Sharma
Senior Principal Scientist
CSIR-National Physical Laboratory
Delhi, India

Dedicated to
the almighty
and my family

ACKNOWLEDGEMENTS

Completing any work of reasonably good proportions is no easy task. At the outset, I am very thankful to the almighty for best owing me with such opportunity to carry out a worthwhile research work. It is my privilege to express my deep gratitude, sincere thanks and appreciation to my research supervisors **Dr. Vikas Rastogi, Dr. R.S. Walia** and **Dr. Rina Sharma** for their valuable guidance, continuous encouragement and unconditional support that paved the way for this research work.

I would like to express my sincere gratitude to **Prof. R.S. Mishra**, Chairman, DRC, Mechanical Engineering Department and **Prof. Vipin**, Head, Mechanical Engineering Department, Delhi Technological University, for their valuable help, motivation and extending all the necessary processing and experimental facilities during my research work.

I am very thankful to **Prof. Mohammed Suhaib, Dr. Abhishek Mishra, Dr. Atul Kumar Agarwal, Dr. Reeta Wattal** and **Dr. Raminder Kaur** for being members of my SRC committee. I am also grateful to **Dr. Qasim Murtaza, Dr. Ranganath M. S. and Dr. Vijay Gautam** for their kind support during this research work. My sincere thanks to all the staff members of Mechanical Engineering Department, Delhi Technological University, for their support during entire course work and research work. I am very grateful to **Mr. Manjeet Singh** and **Mr. Virender** for their valuable technical support.

I would like to extend my sincere gratitude to **Dr. D. K. Aswal**, Director, CSIR – National Physical Laboratory, New Delhi for his kind support and continuous motivation to complete my Ph. D.

I am thankful to my fellow scientists and technical officers of CSIR-National Physical Laboratory, New Delhi who helped me in in every possible way to finish this research work.

I owe a great debt of gratitude to my parents and siblings for their endless efforts to nurture and inspire me. I am unable to express my sincere gratitude in words for the affection, encouragement and support provided by my husband during the entire research work.

I dedicate this Ph.D. thesis to my dearest daughter **Shubhalini Moona** for her unyielding love, patience and encouragement.

Last but not the least; I thank the almighty for giving me strength and perseverance to complete this work in all respects.

May 13, 2020 **(Girija Moona)**

ABSTRACT

Aluminium metal matrix composites (AMMCs) are considered to be new generation potential materials for numerous engineering applications due to their augmented mechanical and physical characteristics. Though, conventional aluminium based composites exhibit enhanced attributes as compared to the unreinforced aluminium alloys, but at the cost of some specific mechanical characteristics which are essential to prevent premature failure of any mechanical component under in service stress. In process of surmounting this issue, fabrication of hybrid composites with reduced interfacial area and reduced meniscus penetration defect is being encouraged in order to adopt them as more dependable and extensible materials.

An extensive research gap can be observed for development of cost-effective and eco-friendly hybrid aluminium composites with augmented characteristics. Past research studies have provided limited literature on some conventional fabrication techniques, with constrained reinforcement combinations and higher reinforcement contents. Influences of various reinforcements on a wider range of characteristics of aluminium composites have also not been reported so far. Hence, there was an enormous scope for present research work, involving development and assessment of economical and environment friendly hybrid aluminium metal matrix composites with upgraded mechanical properties.

Present experimental investigation was carried out to synthesize environment friendly (using hazardously disposed hen eggshells as one of the reinforcements) and cost-effective (maximum total reinforcement content of 5.5% only) hybrid aluminium metal matrix composites through electromagnetic stir casting technique. Al7075-T6 alloy was infused with; eggshell particles (wt.% 0.5, 1and 1.5, particle size ~ 60 µm), silicon carbide particles (wt.% 1, 1.5 and 2, particle size ~ 65 µm) and aluminium oxide particles (wt.% 1.5, 2 and 2.5, particle size ~90 µm) with variable mechanical stirring time (2, 4 and 6 minutes) in accordance with Taguchi's orthogonal array L9. Synthesized aluminium composites have been examined for microstructural studies and elemental compositions using FESEM, X-ray diffractometry and EDS etc. techniques. Hybrid aluminium metal matrix

composites have further been evaluated for various physical and mechanical attributes such as density, porosity, residual stress, microhardness, tensile strength, fatigue life, tribology and machinability followed by process parameter optimization through Taguchi approach and ANOVA analysis. With extensively augmented characteristics, synthesized hybrid aluminium composites strongly advocate their applications in automotives, high strength structures and aerospace etc.

Keywords: Hybrid composites, Electromagnetic stir casting, Microstructure, Characterization, Optimization, Tribology.

LIST OF PUBLICATIONS

Publications in Journals/Proceedings

1. **Girija Moona,** R. S. Walia, Vikas Rastogi and Rina Sharma (2018), Aluminium metal matrix composites: A retrospective investigation, ***Indian Journal of Pure and Applied Physics (NISCAIR)***, Vol. 56, pp. 164-175 **(SCI expanded with impact factor 0.822)**
2. **Girija Moona,** R. S. Walia, Vikas Rastogi and Rina Sharma (2019), Parameter Optimization and Characterization of Environmental Friendly Aluminium Hybrid Metal Matrix Composites, ***Materials Research Express (IOP Science),*** Vol. 6, Number 5, 1165d5 (**SCI expanded with impact factor 1.449)**
3. **Girija Moona,** R. S. Walia, Vikas Rastogi and Rina Sharma (2020), Tribological Characterization of Ecodesigned Aluminium Hybrid Metal Matrix Composites, ***Indian Journal of Engineering and Materials Sciences (NISCAIR)***, Vol. 27 (1), pp. 47-57 **(SCI expanded with impact factor 0.794)**
4. **Girija Moona**, R. S. Walia, Vikas Rastogi and Rina Sharma (2019), Parametric Optimization of Fatigue Behaviour of Hybrid Aluminium Metal Matrix Composites, ***Materials Today Proceedings (Elsevier)*** Vol. 21(3), pp. 1441-1445 **(Scopus indexed, SJR: 0.3)**

Conference Presentations (International/National)

1. **Girija Moona,** R. S. Walia, Vikas Rastogi and Rina Sharma (2019), High Temperature Wear Characterization of Hybrid Aluminium Metal Matrix Composite, *International Conference on Emerging Trends in Electro-Mechanical Technologies and Management (TEMT-2019)*, July 26-27, 2019, HMRITM Delhi
2. **Girija Moona**, R. S. Walia, Vikas Rastogi and Rina Sharma (2019), Parametric Optimization of Fatigue Behaviour of Hybrid Aluminium Metal Matrix Composites, *International Conference on Mechanical and Energy Technologies (ICMET-2019)*, November 7-8, 2019, GCET Noida
3. **Girija Moona,** R. S. Walia, Vikas Rastogi and Rina Sharma (2019), Microstructure and Wear Study of Al7075-T6/Eggshell /SiC/Al_2O_3 Hybrid Composites, *National Conference on Advances in Mechanical Engineering (NCAME-2019)*, March 16, 2019, NIT Delhi

Book Chapter

1. **Girija Moona,** R. S. Walia, Vikas Rastogi and Rina Sharma (2019), Microstructure and Wear Study of Al7075-T6/Eggshell /SiC/Al_2O_3 Hybrid Composites, ***Lecture Notes in Mechanical Engineering (Springer)***, ISBN 978-981-15-1070-0, pp. 471-481 **(Scopus indexed, SJR: 0.14)**

TABLE OF CONTENTS

LIST OF FIGURES

LIST OF TABLES

LIST OF SYMBOLS AND ABBREVIATIONS

Symbol/Abbreviation	Stands For
MMC	Metal Matrix Composites
AMMC	Aluminium Metal Matrix Composites
P_c	Property of Composites
P_m	Property of Matrix Material
Pr	Property of Reinforcement
V_m	Volume Fraction of Matrix Material
V_r	Volume Fraction of Reinforcement
α_c	Coefficient of Thermal Expansion of Composite
α_m	Coefficient of Thermal Expansion of Matrix Material
α_r	Coefficient of Thermal Expansion of Reinforcement
K_c	Thermal Conductivity of Composite
K_m	Thermal Conductivity of Matrix Material
K_r	Thermal Conductivity of Reinforcement
P_{comp}	Porosity in Composite
ρ_{th}	Theoretical Density of Composite
ρ_m	Measured Density of Composite
σ_c	Axial Stiffness of Composite
σ_m	Axial Stiffness of Matrix Material
σ_f	Axial Stiffness of Fiber Reinforcement
V_f	Volume Fraction of Fiber Reinforcement
ε_c	Transverse Stiffness of Composite
ε_m	Transverse Stiffness of Matrix Material
ε_f	Transverse Stiffness of Fiber Reinforcement
E_c	Elasticity of Composite
E_m	Elasticity of Matrix Material
E_f	Elasticity of Fiber Reinforcement

σ_c^{UTS}	Strength of Composite
σ_m^{UTS}	Strength of Matrix Material
σ_f^{UTS}	Strength of Fiber Reinforcement
N	Signal to noise ratio in dB
n	Number of responses
x_i	Quality characteristic value for i^{th} experiment
μ	Mean
σ	Deviation
$N_{Taguchi}$	Number of experiments to be conducted
NV	Number of variables
L	Number of levels
S0	As-cast Al7075-T6
S1	Al7075-T6/Eggshell wt.% 1.5/Sic wt.% 1/Al_2O_3 wt.% 1.5, Stirring time 2 min
S2	Al7075-T6/Eggshell wt.% 0.5/Sic wt.% 1.5/Al_2O_3 wt.% 2, Stirring time 4 min
S3	Al7075-T6/Eggshell wt.% 0.5/Sic wt.% 2/Al_2O_3 wt.% 2.5, Stirring time 6 min
S4	Al7075-T6/Eggshell wt.% 1/Sic wt.% 1/Al_2O_3 wt.% 2, Stirring time 6 min
S5	Al7075-T6/Eggshell wt.% 1/Sic wt.% 1.5/Al_2O_3 wt.% 2.5, Stirring time 2 min
S6	Al7075-T6/Eggshell wt.% 1/Sic wt.% 2/Al_2O_3 wt.% 1.5, Stirring time 4 min
S7	Al7075-T6/Eggshell wt.% 1.5/Sic wt.% 1/Al_2O_3 wt.% 2.5, Stirring time 4 min
S8	Al7075-T6/Eggshell wt.% 1.5/Sic wt.% 1.5/Al_2O_3 wt.% 1.5, Stirring time 6 min
S9	Al7075-T6/Eggshell wt.% 1.5/Sic wt.% 2/Al_2O_3 wt.% 2, Stirring time 2 min
SEM	Scanning Electron Microscope
XRD	X Ray Diffractometer
EDS	Energy Dispersive Spectroscopy
t	Recorded Temperature for Density Measurement

ρ_l	Density of Distilled Water at Recorded
ρ_a	Density of Air at Recorded Temperature
I_{ta}	Weight of Specimen in Air at Recorded
I_{tl}	Weight of Specimen in Distilled Water at Recorded Temperature
ρ_t	Experimental Density of Test Specimen at Recorded Temperature
ρ_{f1}	Density of Eggshell Particles
ρ_{f2}	Density of Silicon Carbide Particles
ρ_{f3}	Density of Aluminium Oxide Particles
ρ_m	Density of Al7075-T6 Alloy used as Metal Matrix
ρ_c	Theoretical Density of Composite
w_{f1}	Weight of Eggshell Particles
w_{f2}	Weight of Silicon Carbide Particles
w_{f3}	Weight of Aluminium Oxide Particles
w_m	Weight of Al7075-T6 Alloy used as Metal Matrix
w_c	Weight of Composite
X_{mp}	Predicted Mean of Quality Characteristic at Optimal Level of Process Parameters
CI	Confidence Interval
f_e	Error Degree of Freedom
V_e	Error Variance
N'	Total Number of Experiments
R	Confirmation Experiment Size
$\bar{G}$	Gross Mean
$\overline{A_3}$	Optimal Level of Eggshell Particles Content (3rd level)
$\overline{B_1}$	Optimal Level of Silicon Carbide Particles Content (1st Level)
$\overline{B_2}$	Optimal Level of Silicon Carbide Particles Content (2nd Level)
$\overline{B_3}$	Optimal Level of Silicon Carbide Particles Content (3rd Level)
$\overline{C_1}$	Optimal Level of Aluminium Oxide Particles Content (1st Level)

$\overline{C_2}$	Optimal Level of Aluminium Oxide Particles Content (2nd Level)
$\overline{D_3}$	Optimal Level of Mechanical Stirring time (3rd
HV	Vicker Hardness
F	Load applied in kgf
d	Arithmetic mean of the two diagonals d1 and d2 in
Ra	Average Surface Roughness
Rz	Average Maximum Height of the Profile
COF	Coefficient of Friction
FF	Frictional Force
MRR	Material Removal Rate

CHAPTER 1

Introduction

1.1 Research Motivation

Aluminium based composites are adequately popular materials for large volume commercial applications. Although significant research work has been carried out for advancement of aluminium composites, yet hybrid aluminium composites remain uncharted. Monolithic aluminium composites may demonstrate several enhanced physical and mechanical properties, but at the cost of other relevant attributes, thereby limiting the applications of aluminium composites and motivating the production of cost-effective hybrid aluminium mental matrix composites, using agricultural waste materials. Disposal of certain waste materials, like eggshells is a strikingly serious hazard to our environment, as they straight away contribute in pollution in terms of odour generation and microbial growth. Present experimental investigation aims to synthesize and characterize economical and eco-friendly hybrid aluminium metal matrix composites with exceedingly augmented characteristics; using eggshell, silicon carbide and aluminium oxide particles as reinforcements. The abutting section elaborates backdrop of composite materials.

1.2 Background: Composite Materials

In recent years, research and development in material science stream has predominantly culminated into evolution of materials, termed a composite material. These materials are observed to be unquestionably advantageous while analysing cost–performance equation in component production. Composites are new generation structural materials cohesively composed by physically infusing two distinct compatible constituents (reinforcement and matrix) at macroscopic level. The matrix phase binds and detains reinforcement phase within [1] and reinforcements manipulate the failure mechanism of composites, hence augment the base metal characteristics by many folds. Monolithic or unreinforced materials often encounter restricted utilizations in response to the unprecedented

requirements of diversified engineering applications, whereas the two phases in composites produce amalgamation of various attributes that can never be observed with traditional materials. Composite materials are considered to be multifunctional materials with enhanced strength, enhanced stiffness, better temperature stability, high thermal conductivity, electrical conductivity and improved wear resistance etc. [2]. Characteristics of composite materials majorly depend upon constituent materials and process parameters. Predominant applications of composite materials include electronics, aerostructures, sports and automobiles etc. The upcoming section discusses classification of composites materials.

1.3 Composite Classification

Depending upon the matrix materials, reinforcements and material structures composites can be divided into distinctive subcategories as shown in Figure 1.1. Brief description of these materials has been deliberated in upcoming sub sections.

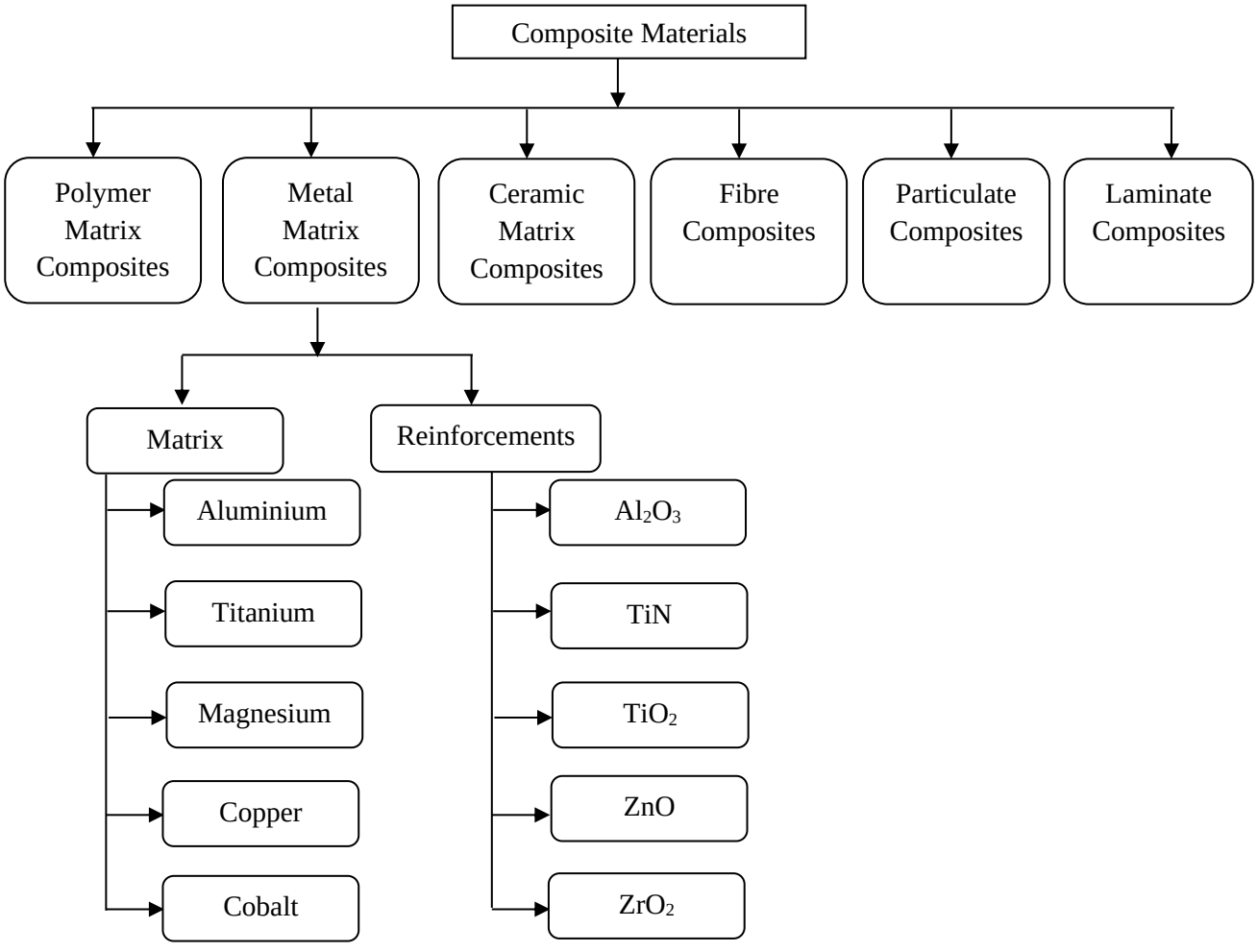

Figure 1.1: Classification of Composites [2]

1.3.1 Polymer Matrix Composites

Polymer matrix composites are prepared by infusing fibrous or particulate reinforcements into polymer resin matrices with good adhesion characteristics. The polymer matrix phases can be classified as thermosets (epoxy resins, vinyl ester resins and melamine formaldehyde etc.) and thermoplastics (aromatic polyamides, aromatic polyesters and polyphenylene oxide etc.).Depending upon mechanical attributes, they are broadly divided into two subcategories, (i) reinforced plastics and (ii) advanced composites [3]. Polymer composites are usually fabricated by a technique known as lay-up, which includes steps like mould preparation, resin glue preparation, cutting glass cloth, hand lay-up pre moulding, curing, de-moulding and finishing. Mechanical properties of polymer composites depend upon size of reinforcements, their orientations and volume content (upto 70% only, as beyond that the matrix amount shall be insufficient to support the infused preforms adequately).

In fiber reinforced polymer composites, the infusion of unidirectional fibers along fiber axis results into enhanced strength and modulus values. Polymer composites have wide application scopes in aircrafts, automobile bodies, construction, shipbuilding industry, electronics and pressure vessels etc. due to light weight, high strength, enhanced stiffness, higher corrosion resistance, improved damping characteristics, reduced cost and elementary fabrication techniques such as sheet moulding, injection moulding, pultrusion and thermal forming etc. [4].

1.3.2 Metal Matrix Composites

Metal matrix composites (MMCs) have been able to accomplish the desiderated conceptions of component designers in order to meet the specified requirements of numerous engineering applications in extreme environmental conditions such as satellites, avionics, automobiles, and structural components. For fabrication of metal matrix composites, hard reinforcements are infused into metal matrix to attain a combination of augmented properties by transferring the load from metal matrix to reinforcement materials, depending upon the interfacial bonding strength between the two phases [5]. Metal matrix composites acquire higher transverse stiffness and strength, enhanced wear resistance, good fatigue response, higher

thermal and electrical conductivity, improved strength and low thermal coefficient of expansion as compared to their unreinforced counterparts.

These are innovative materials whose attributes may be tailored significantly for various applications depending upon selection of relevant process parameters, base metals and reinforcements in terms of their elemental compositions, size and shape, form and geometrical arrangements, content and interface properties [6]. The base metal matrices are prudently selected based upon chemical compatibility, wettability and processing behaviour of reinforcements. For fabrication of metal matrix composites, different metals used are magnesium, titanium, iron, copper, nickel and aluminium. Due to high melting points of Titanium and its alloys, their usage in high temperature and high strength applications is significantly rationalized. Titanium composites developed by infusing various reinforcements have a broad range of high-performance applications in automobile sector [7]. Magnesium is considered a low-density metal with limited plastic deformation at room temperature. Magnesium composites synthesized through squeeze casting and powder metallurgy retain modified mechanical and physical characteristics for various aerospace and automobile applications. Cobalt composites as tool inserts are used for cutting and drilling operations. Nickel metal matrix composites with augmented high temperature creep resistance properties are suitable for various advance engineering applications such as turbine blades of jet engines. Copper composites fabricated through powder metallurgy, internal oxidation and sprays forming etc. acquire enhanced mechanical and thermal conductivities, hence advocating their utilizations in welding electrodes, sliding contacts, nuclear reactors and electronic packaging.

However, the most commonly utilized base metal for synthesis of metal matrix composites is aluminium due to its availability in vast range of alloy compositions, light weight, high strength, superior electrical and thermal properties, reflective properties and cost effectiveness [8]. Aluminium alloys as matrix materials, have consistently enchanted material science researchers because of some more supplementary features such as low viscosity on melting, better corrosion resistance, improved wear attributes and enhanced damping capacity. Based upon the elemental composition of aluminium alloys, the composites

demonstrate variation in their attributes, making engineering components executable. The aerospace, automobile, instrumentation and sports industries require assorted aluminium composite components, to be used in different circumstances; hence extensive research has been carried out in recent years on distinctive aluminium alloys infused with various reinforcements. Metal matrix composites can also be recycled with suitable melting treatments. Numerous processing routes for synthesis of metal matrix composites are classified as:

(i) Solid state methods (powder metallurgy and diffusion bonding)
(ii) Liquid state methods (stir casting, infiltration, spray deposition, infiltration, electroplating and squeeze casting)
(iii) Vapour deposition methods
(iv) Semi-solid-state methods
(i) In-situ fabrication methods

There are some disadvantages also associated with MMCs such as elevated costs, limited service experiences and complicated processing techniques etc. MMCs also have some deprivations in comparison of unreinforced alloys/metals, such as high fabrication cost, reduced ductility, inferior toughness and deteriorated machinability. In addition to this, application of standard fracture mechanism in case of metal matrix composites has not been found suitable due to their microstructural heterogeneity and complicated damage pattern [9]. Also, utilization of metal matrix composites is restricted because of complications in manufacturing due to non-availability of standard procedures for the secondary operations. Welding operations are challenging in fabrication of engineering components using metal matrix composites due to various defects such as chemical degradations, coarse microstructures in fusion zone, excessive formation of eutectic, improper mixing of matrix and reinforcement phases and porosity in fusion zone etc.

1.3.3 Ceramic Matrix Composites

Ceramic matrix composites are developed to enhance toughness, high temperature creep behaviour and resistance to thermal shocks as compared to conventional ceramics with significant reduction in their brittleness, posing them as reasonable materials for high temperature, high stress applications. These composites are

composed to exploit superior high temperature traits of ceramics, by embedding ceramic reinforcements into ceramic matrix with an objective of increasing toughness. The enhanced toughness of ceramic composites is attributed to the fact that on applying load, secondary phases restrict crack propagations of matrix phase. Various strengthening mechanisms present in ceramic matrix composites, like deflection of cracks and fiber pull-outs lead towards enrichment in toughness as compared to their unreinforced counterparts.

Whiskers infused into ceramic matrices cause crack bridging, resulting into enhanced fracture toughness as the stresses in these whiskers connect the crack planes and shut the cracks, impeding crack propagation [10]. In order to inhibit the crack growth, reinforcements in ceramic composites should have high tensile strength with relatively weaker interfacial bonding to pull out the crack extensions. In ceramic composites, controlled interfacial structure is required essentially to intensify the fracture toughness [11]. Ceramic composites can be fabricated through various processing techniques such as powder blending, sintering, hot pressing, chemical vapour impregnation and infiltration etc. depending upon sizes and geometries of reinforcement. They can be widely divided into two subcategories; (i) toughened ceramics reinforced with particulates and whiskers (brittle in nature with improved toughness and strength) and (ii) continuous-fiber ceramic composites (displaying quasi-ductile behaviour). The presence of ceramic reinforcements in ceramic matrices, enhances their high temperature corrosion resistance as compared to the monolithic ceramics because of microstructural and chemical heterogeneity of ceramic composites.

There are some disadvantages associated with ceramic composites because of complexed and costly high temperature processing techniques, which involve only high temperature reinforcements. The reinforcements to be infused should maintain their strength and stiffness at higher processing temperatures to synthesize ceramic composites with augmented characteristics [12]. Additionally, due to difference in thermal coefficient of expansion of reinforcements and matrix, thermal stresses occur during cooling of ceramic composites from high processing temperatures. In case of metal matrix composites, these thermal stresses (tensile or compressive) can be removed by plastic deformation, whereas in case of ceramic

composites crack might initiate during cooling depending upon contraction of reinforcements.

1.3.4 Fiber Composites

In fiber-reinforced composite materials, fibers of high strength are infused into a matrix with recognizable interfaces in order to achieve augmented attributes as compared to the monolithic matrix material. The matrix materials may be polymers, ceramics and metals whereas the common fiber reinforcements are glass fibers, silicon carbide fibers, carbon fibers, boron fibers and various natural fibers such as leaf fibers, bast fibers, reed fibers and core fibers etc.

The reinforcements are, either parallel or braided continuous fibers. Generally, use of metallic fibers is discouraged, due to greater density and tendency to react with matrix alloy. Fiber composites possess high strength/stiffness to weight ratio as compared to the traditional materials [13, 14]. The reinforced fibres in desired locations and orientations act as principal load bearing agents, protecting the matrix materials from plastic deformation. Fiber reinforcements are infused in matrix material in a specified direction, constructing an anisotropic structure and demonstrating directionality in some of their critical mechanical traits such as strength, fatigue, creep and wear behaviour [15].

Though designing of fiber composite components is challenging due to their anisotropic nature, however their properties can be adjusted as per the design requirements. Selected fiber reinforcements can be infused into matrix materials, in the direction of dominant stresses enhancing the directional stiffness of composites. Fiber reinforced composites with long reinforcements are known as continuous fiber reinforced composites whereas composites with short fibers (with sufficient length for significant load transfer and crack growth confinement, to avoid material failure) are called discontinuous fiber reinforced composites. Depending upon directionality of infused fibers, composites can be termed as unidirectional fiber reinforced composites and bi-directional fiber reinforced composites for effortless load transfer form matrix to reinforcements [16].

Mechanical attributes of fiber composite are majorly impinged by characteristics of fibers, their concentration, orientation and the load transmittance

degree to the fibers by matrix material, depending upon the interfacial bonding between the two phases. Critical fiber length, depending upon fiber diameter and its ultimate tensile strength is essential for effective strengthening of the fiber reinforced composite materials. [17, 18]. Also, due to reduced thermal coefficient of expansion, fiber reinforced composites exhibit enhanced dimensional stability over a broad temperature range. Some fiber reinforced composites have high internal damping capacity leading towards enhanced vibrational energy absorption causing reduced noise and vibrations to adjacent structures, mainly in automotive applications [19]. Fiber reinforced composites can be processed through pultrusion, prepeg production processes, open/closed mould processes, tube rolling, compression moulding, centrifugal casting, injection moulding and filament winding etc. Wide spectrum of applications of fiber reinforced composites includes aerospace, automobiles, construction, biomedical, marine, and many other manufacturing industries. In electronics packaging applications also fiber reinforced composites are the most preferred materials because of higher thermal conductivity, lower weight and reduced thermal coefficient of expansion.

1.3.5 Particle Reinforced Composites

Particle reinforced composites are produced by impregnating particle fillers into a matrix through various processing routes. They are most widely used composites due to their enhanced properties, ease of production and cost effectiveness. They are classified into two main categories [20].

- **Dispersion Strengthened Composites**

  With comparatively smaller particles (0.01-0.1μm), exhibit strengthening mechanism identical to precipitation hardening where load is majorly borne by the matrix material and reinforcements play important role in impeding the dislocation mobility. But unlike precipitation hardened composites where strength reduces due to dissolution of precipitate phase, in dispersion strengthened composites the strengthening effect remains undiminished at elevated temperatures due to latency of reinforced particles to chemically react with matrix phase. The interactions between two phases of these

composites are evaluated on molecular level due to fine size of reinforcement particles [21].

- **Particulate Composites**

  They accommodate bigger particles, display intensified mechanical properties as compared to their unreinforced counter parts and employ continuum mechanics to treat particle-matrix interactions. Large reinforcement particles may have different geometries, but they should be equiaxed with uniform dispersion in matrix for effective improvement in composite attributes. Most commonly used particulate composites are cermets (hard ceramic particles reinforced into metal matrix), polymers infused with carbon particulates and concrete. In particulate composites, the reinforcements provide harder phases and bear applied load restricting matrix phase movement. The augmentation in characteristics of these composites significantly depends upon interfacial bonding between matrix phase and filler phase.

Shape, size, chemical affinity and wettability of particle reinforcements have reasonable influence on microstructures and various properties of particle reinforced composites. Particle reinforced composites are noticed to be isotropic in nature and can be subjected to many forming operations such as rolling, forging and extrusion etc. With particle addition to various matrix phases, produced composites exhibit increased hardness, tensile strength, young's modulus, wear resistance etc. and decreased thermal expansion coefficient.

Though enhanced strength of particle reinforced composites may be attributed to various strengthening mechanisms, yet particle reinforcements are considered to be less competent sources for strengthening than continuous reinforcements [22]. Prominent applications of particle reinforced composites include aerospace, microwave and satellite applications, automobiles, structures, nuclear reactors, electrical contacts, creep resistant needs, superconductivity, turbine engines, defence, biomedical, robotics, sports goods and electronic packaging etc.

1.3.6 Laminate Composites

Laminate composites consist of laminas or panels with endorsed directional strength interspersed with fiber reinforcements. These composites are synthesized by arranging layers of fiber reinforcements and matrix material in form of stacks and consolidating them as desired to support applied load or to maintain required deflection. Orientation of fiber reinforcements in every layer and stacking arrangement of these layers significantly influence the physical and mechanical characteristics of laminate composites. Laminate composites with reduced strength can also the produced by using short fibers with random orientation realizing identical physical and mechanical traits in all the directions of composite laminate, hence establishing specific level of isotropy [23].

Though in these composites, usually all the laminas may contain fiber reinforcements oriented either in same direction (with fracture tendency in transverse direction of fibers due to uneven lateral contraction) or in different directions, however interply (different laminas infused with different kind of fibers) and intraply (same lamina infused with different kind of fibers) hybrid composite laminates can also be developed by combining different kind of fibers. Fiber orientation in outer layers are considered as reference direction i.e. 0^0 direction, to determine the middle layer fiber direction for describing laminate composite geometry [24]. Stacking of laminas in these composites essentially has to be balanced and symmetric with respect to the middle plane, in order to bypass any inconsistent deformation. Inelastic behaviour of laminate composites should be interpreted thoroughly for their efficient usage in advance engineering applications. This inelastic behaviour originates from micro damage on increasing load on laminate composite components, due to crack initiation in matrix, transverse to the load direction, resulting into delamination between layers and fiber fracture [25, 26].

Laminate composites are much acclaimed materials due to their augmented attributes and cost effectiveness. Nonetheless, based on the effectiveness of externally applied load; there may be progressive abatements in composite properties. Common materials used in synthesis of laminate composites are plastic matrices, metal sheets, paper and wood etc. Laminate composites have a broad

spectrum of state-of –the art applications due to enhanced fatigue strength, stiffness, corrosion resistance and light weight. The most common applications of laminate composites include structures, aerospace, automotive, damping components, bearing materials, pressure vessels and electrical brushes etc. Polymer laminate fiber reinforced composites are capable of aeroelastic alterations in stiffness of airframe structures by tailoring piling arrangement and fiber orientation angle in each layer, enhancing aerodynamic properties. Thin laminate composites synthesized by infusing boron fibers in aluminium tubes and carbon fiber reinforced epoxy sheets, exhibit isotropy in elastic properties and are contemplated to be suitable for various avionics applications.

1.3.7 Hybrid composites

These are synthesized by infusing two or more reinforcement materials with varying attributes into matrix materials, imparting enhanced properties within composites, as shown in Figure 1.2 (the reinforcements don't react with each other) and mitigating the undesired traits of reinforcements. Conventional composites exhibit superior mechanical properties such as strength and stiffness as compared to unreinforced matrix materials, but with a negative influence on many other mechanical and physical properties which are essential to impede premature failure of mechanical components under in service stress [27, 28].

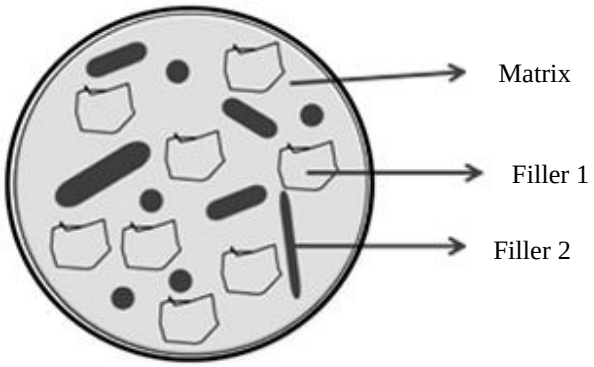

Figure 1.2: Hybrid Composite [29]

These composites exhibit consolidation of characteristics such as impact strength, compressive strength and modulus of elasticity unlike traditional composite materials with single reinforcement. Additionally, hybrid composites have enormous possibilities for alterations in their characteristics for specified requirements. For example, a high modulus material with reasonable load carrying capacity, in order to avoid catastrophic brittle breakdown can be synthesized only as hybrid composite [30].

Hybrid fiber and particulate composites with excellent performances, lower costs, specified functionalities and increased design freedoms are the most preferred advance materials with rapidly increasing implementations. For example, infusion of glass fibers along with carbon fibers into plastic matrix results into a low-density hybrid composite with augmented strength, toughness and impact resistance. Here on applying load, the carbon fibers fail first, transferring the load to glass fibers causing their failure and eventually load is sustained by matrix phase leading towards composite deterioration. Hybrid composites advocate their applications in advance technical pertinences where longitudinal as well as transverse mechanical performances are desired. Prominent hybrid composite application areas include aeronautical applications, electronic applications, renewable energy applications, light weight structural applications, biomedical applications and sports goods etc. as shown in Figure 1.3 [31].

Though there are some complications associated with the phenomena of hybridization during synthesis of hybrid composites, comprising of hybrid ratio, hybrid mode, tendencies of reinforcements, interfacial bonding between matrix and reinforcements phases, processing techniques, component design and strength concept, however hybrid composites are realized to be cost effective materials with remarkable improvement in their physical, mechanical and thermal attributes in comparison of conventional composites and unreinforced alloys. The next section enlists major applications of composite materials.

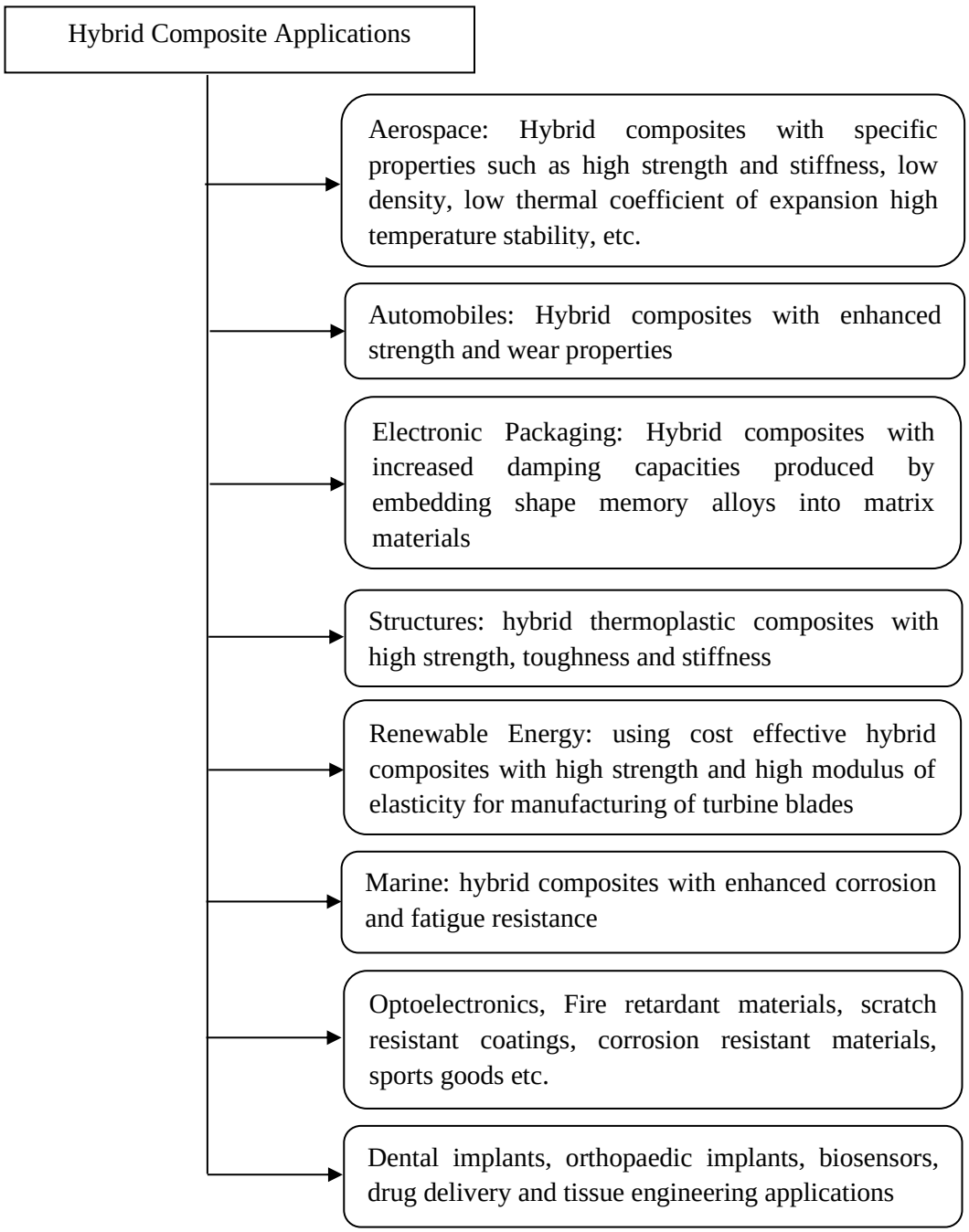

Figure 1.3: Various Applications of Hybrid Composites

1.4 Thesis Scope

The present experimental study has been conducted to synthesize and characterize ecodesigned hybrid aluminium metal matrix composites with enhanced physical and mechanical properties. Various contemplated aspects were literature review, material selection (Al7075-T6 as base alloy and eggshell, silicon carbide, aluminium oxide particles as reinforcements) and synthesis of composites through electromagnetic stir casting technique. This research investigation was essentially concentrated on characterization of produced hybrid aluminium composites to assess them for density, porosity, microhardness, tensile strength, fatigue life, tribological characteristics and machinability followed by process parameters optimization. Present investigation also confronted certain limitations such as fixed stirring speed and agglomeration in reinforcement particles. As anticipated, the synthesized composites showcased phenomenal enrichment in miscellaneous traits. The next section explains contribution of present research work.

1.5 Contribution of Present Work

Main objective of this experimental work is to develop environment friendly and cost-effective hybrid aluminium metal matrix composites with augmented mechanical properties for numerous engineering applications. With exceedingly intensified mechanical, tribological and fatigue attributes, the present study strongly rationalizes wear and fatigue resistant applications of synthesized aluminium hybrid composites with a maximum total reinforcement weight percentage of 5.5% only. Synthesized Al7075-T6 hybrid composites with their ameliorated traits may have extensive spectrum of state-of-the-art applications including automotive, high strength structures, thermally modifiable/ light weight aerospace and defence applications. Organization of thesis is explained in forthcoming section.

1.6 Organization of Thesis

The thesis mainly consists of eight chapters and is organized as follows.

- ***First chapter*** is comprised of discussions on background of composite materials, their classification, scope of thesis, contribution of present work and organization of thesis.

- ***Second chapter*** introduces aluminium metal matrix composites. It presents an exhaustive literature review through assorted research articles spanning the distinctive research contributions in terms of different kinds of reinforcement materials, processing techniques and composite attributes. This chapter includes a brief explanation of various processing techniques for synthesis of aluminium metal matrix composites. It discusses the outcomes of literature review related to aluminium metal matrix composites. This chapter also includes problem statement, research objectives of present research work and research methodology adopted to achieve these objectives.
- ***Third chapter*** deals with Taguchi's approach for design of experiment, selection of orthogonal array and identification of control parameters to synthesize hybrid aluminium metal matrix composites. It also discusses about determination of signal to noise ratio for optimization of specific control factors.
- ***Fourth chapter*** deals with synthesis of hybrid aluminium metal matrix composites through electromagnetic stir casting route followed by preparation of standard test specimens for various mechanical characterizations. It includes discussions on elemental analysis and microstructural studies of composites using various techniques such as XRD, EDS and SEM.
- ***Fifth chapter*** discusses comprehensive mechanical characterization of synthesized hybrid aluminium metal matrix composites and optimization of process parameters.
- ***Sixth chapter*** deals with extensive wear behaviour investigations of all the developed hybrid aluminium metal matrix composites in dry and lubricated wear conditions over a wide range of testing temperatures, followed by parametric optimization for wear loss.
- ***Seventh chapter*** includes investigations towards machinability of developed hybrid aluminium metal matrix composites.

- ***Eighth chapter*** summarizes key findings of the present research work. It also discusses limitations and various future scopes related to the present experimental investigation.

This chapter encompasses research motivation and detailed introduction of composites materials. It highlights the scope of thesis, contribution of present research investigation and organization of thesis. Review of literature shall be excogitated in next chapter.

CHAPTER 2

Review of Literature

2.1 Introduction

The previous chapter contributed to provide an overview of composite materials. Further, there was need of a comprehensive literature review to provide directional discussion of past research related to different aspects of composite materials. This chapter includes detailed introduction of aluminium composites, reinforcement materials, processing techniques, applications and literature review outcomes etc. to provide rationalized review of previous research work. The literature review has been advantageous in selecting matrix and reinforcement materials, synthesis route, equipment and prevalent process parameters to achieve the research objectives. Forthcoming section includes comprehensive description of aluminium based composites.

2.2 Aluminium Composites

Aluminium matrix composites (AMMCs) are contemplated to be next generation potential materials for advance engineering applications. Numerous kinds of reinforcement materials are infused into the aluminium matrix to augment hardness, toughness, wear resistance, fatigue characteristics, electrical attributes and thermal stability in comparison of their unreinforced counterparts [1]. Different properties of aluminium composites predominantly depend upon metal matrix, reinforcement materials, processing parameters and interface bonding between the two phases. Depending upon the reinforcement characteristics, aluminium composites can be divided into three major categories, (i) particulate aluminium metal matrix composites (ii) fiber reinforced aluminium metal matrix composites and (ii) hybrid aluminium metal matrix composites [2]. Various research databases expressed that hybrid aluminium metal matrix composites with uniform dispersion of reinforcements and lower porosity have been more flexible and predictable for various intricate engineering designs [3, 4].

Expanded applications of aluminium matrix composites cause momentous enhancement in product design and development with decreased weight, providing economically reasonable alternatives [5]. Fundamental objective of developing aluminium composites is to achieve desired characteristics by altering matrix composition, reinforcement content, reinforcement shape/ size, synthesis technique and processing parameters. Available literature shows that investigations have been done to interpret the development mechanisms and characteristics analysis related to aluminium metal matrix composites depending upon reinforcement content, reinforcement size and process parameters. Aluminium composites exhibit some phenomenal properties posing tough competition to their monolithic counterparts, as on using appropriate reinforcement the peculiarities of aluminium metal matrix composites can be transformed significantly [6].

In order to assess the mechanical characteristics of aluminium composites such as fracture strength, stiffness and density etc. following model can be considered [7, 8]:

$$P_c = P_m V_m + P_r V_r \tag{2.1}$$

For thermal coefficient of expansion, the rule of mixtures is as given below:

$$\alpha_c = \frac{\alpha_m V_m K_m + \alpha_r V_r K_r}{V_m K_m + V_r K_r} \tag{2.2}$$

Here P is the property, α is coefficient of thermal expansion, V is volume fraction and K is thermal conductivity. Subscripts c, m and r indicate composite, matrix material and reinforcement.

Some of the significant mechanical properties of aluminium metal matrix composites are discussed below [9, 10].

(i) Porosity- Porosity plays an essential role in regulating the mechanical properties of developed composites and can be expressed as:

$$P_{comp} = \frac{\rho_{th} - \rho_m}{\rho_{th}} \tag{2.3}$$

Here ρ_{th} and ρ_m are theoretical and measured densities of composites.

(i) Elasticity- It is of major concern in case of fiber reinforced composites. According to rule of mixtures, we have the following expressions:

For axial stiffness:

$$\sigma_c = (1 - V_f)\sigma_m + V_f \sigma_f \tag{2.4}$$

$$E_c = (1 - V_f)E_m + V_f E_f \quad (2.5)$$

For transversal stiffness:

$$\varepsilon_c = (1 - V_f)\varepsilon_m + V_f \varepsilon_f \quad (2.6)$$

$$E_c = \left(\left(\frac{1-V_f}{E_m}\right) + \frac{V_f}{E_f}\right)^{-1} \quad (2.7)$$

(ii) Fracture behaviour: Fracture strength is nothing but the stress at which the material fails due to fracture. In composites, if the volume content of fiber reinforcement is higher, the composites fail as the fibers break while if the fiber content is less, then the fibers fail before the base material fails. The relevant expressions are given below:

$$\sigma_c^{UTS} = V_f \sigma_f^{UTS} + (1 - V_f)\sigma_m^{UTS} \quad (2.8)$$

$$\sigma_c^{UTS} = (1 - V_f)\sigma_m^{UTS} \quad (2.9)$$

Here σ is stress, *V* is volume fraction, ε is strain, *E* is Young's modulus, and subscript *m*, *f*, and *c* describe the matrix material, fiber reinforcement and composite.

Particle reinforced aluminium composites are probably the most endorsed engineering materials due to easy synthesis and isotropic behaviour. During the development of particle reinforced aluminium composites, there are two major problems faced, one is porosity due to trapped gases and another is agglomeration due to cohesive character of reinforcement particles [11]. Researchers have observed that, generally porosity was increased with reinforcement infusion to the aluminium metal matrix, hence reinforcement content optimization is extremely crucial for non-wetting conditions. On rigorous stirring of aluminium melt and reinforcement mixture, air bubbles enter the slurry causing porosity in composites. Due to porosity, the mechanical characteristics of aluminium metal matrix composites are afflicted severely [12]. Although porosity cannot be avoided completely during casting process, however it can be controlled up to a great extent by using inert gas atmosphere during stirring or creating turbulence only at the bottom region of metal melt during stirring or carrying out casting under pressure or closing the pores by extruding the casting etc. [13].

Distribution of reinforcement particles into aluminium melt predominantly depends upon processing time, reinforcement wetting, processing temperature,

solidification rate and slurry viscosity etc. Uniform reinforcement dispersion regulates the characteristics of aluminium composites and has momentous effects on in-service properties of engineering components manufactured using AMMCs. Additionally, the metal–reinforcement interface which includes chemical reactions and mutual interactions between preform and aluminium matrix, is a crucial phenomenon to determine the properties and performance of composites [14, 15]. Mixing of those reinforcements which are incompatible with aluminium matrix can result into less reliable composites with premature failure tendency.

To strengthen the interfacial bonding of preform and aluminium matrix, various surface treatments have been explored. For example, high intensity ultrasonic cavitation effects were incorporated in aluminium matrix to ensure strong interfacial bonding and uniform distribution of reinforcement [16, 17]. In addition to this, nanostructures such as nano pores on aluminium surfaces, carbon nanotubes and nanofibers were also introduced into composites for strengthening interfacial bonding [18]. Furthermore, in aluminium metal matrix composites the reinforcement wettability usually depends on three main factors: surface energy of reinforcement, molten aluminium metal matrix surface tension and interfacial energy between the two phases. Enhanced surface energies of reinforcements, reduced surface tension of aluminium metal matrix melt and decreased interfacial energy are the basic approaches to enhance wettability [19]. In order to achieve improved wettability, various methods are adopted like coating of reinforcement particles, adding alloying elements to the liquid aluminium matrix and treating the reinforcement particles. For example, the wettability of SiC particles in aluminium/SiC composites was influenced by factors like free silicon in SiC and wetting angle. To overcome this problem, SiC particles were wrapped in aluminium foil, preheated and then infused into aluminium matrix for composite fabrication.

Sometimes, to strengthen the interface bonding between SiC and aluminium matrix, magnesium (<1%) and titanium were added during aluminium metal matrix composite fabrication process [20, 21]. During the analysis of wetting process of aluminium alloy by SiC dip coverage method, some researchers observed that incubation period was decreased by adding silicon, manganese, iron,

chromium, molybdenum and tungsten with aluminium, thus increasing the wettability. Rigorous mechanical stirring and application of external mechanical forces to break the gas layer surrounding reinforcement particles also enhanced the wettability [22]. Filler addition to aluminium alloys resulted into augmented strength through various mechanisms such as hall petch strengthening, orowan strengthening, thermal mismatch strengthening, particle shearing strengthening and load transfer strengthening [23, 24].

In addition to interface phenomena, diversified reinforcement particles distribution patterns in aluminium metal matrix composites also influence the composite characteristics. The types of particle size distribution arrangements are monomodal, bimodal, trimodal and multimodal distributions [25]. Researchers have worked specifically towards investigation of effect of filler size distribution on composite characteristics. Aluminium/SiC particles composites, prepared by pressure less infiltration technique exhibited linear changes in density with increasing particle size distribution while their mechanical properties such as fracture toughness and hardness showed parabolic behaviour [26, 27]. Al/Si/SiC composites with multimodal particle size, fabricated by gas pressure infiltration technique were used for electronic packaging due to their enhanced mechanical characteristics and excellent thermal properties [28]. Aluminium/SiC composites with monomodal size distribution showed linearly increased thermal conductivity, while for bimodal distribution, the thermal conductivity first increased with increasing volume fraction and then turned constant [29]. The abutting section explains various processing techniques for production of aluminium composites.

2.3 Processing Techniques for Fabrication of Aluminium Metal Matrix Composites

Aluminium metal matrix composites can be produced by numerous processing techniques, described in Figure 2.1. The in-situ synthesis processes implicate creation of reinforcements through single step chemical reaction in aluminium matrix, providing better wettability, clean interfaces, stronger bonding and reduced safety hazards [30, 31]. In one of the in-situ processes, molten Al–Mg alloy was infiltrated into the reinforcement to produce composites. Other process

for in-situ synthesis of aluminium metal matrix composites is known as XD process, where a mixture of ceramics and metallic powders is heated above metal melting point, in order to synthesize the composite [32].

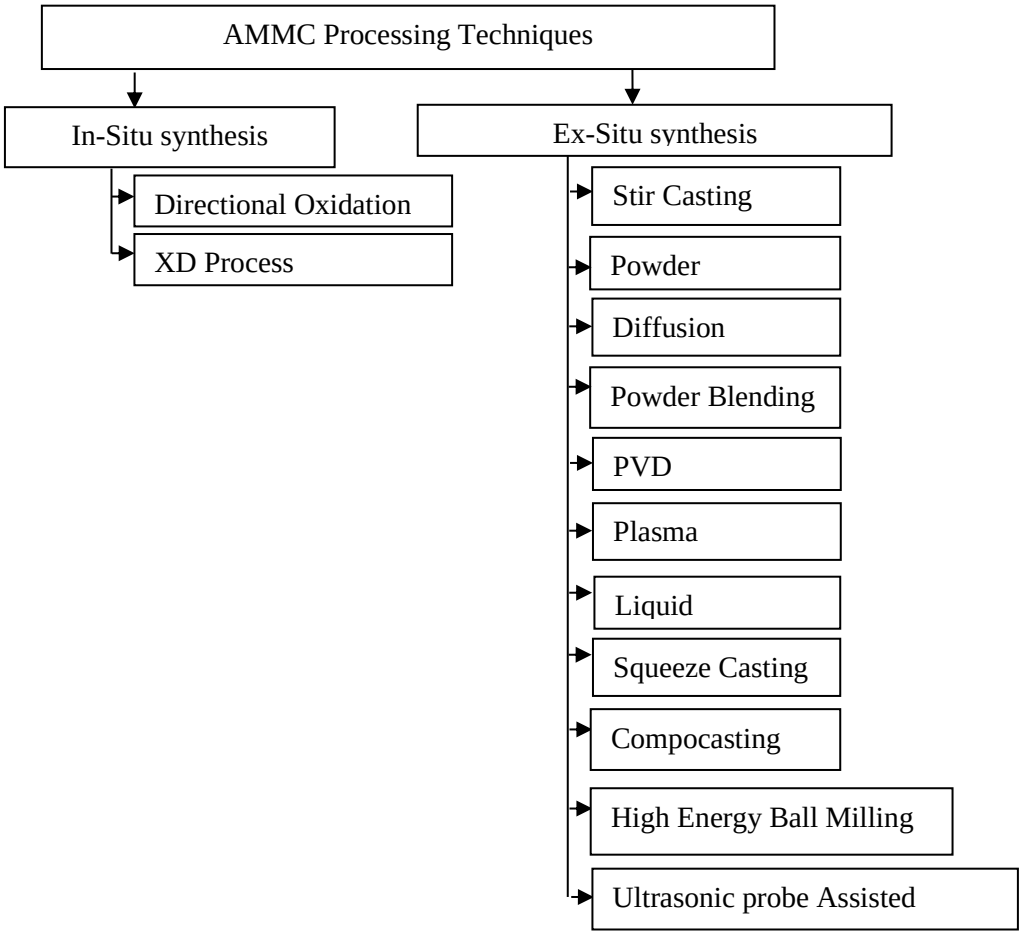

Figure 2.1: AMMCs Processing Techniques

Researchers have also discussed in-situ synthesis of aluminium/Al_2O_3 composite by injecting activated ZnO-Al powder mixture below the melt surface using an injection gun. In this activated powder injection in-situ method, alumina particles of submicron size were formed resulting into almost defect free aluminium metal matrix composite [33]. An innovative fabrication technique, known as pseudo-in-situ was proposed for synthesis of stir cast Al/Ti/Zr/B_4C composite. Large size boron carbide particles were reinforced into aluminium matrix without pre-heating. These B_4Cparticles were subjected to thermal shocks and were converted into fine and contamination free particles with increased wettability resulting into uniform dispersion [34]. For synthesis of inter-metallic

reinforced aluminium metal matrix composites, a contemporary in-situ method was proposed, in which Ni powder was gradually added to molten aluminium by stirring, as a result of which homogeneously dispersed Al_3Ni particles were formed [35]. Controlled gas-liquid reaction methods have also been used for in-situ infusion of carbide, boride, and nitride particles into aluminium matrix [36]. There are certain limitations associated with in-situ synthesis techniques, such as thermodynamic and kinetic restrictions, which limit the composition, nature, shape, size and volume fraction of reinforcement achieved under specified reaction conditions [37].

In ex-situ synthesis, reinforcements are added from outside under controlled processing conditions. Some of the ex-situ processing techniques are explained in following subsections.

2.3.1 Stir Casting

This is the simplest and most widely used fabrication technique. It is also termed as vortex technique. This includes the incorporation of reinforcement particles (upto 30% volume fraction) into aluminium melt in inert atmosphere (as presence of air can cause contamination resulting into chemical and physical changes in the final product), followed by solidification of the mixture as shown in Figure 2.2. The trapped air in molten metal may also be released by flushing the melt with inert gas, reducing porosity. In stir casting technique, particle reinforcements with lower surface to volume ratio and less critical reactivity with metal matrix are preferred as compared to continuous reinforcements [38]. A typical stir casting setup consists of a furnace and a vertical mechanical stirrer (rod connected with electric motor and impeller). The stirrer material should also be able to withstand temperatures higher than the melting point of metal matrix.

By regulating stirrer speed, stirrer angle and vortex cone, good wetting is created between the particulate reinforcement and liquid aluminium alloy melt, which is extremely important in order to avoid porosity and agglomeration in produced aluminium metal matrix composites [37, 38]. Characteristics of composites fabricated by this technique can be altered by varying different process parameters such as melt temperature, processing temperature, preheat

temperature, pouring temperature, stirring speed, stirring time and stirrer position/size etc. [39].

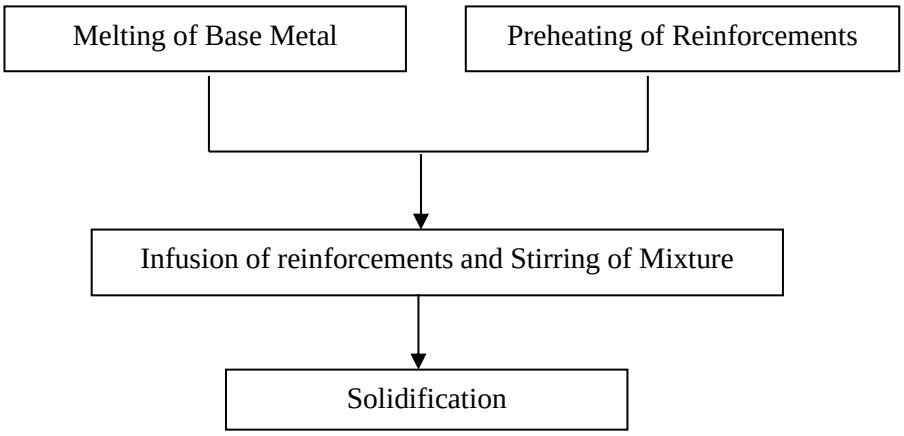

Figure 2.2: Stir Casting Process

2.3.2 Powder Metallurgy

Powder Metallurgy (P/M) is prominent processing technique for synthesis of various composite materials with enhanced mechanical and tribological properties. Here fine powders are blended, pressed into a desired shape, and then heated to bond surfaces as shown in Figure 2.3 [40]. Sufficient diffusion is essentially desired to achieve uniform microstructure and chemical composition of synthesized composites. Generally, ceramic reinforcements (acquiring refractoriness, high hardness and better wear resistance etc.) with dissimilar attributes are infused into aluminium alloy matrixes for production of aluminium metal matrix composites [41]

Properties of aluminium metal matrix composites developed by powder metallurgy depend on purity of matrix phase, reinforcement's shape and size distribution, pressure, sintering temperature, sintering time and finishing treatments [42]. Sometimes the powders are blended with other powders, lubricants and binders to obtain the desired characteristics in developed aluminium composites. The advantages associated with powder metallurgy technique include higher production rate, production of intricate components, good dimensional stability, wide composition variations and less defects such as voids and blow

holes. Whereas the related disadvantages are inferior strength of composites, high tooling cost and density variations.

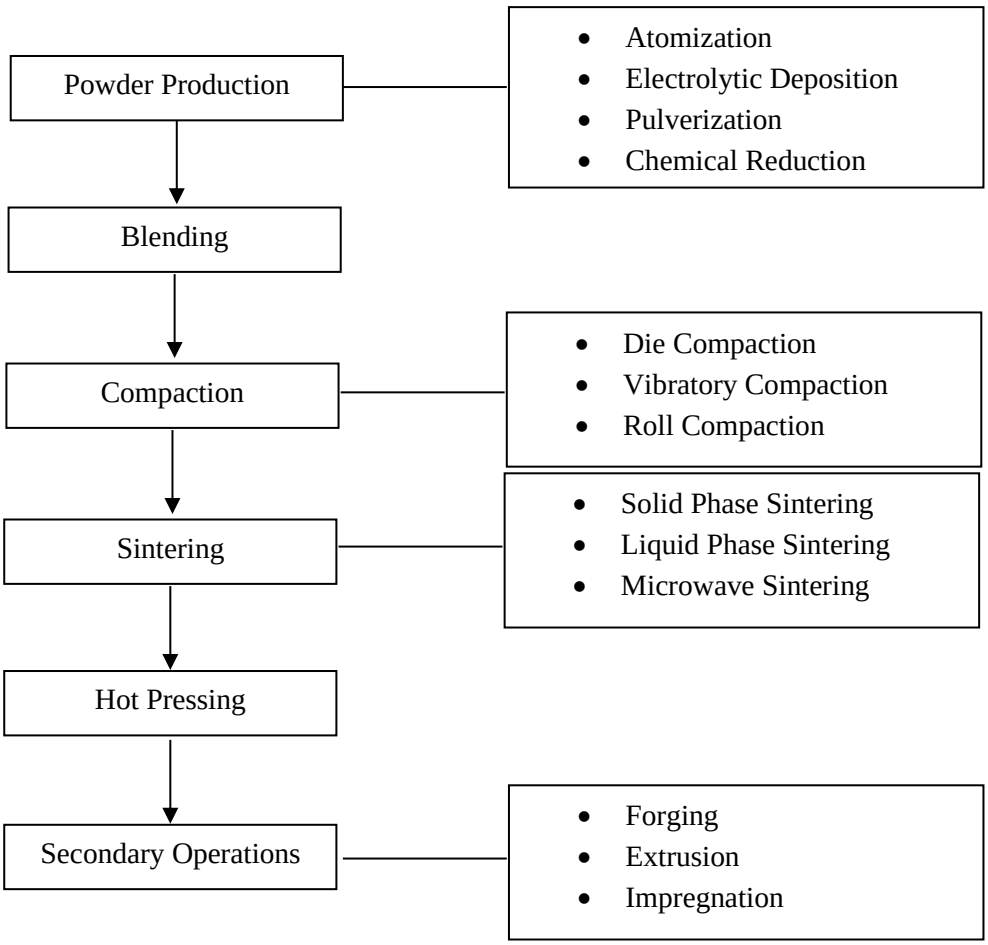

Figure 2.3: Powder Metallurgy Process

2.3.3 Diffusion Bonding

It is a solid-state welding technique and works on the principle of solid-state diffusion, where the atoms of two solid metallic surfaces intersperse themselves over time on applying temperature and pressure. In diffusion bonding, continuous fibers are sandwiched between foils of the matrix material and then subjected to a high pressure on elevated temperature, to establish a bond between the matrix and reinforcement by inter-diffusion. Diffusion bonding involves two main steps; in first step, metal to metal contact is achieved by applying pressure which deforms the surface roughness and disperses the metal layers, whereas in second step active diffusion and grain growth take place to complete the metallic bonding across the contact area [43].

The two diffusion bonding phenomena involve plastic deformation of matrix layers at high temperature resulting into penetration of matrix among fiber reinforcements and interface joint mechanism, when the layers approach each other. Main diffusion bonding methods are vacuum fusion bonding, eutectic bonding, gas pressure bonding and roll bonding etc. To obtain the perfect bonding, the process parameters such as pressure, temperature, surface texture and metallurgical factors should be controlled [44, 45]. The main problem in diffusion bonding is related to the arrangement of reinforcement fibers in intermediate reinforcement layers lying between matrix foils, so that their position remains intact after consolidation.

2.3.4 Powder Blending and Consolidation

It is a versatile method for the fabrication of aluminium metal matrix composites. Amalgamation of aluminium alloy powder with ceramic whiskers/ particles can be conducted dry or in liquid suspension followed by cold compaction, degassing and high temperature consolidations [45].

2.3.5 Physical Vapour Deposition (PVD)

In Physical Vapour Deposition (PVD) atoms/molecules are deposited on a substrate to augment its properties as desired. It is a typical process in which the source material gets vaporized and then forms thin films on condensation. Physical vapour deposition is a high vacuum method used to deposit materials layers with two most common procedures, thermal evaporation and sputtering. In thermal evaporation the source material is heated in vacuum to vaporize, whereas in sputtering accelerated gaseous ions hit the source to create vapours. In physical vapour deposition, molten bath composition has a significant influence on evaporation rate of source material. Here reinforcement fibers are continuously passed through a high partial pressure region of the metal to be used as matrix. On condensation a thick metal coating is produced on the fibers. Further the coated fibers are assembled into an array and consolidated in a hot press [46]. In physical vapour deposition technique uniform dispersion of fiber reinforcements can be achieved by controlling the coating thickness.

2.3.6 Plasma Deposition

This processing technique involves production of composites by mixing ceramic particle reinforcements with metal matrix droplets without any degassing. Plasma (the ionized hot gas containing electrons and ions) is generated between cathode and nozzle in nontransferred mode and is supplied to the work piece for surface coating in order to produce surface composites. Aluminium powder with reinforcement is put into low pressure plasma jet at the nozzle entrance. Metal matrix is heated above melting point in the plasma and accelerated by fast moving plasma gasses. These droplets are then deposited on a substrate, together with the reinforcement particles [47]. The main process parameters of plasma deposition technique are initial temperature, size distribution and velocity of metal droplets, feeding rate of reinforcement, temperature of reinforcement and nature of substrate used for collection of composites [48]. Advantages associated with plasma deposition include rapid solidification and reduced reaction time between matrix and preform phases whereas the disadvantages are residual porosity and considerable material waste during deposition.

2.3.7 Liquid Infiltration

This liquid state fabrication technique is appropriate for synthesis of aluminium metal matrix composites with higher reinforcement content. Here the porous body of a reinforcement phase is held and molten aluminium flows through it, filling all the pores and developing composites with adequate mechanical strength, optimum porosity level and uniform pore distribution. For particle reinforced composites produced by liquid infiltration, lower reinforcement contents are attained by applying unimodal size distributions of filler particles whereas higher reinforcement contents are achieved by using bimodal or multi modal size distributions.

Liquid infiltration technique can be divided into two main categories as shown in Figure 2.4 (i) spontaneous infiltration, where the driving force for infiltration action is capillary force of dispersed phase and (ii) forced infiltration, where external pressure such as mechanical, gaseous, electromagnetic and

centrifugal etc. are applied to molten matrix phase for infiltration of liquid matrix phase through reinforcement.

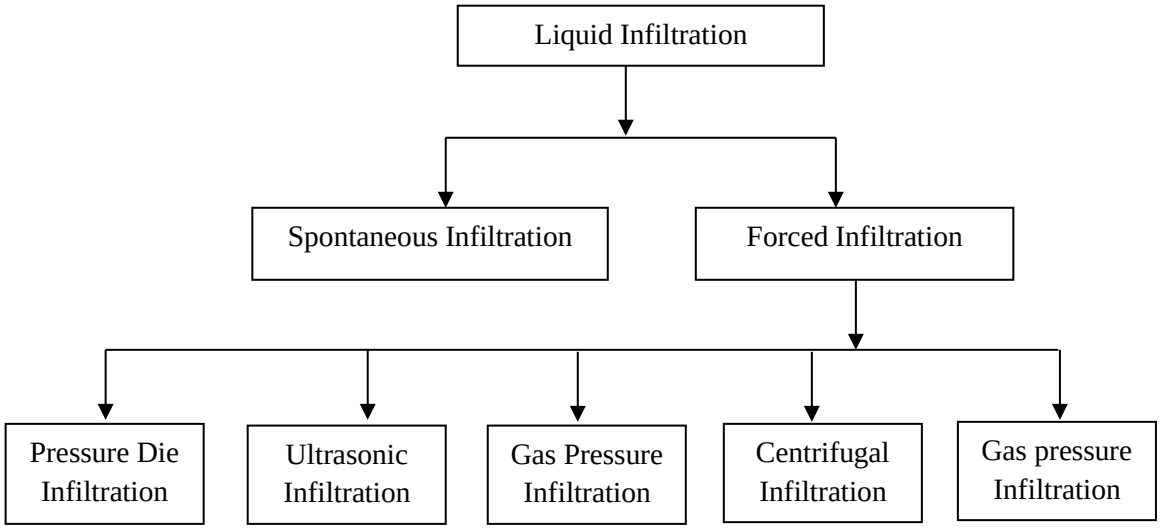

Figure 2.4: Infiltration Processes [49]

The important process parameters are initial composition, temperature of reinforcement phase and infiltrating material, nature and magnitude of the external force exerted on the matrix metal and volume fraction of reinforcement [50, 51]. Composites produced by liquid infiltration technique acquire some captivating attributes such as low density, uniform microstructure, low thermal conductivity and controlled permeability.

2.3.8 Squeeze Casting

It is a unidirectional infiltration technique for fabrication of aluminium composites. This technique is an amalgamation of casting and forging processes with low die filling speed, less turbulence and high pressure applied during melt solidification altering melting point of alloys and improving solidification rate. In squeeze casting process, the metal melt is kept into a die which solidifies due to die pressure, leading towards accelerated heat transfer from molten metal to die, resulting into grain refinement of the metal casting. It is an attractive processing method for development of porosity and shrinkage cavities free AMMCs with uniform microstructures and better mechanical properties.

The dispersion of reinforcement can be made uniform and bond formation can be improved by controlling their wettability in molten metal by applying high pressure. This process is very fast and provides good surface finish. The main process parameters are melt quality and content, preform preheating temperature, molten metal pouring temperature, casting pressure, casting temperature pressurization rate and die temperature [52].

2.3.9 Compocasting

In compocasting, the preheated particulates or short fibers are introduced into partially solid and highly viscous slurries of molten metal by vigorous agitation. Reinforcements are captured between proeutectic phase present in the alloy slurry and there is no gravity segregation also, reducing agglomeration. By continuous stirring the slurry becomes less viscous, leading towards enhanced mutual interactions between metal matrix and reinforcement phases, resulting into increased wetting, strong interfacial bonding and lower porosity [53]. Incorporation of reinforcements with reduced particle sizes into metal matrix through compocasting results into improved ductility as compared to stir-casted composites. Due to lower operating temperatures in compocasting, chemical interactions do not occur between matrix and reinforcements and the molten metal matrix energy is saved, providing longer tool life.

2.3.10 High Energy Ball Milling

It is an effective technique to reduce the grain size of hard phase particulate reinforcement materials and then disperse them uniformly into various base metal matrix including light weight alloys. By optimizing the process parameters and selecting appropriate materials, homogeneous distribution of fine reinforcements can be achieved. Here the mechanical energy is transferred in the form of high impact, from high energy and high frequency balls to the material being developed. This technique is best suited for development of high-density nanostructured metal matrix composite powders with enhanced mechanical properties, which are most appropriate for thermal spray process applications [54].

2.3.11 Ultrasonic Probe Assisted Method

Conventional fabrication methods such as stir casting have many complications in mixing of nano reinforcements into metal matrix due to poor wettability and large surface to volume ratio. Ultrasonic probe assisted method has been proved to be exceedingly efficient in dispersing nanoparticles in base metal matrix. This system includes ultrasonic probe combined with a transducer and power source heating furnace, reinforcement addition mechanism, and inert gas atmosphere. Ultrasonic vibrations are used to degas and purify the metal melt and improve the wettability of particle reinforcement. Strong ultrasonic waves create strong cavitation in metal melt, which further creates transient domains for extreme temperature and pressure variations [55]. The nanoparticle clusters are broken by high temperature shock forces occurred during ultrasonic cavitation and are homogeneously distributed in the metal melt to produce composites with enhanced hardness and tensile strength. Exhaustive analysis of pertinent literature on aluminium composites is carried out in upcoming section.

2.4 Analysis of Literature

Relevant literature has been reviewed extensively and categorized depending on reinforcement materials, fabrication techniques and composite attributes.

2.4.1 Reinforcement Materials

A wide range of reinforcements such as TiB_2, B_4C, SiC, Al_2O_3, TiC, MoS_2, TiO_2, WC, graphite, fly ash, red mud, rice husk ash, bamboo leaf ash, bagasse ash, carbon fibers and glass fibers etc. have been used to develop various aluminium metal matrix composites with enhanced properties [8]. Al7075 was mixed with boron carbide particles and with titanium bromide particles for synthesis of two different aluminium based composites [9]. In another study**,** Al7075 alloy was infused with silicon carbide particles, in variable reinforcement contents i.e. 20, 25 and 30% to synthesize aluminium based composites [10]. Mixing of AlSi18CuNi and Al_2O_3 (weight fraction 2%) by stir casting resulted into a composite with enhanced properties [11].

Aluminium composites were fabricated by mixing aluminium alloy with boron carbide particles (weight fractions 2.5, 5 and 7.5%) [12]. A356-fly ash cenosphere composites were developed using a broad range of reinforcement volume fractions from 20-65% [13]. Mixing of aluminium oxide particles in varying volume fractions from 5-30% was carried out into aluminium alloy matrix to produced aluminium composite. Aluminium composites were synthesized by mixing 6061 Al-Mg-Si alloy with aluminium oxide microspheres with variable volume fraction range from 5-30% [14]. Pure aluminium was infused with 20% Al_2O_3 and Al6061 was mixed with high strength Al_2O_3 fibers to produce aluminium based composites [15].

Hybrid aluminium composites were fabricated by infusion of 3-12 wt.% of garnet and 3 wt.% of carbon particles into LM 13 aluminium alloy [18]. Aluminium alloy was mixed with silicon carbide and bamboo leaf ash, to synthesize hybrid aluminium metal matrix composite [27]. Another hybrid aluminium composite was produced by mixing boron carbide and molybdenum sulphide nanoparticles with Al2219 alloy [29]. Aluminium 6061 alloy infused with variable contents of silicon carbide nanoparticles (0.5, 1.0 and 1.5 volume%) and fixed amount of boron carbide nanoparticles (0.5 volume%), resulted into preparation of hybrid aluminium metal matrix composites [30]. Aluminium intermetallic reinforced composites were produced by adding nickel powder to molten aluminium, forming uniformly dispersed Al_3Ni particles (in-situ formation) [35]. Bamboo leaf ash (weight fractions 0, 2, 3 and 4 %) and silicon carbide particles (maintaining a total reinforcement content of 10 wt.% only) were added to Al-Mg-Si alloy to fabricate hybrid aluminium composites [60]. Al 6061 alloy was infused with titanium oxide particles (volume fraction 5-10%) and graphite particles (fixed volume fraction 3%) to produce hybrid aluminium metal matrix composites [62].

2.4.2 Processing Techniques

Aluminium composites were fabricated through liquid metallurgy route (stir casting) by infusing B_4C particles into LM6 aluminium alloy [12]. Aluminium oxide based polycrystalline microspheres were mixed with aluminium-magnesium-silicon alloy 6061 to synthesize aluminium metal matrix composites

through liquid metallurgy route [14]. Al6061/SiC/B_4C hybrid composites were prepared through solidification process based on ultrasonic cavitation technique [30]. Al7075/ boron carbide composites were prepared through plasma activated sintering. This composite synthesis procedure started with milling of powder mixture followed by sintering and heat treatment [32].

Aluminium/Al_2O_3 composites were also synthesized by in-situ processing technique, where activated powder mixture was injected into molten aluminium [33]. Al/Ti/Zr/B_4C hybrid aluminium metal matrix composite were produced through stir casting route, without any preheating of boron carbide particles [34]. In order to prepare aluminium alloy Al2024-nano Al_2O_3 composites, solid-liquid casting method was adopted in combination with ultrasonic treatment to obtain uniform dispersion of reinforcement particles into metal matrix [36].

LM13/garnet/carbon aluminium composites were fabricated by chill casting method, using sand mould attached with a chill to maintain appropriate cooling rate during solidification [39]. Aluminium/Al_2O_3/graphite hybrid composites were prepared through powder metallurgy technique [41]. An innovative processing technique, involving stirring of uncoated heat treated ceramic reinforcement particles was adopted for fabrication of aluminium composites [52].

Aluminium alloy/bamboo leaf ash/silicon carbide particulate composite were produced through two step casting method. The base metal was first melted and allowed to solidify upto a semi-solid state. Preheated reinforcements were added to semi-solid metal matrix and stirring was carried manually, followed by superheating of composite slurry and mechanical stirring [60]. Combination of two generic processing techniques powder metallurgy and liquid metallurgy was used synthesize aluminium/silicon carbide/graphite hybrid composites [61]. TiO_2 and graphite particles were infused into aluminium 6061 alloy through stir casting technique for production of aluminium hybrid metal matrix composites [62]. Conventional stir casting technique, in conjunction with disintegrated melt deposition approach was adopted to fabricate Al-Cu/SiC composites [68].

Titanium diboride reinforced aluminium composites were synthesized by in-situ process through chemical reaction among aluminium, titanium oxide and

boric anhydride [70]. Aluminium/lithium/silicon carbide particulate composite were fabricated using compound billet method to surmount various challenges encountered during composite extrusion [73]. High energy ball milling and reaction sintering routes were used to prepare Al-Zn/aluminium oxides and Al-Zn-Cu/aluminium oxide composites [76]. To produce Al-Zn/Al_2O_3 nanocomposites, aluminium and ZnO_2 powders were ball milled and hot pressed [78].

2.4.3. Composite Properties

Aluminium 6061 alloy mixed with silicon carbide and boron carbide demonstrated enhanced hardness and tensile strength, whereas the impact strength and ductility were slightly reduced [30]. A decline in coefficient of friction and thermal conductivity along with enhancement in transition temperature and transition load during wear test, was observed for Al6061/Al_2O_3 metal matrix composites [37]. A356/Al_2O_3 nanocomposites indicated grain refinement of matrix material and uniform dispersion of fillers. These composites also showed augmented hardness, tensile strength and ductility [48].

Increased yield strength, good flowability and improved hardness was displayed by pure Al/Al_2O_3 nanocomposites [54]. Composites synthesized by using a mixture of aluminium alloy, aluminium oxide and rice husk ash exhibited increased strength, increased fraction toughness, reduced density and reduced hardness [58]. Aluminium metal matrix composites synthesized by mixing Al-Mg-Si alloy, SiC particles and bamboo leaf ash particles showed enhanced fracture toughness and corrosion resistance. Other crucial attributes of these composites such as density, tensile strength and hardness were deteriorated [60]. Increased tensile strength and decreased density were observed for Al6061/SiC/Gr composites as compared to unreinforced Al6061 alloy [61]. Titanium oxide and graphite particles mixed with Al6061 alloy, produced aluminium metal matrix composites with upgraded hardness and tensile strength [62]. Augmented tribological characteristics and improved hardness were noticed for Al7075/B_4C composites [66].

AA6082/Si_3N_4/Gr composites exhibited increased tensile strength and hardness with deteriorated percentage elongation [69]. Aluminium composite with

A356.2 alloy as base metal and silicon carbide and rice husk ash as reinforcement demonstrated enhanced hardness, enhanced tensile strength, decreased density and decreased thermal coefficient of expansion in comparison of A356.2 alloy [72]. Al8090/SiC/calcinated fly ash composites offered resistance to chemical deterioration in extreme environment [73]. Al6061/Al_2O_3 and Al2124/SiC composites displayed improved wear characteristics, increased tensile strength and increased hardness [75].

Aluminium metal matrix composites Al (Zn)/Al_2O_3 and Al (Zn)–4Cu/Al_2O_3 showed decreased wear due to presence of load bearing reinforcement particles [76]. Enhanced thermal stability was observed for Al/Zn/Al_2O_3 composites [78]. Lower porosity and better corrosion resistance were ascertained for AK12 aluminium alloy and fly ash composites [81]. Aluminium alloy Al6063 was reinforced with zircon sand ($ZrSiO_4$) and aluminium oxide to produce composites, exhibiting increased hardness and tensile strength [83]. LM25/SiC/Gr hybrid aluminium composites demonstrated enhanced hardness in addition with exceptional wear properties [89]. A 356.1 alloy infused with MgO displayed increased compressive strength and increased hardness [91]. Multi-walled carbon nanotubes mixed with Al2024 alloy, produced aluminium composites with high damping capabilities at elevated temperatures without sacrificing the mechanical strength and stiffness of metal matrix [96].

Various aluminium metal matrix composites with different reinforcements, processing techniques and attributes have been consolidated in Table 2.1 [56].

Table 2.1: Aluminium Metal Matrix Composites with Various Reinforcements, Processing Techniques and Properties

Sl. No.	Components	Processing Technique	Properties
1	AlSi18CuNi/Al_2O_3p (2%)	Stir casting	Increased tensile strength and increased hardness. Better wear resistance [10]
2	AA 6061/SiC/B_4C (0.5-1.5%)	Ultrasonic cavitation based	Increased hardness, increased tensile strength, slightly

		solidification process	reduced ductility, and marginally lower impact energy [30]
3	Al 356/Al_2O_3	Stir casting	Increased hardness [48]
4	Al2219/B_4C/ MoS_2	Liquid metallurgy	Decreased densities, increased micro hardness, decreased tensile strength, decreased ductility and better wear resistance [57]
5	Al-Mg-Si/Al_2O_3/Rice husk ash (0-10%)	Stir casting	Decreased density, hardness and tensile strength. Increased specific strength, percent elongation and fracture toughness [58]
6	Al-Mg-Si alloy (6000 series)/SiC/Bamboo leaf ash (0-10%)	Two step stir casting	Reduction in tensile strength and hardness. Increased fracture toughness, improved corrosion resistance and decrease in density [59, 60]
7	Al6061/SiC/Gr (5-15%)	Stir casting	Increased tensile strength and decreased density [61]
8	Al6061/TiO_2/Gr (3-10%)	Stir casting	Increased hardness and tensile strength [62]
9	Al6061/SiC and Al7075/Al_2O_3 (2-6%)	Liquid metallurgy	Higher tensile strength, improved wear properties, increased hardness and decreased density of composites. Decrease in thermal conductivity, thermal capacity and thermal expansivity in Al6061+SiC composites [63]

10	Al6061-T6/SiC/Gr/ Al_2O_3	Friction stir processing	Decreased micro-hardness, increased wear resistance and better machinability with good surface quality using EDM, excellent dimensional stability, reduced thermal properties and better wear resistance [64]
11	Al7075/B_4C (5-20%)	Stir casting	Increased hardness and increased wear resistance [65, 66]
12	A356/SiC/Gr	Compocasting	Enhanced tribological properties [67, 68]
13	AA6082/Si_3N_4/Gr	Stir casting	Increased hardness and tensile strength Reduced percentage elongation [69, 70]
14	Al 8090/SiC (5-20%)	Stir casting	Variation in density, porosity and in thermal properties. Increased micro-hardness [71]
15	A356.2/SiC/Rice husk ash (2-8%)	Double stir casting	Increased hardness, increased porosity, increased tensile strength, decreased density and decreased thermal coefficient of expansion [72]
16	Al 8090/SiC/ Calcinated fly ash	Stir casting	Enhanced chemical deterioration in extreme environmental conditions [73]
17	Al 5083/B_4C	Cryomillling and consolidation	Enhanced strength [74]

18	Al6061/Al_2O_3 and Al2124/SiC (6-12%)	Stir casting	Increased hardness, increased tensile strength and enhanced wear characteristics [75]
19	Al/ ZnO/ CuO	Powder metallurgy	Decreased wear rate [76]
20	Al/Al_2O_3 (20%)	Powder metallurgy	Increased hardness [77]
21	Al/Zn/Al_2O_3	Powder metallurgy	Enhanced thermal stability [78]
22	A6082/ Al_2O_3	Friction stir casting	Increased wear resistance [79]
23	Al 6061/Ni coated Si_3N_4 Particles	Stir casting	Lower wear rate [80]
24	Ak12/Fly ash (9%)	Squeeze casting	Lower porosity and better corrosion resistance [81]
25	Al 6061/Fly ash (10-20%)	Stir casting	Increased tensile strength and hardness and decreased ductility [82]
26	Al6063/$ZrSiO_4$/ Al_2O_3 (0-8%)	Stir casting	Increased hardness and tensile strength [83]
27	Pure Al/TiO_2 (5%)	Stir casting	Improved tensile strength and hardness [84]
28	Al7075/TiB_2	Stir casting	Increased micro-hardness, increased tensile strength and increased yield strength [85]
29	Al 2014/TiC (5-10%)	Stir casting	Increased hardness and strength [86]
30	Al 6063/SiC/ Al_2O_3	Stir casting	Increased wear resistance [87]
31	Al 7009/ SiC	Stir casting	Increased hardness [88]
32	LM 25/SiC/Gr	Stir casting	Increased hardness and reduced wear rate [89]

33	Al6063/SiC (3-12%)	Two step stir casting	Improved tensile strength and fracture toughness [90]
34	A 356.1/MgO (1.5-5%)	Stir casting	Increased hardness and compressive strength [91]
35	A359/ Al_2O_3	Electromagnetic stir casting	Increased hardness and tensile strength [92]
36	Al 6061/TiB_2/Gr	Stir casting	Better wear properties [93]
37	Al/Cu (4%)/SiC (5%)	Stir casting	Increased hardness, impact strength and tensile strength [94]
38	Nanostructured composites Al/Al_2O_3	In-situ consolidation during back pressure equal channel angular pressing	Increased compressive strength [95]
39	Al2024/MWCNTs	Cold isostatic press and hot extrusion	Enhanced damping capabilities at elevated temperature [96]
40	Al 2024/Ag	Powder metallurgy	Increased tensile strength and hardness [97]
41	Al6063/Al_2O_3/Y_2O_3 (0.75-1.5%)	Powder blending and mechanical alloying	Increased micro-hardness [98]
42	Al-Ti-Cr/L12–Al3Ti	Rapid solidification processing	Increased micro-hardness [99]
43	Al/AlN (0-39%)	Arc plasma evaporation followed by consolidation	Improved hardness and elastic modulus [100]

44	Al-Si7-mg2/SiC (5-15%)	Squeeze casting	Increased tensile strength and hardness and decreased toughness [101]
45	Al7075/Fly ash/ E-glass short fibers	Stir casting	Increased tensile strength, increased hardness and wear resistance [102]
46	AA6063/Al_2O_3/RHA/Gr	Two step stir casting	Increased tensile strength, decreased hardness and enhanced wear resistance [103]
47	Al6063/BLA/SiO_2 (2.5-10%)	Two step stir casting	Improved wear resistance, decreased density and hardness [104]
48	Al-Cu/SiC/Fly ash	Stir casting	Increased hardness, wear resistance, impact strength and tensile strength [105]
49	Al+TiO_2 (0-12%)	Powder metallurgy	Increased micro-hardness and increased wear resistance [106]
50	LM6/Al_2O_3/SiC (0.5-2%)	Stir casting	Increased hardness and tensile strength. Better tribological properties [107]
51	Al6061/Gr	Stir casting	Increased hardness, ultimate tensile strength and reduced ductility [108]
52	AA6061/ZrB_2	In situ method	Enhanced tribological properties [109]
53	Al/B_4C	Liquid metallurgy	Increased hardness and reduced density [110]
54	A384/SiC	Stir casting	Increased hardness [111]
55	AA7075/TiC	Stir casting	Increased hardness and ultimate tensile strength [112]
56	Al 2024/SiC/ Flyash	Two step stir casting	Increased tensile strength and increased hardness [113]

57	Al-4.5%Cu/10TiC	In-Situ method	Ultimate tensile strength and hardness were increased [114]
58	Al7075/TiC	Stir casting	With increased content (wt.%) of TiC, the specific wear rate and coefficient of friction were reduced [115]
59	(Al-Si10Mg)/ alumina/ graphite	Stir casting	Improved wear resistance due to graphite as a primary filler and alumina as secondary [116]
60	Al 2024/ Beryl Particles	Liquid metallurgy	Decreased wear rate [117]
61	Al6061 / Nickel coated Si_3N_4	Liquid metallurgy	Coefficient of friction decreases for increased load and increases on increasing velocity. Increased wear rate with increased load and sliding velocity [118]
62	Al/ Carbon nanotubes	Spark plasma sintering followed by hot-extrusion processes	Enhanced tensile strength and no decrease in elongation [119]
63	Al/ Carbon nanotubes	High energy ball milling	Limited strain hardening of the aluminium powder and significantly improved mechanical properties [120]
64	Al-4.5% Cu/ Flyash	Stir and squeeze casting	Hardness and impact values were increased whereas porosity and other casting defects such as shrinkage cavities were minimized [121]

65	Al/TiC	Semisolid stir casting	Improved specific strength, high temperature wear resistance and hardness [122]
66	A-S7go$_3$ and A-S$_4$G composites	Stir casting	Significant improvement in mechanical properties due to presence of eutectic silicon in form of fine spheres [123]
67	Al/SiC/Cu	Stir casting	Increased hardness and tensile strength [124]
68	Al/CNT	Cold isostatic pressing followed by hot extrusion techniques	Increase in tensile strength [125]
69	AA 6061/TiC	Stir casting	Increased tensile strength [126]
70	Al7075/ Fly ash/ TiC	Stir casting	Increased hardness and tensile strength [127]
71	Al/SiC/Mica	Stir casting	Increased strength and hardness [128]
72	Al/ TiO2	Hot Pressing	Reduced coefficient of friction and wear rate [129]
73	Al/B_4C (0.5vol%) /SiC(0.5,1%1.5	Ultrasonic cavitation method	Increase in hardness, tensile strength with grain size refinement [130]
74	Al/Al_2O_3/B_4C	Stir casting	Improved wear characteristics with increase % of B_4C [131]
75	Al 6061/TiB_2/12P	in-situ procedure	Higher values of hardness, tensile strength and Young's modulus with poor machinability [132]

The forthcoming section includes discussion on predominant applications of aluminium composites.

2.5 Applications of Aluminium Metal Matrix Composites

There is huge application scope for aluminium metal matrix composite due to their superior and tailor made characteristics.

- **Aerospace applications:** Aluminium metal matrix composites have emerged as potential materials with numerous space and avionics applications, substituting current aerospace components. Their coefficient of thermal expansion, that can be tailored to zero make AMMCs suitable for aerospace applications. The vital aerospace components fabricated using aluminium composites are brakes, wing slat tracks, vertical tails, wheels bulkheads, doors and landing gear parts etc. [133].
- **Automotive applications:** Aluminium metal matrix composites possess reduced weight, augmented tribological characteristics, better thermal conductivity, capacity to withstand extreme working conditions, increased component durability, higher damping capacity, self-cleaning and self-healing capabilities etc. [134]. Light weight automotive parts result into decreased fuel consumption, diminished emission level and increased reliability of the system, thus meeting the emissions regulations and consumer expectations [135]. Different automotive parts manufactured using aluminium based composites are pistons and cylinder liners, main bearings, connecting rods, A/C pump bracket, chassis, suspensions components, chain covers, transmission housings, valve covers, brakes and intake manifolds etc.
- **Structural applications:** Aluminium metal matrix composites are used to fabricate various structural components such as platforms, walkways, roof structures, bridge structures, window frames, door panels, storage containers, large signages, marine/offshore structures power plant structures and handrail components etc. Ductile and tough aluminium alloys blended with hard and strong ceramic reinforcements produce composites that are appropriate for structural applications [136]. In addition

to these, AMMCs possess resistance to extreme environmental conditions, high bearing strength, resistance to out gassing, good wear resistance, good erosion resistance, good thermal conductivity, better dimensional stability, high temperature resistance and high impact resistance, providing better response in the area of structural components [137, 138].

- **Electronics and communication applications:** The prime challenges faced in modern electronic systems are increased power density, ability to withstand extreme operating conditions and high level of integrations [139]. Aluminium metal matrix composites have emerged as good thermal management materials for high reliability applications in power electronics. Al/Gr, Al/SiC and Al/B composites are unmatched packaging materials for high performance thermal management packaging systems due to their lightweight, higher specific strength, better wear resistance, high thermal conductivity and compatible coefficient of thermal expansion [140, 141].
- **Thermal applications:** Monolithic aluminium alloys with higher thermal expansion coefficient and inferior tribological attributes are being superseded by different aluminium metal matrix composites for various thermal applications like automotive/aerospace components, power electronics components and semiconductor devices [134]. Al/SiC, Al/Al_2O_3, Al/TiB_2 composites can be useful for different thermal applications like satellite microwave system, networking, engine pistons, intake-exhaust valves, cylinders, connecting rods and gears, etc. demonstrating reduced thermal impacts, reduced wear, reduced fatigue at elevated temperatures and better dimensional stability with narrow tolerances [135, 136].
- **Precision applications:** Aluminium composites are used for manufacturing dimensionally stable spacecraft structures such as space telescope, space shuttle mid fuselage main frame, landing gear drag link of the space shuttle orbiter and antenna etc. Al/Gr composites with desired stiffness, low coefficient of thermal expansion and excellent electrical conductivity are used in high gain antenna [137]. Aluminium metal matrix composites like Al/Al_2O_3, $Al/ZrSiO_4$ and Al/fly ash which are developed

through powder metallurgy route are used for fabrication of precision parts for automotive. Beryllium reinforced aluminium metal matrix composites processed through powder metallurgy based semisolid metal forming process, exhibiting high modulus, low density, high thermal conductivity and high heat capacity are used in satellite and avionics precision applications [138, 139]. Many other precision applications of AMMCs are atomic force microscope support frame, robotic arms, video recording heads and advance manufacturing instruments requiring adequate thermal and load resistance.

- **Wear resistant applications:** Some contemporary studies have been conducted to observe various features of Al/SiC composites, projecting aluminium composites as potential materials for wear resistant applications [140]. Al/Sic and Al/ Al_2O_3composites, used for numerous automotive and marine applications, demonstrate superior tribological characteristics as compared to the unreinforced metal. Reinforcement of TiB_2 particles into aluminium by liquid aluminium infiltration exhibits increased wear resistance, which may be attributed to the capability of TiB_2 particles to protect the softer metal matrix from abrasion [141]. Due to augmented wear attributes aluminium based composites are being used in manufacturing of cylinder, piston and brake pads etc. leading towards better fuel economy and controlled emission.
- **Recreational activities:** Aluminium metal matrix composites are also used in sports activities and recreational goods such as tennis rackets, badminton rackets, pole vaults, golf rods, polo rods and bicycles. Aluminium composite materials (infused using silicon carbide and boron carbide particles as reinforcements) with cost effectiveness, increased strength and modulus of elasticity provide design advantages for numerous sports products [142].
- **Electrical transmission:** With augmented attributes such as low density, increased strength, high corrosion resistance and high electrical conductivity, aluminium composite materials are considered perfect for

transmitting electric power from power generation stations to houses and offices [142].

- **Rail Transport:** Aluminium composites are preferred materials for railroad cars due to reduced welding needs, high load carrying capacity and light weight resulting into reduced fuel cost. Aluminium composites also offer increased corrosion resistance and strength in extreme environmental conditions justifying their applications in rail transport [142].
- **Marine transport:** Aluminium metal matrix composites have emerged as revolutionary materials for various marine applications as they enhance their vessel speed, load capacities, fuel efficiency and seaworthiness and reduce maintenance cost [142]. The manoeuvrability of marine transport means (manufactured through friction stir welding and structural bonding routes) can also be increased by using aluminium composites being able to deal with impact, compression and torsional loads during water travel.
- **Offshore applications:** Aluminium composites are adequately used in production of seawells, helidecks, telescoping bridges, cable ladders and offshore platforms due to light weight, high strength, increased corrosion resistance, reliability and lower maintenance cost. Smooth manufacturing associated with aluminium composites in terms of easy extrusion, better weldability and non-combustible nature offers them an extra edge while selecting material for offshore applications [142].

Some of the proven commercial applications of AMMCs are as given below [143]:

- Brake rotors made form aluminium composites (AlSi7Mg+SiC particulates) for German high speed train ICE-1 and ICE-2 developed by Knorr Bremse AG
- AMMC continuous fiber reinforced pushrods produced by 3M for racing engines. These pushrods weigh 40% of steel
- AMMC wires also developed by 3M for the core of an electrical conductor
- Pistons, brake rotors, calipers, liners and propeller shafts manufactured by Duraclan, Martin Mareitta, GKN and Lanxide using Al-SiC particle composites
- Connecting rods of Nissan using Al-SiC whiskers composites

- Connecting rods of DuPont, Chrysler and Piston rings of Toyota using Al-Al_2O_3 composite
- Pistons and connecting rods of Martin Mareitta using Al-TiC particle composite
- Engine blocks of Honda using Al-Al_2O_3-carbon fiber hybrid composites
- Brake rotors of Lotus Elisse, Chrysler and Volkswagen using Al-SiC particle composites. Rear brake drum, drive shaft and engine cradle of General Motors using Al-SiC particle composites

Assorted outcomes of comprehensive review of literature are explained in following section.

2.6 Outcomes of Literature Review

There are various issues related to the engineering competence, commercial viability, development and widespread usage of aluminium metal matrix composites. Increased processing cost, deteriorated machinability, lack of theoretically predicted properties, lack of knowledge about potential applications, lack of available design data, degradation in mechanical properties during secondary processing, increased nano-reinforcement costs, deteriorated ductility and toughness are some of the fundamental reasons that restrain the applications of aluminium composites in different sectors despite of their augmented characteristics. Economical synthesis of aluminium based composites is need of the hour for making them more acclaimed engineering materials. Though aluminium composites are being used in numerous commercial and defence applications, however more opportunities are yet to be explored. Some of the prominent challenges are as discussed below:

- Disposal of industrial and agricultural waste materials such as fly ash, red mud, palm oil fuel ash, palm oil clinker, rice husk, coconut husk and sugarcane bagasse etc. is a threat to environment, thus more focus should be on recycling them and using them for development of environment friendly and cost effective composites [144].
- Mechanisms behind different processing techniques are to be understood thoroughly in order to achieve uniform dispersion of reinforcement, strong

interfacial bonding and improved wettability without affecting the microstructural integrity of aluminium metal matrix composites [145]. More emphasis should be given on development of modified processing techniques and controlled process parameters, so that there is no compromise with damage tolerant properties of composites like ductility and fracture toughness, as the infusion of reinforcements into aluminium matrix reduces the ductility, making them worse for secondary forming operations.

- Various manufacturing technologies for aluminium composite components to maintain the reliability, durability and machinability of components such as filament winding, pultrusion, sandwich panelling, forming, rolling and 3D weaving etc. are to be developed further [146].
- Cast composites usually do not hold well when processed further. So, the processing techniques need to be sub-classified in accordance with the production factors, microstructures and applications of aluminium composites.
- There is an urgent need to explore secondary processing techniques and recyclability for development of aluminium based nanocomposites with uniform distribution, preserved nanostructures and restricted grain growth.
- Performance of aluminium metal matrix composites also depends upon the volume fraction, shape, size and nature of reinforcements, so more work is to be done to produce low cost reinforcements and to develop AMMCs from nonstandard low cost aluminium alloys with desired mechanical, thermal, electrical, tribological and corrosion properties to withstand extreme working conditions [147].
- Sufficient attention is to be paid in order to avoid health hazards while dealing with ultrafine nano-reinforcements during production of aluminium metal matrix nanocomposites.
- In hybrid aluminium metal matrix composites, it becomes very important to understand the role of individual reinforcement component in order to achieve desired properties and optimize prevalent process parameters. Often the use of hybrid aluminium composites is limited, due to their

difficult machinability. The major problems faced are rapid electrode wear, inconsistent material removal rate, difficult to cut intricate geometries, poor surface finish, requirement of large pulse current and low machining rate etc. [148].

- The corrosion behaviour of aluminium composites is a strong criterion for selection of aluminium alloys and reinforcements, because processing condition of AMMCs can cause rapid corrosion of composite as compared to the unreinforced alloy. The main kind of corrosion in AMMCs is galvanic corrosion, which occurs due to the chemical degradation of matrix and reinforcement phases. This can be avoided by controlling processing parameters, microstructure of composites, and interactions at the interfaces [149].

Next section defines problem statement of present research investigation.

2.7 Problem Statement

In present industrial scenario, a humongous research gap can be contemplated for development of eco-friendly materials with distinctive mechanical attributes to cater specialized needs. In reference to hybrid aluminium composites, previous research investigations have demonstrated limited studies on some conventional fabrication techniques, with constrained reinforcement combinations (utmost two reinforcements) and higher reinforcement contents. Exhaustive explorations to observe the influence of various reinforcements on a wider range of mechanical/physical characteristics of aluminium composites have also not been reported so far. With this background, present research work aims to develop and characterize economical and ecodesigned hybrid aluminium metal matrix composites with upgraded mechanical properties through an unconventional processing technique, for contemporary industrial applications

The upcoming section explains thesis objectives.

2.8 Thesis Objectives

From aforementioned research gaps, the present thesis aspires to achieve the following objectives:

(i) Development of hybrid aluminium metal matrix composites using three reinforcements, out of which two are inorganic reinforcements and one is agricultural waste material reinforcement.

(ii) Characterization of developed hybrid composite for microstructure and elemental composition using different characterization techniques such as SEM, EDS and XRD.

(iii) Evaluation of synthesized hybrid aluminium metal matrix composites for various mechanical and physical attributes such as density, percentage porosity, residual stresses, hardness, tensile strength, fatigue life and tribological characteristics.

(iv) To investigate influence of various reinforcements on attributes of developed hybrid composites. Optimization of prevalent process parameters (weight fraction of reinforcements in metal matrix and mechanical stirring time) for prediction of optimal composition of constituent elements using ANOVA.

(v) To study the effect of surface roughness on fatigue behaviour of developed hybrid aluminium metal matrix composites.

(vi) Exploring the machinability of developed hybrid aluminium metal matrix composites.

Research methodology endorsed for present research work has been discussed in next section.

2.9 Research Methodology

The research methodology adopted to fulfil various research objectives of proposed research work involved the following steps:

- The methodology begins with literature review that relates to this work for better understanding of subject and knowing state of the art
- To identify the relevant aluminium alloy as base metal
- To identify appropriate reinforcements
- Design of experiment for synthesis of hybrid aluminium metal matrix composites with four control factors retaining three levels using Taguchi's orthogonal array L9

- Synthesis of hybrid aluminium metal matrix composites by electromagnetic stir casting technique in conjunction with conventional stir casting method
- Preparation of standard specimens for various characterizations
- Microstructural, elemental, physical and mechanical characterization of developed hybrid composites
- Depending upon characterization outcomes, parametric optimization of control factors for enhanced physical and mechanical properties
- Investigations for surface roughness and machinability of developed composites
- Exhaustive investigation for tribological behaviour of synthesized hybrid aluminium metal matrix composites

Research methodology was broadly divided into four phases as shown below:

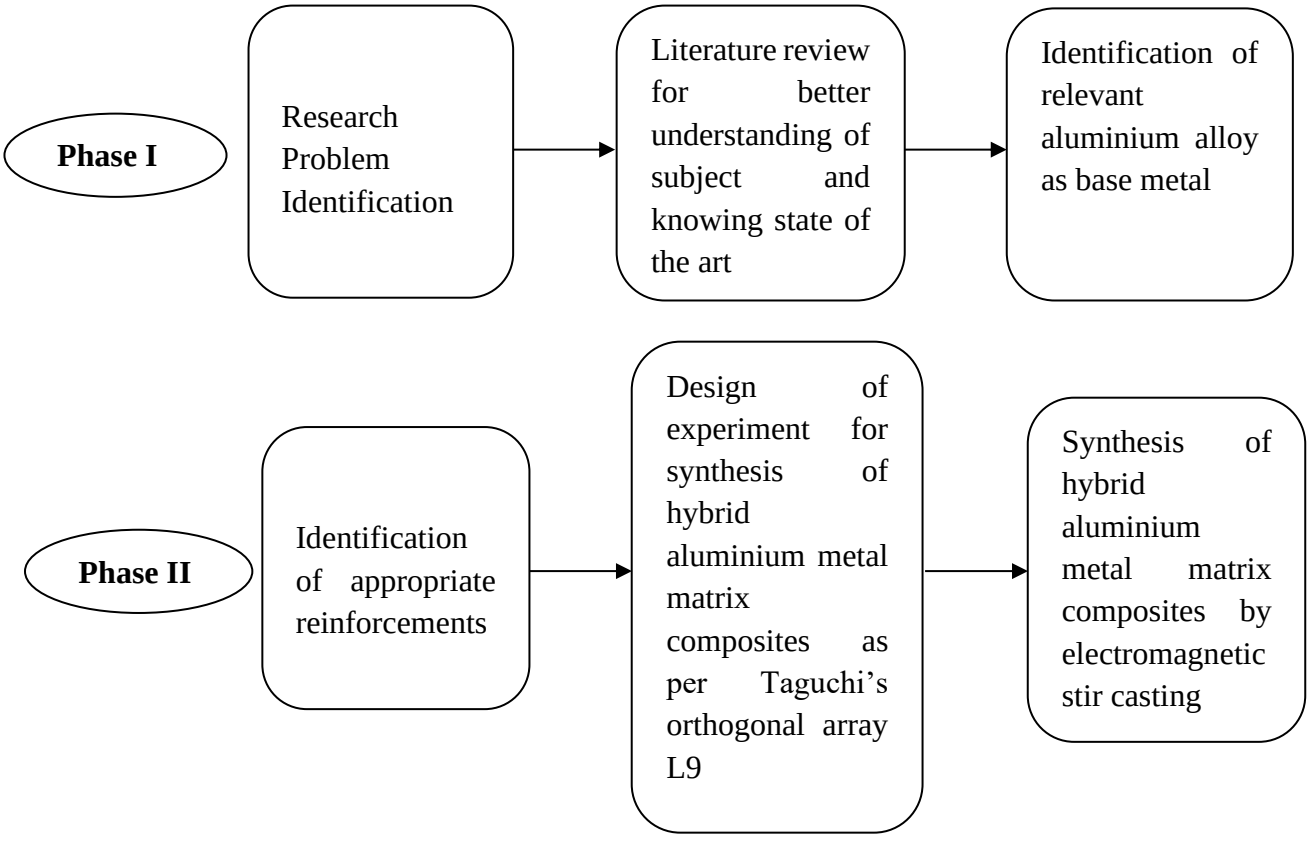

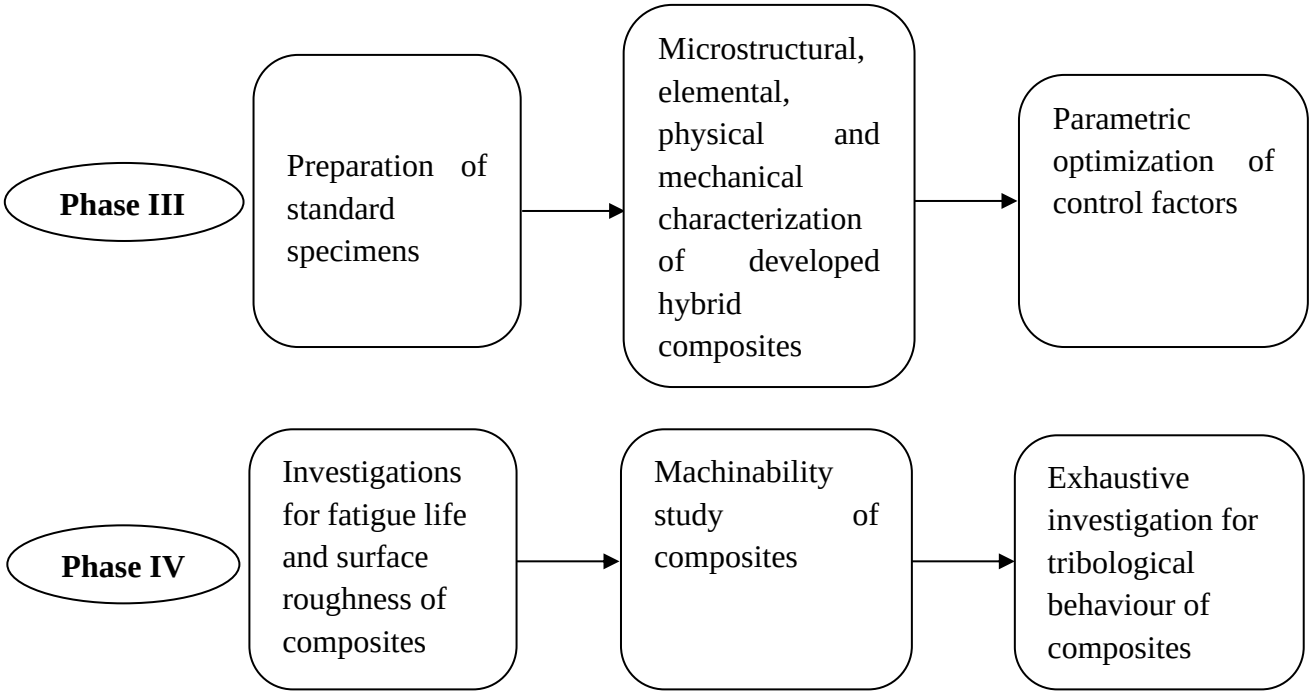

Summary of present chapter has been conferred in a nutshell in next section.

2.10 Summary

The present chapter discusses salient features of research work carried out by various researchers in recent years. Different phases and aspects related to the development of aluminium metal matrix composites have been discussed. Proposed design of experiment using Taguchi approach, selection of orthogonal array and estimation of signal to noise ratio have been discussed in next chapter.

CHAPTER 3

Design of Experiment

3.1 Introduction

For precise outcomes, the experimental investigation needs to be systematically planned and executed. Design of experiment is a scientific approach to discover empirical cause-effect relationship and to draw authentic interpretations about various parameters, based on the data collected from experimental studies. It is an essential approach for process and product optimization with less performance variations. By investigating influence of diversified components on quality characteristics, minimum performance variations through robust design can be assured in terms of improved product quality and process effectiveness [150].

This chapter presents detailed description of design of experiment through Taguchi approach, followed by estimation of signal to noise ratio. Design of experiment required for present experimental study, identification of prevalent process parameters and orthogonal array selection has been also covered in this chapter. The upcoming section deliberates design of experiment through Taguchi approach.

3.2 Taguchi Approach for Design of Experiment

Design of experiment implicates execution of planned experimental runs with all the pertinent variable process parameters which depend upon preliminary experimentation and systematic data. While carrying out a designed experiment, input variable (factors) can be altered, observing respective modifications in output variables (response). Advantages associated with design of experiment include collection of more data with lesser experimentation, more precise estimated responses and systemized estimation of cross talks between process factors. There are numerous experiment design techniques adopted by previous researchers such as randomized complete block design, fractional factorial, full factorial, Taguchi approach and response surface design etc.

Design of experiment as per Taguchi approach to obtain reproducible results and robust product is the most preferred technique due to a standardized method following a set of well-defined guidelines. This approach was developed primarily to explore the influence of different process parameters on mean and variance of performance characteristics to ensure the process functioning. It comprises of significant reduction in process alterations through robust design of experiments. Taguchi approach for design of experiment is capable of dealing with larger number of experiments following an explicit method for noise treatment where the consistency of performance is obtained by conducting trail experiments under the impact of different uncontrollable variables (noise factors) [151]. Taguchi methodology is formulated for identification of optimal factor combinations for given response and process optimization. It optimizes performance parameters by reducing the system performance sensitivity through the settings of process parameters.

A typical statistical design of experiment as per Taguchi methodology involves four main steps; (i) performance characteristics selection (ii) control factor identification (iii) control factor levels selection for each experimental run (iv) observing noise factors etc. as shown in Figure 3.1:

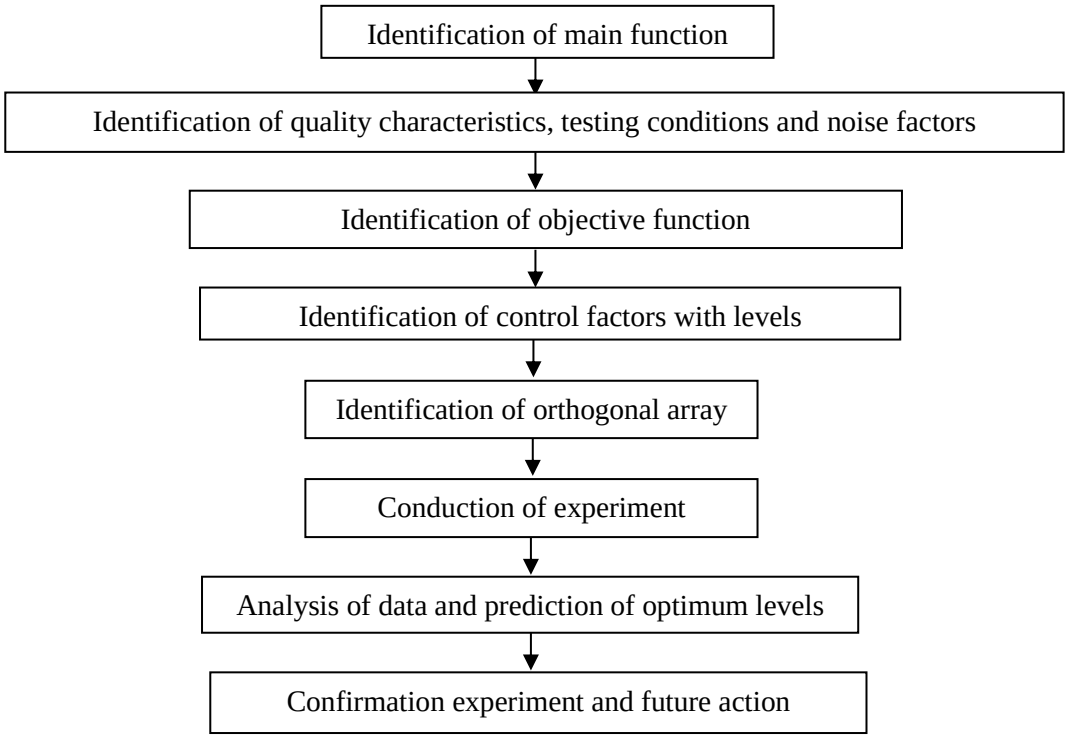

Fig. 3.1: Taguchi Methodology Steps

Here, basic knowledge about the system and process parameters is utilized for effective experimental investigations by omitting extra efforts for examining interactions and reducing the number of factors which influence the quality characteristics. The factors in Taguchi approach are categorized as follows:

(i) Control factors: These can be specified and controlled by the designer. These can be set at stated level during the process.

(ii) Noise factors: These cannot be controlled by the designer and their influences are not known. They cause deviations from specified signal factor values and result into loss of quality. To determine robust design for Taguchi's approach, experiments are deliberately performed under the effect of different noise factors.

Taguchi approach for design of experiment through robust design is a scheme to find the controllable parameters settings in order to prepare the process's functional characteristics, insensitive of the noise factors causing variability. Here the experimental investigation is systematically planned in order to obtain reliable information about variables involved by improving quality, defined as the consistency of performance. The two main targets of robust design are minimum variations in process parameters due to noise factors without eliminating them and to make the mean value near to the target value. Robust design can be obtained by optimizing the process to make it less sensitive to the variation cause (noise factors) through parameters design utilizing signal to noise ratio and orthogonal array. The design selected for controlled variables is called inner array and for noise factors is called outer array. Combination of the two arrays is known as cross array, which includes all the experiments to be conducted by Taguchi approach and provides information about parameters that are significant for robust system design [152].

Additionally, in Taguchi approach for robust design of experiment, additive model or main-factor cause-effect model is adopted, which avoids the interaction study and assumes that main influences of independent variables on performance characteristics are distinct, resulting into significant reduction in number of experimental runs. The additivity assumption suggests that, cross product effects do not exist among the main factors, whereas every factor can have linear or higher order effect on performance characteristic, which means distinct level settings of an

independent variable do not influence the outcome of any other independent variable on performance parameter. In case of violation of additivity assumption, the independent variables may interact. To deliver robustness in design of experiment, the control factors and signal factors can be handled depending upon the main factor effects on performance characteristic. The next section presents concept and philosophy of signal to noise ratio.

3.3 Signal to Noise (S/N) Ratio

Performance characteristic may also be characterized by using quality loss function, which is a continuous function demonstrating deviation of design parameters from target value. Quality loss function value as signal to noise ratio (S/N, where S stands for standard deviation of performance characteristic and N stands for total number of experiments) displays the effect of noise factors on performance characteristic.

Functional variations in performance characteristic are demonstrated by signal to noise ratio leading toward the estimation of control parameter settings, which are responsible for making the process unresponsive to the noise factors. Signal to noise ratio can be termed as mathematically defined form for performance characteristic, whose maximization minimizes the quality loss and improves additivity assumption control factor effect. Since S/ N ratio is inversely proportional to the variance, hence by maximizing the signal to noise ratio, process variability against inadmissible changes in noise factors can be diminished [153]. It represents the ratio of desired value (mean value of performance characteristic) and undesired value (deviation of performance characteristic) and is expressed as a logarithmic function, used in process optimization and variability minimization.

The signal to noise ratio characteristics are classified in three categories.

- **Smaller-the-better:** The performance characteristic is non-negative and continuous a target value of zero. It is chosen for undesirable characteristic to minimize the response and is expressed as:

  $$N = -10log_{10}[Mean\ of\ sum\ of\ squares\ of\ measured\ data\ ]$$

  $$N = -10log_{10}[\sum_{i=1}^{n}(x_i^2)/n] \quad (3.1)$$

- **Larger-the-better:** The performance characteristics to be continuous and non-negative. This is selected for desirable characteristics with value as large as possible in order to maximize the response and is expressed as:

  $N = -10log_{10}[Mean\ of\ sum\ squares\ of\ reciprocal\ of\ measured\ data]$

  $N = -10log_{10}[\sum_{i=1}^{n}(1/x_i^2)/n]$ (3.2)

- **Nominal-the-better:** This is considered when a specific value is desired and requires performance value to be as near as possible to the target value. Nominal-the-better S/N ratio is expressed as:

  $N = -10log_{10}\frac{Square\ of\ mean}{Variance}$

  $N = -10log_{10}\frac{\mu^2}{\sigma^2}$ (3.3)

Here, *N*: Signal to noise ratio in dB

n: Number of responses

x_i: Quality characteristic value for i^{th} experiment

μ: Mean

σ: Standard deviation.

The signal to noise ratio for every experimental response is estimated in a different way depending upon the type of quality characteristic and therefore irrespective of the category it correlates to a better quality characteristic. Evidently, design of experiment includes the identification and selection of independent variables that affect the investigation outcomes. After choosing the prevalent independent variables, their levels are finalized depending upon the influence of different level settings on performance characteristic. Number of level settings is estimated according to the relationship between performance parameter and independent variables followed by the analysis of experimental data for percentage contribution of independent variables and error calculations. Further the appropriate orthogonal array is selected in continuation with the finalization of least number of experimental runs to be carried out.

Design of experiments through orthogonal arrays is considered to be a potential method in comparison of other statistical designs. In Taguchi method, the minimum number of experimental investigations to be performed is determined

depending upon the degrees of freedom approach, as shown by the equation below [154]:

$$N_{Taguchi} = 1 + NV(L - 1) \quad (3.4)$$

Here, $N_{Taguchi}$: Number of experiments to be carried out

NV: Number of variables

L: Number of levels

In Taguchi approach, orthogonal arrays to coordinate the parameters influencing processes are involved, they reduce the number of experimental runs and provide concise guidelines for factor optimization. With the help of orthogonal arrays, we choose level combinations of input variables for each experimental run and designated number of experiments is conducted to attain complete information about prevalent control factors influencing the performance characteristics. Instead of verifying all feasible combinations as in factorial design approach, Taguchi method examines pairs of combinations. Hence, accumulation of essential data is possible to identify various factors majorly affecting the product quality with a specified extent of experimentation. Standard orthogonal arrays depending upon number of independent input variables and their levels recommend the minimum number of experimental runs to be performed.

These orthogonal arrays bear a balancing property, as in each vertical column under different input variables the level settings emerge for equal number of times. Also, the orthogonality of array is maintained by adhering to the unchanged sequence of levels for experimental runs. Order of independent variables in vertical column of the orthogonal array and associated level setting is extremely critical as the percentage contribution of each independent variable relates to the level assigned. After choosing orthogonal array, all the experiments are necessarily conducted according to the level combinations specified followed by observing the performance parameter value for each experimental run in order to conduct the sensitivity analysis [155].

The experimental observations are further analysed to establish optimal conditions for a process, to determine contribution of each independent variable and to estimate performance response under optimal conditions. In Taguchi design of experiment, the most important step involves segregation of respective influence of

each independent variable on performance characteristic value for each experiment, which has a specific sequence of different factor levels. Data analysis is done by adding the quality characteristic values for respective level settings. After calculating grand mean and mean value for every level of a certain independent variable, the calculation for sum of square of difference of every mean value from grand mean is conducted. The sum of square of deviation for a certain independent variable demonstrates the sensitivity of performance characteristic with variation in level setting.

The insignificant value of sum of square indicates that design variable does not influence the outcome considerably. The predominance and percentage contribution (calculated by ratio of each sum of square for a specific independent variable and total sum of square) of independent variables can be assessed by performing the sensitivity analysis and analysis of variance (ANOVA). By using ANOVA, observations of orthogonal array experiments in process design are analysed and variations in quality affecting factors are identified. A typical ANOVA consist of the following steps:

- Identification of sources of variation
- Computation of square sum for distributions of all experimental data
- Calculation of degrees of freedom
- Obtaining unbiased variance
- Calculation of variance ratio

Further, to establish the efficacy of additivity assumption for attempted optimization through Taguchi design of experiment and sensitivity analysis, a confirmation/ verification experiment is conducted with optimum values of all the considered independent variables, where the observed value of performance parameter is compared with the predicted value depending upon main-factor cause-effect model. The extent of closeness between observed and estimated values of performance characteristic establishes competence and reasonability of additivity assumption in Taguchi approach [156].

Taguchi method is broadly accepted, as it ensures that the process functions robust in presence of noise also. Taguchi robust design has emerged as time saving and user-friendly method which improves quality of a process by providing optimal

level settings for independent variables. Taguchi methodology accentuates the mean performance parameter value close to the target value rather than a value within specified limits. There are some disadvantages also associated with Taguchi approach such as the results obtained from Taguchi optimization are only relative; there is difficulty in addressing cross talks between independent variables and inability in handling dynamically changing processes [157]. The upcoming section explains design of experiment for present experimental investigation.

3.4 Design of Experiment Layout for Present Experimental Work

Taguchi method is based on predefined instructions and uses a set of arrays to designate a procedure for carrying out minimum number of experiments being able to provide complete information related to the performance parameters. In Taguchi approach, for an orthogonal experimental design the influence of control factors can be segregated in terms of mean response and signal to noise ratio [158].

In present experimental work, Taguchi approach was adopted for design of experiment including selection of orthogonal array and identification of control parameters to synthesize hybrid aluminium metal matrix composites along with estimation of signal to noise ratio for optimization of specific control factors. Mean objectives/response functions were analysed using data from designed experiments in order to calculate signal to noise ratio. Analysis of variance (ANOVA) was conducted to explore the influence of process parameters on specific performance characteristics in terms of F-ratio and percentage contribution. The selected prevalent process parameters for ongoing investigation were:

(i) Eggshell particles content (wt.%)
(ii) Silicon carbide partiales content (wt.%)
(iii) Aluminium oxide particles content (wt.%)
(iv) Mechanical stirring time in minutes

To realize the influence of control factors on considered performance characteristics such as percentage porosity, residual stress, microhardness, tensile strength, fatigue life and wear properties; three levels of all four control factors were considered (because they may affect the performance attributes nonlinearly), as shown in Table 3.1, in order to observe maximum potential variations and reduce

error. In most of the recent research studies, for significant enhancement in mechanical properties of aluminium composites, the total reinforcement content used was more than 15 wt.%. Present experimental investigation was conducted to develop cost efficient hybrid aluminium metal matrix composites with improved mechanical properties by using an effective combination of various reinforcements with minimal filler contents (lower wt.%) and appropriate mechanical stirring time range for reasonable stirring.

Table 3.1: Control Factors and their Levels

Control factors	**Factors Designation**	**Level 1 (Low)**	**Level 2 (Medium)**	**Level 3 (High)**
Eggshell weight %	A	0.5	1	1.5
SiC weight %	B	1	1.5	2
Al_2O_3 weight %	C	1.5	2	2.5
Mechanical stirring time (min)	D	2	4	6

In present study, 9 hybrid aluminium composites were synthesized by considering four prevalent control factors with three specified levels, in accordance with the design matrix using Taguchi L9 orthogonal array. The actual design of experiment layout with control factor level values (assuming that there is no cross-product effect between any two factors) and other process parameters with fixed values to conduct experimental study for synthesis of hybrid aluminium metal matrix composites is presented in Table 3.2. After synthesis, the hybrid composites specimens (in three replications) were evaluated for various physical and mechanical characteristics as described below:

(i) For percentage porosity measurement of specimens with respective signal to noise ratio for “smaller-the-better” type of performance characteristic
(ii) For residual stress, signal to noise ratio as “smaller-the-better” type of quality characteristic specimens
(iii) The microhardness of specimens with signal to noise ratio calculation for “larger-the-better” type of quality characteristic

(iv) To analyse tensile strength, signal to noise ratio as "larger-the-better" type of quality attribute

(v) For fatigue Life, with signal to noise ratio for "larger-the-better" type of quality characteristic

(vi) For wear loss, with signal to noise ratio for "larger-the-better" type of quality characteristic

Table 3.2: Design of Experiment Layout

Hybrid Composite Specimen Number (S1 to S9)	**Eggshell wt.%**	**Silicon Carbide wt.%**	**Aluminium Oxide wt.%**	**Mechanical Stirring Time (min)**
S1	0.5	1	1.5	2
S2	0.5	1.5	2	4
S3	0.5	2	2.5	6
S4	1	1	2	6
S5	1	1.5	2.5	2
S6	1	2	1.5	4
S7	1.5	1	2.5	4
S8	1.5	1.5	1.5	6
S9	1.5	2	2	2
S0	As-cast Al7075-T6 specimen (Base metal with no reinforcement)			
Mechanical stirring speed	150 rpm			
Stirring temperature	850^0 C			
Reinforcement preheat temperature	500^0 C			
Electromagnetic stirring speed	960 rpm			
Electromagnetic stirring time (minutes)	0.5 min			

Further, optimization of prevalent process parameters was conducted through ANOVA followed by computation of predicted mean of quality characteristics at optimal level of process parameters, confidence interval at 95% confidence level

and a confirmation experiment to observe the degree of agreement between observed and predicted value of performance parameter based on main-factor cause-effect model. The next section contributes to provide essence of present chapter.

3.5 Summary

Present chapter discusses Taguchi design of experiment for experimental investigation. Classifications and relevant calculations for Signal to Noise have been discussed. This chapter also includes discussions on suitability of various orthogonal arrays for robust design and analysis of variance for process parameter optimization. Here, four prevalent process variables along with three levels have been finalized in accordance with orthogonal array L9 for synthesis of composites. Detailed synthesis process of hybrid aluminium metal matrix composites as per design of experiment will be presented in next chapter.

CHAPTER 4

Synthesis and Microstructural Characterization of Hybrid Aluminium Composites

4.1 Introduction

Hybrid aluminium composites are being developed keeping in view the reasonable enhancement in their properties by exploiting different virtues of various reinforcements without any noticeable deterioration in composite attributes. They behave in a balanced manner between the advantages and disadvantages of different reinforcements and demonstrate enhanced mechanical characteristics caused due to reduced meniscus penetration defect and decreased interfacial area. This chapter deliberates synthesis of hybrid aluminium composites, elemental composition analysis and microstructural investigation of base metal, reinforcements and synthesized composites.

The present experimental investigation has been carried out to synthesize hybrid aluminium metal matrix composites (in accordance with Taguchi orthogonal array L9) with three reinforcements in minimal amount through electromagnetic stir casting: an uncommon fabrication technique. Al7075-T6 alloy was infused with three reinforcements; (i) eggshell particles (wt.% 0.5, 1 and 1.5) (ii) silicon carbide particles (wt.% 1, 1.5 and 2) and (iii) aluminium oxide particles (wt.% 1.5, 2 and 2.5) with variable mechanical stirring time (2, 4 and 6 minutes), as shown in Table 4.1. Relevant ceramic particulate reinforcements have been utilized to upgrade desired composite characteristics such as hardness, strength, fatigue and wear resistance. These eco-designed hybrid aluminium composites have been fabricated using eggshell waste (a severe environmental jeopardy) as one of the reinforcements and the maximum total reinforcement content was fixed only upto 5.5wt.%, producing hybrid aluminium composites with reasonable cost. The experimental investigation plan is shown in Figure 4.1, whereas crucial aspects such as selection of base material, reinforcement materials, composite synthesis, standard specimen fabrication and microstructural investigations are discoursed in detail in following sections.

Table 4.1: Specimen Details

Specimen Number	Eggshell wt.%	Silicon Carbide wt.%	Aluminium Oxide wt.%	Mechanical Stirring Time (min)
S0	As-cast Al7075-T6 (Base metal with no reinforcement)			
S1	0.5	1	1.5	2
S2	0.5	1.5	2	4
S3	0.5	2	2.5	6
S4	1	1	2	6
S5	1	1.5	2.5	2
S6	1	2	1.5	4
S7	1.5	1	2.5	4
S8	1.5	1.5	1.5	6
S9	1.5	2	2	2

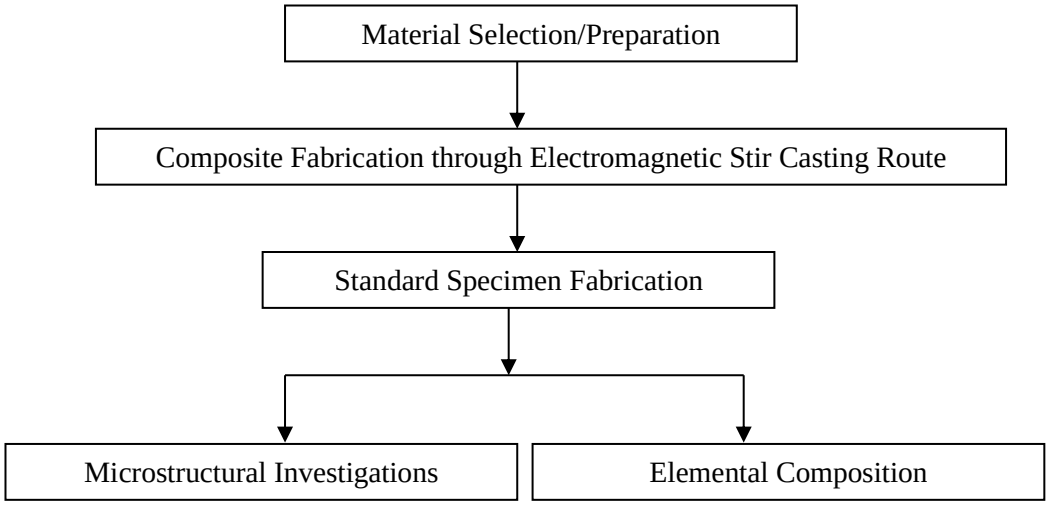

Figure 4.1: Investigation Plan

4.2 Materials

Matrix material and reinforcement materials used for present experimental investigation are discussed in forthcoming sub-sections.

4.2.1 Base Material

Previous series of aluminium alloys have already been explored extensively for numerous experimental investigations. The metal matrix used for present study was Al7075-T6 alloy due to low density, compatibility with reinforcement

materials, thermal Stability and economic efficiency. Chemical compositions of Al7075-T6 alloy is given in Table 4.2.

Table 4.2: Composition of Al7075-T6 [159]

Sl. No.	Component	Weight %	Sl. No.	Component	Weight %
1.	Al	87-91	6.	Mn	>0.3
2.	Cr	0.18-0.28	7.	Si	>0.4
3.	Cu	1.2-2	8.	Ti	>0.2
4.	Fe	>0.5	9.	Zn	6
5.	Mg	2.1-2.9	10.	Others	Balance

Chemical compositions of various materials used in present experiment were demonstrated through energy dispersive spectroscopy (EDS) conducted by X-ray diffractometer (make: Rigaku Japan, model- Miniflex-II) and field emission scanning electron microscope as displayed in Figures 4.2 and 4.4. In X-ray diffraction (XRD), the atomic planes of a material caused an incident beam of X-rays to interfere with one another as they left the crystal. This analysis depended on X-rays and crystalline sample's constructive interference, satisfying Bragg's law. A cathode ray tube produced X-rays, which after filtration generated collimated monochromatic radiation directed towards specimen. A constructive interference was originated, depending upon interaction of specimen and incident X-ray. By scanning the sample for diffraction angle 2Ɵ range, feasible diffraction directions of the lattice were obtained. Further, the diffraction peaks were converted to d-spacings and identified the compound [160].

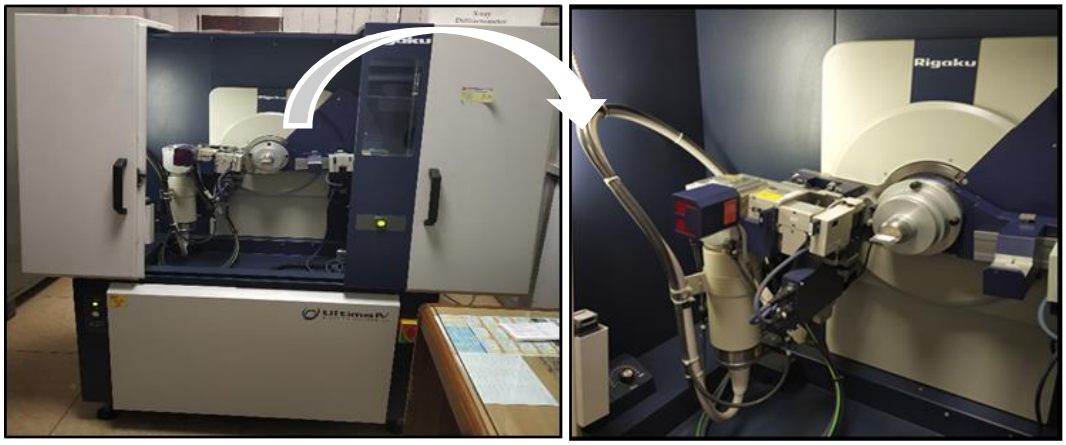

Figure 4.2: X-Ray Diffractometer

The XRD spectrogram of as-cast Al7075-T6 as shown in Figure 4.3 demonstrated diffraction peaks for its chemical constituents at diffraction angle $2\Theta \approx 36.9^0$, 38.33^0, 42.90^0, 44.58^0, 64.91^0 and 69.32^0 whereas diffraction peaks corresponding to impurities present in base metal were not observed in the XRD pattern. However, energy dispersive spectroscopy (EDS) is a technique used to analyse the elemental composition of a sample. It investigated interaction between the sample and X-ray excitation source, when the sample was bombarded by electron beam. Electrons were ejected from the sample surface and created electron vacancies. These electron vacancies were further occupied the high energy state electrons, emitting an x-ray, which balanced the energy difference between two energy states. This emitted X-ray energies were the characteristic of different elements present in the sample [160]. Various set of peaks corresponding to electromagnetic emission spectrum for major constituent elements of as-cast Al-7075-T6 (aluminium, magnesium and zinc) were observed in EDS spectrograms, as shown in Figure 4.3. EDS spot analysis displayed that base metal matrix contained aluminium as a dominant component whereas mg and Zn were present in smaller amounts, as per element concentrations given in Table 4.3.

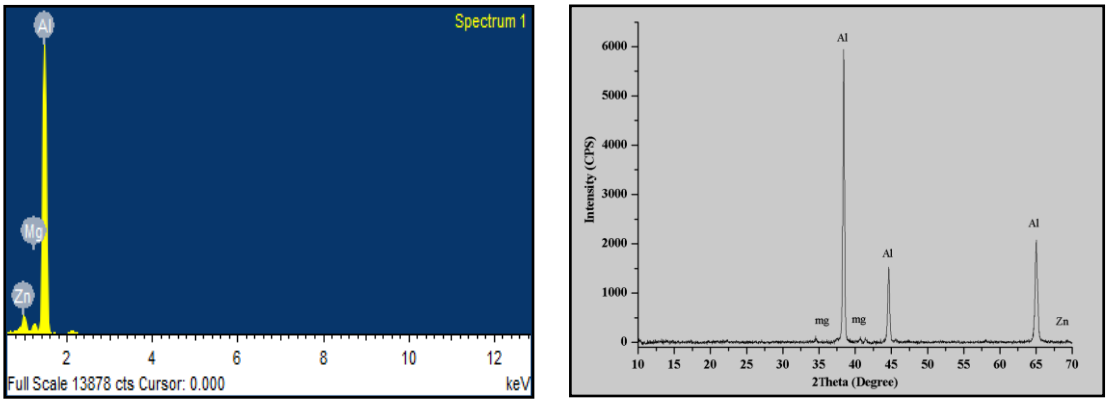

Figure 4.3: Elemental composition of as-cast Al7075-T6 (Specimen S0)

Table 4.3: Elemental Concentrations in as-cast Al7075-T6 as per EDS analysis

Element	**Weight %**	**Atomic %**
Mg	2.33	2.68
Al	89.72	93.73
Zn	6.55	2.80
Others	1.4	0.79
Total	100	

The optical micrographs for microstructural studies of distinct specimens were obtained by using scanning electron microscope (make: OXFORD Instruments, model: 7718) and field emission scanning electron microscope (make: Zeiss, model: Supra 40 VP) as shown in Figure 4.4. In scanning electron microscope (SEM), the sample was bombarded with a high energy electron beam emerging from a thermionic source. Thermionic sources had certain limitations such as low brightness, cathode material evaporation and thermal drift during operation. To surmount these constraints, field emission method of electron generation was adopted. In field emission scanning electron microscopes, the source was placed in huge electrical potential gradient to produce electron beam. These primary electrons of electron beam interacted with specimen in a specimen chamber and provided energy to the atomic electrons of specimen. These electrons were released as secondary electrons from the specimen and created image, depending upon the receiving of signals generated from the electron beam and specimen interaction. SEM essentially operated in vacuum to prevent interactions of electrons with gas molecules to achieve high resolution [161].

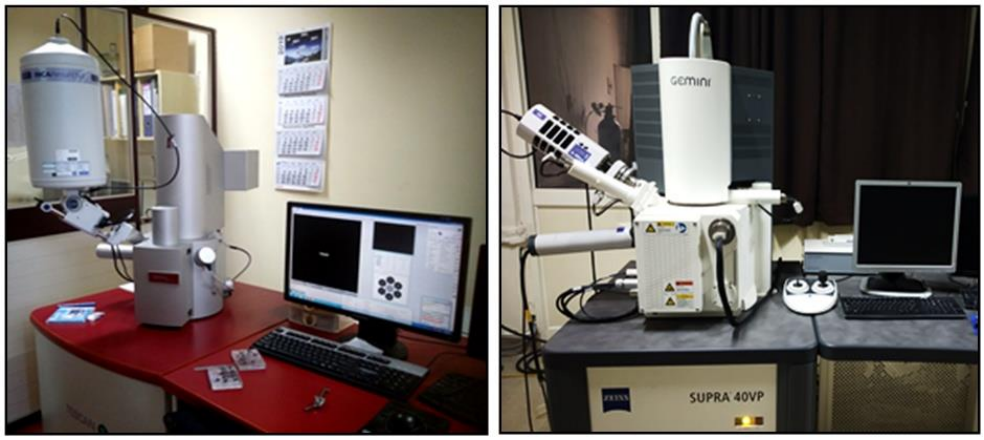

Figure 4.4: Scanning Electron Microscope and Field Emission Scanning Electron Microscope

The surface morphology and grain structure of as-cast Al7075-T6 (specimen S0) at 500X magnification are shown in Figure 4.5.

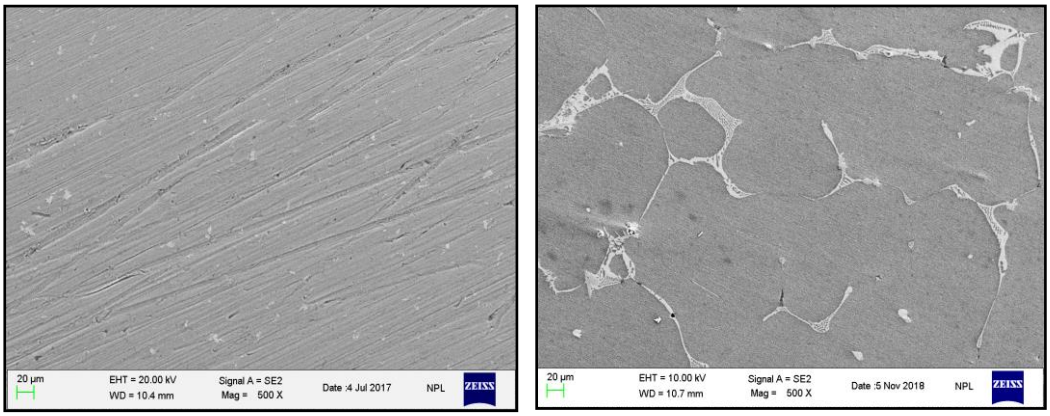

Figure 4.5: Microstructure of as-cast Al7075-T6 (Specimen S0)

4.2.2 Reinforcement Materials

Reinforcement materials are the hard fillers infused into base metal matrix for significant enhancement of composite attributes (both extrinsic and intrinsic) in terms of strength, toughness, stiffness, wear resistance and cost effectiveness. Each reinforcement used for present investigation had specific characteristics, thus when mixed with molten metal, they contributed towards enhancement of distinct properties of synthesized composites as compared to the unreinforced metal.

In present experimental investigation, hybrid aluminium metal matrix composites were prepared by infusing three fillers (eggshell, silicon carbide and aluminium oxide particles) to tailor the characteristics of synthesized composites as per the desired applications. The reinforcement specifications are explained below:

- Disposal of certain natural waste matter such as eggshells is extremely harmful for our environment, hence after recycling; these can be used as natural reinforcements to develop composites. Eggshell powder was prepared by following the procedure given below, using ball mill and muffle furnace as shown in Figures 4.6 and 4.7:

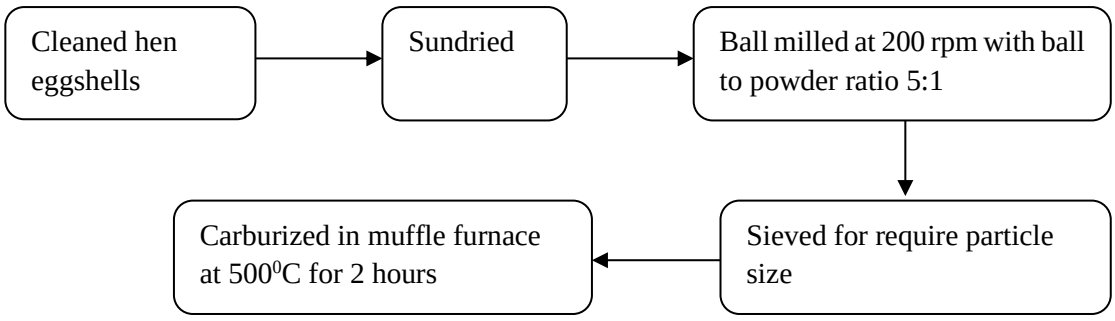

Figure 4.6: Ball Mill used for Preparation of Eggshell Powder

Figure 4.7: Muffle Furnace and Carburized Eggshell Powder

Density: 2.15 g/cc

Mesh Size: 230 mesh (Average particle size ≈ 60 microns)

- Silicon carbide (SiC), Commercially available

Make: CDH

Density: 3.21 g/cc

Mesh Size: 220 mesh (Average particle size ≈ 65 microns)

- α Aluminium oxide (Al_2O_3), Commercially available

Make: CDH

pH value: 6.5-7.5

Density: 3.95 g/cc

Mesh Size: 100-300 mesh (Average particle size ≈ 90 microns)

Optical micrographs, EDS spectra and XRD plots of reinforcement materials displaying their microstructures and elemental compositions are shown in Figures 4.8, 4.9 and 4.10. Reinforcement particle sizes were determined by SEM

micrographs obtained at 200X magnification. Average particle sizes observed were; eggshell particles ≈60 μm, silicon carbide particles ≈65 μm and aluminium oxide particles ≈90 μm. Very small sized reinforcement particles cause agglomeration and weak interfacial bonding, reducing the material strength whereas very large reinforcement particles degrade mechanical characteristics due to less dense dislocations of reinforcements. Hence moderate and comparable sizes of reinforcement particles was preferred for present experimental study in order to avoid agglomeration and obtain their uniform dispersion in metal matrix.

From EDS spectra, elemental composition of eggshell particles demonstrated presence of calcium (39.52 wt.%), oxygen (51.25 wt.%) and carbon (9.23 wt.%). Silicon carbide particles were comprised with silicon (75.84 wt.%) and carbon (24.16 wt.%). Aluminium oxide particles were constituted by aluminium (53.75 wt.%) and oxygen (46.25 wt.%).

XRD intensity data for reinforcement materials were taken for diffraction angle 2Θ range of 10-100^0.

- For eggshell particles, the diffraction peaks were observed at diffraction angle 2Θ≈23.58^0, 30^0, 37.76^0, 40^0, 44.89^0 and 50^0
- For silicon carbide particles the intensity peaks occurred at diffraction angle 2Θ≈38.52^0, 41.96^0, 60^0 and 73.84^0.
- X-ray diffraction spectrogram of aluminium oxide particles displayed distinctive peaks at diffraction angle 2Θ≈25.9^0, 35.41^0, 37^0, 44.25^0, 52.72^0, 57^0, 68.78^0 and 77^0.

Detailed procedure for composite synthesis has been described in forthcoming section.

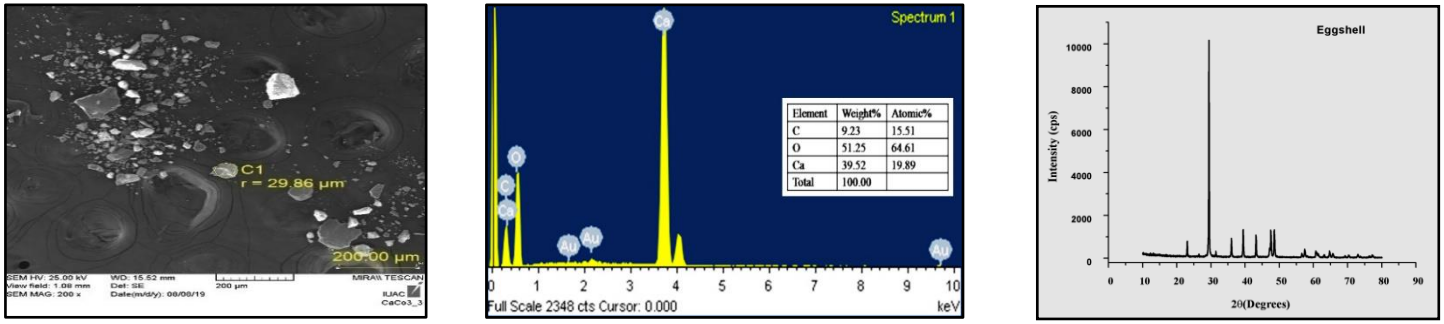

Figure 4.8: Particle Size and Elemental Composition of Eggshell Powder

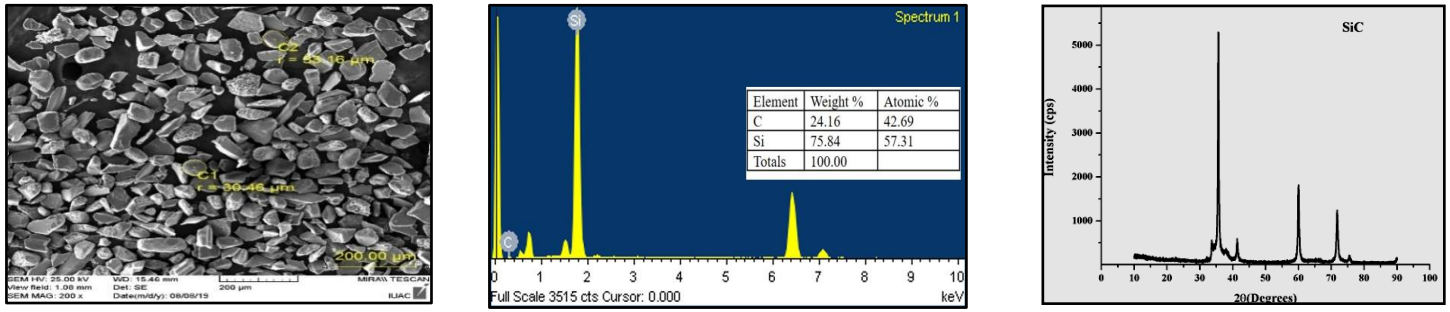

Figure 4.9: Particle Size and Elemental Composition of Silicon Carbide Powder

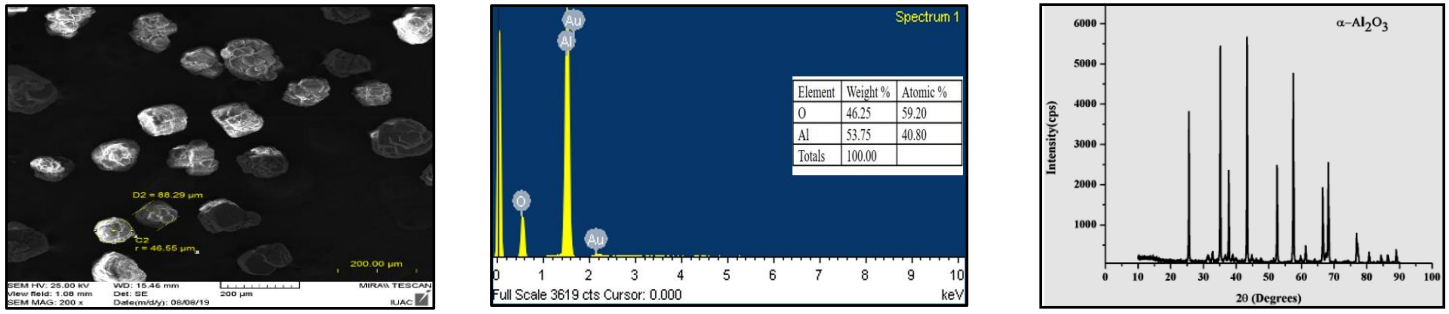

Figure 4.10: Particle Size and Elemental Composition of Aluminium Oxide Powder

4.3 Composite Synthesis

Synthesized hybrid aluminium composites with enhanced attributes may have enormous application scope. These applications include high strength structural applications, thermally modifiable and light weight aerospace applications, automotive applications due to better tribological and fatigue properties, electronics applications due to higher specific strength for power electronics & packaging materials and numerous defence applications due to low density, dimensional stability at higher temperatures, high heat capacity and high thermal conductivity.

Among various fabrication techniques for development of particulate reinforced aluminium metal matrix composites, stir casting is contemplated to be the most advantageous due to its cost effectiveness, ability to handle large volume, simplicity and capacity to control metal matrix structure. In stir casting process, composites are produced by continuous stirring of base metal melt followed by infusion of reinforcements. Desired particulate reinforcements with reasonable wettability are incorporated into molten aluminium matrix followed by solidification of the mixture. Composites developed by stir casting technique demonstrate modifiable properties depending upon distinct process parameters like reinforcement content, stirring temperature, stirring time, reinforcement preheat temperature, stirring speed and stirrer position etc. [162].

In this research work, nine hybrid aluminium composites were fabricated using Al7075-T6 as metal matrix, infused with variable weight percentage of three reinforcements (eggshell particles weight percentage 0.5%, 1%, 1.5%, average particle size ≈60 µm, SiC particles weight percentage 1%, 1.5% and 2%, average particle size ≈65 µm and Al_2O_3 particles weight percentage 1.5%, 2% and 2.5%, average particle size ≈90 µm) with varied mechanical stirring time (2 min, 4 min and 6 min) in accordance with the design matrix using Taguchi L9 orthogonal array as discussed in chapter three. Taguchi L9 orthogonal array was adopted for present experiment, as it was conducted to estimate the effect of four independent factors (eggshell particles wt.%, SiC particles wt.%, Al_2O_3 particles wt.% and mechanical stirring time) with three different factor level values assuming that there is no cross product effect between any two factors. To

synthesis composites, weighed Al7075-T6 ingots were cleaned and melted in a customized graphite crucible in the electric furnace of conventional stir casting setup (consisted of a furnace, stirrer impeller rotating at 150 rpm, temperature sensors and control panel, as shown in Figure 4.11) at 900^0 C.

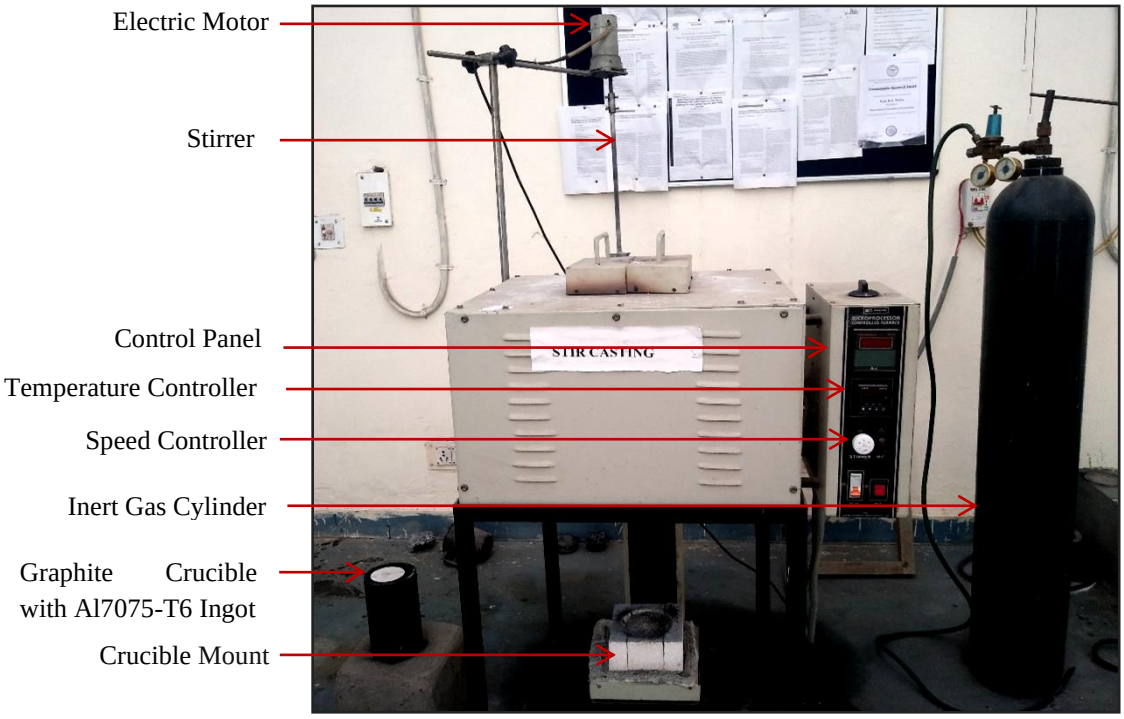

Figure 4.11: Mechanical Stir Casting Setup

Meanwhile required amounts of various reinforcements were weighed and wrapped in aluminium foil and preheated in a muffle furnace (as shown in Figure 4.12) up to 500^0 C for one hour in order to remove absorbed gases from reinforcement's surface, avoid temperature drop on infusion of reinforcement particles into molten metal and obtain improved wettability. The temperature of metal melt was slightly reduced, and reinforcements were added in three steps to avoid agglomeration and attain uniform dispersion of reinforcements into molten metal. In order to enhance mechanical attributes of developed hybrid composites and avert agglomeration, hard particles of comparable sizes were used as reinforcements in present experimental investigation. The preheated stirrer of conventional stir casting setup was used to stir the mixture (Figure 4.13) in inert atmosphere at 150 rpm for variable time intervals as per the design of experiment. Stirring process was carried out in presence of inert gas (Ar) to avoid any kind of

contamination due to presence of air molecules, which may deteriorate the physical and mechanical characteristics of synthesized composites. Additionally, the supply of inert gas flushes out trapped air within the molten mixture reducing porosity and solidification defects.

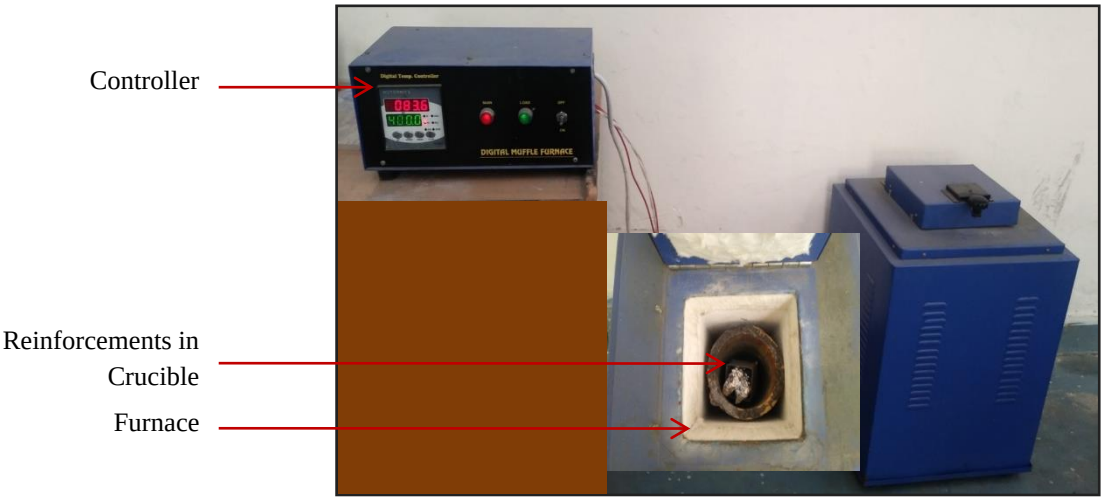

Figure 4.12: Muffle Furnace for Reinforcement Preheating

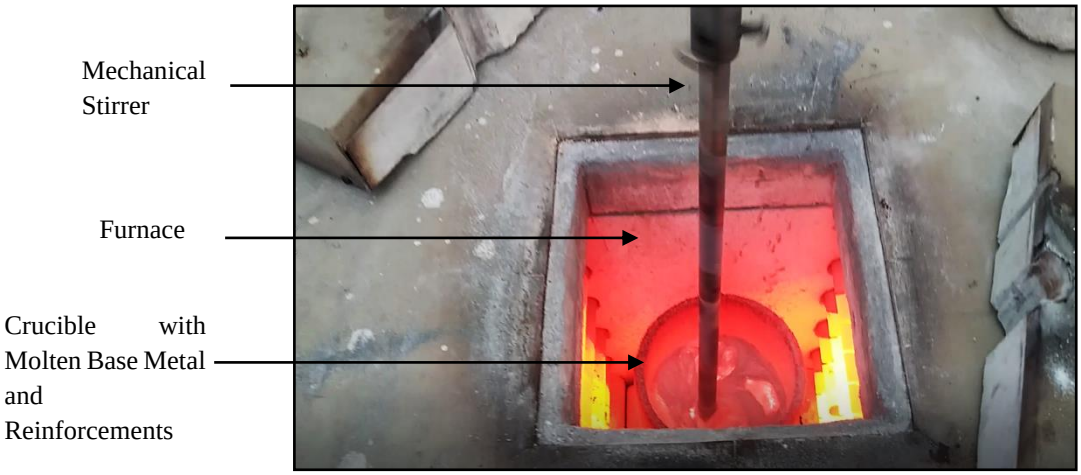

Figure 4.13: Stirring in Conventional Stir Casting Setup

Fundamental complications experienced during stir casting were improper wetting due to poor interfacial bonding between reinforcement and matrix material and non-uniform dispersion of reinforcement particles due to agglomeration. To improve interfacial bonding of filler and metal matrix, various surface treatments have been performed by past researchers, including ultrasonic cavitation effect and inclusion of nanostructures into composites. For enhanced wettability, either

alloying elements were added to molten metal matrix or coating of reinforcements was carried out [163].

Even with such critical corrective actions, in stir casting process the reinforcement particles get repelled away from the mechanical stirrer because of the centrifugal force of rotating melt, resulting into non uniform dispersion. To overcome this complication, in present study, modifications were implemented to existing mechanical stir casting setup in form of electromagnetic stirrer as shown in Figure 4.14. After mechanical stirring, the crucible containing molten metal and reinforcement materials was placed on glass wool insulated electromagnetic stirrer. An electromagnetic stirrer originally was an electric motor, which used a rotating magnetic field causing a whirling motion in molten metal. When a three phase AC voltage was applied to the motor, its magnetic coil generated a moving magnetic field and electromagnetic force was developed in the metal melt causing its stirring [164].

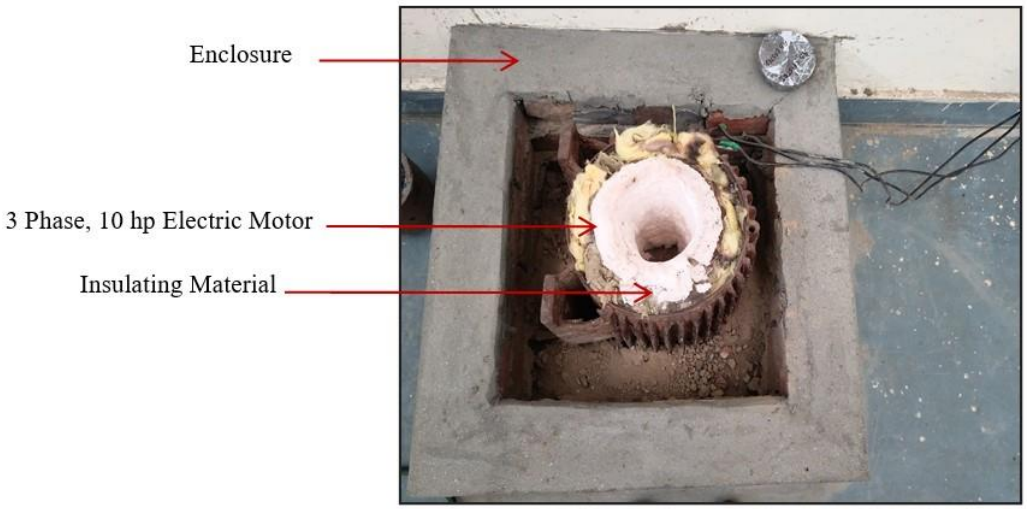

Figure 4.14: Electromagnetic Stirrer

The rotational speed of electromagnetic stirrer with 6 poles and 18 coils used in present experiment was evaluated as:

$$RPM = \frac{120 \times Frequency}{Number\ of\ poles} = \frac{120 \times 50}{6} = 1000 \quad (4.1)$$

The electromagnetic stirrer ideally had a rotational speed of 1000 rpm but due to eddy current and heating losses the speed was reduced to 960 rpm. Base metal and reinforcement mixture in crucible was stirred by electromagnetic stirrer rotating at 960 rpm for 30 seconds as shown in Figure 4.15.

Figure 4.15: Stirring in Electromagnetic Stirrer

The composite castings (Figure 4.16) were allowed to solidify and various test standard specimens were processed for mechanical testing. In order to evaluate mechanical and physical characteristics of composites, ten specimens (one as-cast Al7075-T6 and nine Al7075-T6/ egg shell/ SiC/ Al_2O_3 hybrid composites) in three replications, for each characterization were prepared using wire cut EDM (electric discharge machining) machine, as shown in Figure 4.17.

Figure 4.16: Solid Castings (One as-cast Al7075-T6 and Nine Hybrid Composites)

In electric discharge machining, material was removed precisely from a conducting material with the help of an electrode, which controlled the electric spark for material erosion. Electrode and workpiece were not in contact and the spark gap between them increased as electrode moved closer to the workpiece. The

discharge that occurred in a small gap between electrode and workpiece, heated the workpiece material, melting away small amounts. In electric discharge machining, the electrode and workpiece were submerged in a dielectric fluid, which removed this extra material, worked as coolant and controlled the spark.

Figure 4.17: Wire Cut EDM for Standard Specimen Fabrication

For micro hardness (at constant load, loading time, creep time and load release time), density (specimens weighed in air and distilled water), porosity (from experimental and theoretical densities) and residual stress measurement (at fixed pitch, X-ray incident angle and X-ray irradiation time) specimen palates (conventionally polished up to Ra $\simeq$ 0.1 µm) of size 10×10×5 mm^3 were prepared as demonstrated in Figure 4.18.

For tensile strength evaluation (at constant strain rate and crosshead speed) the sub-size dog bone plate type specimens were prepared as per ASTM E8-M11, as shown in Figure 4.19. To examine low cycle fatigue life (at constant load and constant speed) and surface roughness, standard specimens were fabricated in accordance with ASTM E 468/606, as shown in Figure 4.20. Standard pin test specimens as per ASTM G99-17 and EN 31 disk were prepared for tribological characterization (at constant load, sliding distance, sliding speed and wear track diameter), as displayed in Figure 4.21, whereas machinability study specimens are shown in Figure 4.22.

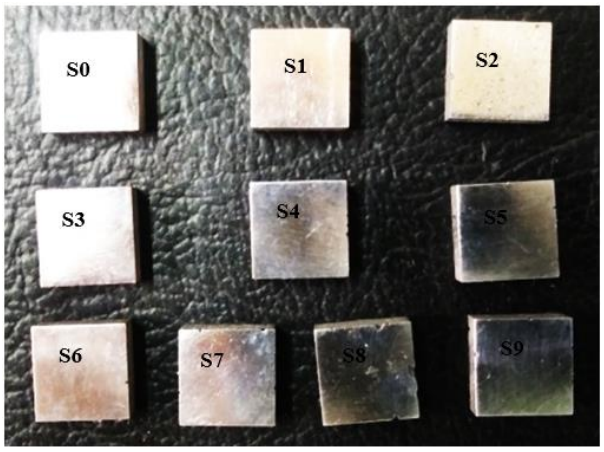

Figure 4.18: Specimens for Density, Porosity, Microhardness and Residual Stress Measurements

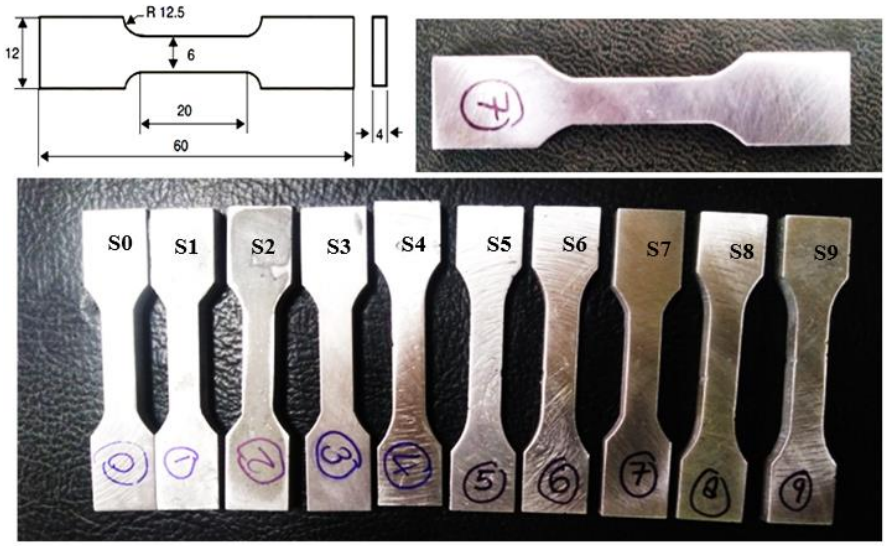

Figure 4.19: Standard Specimens for Tensile Strength Testing (All dimensions are in mm)

Figure 4.20: Standard Specimens for Fatigue Life Testing

Figure 4.21: Standard Wear Test Specimens as per ASTM G99-17 and EN 31 Disk

Figure 4.22: Machinability Study Specimens

Standard test specimens of as-cast Al7075-T6 and hybrid aluminium metal matrix composites were assessed for mechanical, physical and microstructural investigations. Details of microstructural characterization and elemental composition of composites are presented in next section.

4.4 Microstructural Characterization of Composites

Scanning electron microscopy evaluated the reinforcement/matrix interface, elemental composition, and refinement of grains in composites. This section elucidates the correlation between processing parameter variations and microstructures of developed composites. The field emission scanning electron microscope (FESEM) Zeiss Supra 40VP (with maximum acceleration voltage of 30 kV and software SmartSEM) was used for microstructural characterization of the specimens. Zeiss Supra 40VP FESEM is a high-performance field emission scanning electron microscope combined with EDS system. It provided high

resolution surface imaging with three-dimensional display, with maximum resolution of 1 nm and magnification range of 12X to 9, 00,000X.

Specimens were metallographically polished using emery cloths of grit sizes 220 and 320 followed by buffing on leather buffing wheel using alumina paste to attain average roughness value Ra $\simeq$ 0.1 μm. The optical micrograph of base alloy (shown in Figure 4.3) displayed uniform fine grain sizes, whereas in composites micrographs as shown in Figures 4.23 to 4.27, occurrence of some uneven grains may be associated with infusion of reinforcement particles. The microstructures of hybrid composites exhibited significantly finer grain structure, because of the occurrence of heterogeneous nucleation due to reinforcement addition into base metal. In particulate reinforced composites, grains grew finer as the recrystallization by particle stimulated nucleation dominated during thermomechanical processing. The microscopic particles may have demonstrated some alloying elements of base metal. Uniform dispersion of reinforcement particles without any segregation, was observed in composite micrographs, establishing superior characteristics such as enhanced hardness and strength. The progressive precipitation process may also have contributed significantly in hardness augmentation. Uniformly distributed reinforcement particles, impeded dislocation mobility in matrix material, hence increasing hardness of synthesized composites. In some of the hybrid aluminium metal matrix composites, reduced ductility may have been observed due to stress concentrations in reinforcement particles and advance initiation of void nucleation with reinforcement addition to metal matrix.

Few dendrite structures in specimens S3, S6 and S8 were observed, justifying presence of reinforcement particles during solidification. In SEM micrographs, fine composite microstructures represented rationally acceptable interfacial bonding between metal matrix and reinforcement phases. Synthesized composite micrographs exhibited some traces of porosity and detrimental pores due to various process induced effects such as gas trapped in metal melt during mixing, shrinkage due to composites solidification, presence of moisture on reinforcement particles surfaces, evolution of hydrogen and inappropriate casting parameters during fabrication creating isolated areas in composites which get

solidify at last and generate voids. However, lower porosity was observed in synthesized hybrid aluminium metal matrix composite castings in comparison of the unreinforced base metal casting due to inconsequential agglomeration and uniform distribution of reinforcement particles into aluminium matrix. It has been realized that with increased reinforcement content, uniform reinforcement dispersion and negligible porosity was present in composites. Reduction in shrinkage cavities and enhanced packing densities of composites may be attributed to adequate stirring of the molten mixture, accelerated solidification of composite castings and higher reinforcement content infusion to matrix material.

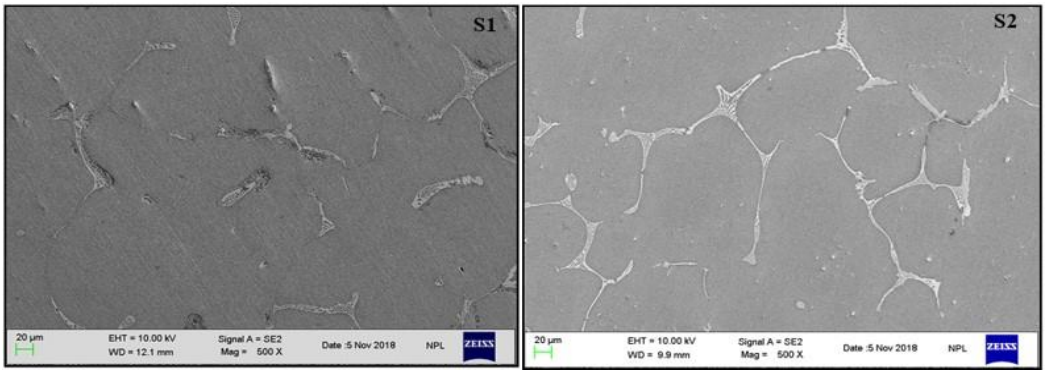

Figure 4.23: Microstructures of Specimens S1 (Al-7075-T6/0.5 wt.% eggshell/1 wt.% SiC/1.5 wt.% Al_2O_3) and S2 (Al-7075-T6/0.5 wt.% eggshell/1.5 wt.% SiC/2 wt.% Al_2O_3)

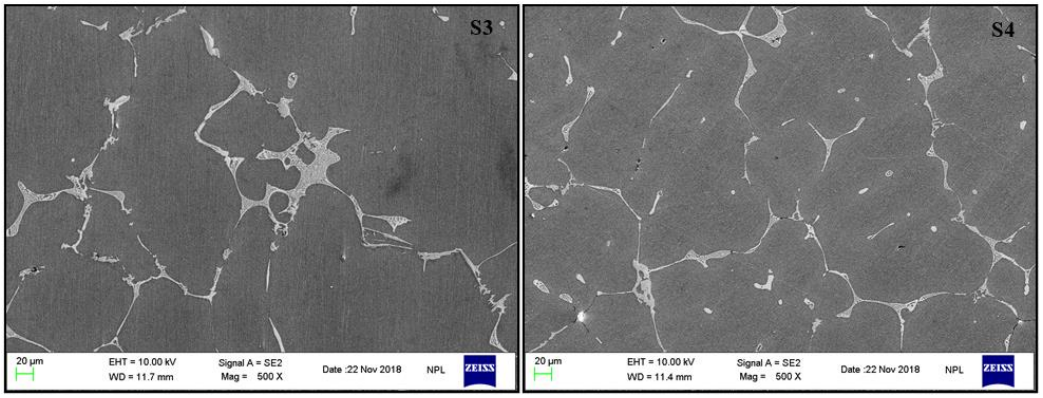

Figure 4.24: Microstructures of Specimens S3 (Al-7075-T6/0.5 wt.% eggshell/2 wt.% SiC/2.5 wt.% Al_2O_3) and S4 (Al-7075-T6/1 wt.% eggshell/1 wt.% SiC/2 wt.% Al_2O_3)

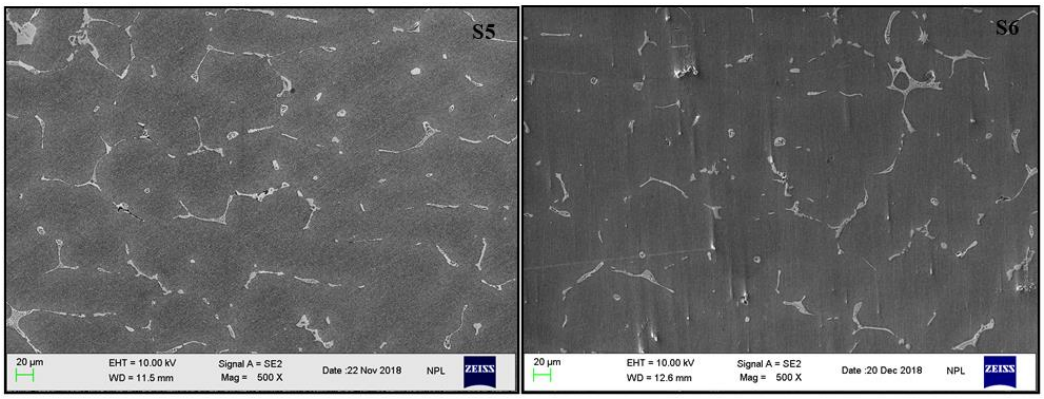

Figure 4.25: Microstructures of Specimens S5 (Al-7075-T6/1 wt.% eggshell/1 wt.% SiC/2.5 wt.% Al_2O_3) and S6 (Al-7075-T6/1 wt.% eggshell/2 wt.% SiC/1.5 wt.% Al_2O_3)

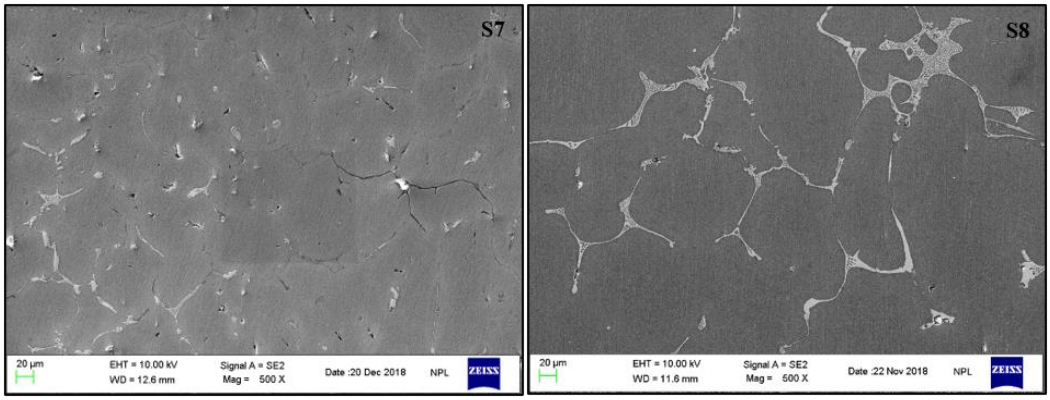

Figure 4.26: Microstructures of Specimens S7 (Al-7075-T6/1.5 wt.% eggshell/1 wt.% SiC/2.5 wt.% Al_2O_3) and S8 (Al-7075-T6/1.5 wt.% eggshell/1.5 wt.% SiC/1.5 wt.% Al_2O_3)

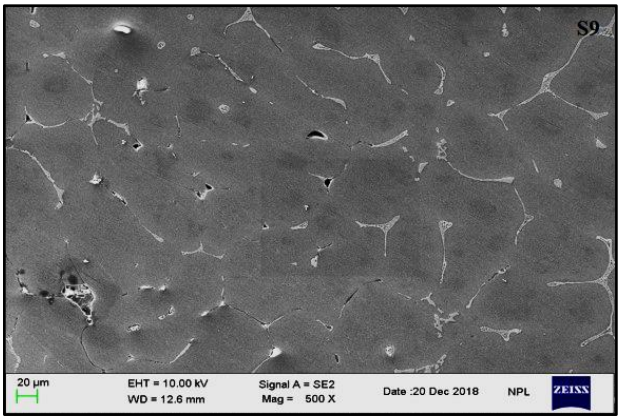

Figure 4.27: Microstructure of Specimen S9 (Al-7075-T6/1.5 wt.% eggshell/2 wt.% SiC/2 wt.% Al_2O_3)

Besides SEM, the energy-dispersive spectroscopy (EDS) technique was also used to carry out area wise qualitative elemental analysis for as-cast Al7057-T6 specimen (as shown in Figure 4.5) and hybrid composite specimens with varying reinforcement content as shown in Figures 4.28 to 4.36. Presence of

noticeable amounts of reinforcement materials, eggshell (as Ca, C and O), silicon carbide (as Si and C) and aluminium oxide (as Al and O) in synthesized hybrid composites was confirmed from X-ray emission spectrum peaks due to their distinctive atomic structures. In EDS graphs of composites, highest pinnacles as characteristics peaks of unique energy confirmed the presence of aluminium as base metal (in largest amount) whereas the low peaks affirmed the existence of additional alloying elements and reinforcements such as magnesium, zinc, silicon, calcium, oxygen and carbon.

During elemental characterization of fabricated hybrid aluminium composites through EDS, the normalized concentrations of various elements were revealed in EDS spectrums in tabular form. An observable difference was noticed in the relative concentrations of various elements, depending upon infused reinforcement contents in different hybrid aluminium metal matrix composites. Oxygen and carbon existing as individual components in EDS graphs, may have majorly been escaped due to decomposition of eggshell, silicon carbide and aluminium oxide during mixing. Presence of voids in solidified castings may also be attributed to the evolution of liberated oxygen from surface. Occurrence of identical components during elemental analysis of produced hybrid aluminium composites discloses degree of perfection in the fabrication route.

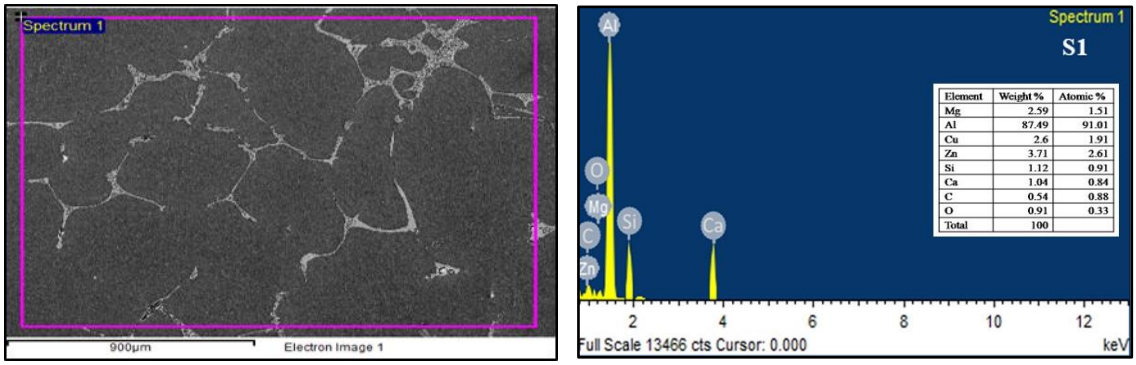

Figure 4.28: EDS Spectrum of Specimen S1 (Al-7075-T6/ 0.5 wt.% eggshell/1 wt.% SiC/1.5 wt.% Al_2O_3)

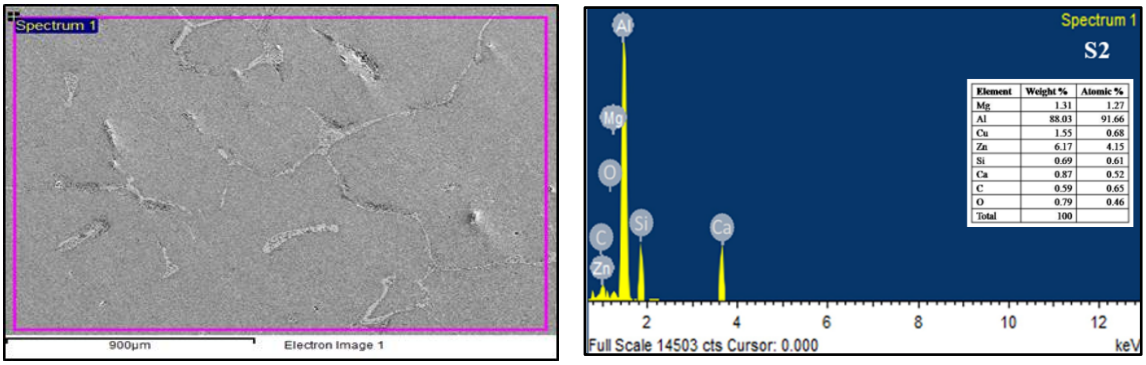

Figure 4.29: EDS Spectrum of Specimen S2 (Al-7075-T6/ 0.5 wt.% eggshell/1.5 wt.% SiC/2 wt.% Al_2O_3)

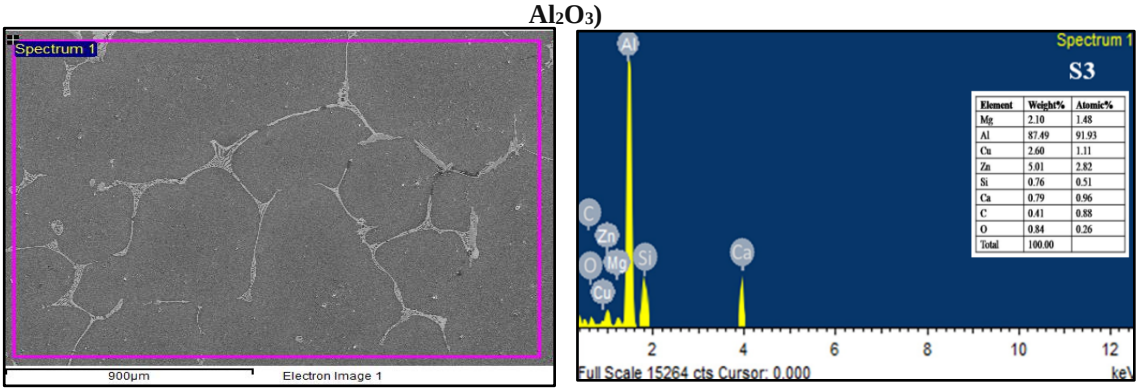

Figure 4.30: EDS Spectrum of Specimen S3 (Al-7075-T6/ 0.5 wt.% eggshell/ 2 wt.% SiC/ 2.5 wt.% Al_2O_3)

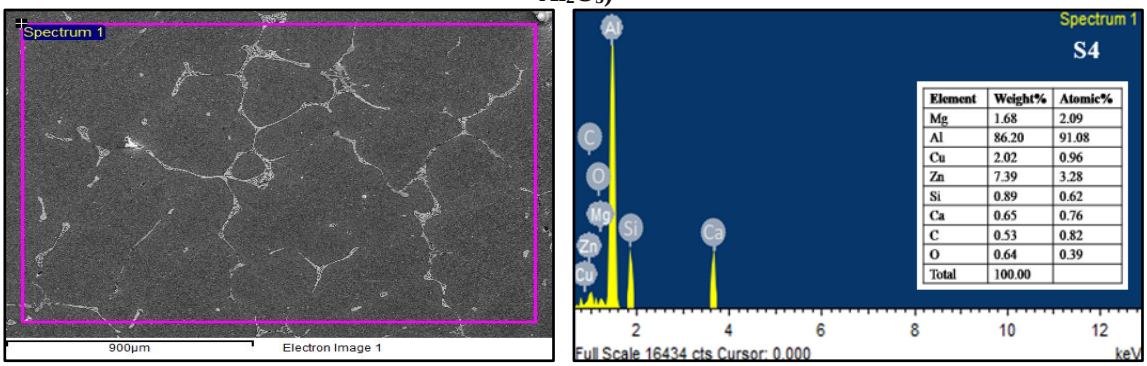

Figure 4.31: EDS Spectrum of Specimen S4 (Al-7075-T6/ 1 wt.% eggshell/1 wt.% SiC/2 wt.% Al_2O_3)

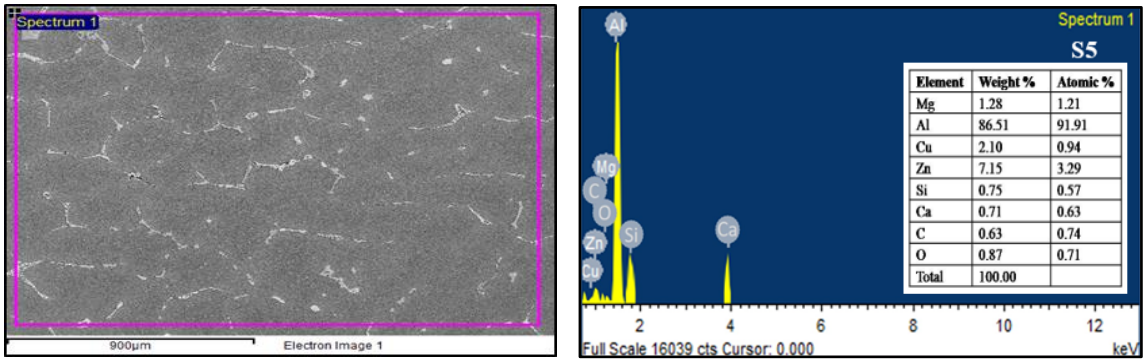

Figure 4.32: EDS Spectrum of Specimen S5 (Al-7075-T6/ 1 wt.% eggshell/1.5 wt.% SiC/2.5 wt.% Al_2O_3)

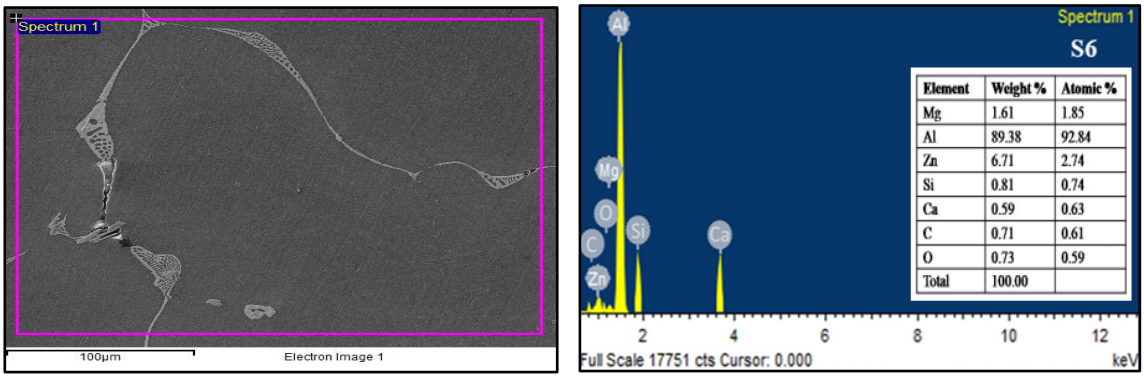

Figure 4.33: EDS Spectrum of Specimen S6 (Al-7075-T6/ 1 wt.% eggshell/2 wt.% SiC/1.5 wt.% Al_2O_3)

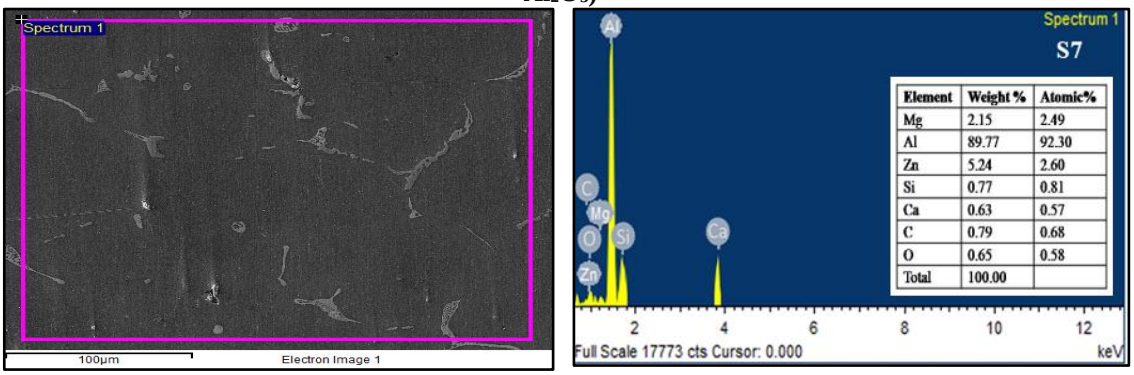

Figure 4.34: EDS Spectrums of Specimen S7 (Al-7075-T6/ 1.5 wt.% eggshell/1 wt.% SiC/2.5 wt.% Al_2O_3)

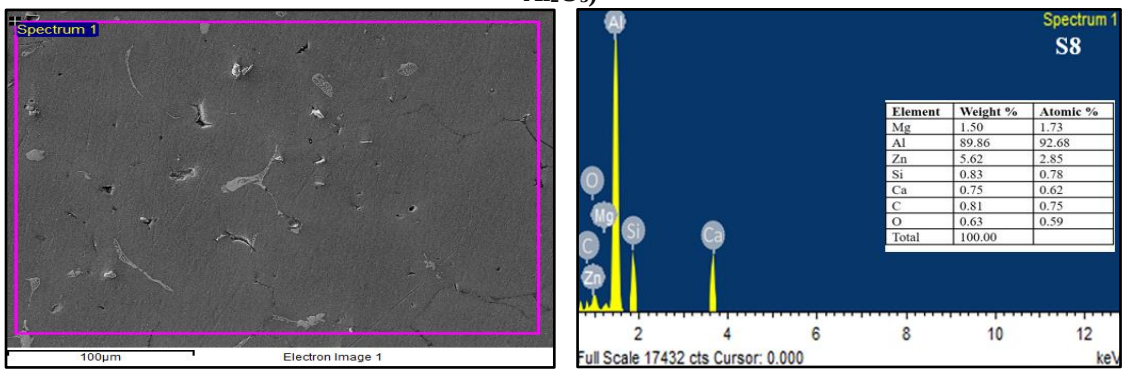

Figure 4.35: EDS Spectrums of Specimen S8 (Al-7075-T6/ 1.5 wt.% eggshell/1.5 wt.% SiC/1.5 wt.% Al_2O_3)

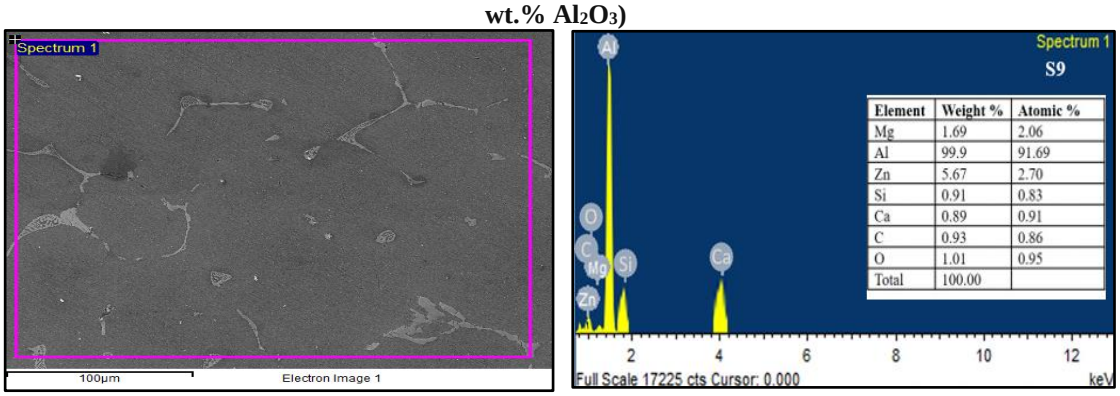

Figure 4.36: EDS Spectrum of Specimen S9 (Al-7075-T6/ 1.5 wt.% eggshell/2 wt.% SiC/2 wt.% Al_2O_3)

Additionally, X-ray diffraction analysis was carried to investigate the interface between metal matrix and reinforcements. XRD spectrograms of produced hybrid composites as shown in Figures 4.37 to 4.45 exhibit intensity peaks for aluminium at diffraction angle $2\Theta \approx 38^0$, 45^0 and 65^0, for eggshell at 22^0 and 45^0, for silicon carbide at 35^0 and 42^0 and for aluminium oxide at 38^0 and 57^0. Appreciable presence of reinforcement components in synthesized composites, established by different characterization techniques indicate improved wettability, uniform dispersion and strong interfacial bonding between matrix phase and reinforcement phases.

The abutting section demonstrates a compendious crux of present chapter.

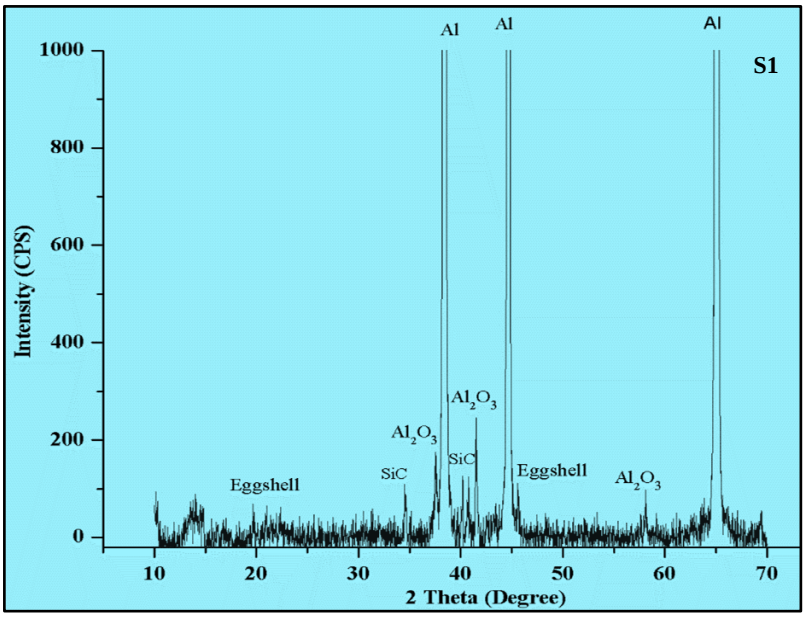

Figure 4.37: XRD Spectrogram of Specimen S1 (Al-7075-T6/ 0.5 wt.% eggshell/1wt.% SiC/1.5 wt.% Al_2O_3)

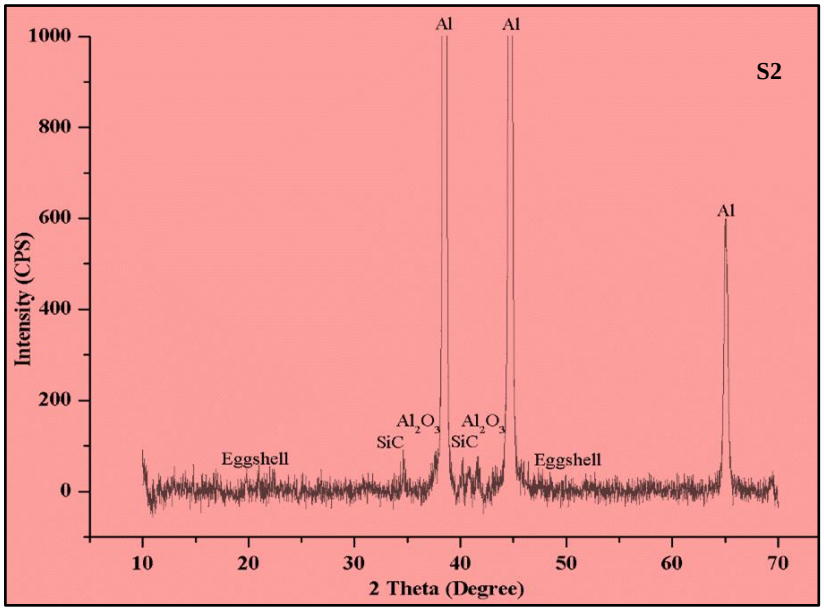

Figure 4.38: XRD Spectrogram of Specimen S2 (Al-7075-T6/ 0.5 wt.% eggshell/1.5 wt.% SiC/2 wt.% Al_2O_3

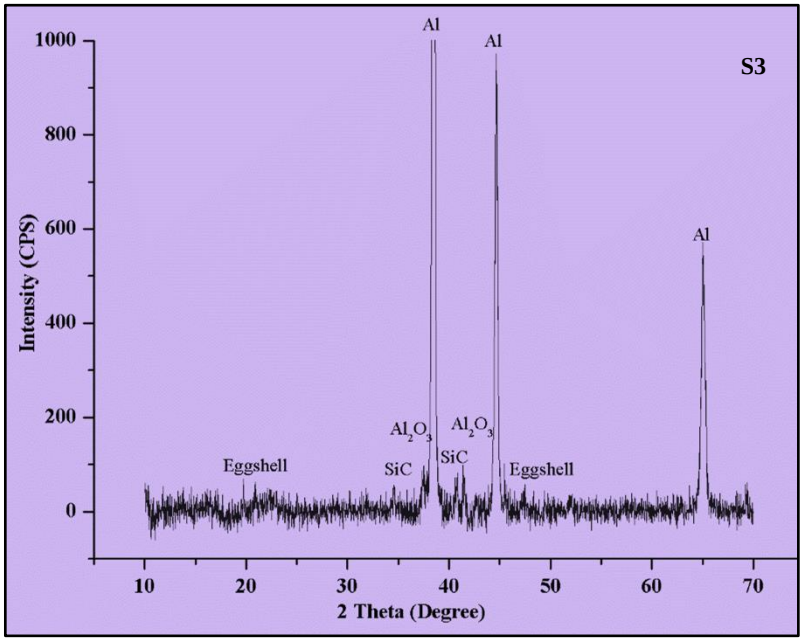

Figure 4.39: XRD Spectrogram of Specimen S3 (Al-7075-T6/ 0.5 wt.% eggshell/2 wt.% SiC/2.5 wt.% Al_2O_3)

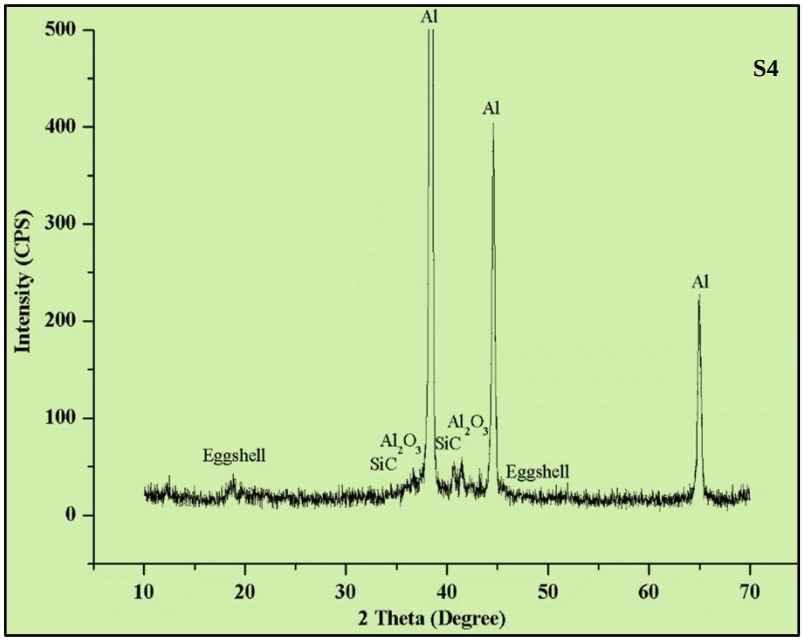

Figure 4.40: XRD Spectrogram of Specimen S4 (Al-7075-T6/ 1 wt.% eggshell/1 wt.% SiC/2 wt.% Al_2O_3

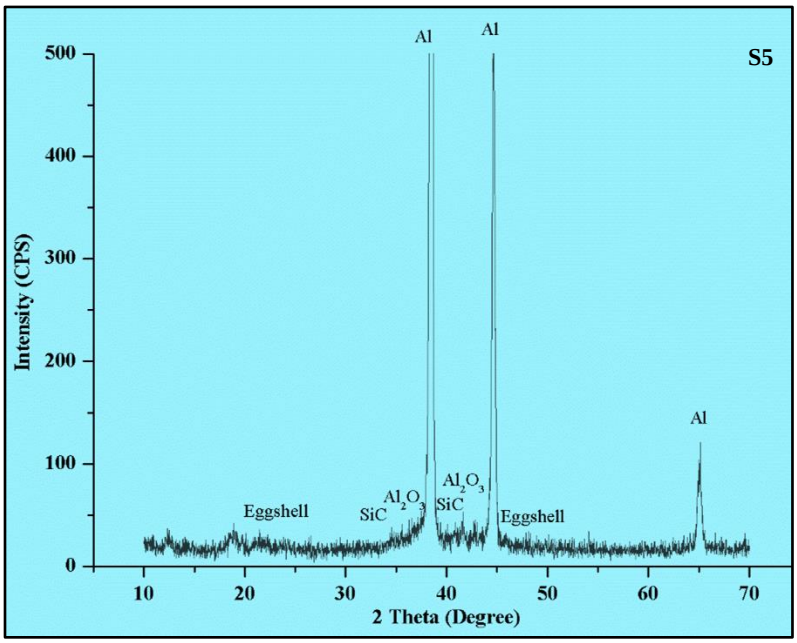

Figure 4.41: XRD Spectrogram of Specimen S5 (Al-7075-T6/ 1 wt.% eggshell/1.5wt.% SiC/2.5 wt.% Al_2O_3)

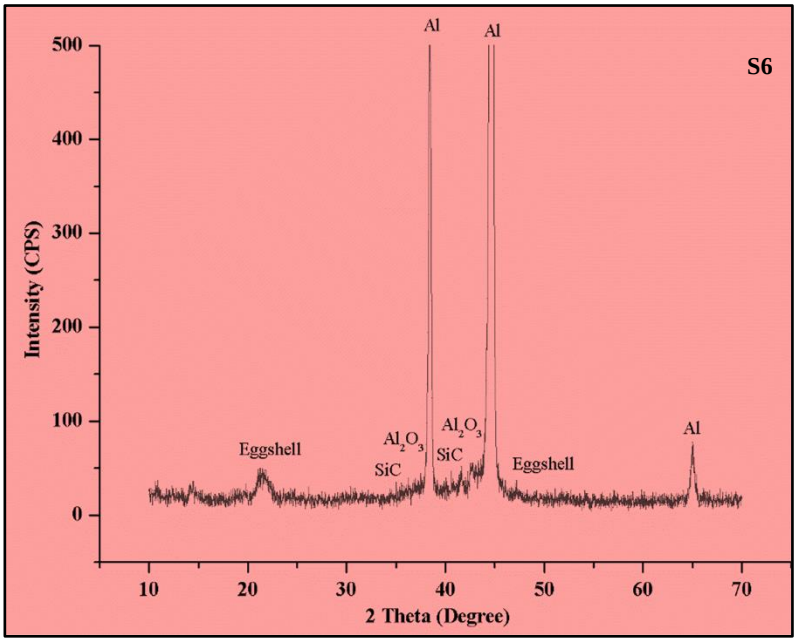

Figure 4.42: XRD Spectrogram of Specimen S6 (Al-7075-T6/ 1 wt.% eggshell/2 wt.% SiC/1.5 wt.% Al_2O_3

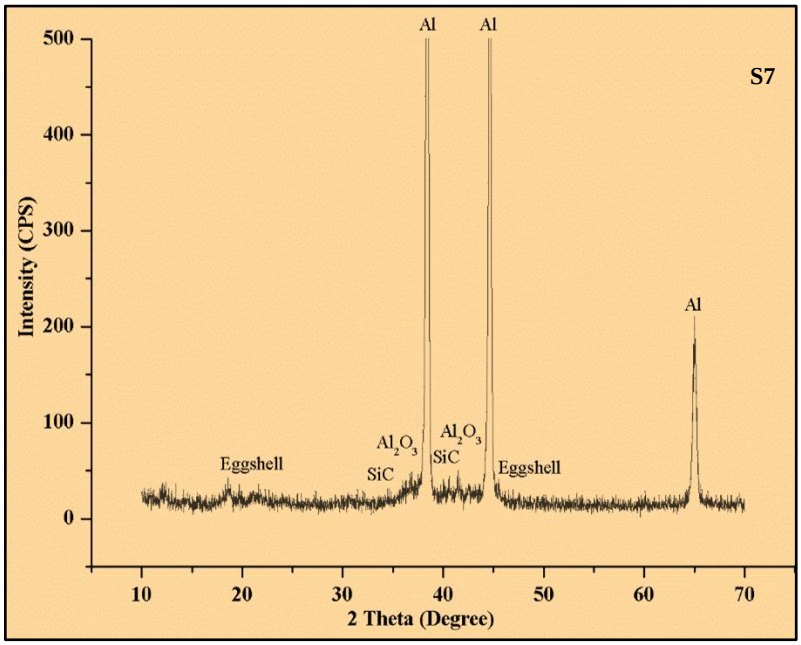

Figure 4.43: XRD Spectrogram of Specimen S7 (Al-7075-T6/ 1.5 wt.% eggshell/1 wt.% SiC/2.5 wt.% Al_2O_3)

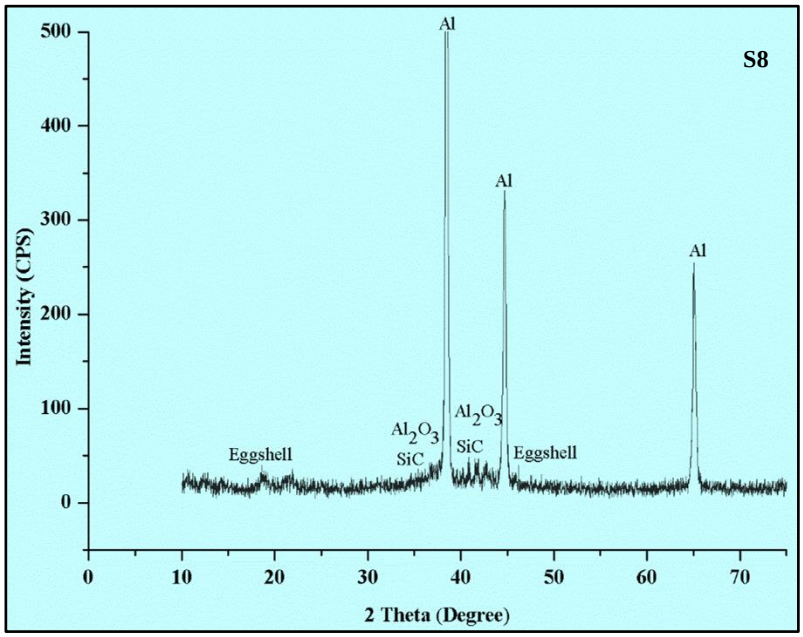

Figure 4.44: XRD Spectrogram of Specimen S8 (Al-7075-T6/ 1.5 wt.% eggshell/1.5 wt.% SiC/1.5 wt.% Al_2O_3

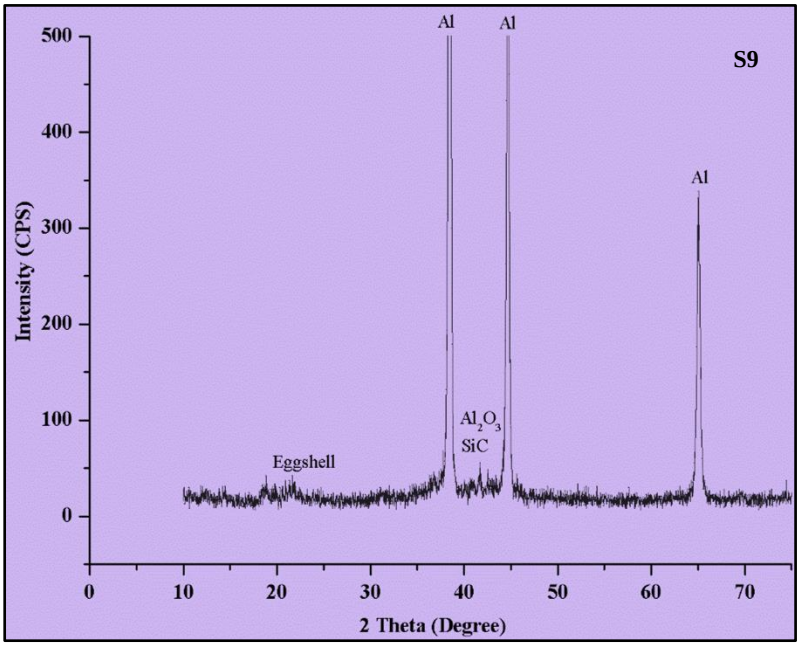

Figure 4.45: XRD Spectrogram of Specimen S9 (Al-7075-T6/ 1.5 wt.% eggshell/2 wt.% SiC/2 wt.% Al_2O_3)

4.5 Summary

This chapter includes synthesis, analysis of chemical composition and microstructural investigation of base metal and reinforcements through scanning electron microscopy (SEM), energy dispersive spectroscopy (EDS) and X-ray diffraction (XRD) techniques. Synthesis of hybrid aluminium composites as per design of experiment through electromagnetic stir casting technique has been discussed in detail. Microstructural and elemental composition investigations of produced composites have been conducted to compare them with unreinforced base metal. The grain size in composites, displaying presence of various alloying elements and reinforcement components was realized to be finer. Evaluation of synthesized hybrid aluminium metal matrix composites for different mechanical and physical attributes and prevalent process parameter optimization has been elaborated in next chapter.

CHAPTER 5

Mechanical Characterization of Synthesized Hybrid Aluminium Composites and Optimization of Prevalent Process Parameters

5.1 Introduction

This chapter includes assessment of synthesized composites for various mechanical and physical characteristics such as density, porosity, residual stress, microhardness, tensile strength and low cycle fatigue life in comparison of their unreinforced counterpart. Repeated measurements mean values and S/N ratio calculations for each attribute have been reported in accordance with Taguchi L9 orthogonal array. ANOVA analysis has been used to observe influence of prevalent process parameters on quality characteristics. Mean predicted value of quality characteristics and confidence interval for predicted value have been calculated by Taguchi approach followed by a confirmation experiment. The four control factors with three levels, because they may affect the performance attributes nonlinearly, are shown in Table 5.1.

Table 5.1: Various Control Parameters and Levels

Control Parameters	**Factor Nomination**	**Level 1**	**Level 2**	**Level 3**
Eggshell Particles Weight %	A	0.5	1	1.5
Silicon Carbide Particles Weight %	B	1	1.5	2
Aluminium Oxide Particles Weight %	C	1.5	2	2.5
Mechanical Stirring Time (Minutes)	D	2	4	6
Mechanical Stirring Speed	150 rpm			
Stirring Temperature	850^0 C			
Reinforcement Preheat Temperature	500^0 C			
Electromagnetic Stirring	960 rpm			
Electromagnetic Stirring Time (minutes)	0.5 min			

Consecutive sections include detailed discussion on various physical and mechanical attributes of composites.

5.2 Density and Porosity

Density measurement of specimens was conducted using gravimetric method/ hydrostatic weighing method as per standard OIML-r111 on a Mettler Toledo weighing balance, as shown in Figure 5.1.

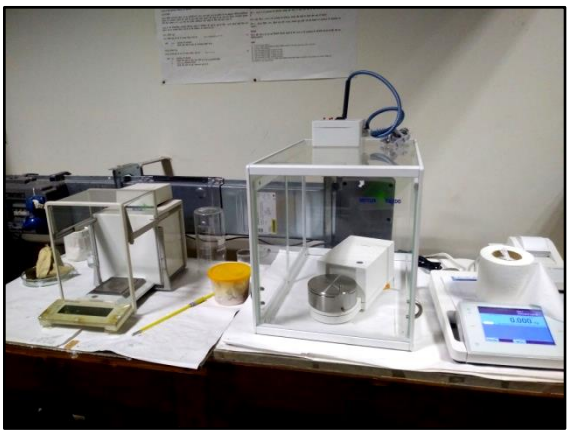

Figure 5.1: Weighing Balance

At recorded temperature, each specimen was first weighed in air and then weighed in distilled water. Density of distilled water is calculated by an empirical formula given in equation 5.1.

$$\rho_1 = 0.99997495\left[1 - \frac{(t-3.983035)^2\,(t+301.797)}{522528.9 \times (t+6934881)}\right] \quad (5.1)$$

Here t: Recorded temperature in ^{0}C

Density of each test specimen was obtained by equation 5.2.

$$\rho_t = \frac{(I_{ta} \times \rho_l) - (I_{tl} \times \rho_a)}{I_{ta} - I_{tl}} \quad (5.2)$$

Here ρ_t: Density of test specimen at recorded temperature

ρ_l: Density of distilled water at recorded temperature

ρ_a: Density of air at recorded temperature

I_{ta}: Weight of test specimen in air at recorded temperature

I_{tl}: Weight of test specimen in distilled water at recorded temperature

Theoretical densities of synthesized hybrid composites were computed by using mixture rule as explained by equation 5.3.

$$\frac{1}{\rho_c} = \frac{1}{\rho_{f1}}\left(\frac{w_{f1}}{w_c}\right) + \frac{1}{\rho_{f2}}\left(\frac{w_{f2}}{w_c}\right) + \frac{1}{\rho_{f3}}\left(\frac{w_{f3}}{w_c}\right) + \frac{1}{\rho_m}\left(\frac{w_m}{w_c}\right) \quad (5.3)$$

Here ρ_c and w_c: Density and weight of composite

ρ_{f1} and w_{f1}: Density and weight of eggshell particles

ρ_{f2} and w_{f2}: Density and weight of Silicon carbide particles

ρ_{f3} and w_{f3}: Density and weight of Aluminium oxide particles

ρ_m and w_m: Density and weight of Al 7057-T6 alloy used as metal matrix

Experimentally obtained and theoretically calculated mean values of density for as-cast Al7075-T6 specimen and 9 composites specimens (in three replications) are shown in Figure 5.2. It was observed that there was no significant variation in density of composites as compared to the base metal (only upto 2.2 %) due to comparable densities of infused reinforcements.

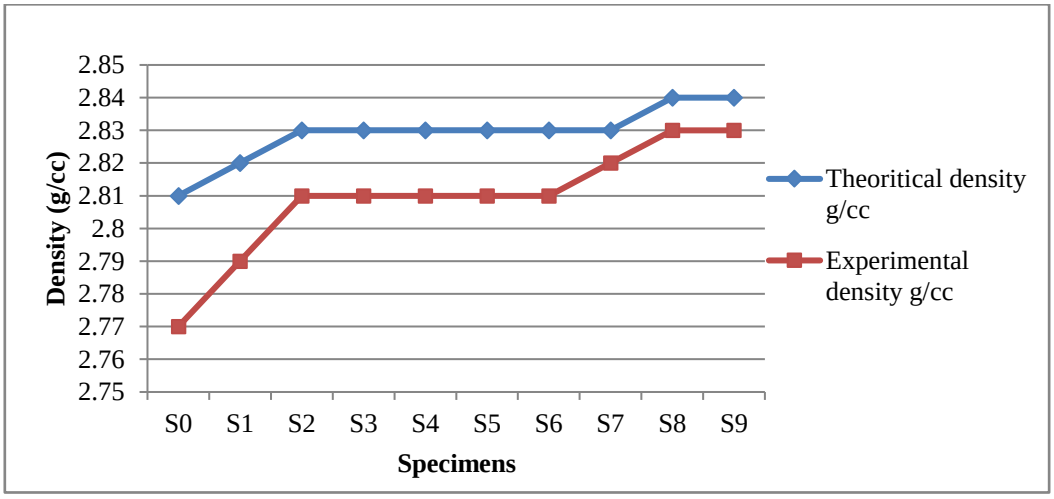

Figure 5.2: Density of Composites

Porosity is described as the volume fraction of voids in materials due to independent air bubbles, moisture on reinforcement surfaces, air enveloping reinforcement particles, shrinkage during solidification and water vapours from atmosphere etc. Percentage porosity of developed composites was calculated by expression given in equation 5.4 [164].

$$\% \text{ Porosity} = \left\{\left(\frac{\rho_c - \rho_t}{\rho_c}\right)\right\} \times 100\ \% \quad (5.4)$$

Here ρ_c: Theoretical density of composites

ρ_t: Experimental density of composites at recorded temperature (t^0C)

Table 5.2 demonstrates three observations corresponding to three replications for percentage porosity measurement of developed hybrid composite specimens with respective S/N ratio for "smaller the better" kind of quality characteristic.

Table 5.2: Observations for Percentage Porosity and S/N Ratio

Percentage Porosity					
Average Percentage Porosity of as-cast Al7075-T6 Specimen S0: 1.42					
Composite Specimen	**Observation 1**	**Observation 2**	**Observation 3**	**Mean Value**	**S/N Ratio (dB)**
S1	1.06	1.13	0.81	1.00	-0.08
S2	0.71	0.65	0.64	0.67	3.51
S3	0.72	0.96	0.48	0.72	2.54
S4	0.82	0.65	0.71	0.73	2.73
S5	0.71	0.85	0.65	0.74	2.60
S6	0.91	0.71	0.53	0.72	2.69
S7	0.47	0.28	0.35	0.37	8.52
S8	0.3	0.35	0.38	0.34	9.25
S9	0.35	0.42	0.26	0.34	9.13

Generally, porosity in composites is increased with infusion of fillers, as the reinforcement particles entering metal matrix trap air and cause voids. Stress concentrations occur in proximity of micro-pores created due to porosity, deteriorating the mechanical attributes of composites in terms of reduced ductility, accelerated fatigue crack initiation, reduced tensile strength, reduced hardness, decreased corrosion resistance and inferior surface finish [165]. To reduce porosity, it is essential to maintain a balance between void sources (features or mechanisms that cause porosity such as moisture layers and trapped air) and void sinks (features or mechanisms that diminish porosity such as bubble mobility and vacuum evacuation). However, in present experiment, electromagnetic stirring resulted into strong interfacial bonding and uniform distribution of reinforcement particles into metal matrix, filling the micropores and reducing porosity in synthesized hybrid composites. Additionally, faster cooling rate, improved wettability and controlled process parameters also reduced porosity in synthesized composites [166]. Plots in Figure 5.3 feature the effect of different process

parameters on S/N ratio and percentage porosity in synthesized composites. It is displayed that with increased reinforcements content (Figures 5.3a, 5.3b and 5.3c) and longer mechanical stirring time (Figure 5.3d) percentage porosity of developed hybrid aluminium metal matrix composites was reduced significantly. It was inferred that for minimum percentage porosity and S/N ratio, 3rd level of eggshell content (A_3), 2nd level of SiC content (B_2), 2nd level of Al_2O_3 content (C_2) and 2nd level of mechanical stirring time (D_2) were optimum levels. Table 5.3 represents average values of percentage porosity and S/N ratio for each process parameter at all levels.

Table 5.3: Response Table: Percentage Porosity

Process Parameter	**Level**	**Eggshell Particles wt.%**		**SiC Particles wt.%**		**Al_2O_3 Particles wt.%**		**Mechanical Stirring Time**	
Type of Data	-	Raw Data	S/N Ratio	Raw Data	S/N Ratio	Raw Data	S/N Ratio	Raw Data	S/N Ratio
Average Values	L1	0.80	1.99	0.70	3.72	0.69	3.95	0.69	3.88
	L2	0.73	2.68	0.58	5.12	0.58	5.13	0.58	4.91
	L3	0.35	8.97	0.59	4.79	0.61	4.55	0.60	4.84
Main Effects	L2-L1	-0.07	0.68	-0.12	1.40	-0.11	1.17	-0.11	1.03
	L3-L2	-0.38	6.29	0.01	-0.33	0.03	-0.57	0.01	-0.07
Difference (L3-L2)-(L2-L1)		-0.31	5.61	0.13	-1.72	0.14	-1.74	0.12	-1.09
L1, L2 and L3 display the process parameter levels. (L2-L1) represents main effect while corresponding process parameter changes from level 1 to level 2. (L3-L2) denotes main effect during process parameter change from level 2 to level 3.									

ANOVA is a statistical technique that is capable of analysing any experimental data and drawing significant conclusions in terms of F ratio, percentage contribution and error variance [167, 168]. Table 5.4 shows ANOVA results computed at 95% confidence level, with demonstration of F-ratio and percentage contribution of various factors toward quality characteristic. It was noticed that eggshell particles wt.% (P=66.82%) had significant effect on percentage porosity of synthesized hybrid composites, whereas other control factors remained insignificant. After analysing S/N ratio and mean response characteristic, optimum levels of physically and statistically significant factors were determined to be A_3. Table 5.5 presents ANOVA results enumerated at 95% confidence level, with demonstration of F-ratio and percentage contribution of various factors for S/N

ratio. The predicted mean of percentage porosity at optimal level of process parameters was enumerated using equation 5.5 [169, 170].

$$X_{mp} = \overline{G} + \left(\overline{A_3} - \overline{G}\right) \quad (5.5)$$

Here X_{mp} denoted the predicted mean of percentage porosity at optimum condition and $\overline{G}$ was the grand average of all 27 observations of utility characteristics from Table 5.2. $\overline{A_3}$ represented the average value of percentage porosity at optimal level of significant process parameter.

Table 5.4: Analysis of Variance (ANOVA) for Percentage Porosity

Factor	**Sum of Squares (SS)**	**Degrees of Freedom**	**Variance (V)**	**Percentage Contribution (P)**	**F-Ratio**
Eggshell Particles wt.%	1.03	2	0.51	66.82	29.20*
SiC Particles wt.%	0.07	2	0.04	4.75	2.07
Al_2O_3 Particles wt.%	0.06	2	0.03	3.63	1.59
Mechanical Stirring Time	0.06	2	0.03	4.21	1.84
Others/Errors	0.32	18	0.02	20.60	-
Total	1.54	26	-	100	-
***Significant factor at confidence level of 95%, F critical =3.55 (Value from table)**					

Table 5.5: Analysis of Variance (ANOVA) for S/N Ratio

Factor	**Sum of Squares (SS)**	**Degrees of Freedom**	**Variance (V)**	**Percentage Contribution (P)**	**F-Ratio**
Eggshell Particles wt.%	88.67	2	44.33	92.46	44.88*
SiC Particles wt.%	3.19	2	1.60	3.33	1.61
Al_2O_3 Particles wt.%	2.06	2	1.03	2.15	1.04
Mechanical Stirring Time	1.98	-	-	-	-
Others/Errors	1.98	2	0.99	2.06	-
Total	95.90	8	-	100	-
***Significant factor at confidence level of 95%, F critical =19 (Value from table)**					

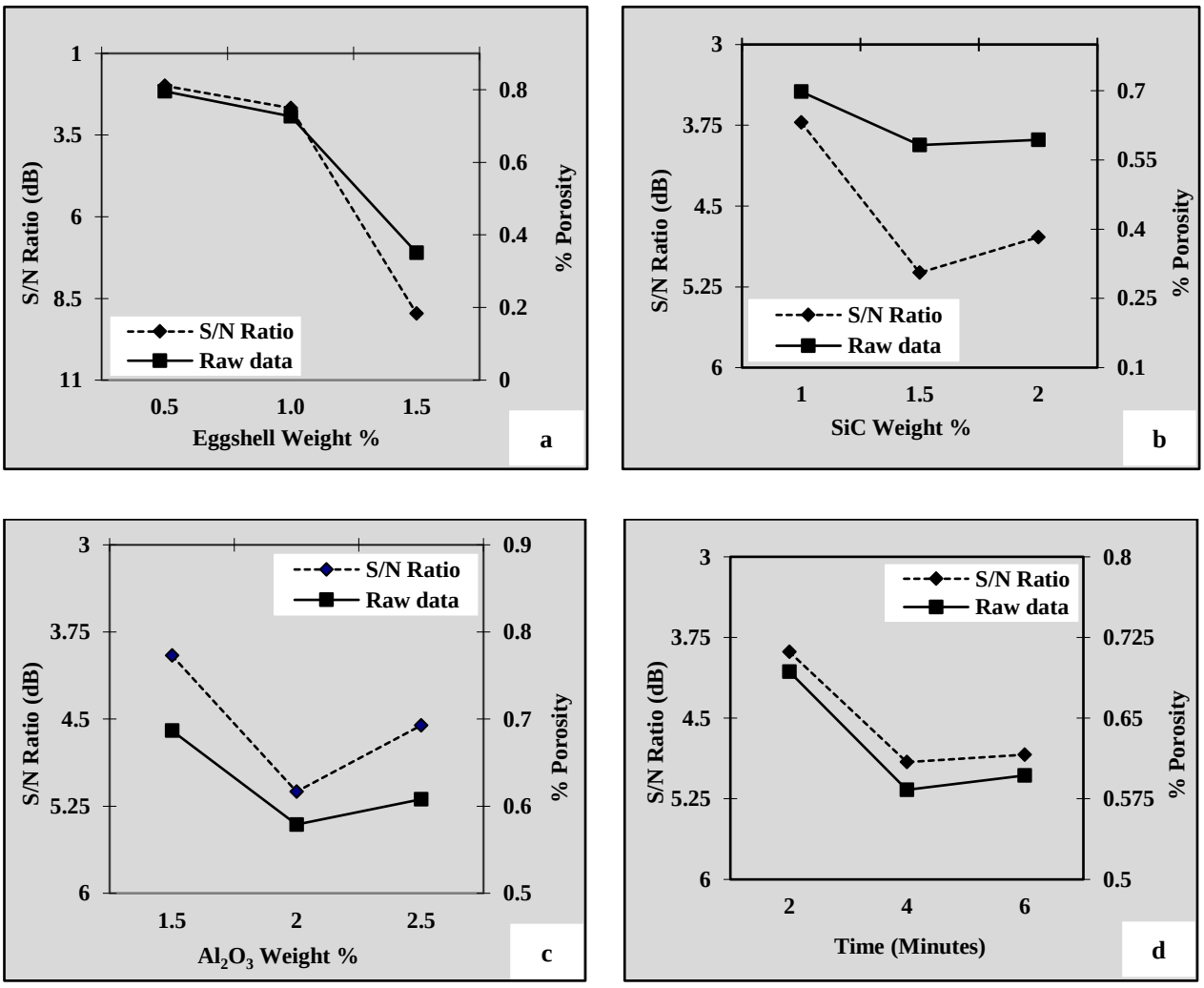

Figure 5.3: Effect of (a) Eggshell Particles wt.% (b) SiC Particles wt.% (c) Al_2O_3 Particles wt.% (d) Mechanical Stirring Time on Percentage Porosity and S/N Ratio

The pooled versions of ANOVA for percentage porosity raw data and S/N ratio are provided in Tables 5.6 and 5.7.

On submitting estimated values of various response averages as $\overline{G} = 0.62$ and $\overline{A_3} = 0.35$ in equation 5.5, predicted mean optimum value of percentage porosity was realized to be 0.35. From Table 5.4 the values were obtained for error variance (0.02) and degree of freedom (DOF) for error (18) whereas F-ratio value at 95% confidence interval was determined from standard statistical table. Further, confidence interval (CI) was calculated to be ± 0.23, using equation 5.6.

$$CI = \sqrt{F(\alpha, 1, f_e)V_e\left[\frac{1}{n_{eff}} + \frac{1}{R}\right]} \quad (5.6)$$

Here $F(\alpha, 1, f_e)$= Critical value of F from statistical Table

f_e = Error degree of freedom

V_e = Error variance value form ANOVA table

$n_{eff} = \frac{N}{1+Degree\ of\ freedom\ for\ estimated\ mean\ response}$

N' = Total number of experiments =27 (experimental runs=9, iterations=3)

R = Confirmation experiment size

Table 5.6: Pooled ANOVA for Porosity Raw Data

Factor	**SS**	**Degrees of Freedom (Pooled)**	**V (Pooled)**	**SS'**	**P % (Modified)**	**F-Ratio**
Eggshell Particles wt.%	1.03	2	0.51	0.99	64.53	29.20*
SiC Particles wt.%	0.07	2	0.04	0.04	2.46	2.07
Al_2O_3 Particles wt.%	0.06	2	0.03	0.02	1.35	1.59
Mechanical Stirring Time	0.06	2	0.03	0.03	1.92	1.84
Others/Errors	0.32	18	0.02	0.46	29.75	-
Total	1.54	26	-	1.54	100	-
***Significant factor at confidence level of 95%, F critical =3.55 (Value from table)**						

Table 5.7: Pooled ANOVA for Porosity S/N Ratio

Factor	**SS**	**Degrees of Freedom (Pooled)**	**V (Pooled)**	**SS'**	**P % (Modified)**	**F-Ratio**
Eggshell Particles wt.%	88.67	2	44.33	86.69	90.40	44.88*
SiC Particles wt.%	3.19	2	1.60	1.21	1.27	1.61
Al_2O_3 Particles wt.%	2.06	2	1.03	0.09	0.09	1.04
Mechanical Stirring Time	-	-	-	-	-	-
Others/Errors	1.98	2	0.99	7.90	8.24	-
Total	95.90	8	-	95.90	100.00	-
***Significant factor at confidence level of 95%, F critical =19 (Value from table)**						

Hence confidence interval with respect to 95% confidence level of predicted optimum percentage porosity was 0.12 < percentage porosity (PP) < 0.58. In accordance with Taguchi's optimization approach, a confirmation experiment was conducted by running three more replications for percentage porosity of produced hybrid aluminium composites at optimal levels of prevalent process parameters as given in Table 5.8 in order to authenticate the predicted results. It is realized from Table 5.8 that confirmation experiment result obtained for percentage porosity of composites was covered within the predicted confidence interval 0.12 < PP < 0.58.

Table 5.8: Confirmation Experiment for Percentage Porosity

Quality Characteristic	**Replications**			**Mean**
Percentage Porosity of Composites	Replication 1	Replication 2	Replication 3	
	0.44	0.29	0.32	0.35

5.3 Residual Stress

Residual stresses are those internal stresses which remain in solid material after the original cause of stress is removed. Residual stress might occur in synthesized hybrid composite specimens due to temperature gradients and machining forces resulting into premature failure. Residual stresses can be measured by various destructive and non-destructive techniques. In present experimental study, measurements of residual stresses in specimens were carried out by X-ray diffraction technique using a non-destructive X-ray analyzer (μ-X360) as shown in Figure 5.4. It consisted of a position sensitive detector unit with scintillation counter for measuring the residual stress in metallic surfaces by detecting and comparing the full Debye ring data (Figure 5.5) from a single incident X-ray angle with non-stressed state. X ray diffraction method determined the residual stress by measuring the distance between crystallographic planes using the angles at which maximum intensity took place when a sample was subjected to X-ray exposure. From these angles we could find out changed spacing between diffraction planes due to any kind of deformation, which corresponded to the magnitude of residual stress [171]. As we knew the wavelength and from measured shift of Bragg's angle the change in interplanar spacing and strain in a layer was calculated, hence by knowing elastic

constant of material, residual stress could be obtained. The measurement conditions for residual stress were as given below:

Pitch: 50 um

X-ray incidence angle: 25.0 Degree

X-ray irradiation time (Setup): 90 Second

X-ray wavelength (K-Alpha): 2.29093 Å

X-ray irradiation time (Meas.): 47 Second

X-ray irradiation time (Max): 82 Second

Sample distance (Monitor): 29.000 mm

Total measurement count: 7498

Sample distance (Analysis): 29.611 / 30.304 mm

Detection sensitivity: 52.8 %

Temperature: 35.88 Degree Centigrade

Peak analysis method: Fitting Lorentz

In this experimental work, as-cast Al7075-T6 specimen and hybrid composite specimens (all in three replications) were characterized for residual stresses. Table 5.9 shows S/N ratio calculation from experimental data (three set of observations for three replications) for residual stress as "smaller the better" type of quality characteristic of developed composites. In present investigation, it was noticed that generally residual stresses were lower for composites with higher reinforcement content. Residual stresses measurements for all the specimens are shown in Figure 5.6.

Figure 5.4: X-ray Analyzer (μ-X360)

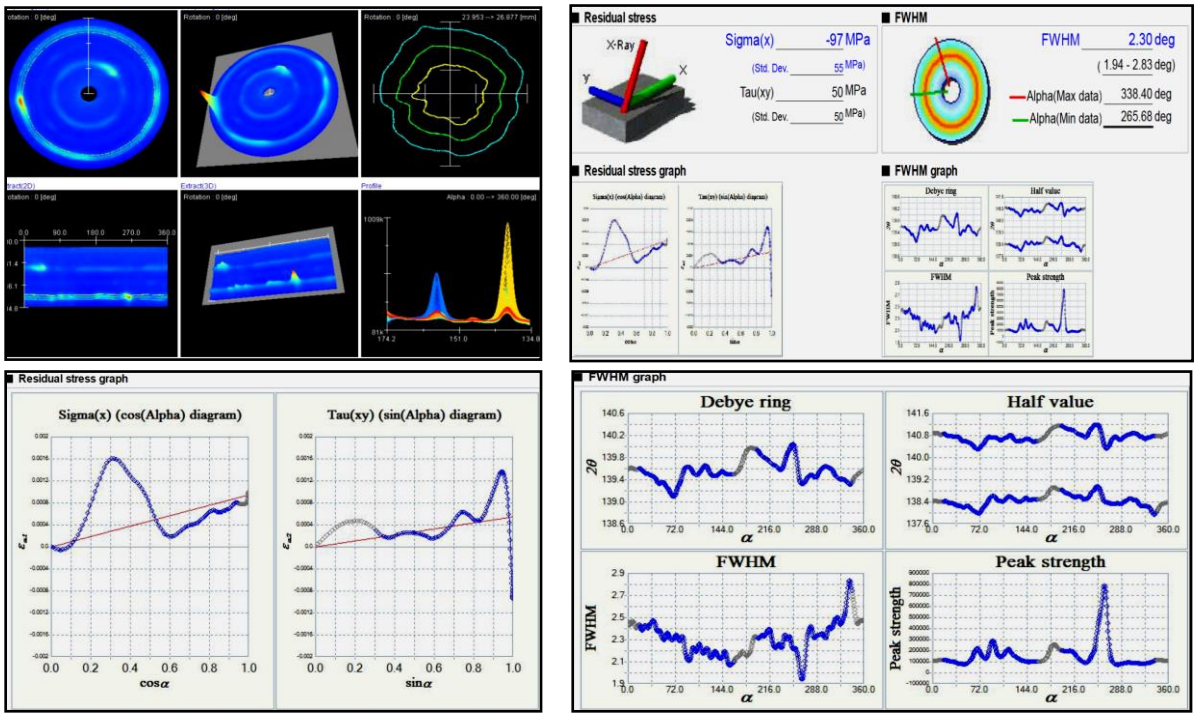

Figure 5.5: Residual Stress Measurement Using X-ray Diffraction

Residual stresses or strain fields were developed within the composites because of thermomechanical mismatch in the characteristics of metal matrix and reinforcement during cooling from fabrication temperature, presence of moisture, fluctuation in material properties, difference in amount of reinforcement and tool-part interaction during machining [172].

Table 5.9: Observations for Residual Stress and S/N Ratio

Residual Stress					
Average Residual Stress in as-cast Al7075-T6 Specimen S0: 89 Mpa					
Composite Specimen	**Observation 1 (Mpa)**	**Observation 2 (Mpa)**	**Observation 3 (Mpa)**	**Mean Value (Mpa)**	**S/N Ratio (dB)**
S1	97	99	89	95.00	-39.56
S2	155	84	129	122.67	-42.02
S3	215	119	208	180.67	-45.38
S4	60	54	32	48.67	-34.00
S5	18	34	26	26.00	-28.57
S6	44	36	48	42.67	-32.66
S7	40	14	36	30.00	-30.13
S8	36	13	14	21.00	-27.43
S9	60	57	86	67.67	-36.77

Variations in residual stresses of synthesized hybrid composites (maximum relative abatement observed in residual stress of hybrid composite specimen S8 was 76% as compared to their unreinforced counterpart specimen S0) may primarily be associated with thermal residual stresses generated during electromagnetic stir casting process, distinct weight percentage of reinforcements infused and residual stresses developed during machining of hybrid composites. Specimens S0 was subjected to higher residual stresses while specimens S8 with higher filler content exhibited lower residual stresses. Infusion of reinforcement particles into metal matrix resulted into grain size refinement and increased dislocation density due to difference in coefficient of thermal expansion of metal matrix and reinforcement [173]. Hence, when material was stressed, the dislocations and reinforcements interacted creating positive dislocation stress fields and negative particle stress fields. When the net effect was positive, the particle stress fields were overcome, and material failed. When net effect was negative, the dislocations were annihilated, their motion was impeded, and material did not fail.

Specimen S3 was an exception with higher reinforcement content and higher residual stress and this possibility may be attributed to the phenomenon of plastic deformation which got enhanced with reduced dislocation density, as sometimes addition of reinforcement particles also pinned down the dislocations (if the reinforcement particle size was not very small).

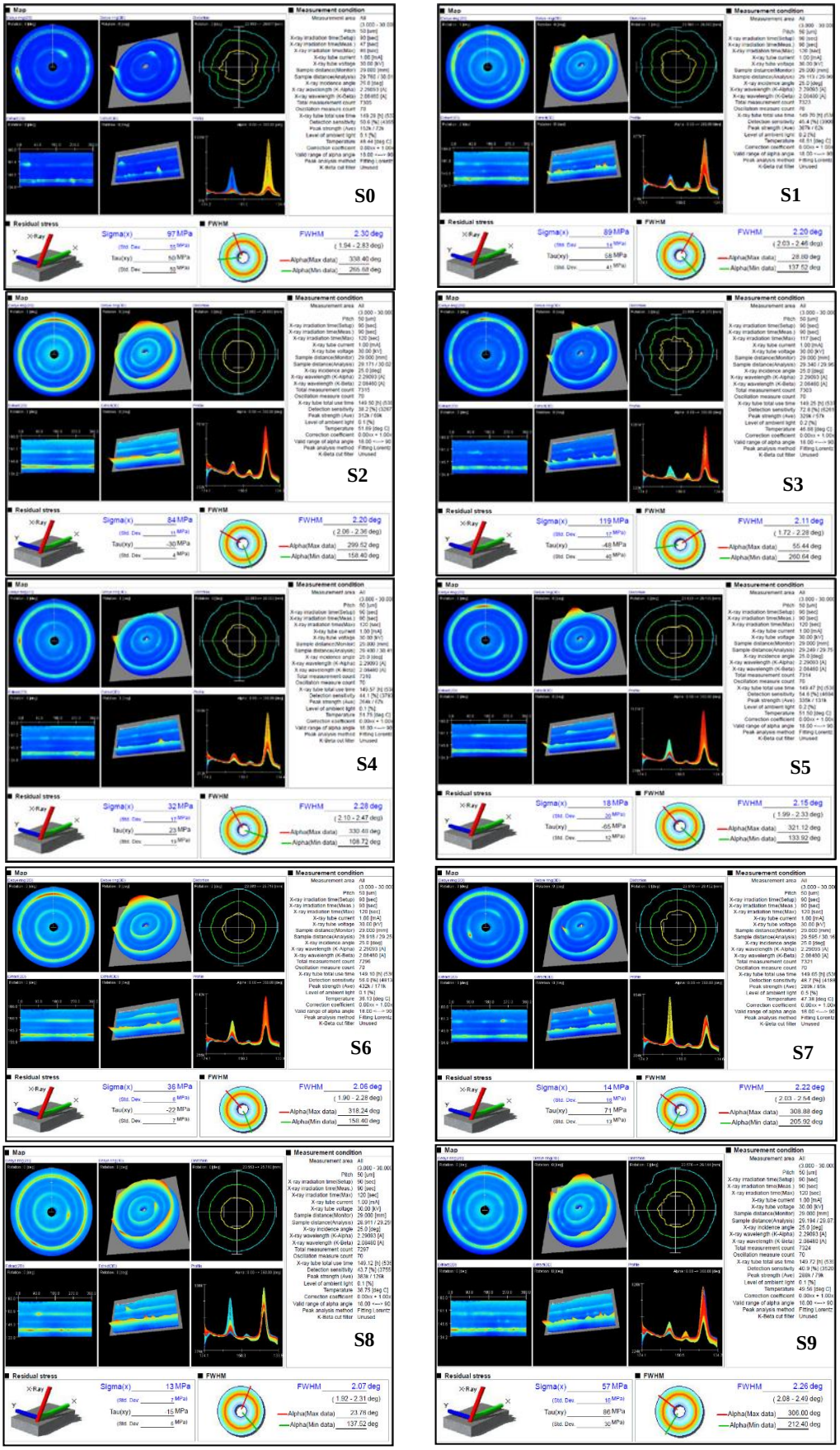

Figure 5.6: Residual Stress Measurement of Specimens

Effects of all the process parameters considered during composite fabrication on S/N ratio and residual stress were studied and plotted as in Figure 5.7. Graph in Figure 5.7a displays that on increasing wt.% of eggshell particles, residual stress in composites was decreased whereas from Figures 5.7b, 5.7c and 5.7d it can be ascertained that on increasing SiC particles wt.%, Al_2O_3 particles wt.% and mechanical stirring time residual stresses in composites were increased. Various graphs from Figure 5.7 explain that for minimum residual stress in synthesized hybrid aluminium composites and S/N ratio optimum process parameter levels were 3rd level of eggshell particles content (A_3), 2nd level of SiC particles content (B_2), 1st level of Al_2O_3 particles content (C_1) and 1st level of mechanical stirring time (D_1). Table 5.10 represents average values of residual stress and S/N ratio for each process parameter at all levels.

Table 5.10: Response Table: Residual Stress

Process Parameter	**Level**	**Eggshell Particles wt.%**		**SiC Particles wt.%**		**Al_2O_3 Particles wt.%**		**Mechanical Stirring Time**	
Type of Data	-	Raw Data	S/N Ratio	Raw Data	S/N Ratio	Raw Data	S/N Ratio	Raw Data	S/N Ratio
Average Values	L1	132.8	-42.3	57.9	-34.6	52.9	-33.2	62.9	-34.9
	L2	39.1	-31.7	56.6	-32.7	79.7	-37.6	65.1	-34.9
	L3	39.6	-31.4	97.0	-38.3	78.9	-34.7	83.4	-35.6
Main Effects	L2-L1	-93.7	10.6	-1.3	1.9	26.8	-4.4	2.2	0.03
	L3-L2	0.44	0.30	40.4	-5.6	-0.8	2.9	18.3	-0.67
Difference (L3-L2) - (L2-L1)		94.1	-10.3	41.9	-7.5	-27.6	7.3	16.1	-0.70
L1, L2 and L3 display the process parameter levels. (L2-L1) represents main effect while corresponding process parameter changes from level 1 to level 2. (L3-L2) denotes main effect during process parameter change from level 2 to level 3.									

ANOVA at 95% confidence level was carried out to study effect of process parameters on utility function. Table 5.11 shows percentage contribution and F-ratio of different factors affecting the residual stress. Table 5.12 presents ANOVA results computed at 95% confidence level, with display of F-ratio and percentage contribution of various factors for S/N ratio. The pooled versions of ANOVA for residual stress raw data and S/N ratio are provided in Tables 5.13 and 5.14.

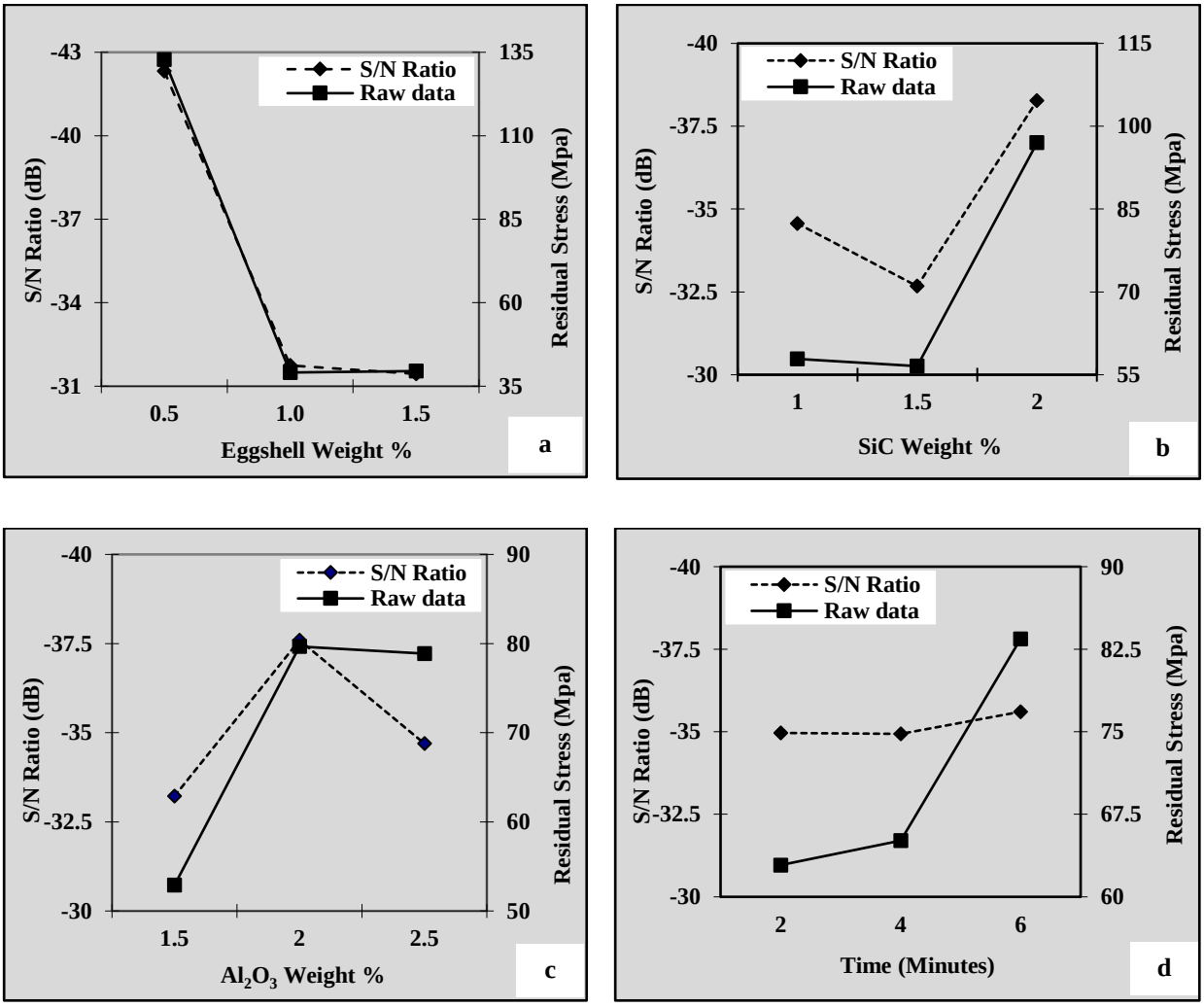

Figure 5.7: Effect of (a) Eggshell Particles wt.% (b) SiC Particles wt.% (c) Al_2O_3 Particles wt.% (d) Mechanical Stirring Time on Residual Stress and S/N Ratio

Table 5.11: Analysis of Variance (ANOVA) for Residual Stress

Factor	**Sum of Squares (SS)**	**Degrees of Freedom**	**Variance (V)**	**Percentage Contribution (P)**	**F-Ratio**
Eggshell Particles wt.%	52392.07	2	26196.04	66.65	46.04*
SiC Particles wt.%	9501.63	2	4750.81	12.09	8.35*
Al_2O_3 Particles wt.%	4180.96	2	2090.48	5.32	3.67*
Mechanical Stirring Time	2290.74	2	1145.37	2.91	2.01
Others/Errors	10241.33	18	568.96	13.03	-
Total	78606.74	26	-	100	-
***Significant factor at confidence level of 95%, F critical =3.55 (Value from table)**					

Table 5.12: Analysis of Variance (ANOVA) for S/N Ratio

Factor	Sum of Squares (SS)	Degrees of Freedom	Variance (V)	Percentage Contribution (P)	F-Ratio
Eggshell Particles wt.%	230.33	2	115.17	74.40	267.11*
SiC Particles wt.%	48.66	2	24.33	15.72	56.43*
Al_2O_3 Particles wt.%	29.74	2	14.87	9.61	34.49*
Mechanical Stirring Time	0.86	-	-	-	-
Others/Errors	0.86	2	0.43	0.28	-
Total	309.59	8	-	100.00	-
***Significant factor at confidence level of 95%, F critical =19 (Value from table)**					

Table 5.13: Pooled ANOVA for Residual Stress Raw Data

Factor	SS	Degrees of Freedom (Pooled)	V (Pooled)	SS'	P % (Modified)	F-Ratio
Eggshell Particles wt.%	52392.07	2	26196.04	51254.15	65.20	46.04*
SiC Particles wt.%	9501.63	2	4750.81	8363.70	10.64	8.35*
Al_2O_3 Particles wt.%	4180.96	2	2090.48	3043.04	3.87	3.67*
Mechanical Stirring Time	2290.74	2	1145.37	1152.81	1.47	2.01
Others/Errors	10241.33	18	568.96	14793.04	18.82	-
Total	78606.74	26	-	78606.74	100	-
***Significant factor at confidence level of 95%, F critical =3.55 (Value from table)**						

Table 5.14: Pooled ANOVA for Residual Stress S/N Ratio

Factor	SS	Degrees of Freedom (Pooled)	V (Pooled)	SS'	P % (Modified)	F-Ratio
Eggshell Particles wt.%	230.33	2	115.17	229.47	74.12	267.11*
SiC Particles wt.%	48.66	2	24.33	47.80	15.44	56.43*
Al_2O_3 Particles wt.%	29.74	2	14.87	28.88	9.33	34.49*
Mechanical Stirring Time	-	-	-	-	-	-
Others/Errors	0.86	2	0.43	3.45	1.11	-
Total	309.59	8	-	309.59	100.00	-
***Significant factor at confidence level of 95%, F critical =19 (Value from table)**						

It was realized from Table 5.11 that eggshell particles wt.% with percentage contribution P=66.65%, SiC particles wt.% with percentage contribution P=12.09 % and Al_2O_3 particles wt.% with percentage contribution P=5.32 % influenced the residual stresses significantly, whereas mechanical stirring time with percentage contribution P=2.91 % had insignificant influence on residual stresses. S/N ratio and mean response characteristics analysis was conducted followed by realization of optimum levels of significant factors as A_3, B_2 and C_1 for prediction of mean residual stress (X_{mp}). Following response average components were evaluated using experimental data from Table 5.9.

$$\overline{G} = 70.48,\ \overline{A_3} = 39.56,\ \overline{B_2} = 56.56 \text{ and } \overline{C_1} = 52.89$$

$$X_{mp} = \overline{G} + \left(\overline{A_3} - \overline{G}\right) + \left(\overline{B_2} - \overline{G}\right) + \left(\overline{C_1} - \overline{G}\right) \quad (5.7)$$

Predicted mean optimum value of residual stress X_{mp} = 25.63 Mpa was calculated form equation 5.7. From Table 5.11, error variance = 568.96 and DOF for error =18 were obtained. F-ratio value at 95% confidence interval was determined from standard statistical table. The confidence interval (CI) calculated from equation 5.6, was ± 40.9. Confidence interval with respect to 95% confidence level of predicted

optimum residual stress was -15.29< Residual Stress (RS in Mpa) <66.55. Additionally, a confirmation experiment was carried out by running three more replications for residual stress in developed hybrid composites at optimal levels of prevalent process parameters. Results of confirmation experiment were reported in Table 5.15 and it was realized that mean value of residual stress 31.5 Mpa fell within the confidence interval -15.29< RS (Mpa) <66.55.

Table 5.15: Confirmation experiment for Residual Stress

Quality Characteristic	**Replications**			**Mean**
Residual Stress in Composites (Mpa)	Replication 1	Replication 2	Replication 3	
	37.1	29.9	27.5	31.5 Mpa

5.4 Microhardness

Each of the specimens (one as-cast Al7075-T6 specimen and nine hybrid specimens, in three replications) was tested for microhardness (on Fischer HM 2000S, as shown in Figure 5.8).

For microhardness test of a material, the applied load should be less than 10 N, samples should be small with polished surfaces as rough sample surfaces may not give accurate data. Microhardness is commonly measured by two most common tests; (i) Vickers hardness and (ii) Knoop hardness. In Vickers microhardness test, the diamond shape indenter was capable of creating geometrically identical impressions, irrespective of its size. The indenter impression had explicit points of measurement and the indenter itself had high resistance to self-deformation. The indenter was in the shape of a right pyramid with a square base and an angle of 136^0 between opposite faces, as shown in Figure 5.9.

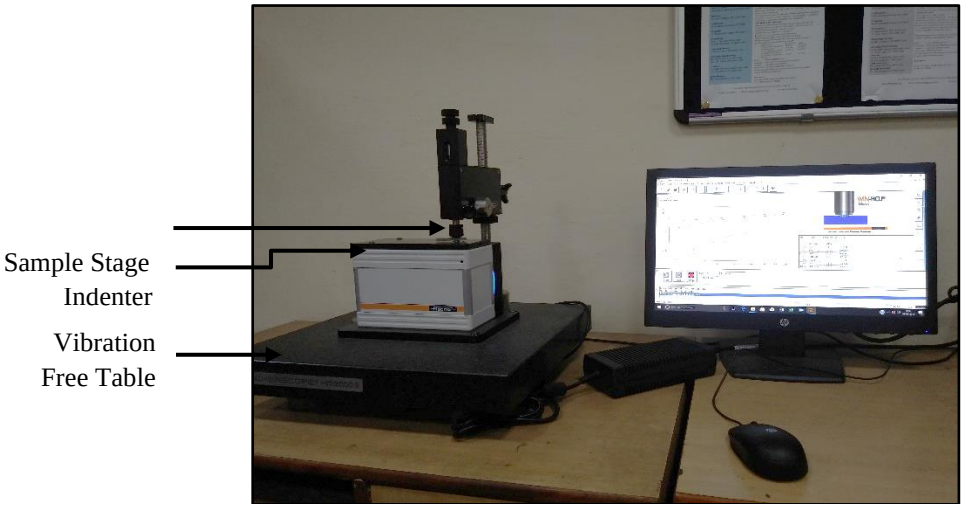

Figure 5.8: Microhardness Tester

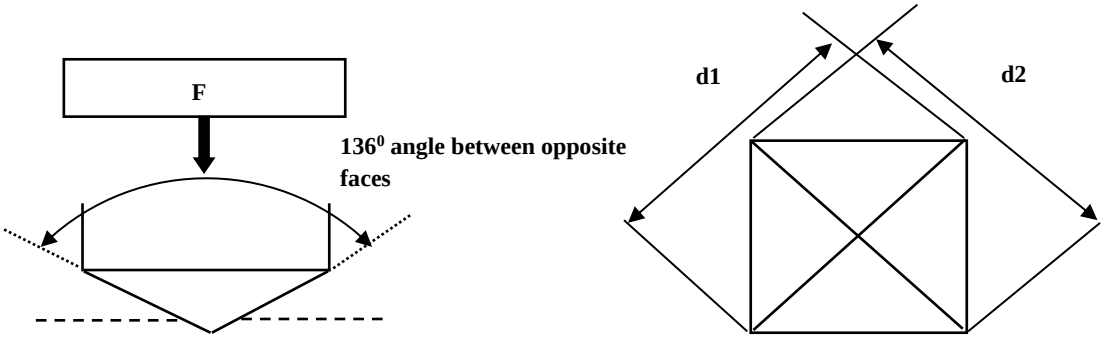

Figure 5.9: Vickers Hardness Test Scheme

Vickers hardness HV was calculated using equation number 5.8.

$$HV = \frac{2F\sin\frac{136^0}{2}}{d^2} = 1.854\frac{F}{d^2} \quad (5.8)$$

Where F: load applied in kgf

d: Arithmetic mean of the two diagonals d1 and d2 in mm

During microhardness test in present investigation, a load of 300 mN was applied for 20 seconds keeping creep time 5 seconds and load release time 20 seconds. The microhardness of as-cast Al7075-T6 specimen and composite specimens (in three replications) with varying reinforcement ratios along with S/N ratio calculation for "larger the better" type of quality characteristic is given in Table 5.16.

Table 5.16: Observations for Microhardness and S/N Ratio

Microhardness					
Average Microhardness of as-cast Al7075-T6 Specimen S0: 167.5 HV					
Composite Specimen	**Observation 1 (HV)**	**Observation 2 (HV)**	**Observation 3 (HV)**	**Mean Value (HV)**	**S/N Ratio (dB)**
S1	196.82	197.7	196.5	197.01	44.13
S2	202.55	212.55	207.55	207.55	44.58
S3	213.62	218.6	217.8	216.67	44.95
S4	209.01	210.29	211.39	210.23	44.69
S5	225.52	229.01	230.01	228.18	45.40
S6	277.52	278.52	280.52	278.85	47.15
S7	226.34	228.34	238.34	231.01	45.50
S8	303.25	309.25	307.25	306.58	47.97
S9	286.4	286.4	288.4	287.07	47.40

Microhardness measurements of some specimens are shown in Figure 5.10. All the composite specimens showed improved microhardness as compared to the unreinforced base metal specimen (maximum relative enhancement of 83% in microhardness of synthesized hybrid composite specimen S8 was observed as compared to unreinforced base metal specimen S0), due to the hardness properties of incorporated reinforcement particles (predominantly eggshell and silicon carbide particles). As compared to the unreinforced metal matrix, the presence of reinforcement particles in base metal restrained mechanical dislocations within the composites [174, 175] causing enhanced strength and hardness.

Influences of various process parameters on S/N ratio and mean response were investigated for microhardness and plotted as in Figure 5.11. Figures 5.11a, 5.11b and 5.11d display that on increasing wt.% of eggshell particles, wt.% of SiC particles and mechanical stirring time, hardness of composites was increased. Whereas, the composites hardness was decreased with increasing wt.% of Al_2O_3 particles as exhibited by plot in Figure 5.11c. It was observed from Figure 5.11 that for maximum microhardness and S/N ratio, 3rd level of eggshell particles content (A_3), 3rd level of SiC particles content (B_3), 1st level of Al_2O_3 particles content (C_1) and 3rd level of mechanical stirring time (D_3) were optimum levels. Table 5.17 represents average values of microhardness and S/N ratio for each process parameter at all levels.

Table 5.17: Response Table: Microhardness

Process Parameter	Level	Eggshell Particles wt.%		SiC Particles wt.%		Al_2O_3 Particles wt.%		Mechanical Stirring Time	
Type of Data	-	Raw Data	S/N Ratio	Raw Data	S/N Ratio	Raw Data	S/N Ratio	Raw Data	S/N Ratio
Average Values	L1	207.1	44.6	212.8	44.8	260.8	46.4	237.4	45.6
	L2	239.1	45.8	247.4	46.0	234.9	45.6	239.1	45.7
	L3	274.9	47.0	260.9	46.5	225.3	45.3	244.5	45.9
Main Effects	L2-L1	32.0	1.2	34.7	1.2	-25.9	-0.9	1.7	0.1
	L3-L2	35.8	1.2	13.4	0.5	-9.7	-0.3	5.4	0.1
Difference (L3-L2) - (L2-L1)		3.8	0.0	-21.3	-0.7	16.2	0.6	3.6	0.03
L1, L2 and L3 display the process parameter levels. (L2-L1) represents main effect while corresponding process parameter changes from level 1 to level 2. (L3-L2) denotes main effect during process parameter change from level 2 to level 3.									

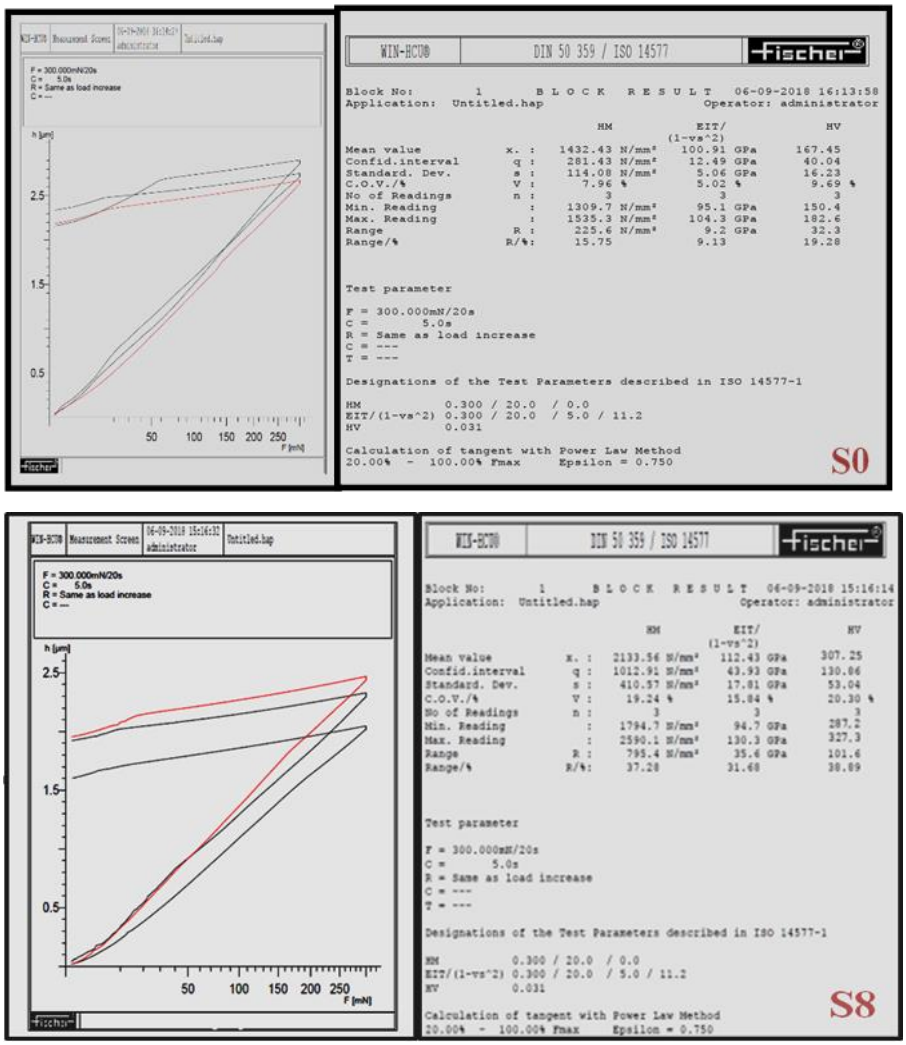

Figure 5.10: Microhardness Measurement of Some Specimens

Table 5.18 represents ANOVA results for microhardness measurements performed at 95% confidence level in terms of F-ratio and percentage contribution of various factors. Microhardness of synthesized hybrid composites appeared to be influenced significantly by eggshell particles wt.% (P=54.06%), SiC particles wt.% (P=28.96%), Al_2O_3 particles wt.% (P=15.85%) and mechanical stirring time (P=0.64%). Table 5.19 shows ANOVA values computed at 95% confidence level with F-ratio and percentage contribution for S/N ratio. To compute predicted mean of microhardness (X_{mp}), S/N ratio and mean response characteristics analysis was conducted followed by realization of optimum levels of significant factors as A_3, B_3, C_1 and D_3. In present study for microhardness of developed hybrid composites following response average components were evaluated using experimental data from Table 5.16.

$$\overline{G} = 240.35, \overline{A_3} = 274.89, \overline{B_3} = 260.86\ , \overline{C_1} = 260.81\ , \overline{D_3} = 244.5$$

$$X_{mp} = \overline{G} + \left(\overline{A_3} - \overline{G}\right) + \left(\overline{B_3} - \overline{G}\right) + \left(\overline{C_1} - \overline{G}\right) + \left(\overline{D_3} - \overline{G}\right) \quad (5.9)$$

Table 5.18: Analysis of Variance (ANOVA) for Microhardness

Factor	**Sum of Squares (SS)**	**Degrees of Freedom**	**Variance (V)**	**Percentage Contribution (P)**	**F-Ratio**
Eggshell Particles wt.%	20712.71	2	10356.36	54.06	993.18*
SiC Particles wt.%	11096.66	2	5548.33	28.96	532.09*
Al_2O_3 Particles wt.%	6073.83	2	3036.91	15.85	291.24*
Mechanical Stirring Time	245.30	2	122.65	0.64	11.76*
Others/Errors	187.69	18	10.43	0.49	-
Total	38316.19	26	-	100	-
***Significant factor at confidence level of 95%, F critical =3.55 (Value from table)**					

The pooled versions of ANOVA for microhardness raw data and S/N ratio are provided in Tables 5.20 and 5.21.

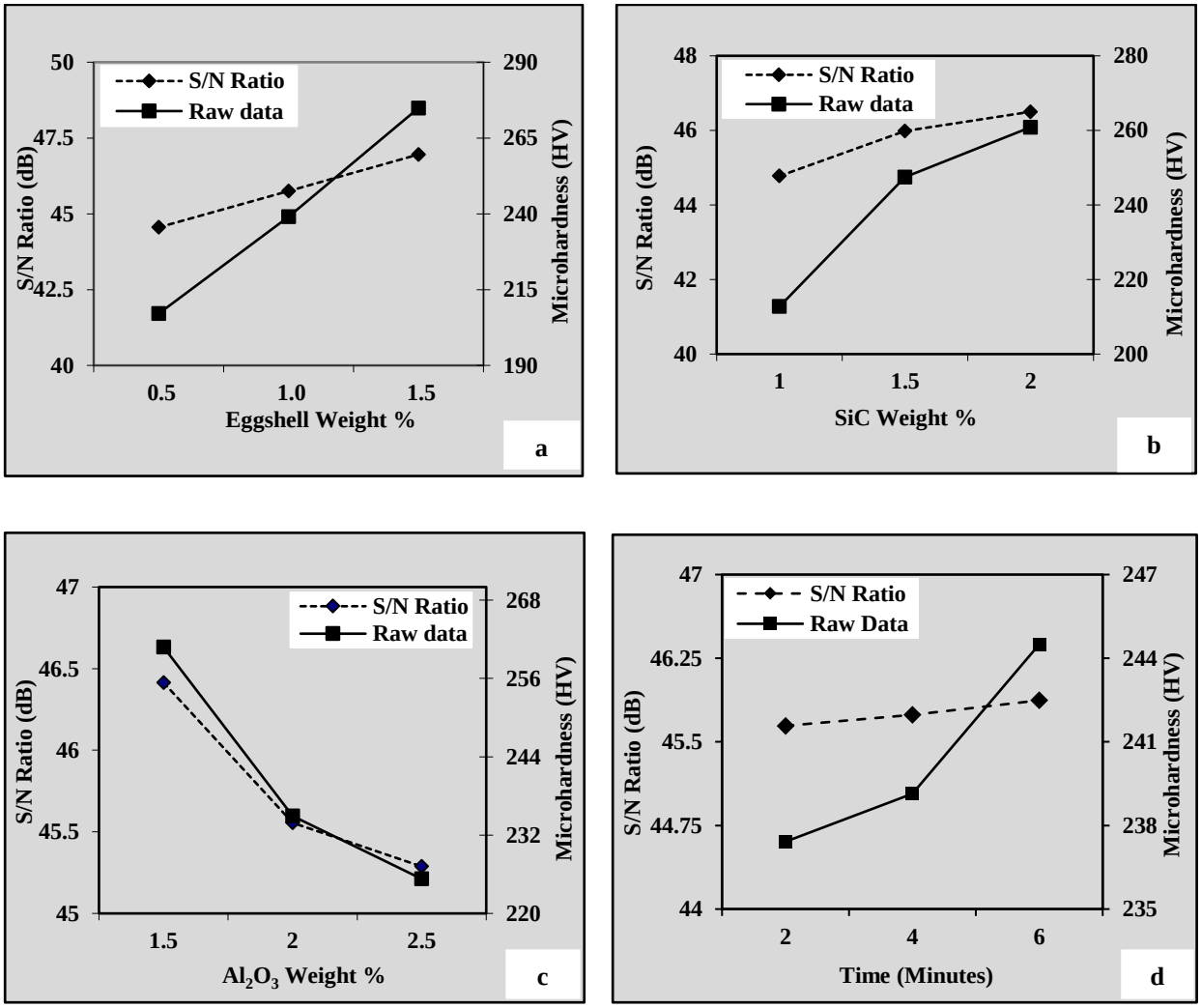

Figure 5.11: Effect of (a) Eggshell Particles wt.% (b) SiC Particles wt.% (c) Al_2O_3 Particles wt.% (d) Mechanical Stirring Time on Microhardness and S/N Ratio

Table 5.19: Analysis of Variance (ANOVA) for S/N Ratio

Factor	Sum of Squares (SS)	Degrees of Freedom	Variance (V)	Percentage Contribution (P)	F-Ratio
Eggshell Particles wt.%	8.67	2	4.34	55.85	110.31*
SiC Particles wt.%	4.70	2	2.35	30.25	59.75*
Al_2O_3 Particles wt.%	2.08	2	1.04	13.39	26.46*
Mechanical Stirring Time	0.08	-	-	-	-
Others/Errors	0.08	2	0.04	0.51	-
Total	15.53	8	-	100.00	-
***Significant factor at confidence level of 95%, F critical =19 (Value from table)**					

Table 5.20: Pooled ANOVA for Microhardness Raw Data

Factor	SS	Degrees of Freedom (Pooled)	V (Pooled)	SS'	P % (Modified)	F-Ratio
Eggshell Particles wt.%	20712.71	2	10356.36	20691.86	54.00	993.18*
SiC Particles wt.%	11096.66	2	5548.33	11075.80	28.91	532.09*
Al_2O_3 Particles wt.%	6073.825	2	3036.91	6052.97	15.80	291.24*
Mechanical Stirring Time	245.3016	2	122.65	224.45	0.59	11.76*
Others/Errors	187.6942	18	10.43	271.11	0.71	-
Total	38316.19	26	-	38316.19	100	-
***Significant factor at confidence level of 95%, F critical =3.55 (Value from table)**						

Table 5.21: Pooled ANOVA for Microhardness S/N Ratio

Factor	SS	Degrees of Freedom (Pooled)	V (Pooled)	SS'	P % (Modified)	F-Ratio
Eggshell Particles wt.%	8.67	2	4.34	8.59	55.34	110.31*
SiC Particles wt.%	4.70	2	2.35	4.62	29.75	59.75*
Al_2O_3 Particles wt.%	2.08	2	1.04	2.00	12.89	26.46*
Mechanical Stirring Time	-	-	-	-	-	-
Others/Errors	0.08	2	0.04	0.31	2.03	-
Total	15.53	8	-	15.53	100.00	-
***Significant factor at confidence level of 95%, F critical =19 (Value from table)**						

From equation 5.9, predicted mean optimum value of microhardness X_{mp} was observed to be 320.01. Table 5.18 demonstrates values of error variance (10.43) and DOF for error (18). F-ratio value at 95% confidence interval was determined from standard statistical table. The computed confidence interval (CI) using equation 5.6, was ± 5.54. Therefore, the confidence interval with respect to 95% confidence level of predicted

optimum microhardness was 314.47 < HV (Vickers Hardness Number) < 325.55. A confirmation experiment was conducted by running three more replications for microhardness of developed hybrid composites at optimal levels of significant process parameters and it was noticed that mean value of microhardness 312.28 as reported in Table 5.22 was lying within the confidence interval 314.47 < H (VHN) < 325.55.

Table 5.22: Confirmation Experiment for Microhardness

Quality characteristic	**Replications**			**Mean**
Microhardness of composites (HV)	Replication 1	Replication 2	Replication 3	
	309.43	315.55	329.85	318.28 (HV)

5.5 Tensile Strength

In order to investigate the tensile behaviour of developed hybrid aluminium composites, specimens (in three replications) were characterized as per ASTM E8-M11 for ultimate tensile strength on universal testing machine (Tinius Olsen, H 50 K-S, Cross head speed: 2.5mm/min, Strain rate : 0.002 s^{-1}), as shown in Figure 5.12. Each specimen was subjected to axial tensile load and the ultimate tensile strength values were observed. Tensile strength measurement of some specimens are shown in Figures 5.13 to 5.17, one of the fractured specimens is shown in Figure 5.18 a. The ultimate force ranged from 918 N to 1910 N and the ultimate tensile strength was observed to be increasing with infusion of reinforcement particles. Stress-strain diagrams of as-cast Al7075-T6 and composite specimens are shown in Figure 5.18 b. To analyse mean response function, S/N ratios ("larger the better" type of quality attribute) calculated from designed experimental data are expressed in Table 5.23.

Table 5.23: Observations for Tensile Strength and S/N Ratio

Tensile Strength					
Average Tensile Strength of as-cast Al7075-T6 Specimen S0: 38.3 Mpa					
Composite Specimen	**Observation 1 (Mpa)**	**Observation 2 (Mpa)**	**Observation 3 (Mpa)**	**Mean Value (Mpa)**	**S/N Ratio (dB)**
S1	36.7	35.6	38.3	36.87	29.56
S2	47.5	43.6	46.7	45.93	31.46
S3	40.9	42.9	41.9	41.90	30.68
S4	53.4	46.9	51.3	50.53	32.27
S5	46.3	59.1	51.8	52.40	32.50
S6	72.3	63.8	55.7	63.93	34.21
S7	43.1	50.1	36.7	43.30	30.76
S8	82.1	79.5	75.1	78.90	36.16
S9	48.7	54.1	58.2	53.67	32.76

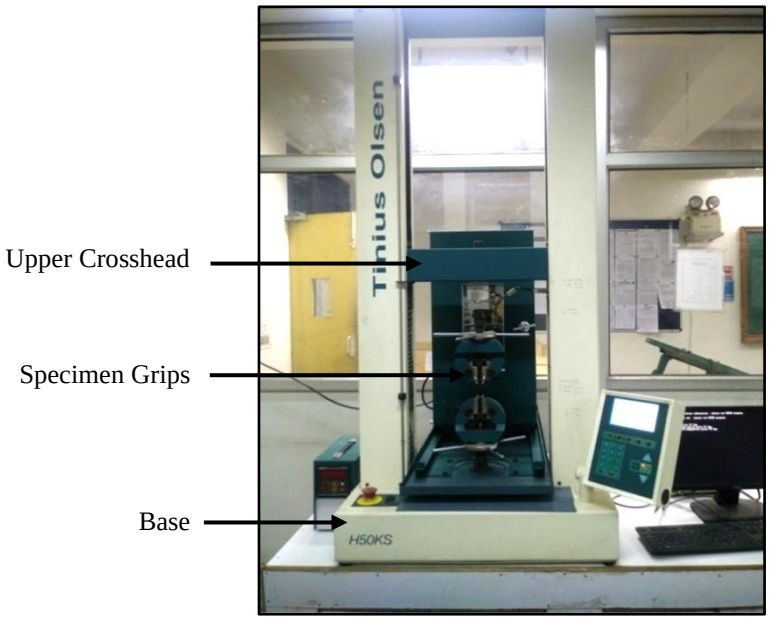

Figure 5.12: Universal Testing Machine

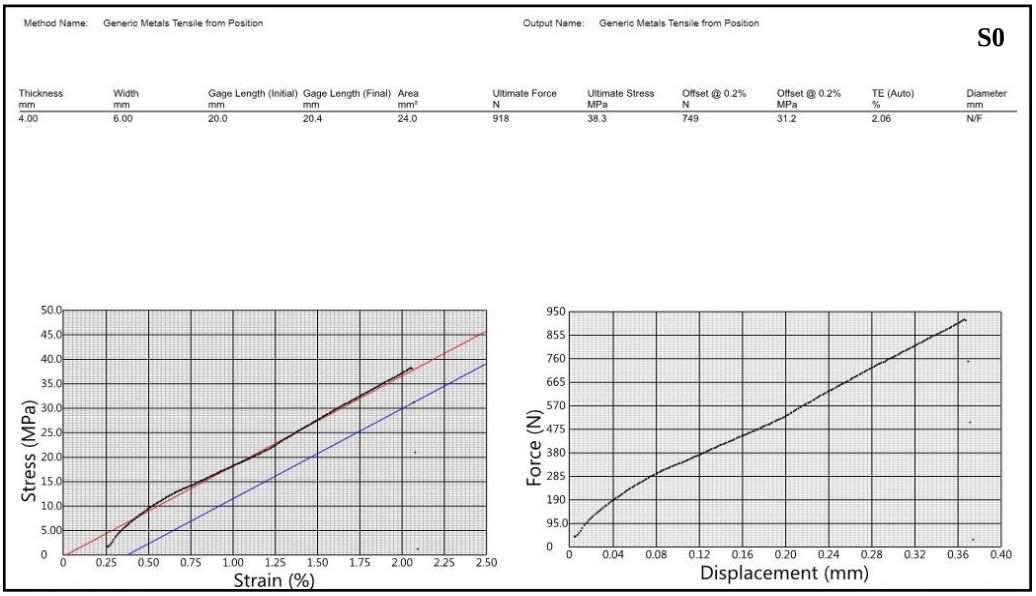

Figure 5.13: Tensile Strength Measurement of Specimen S0

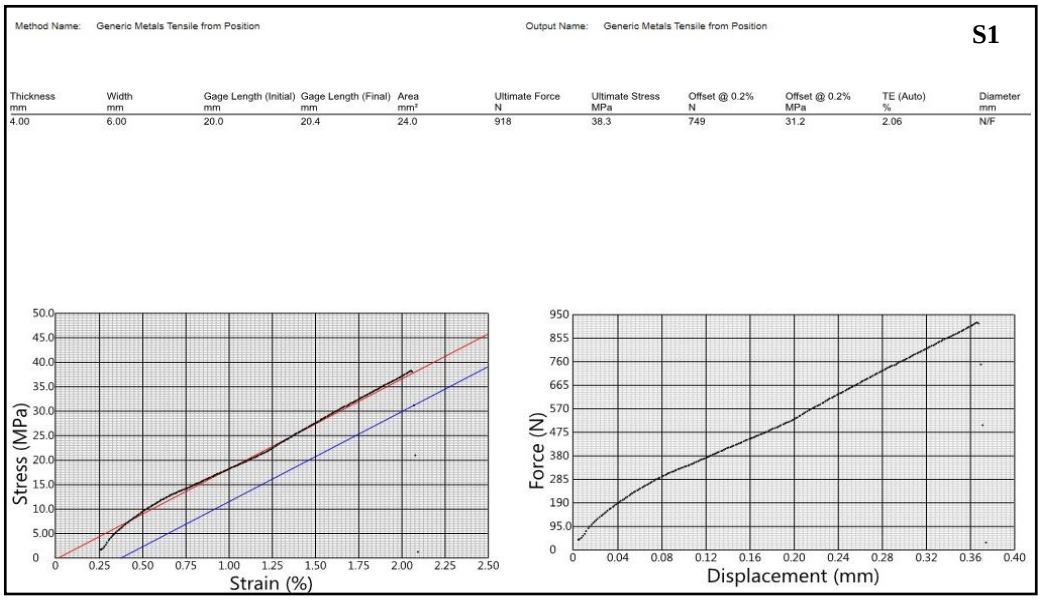

Figure 5.14: Tensile Strength Measurement of Specimen S1

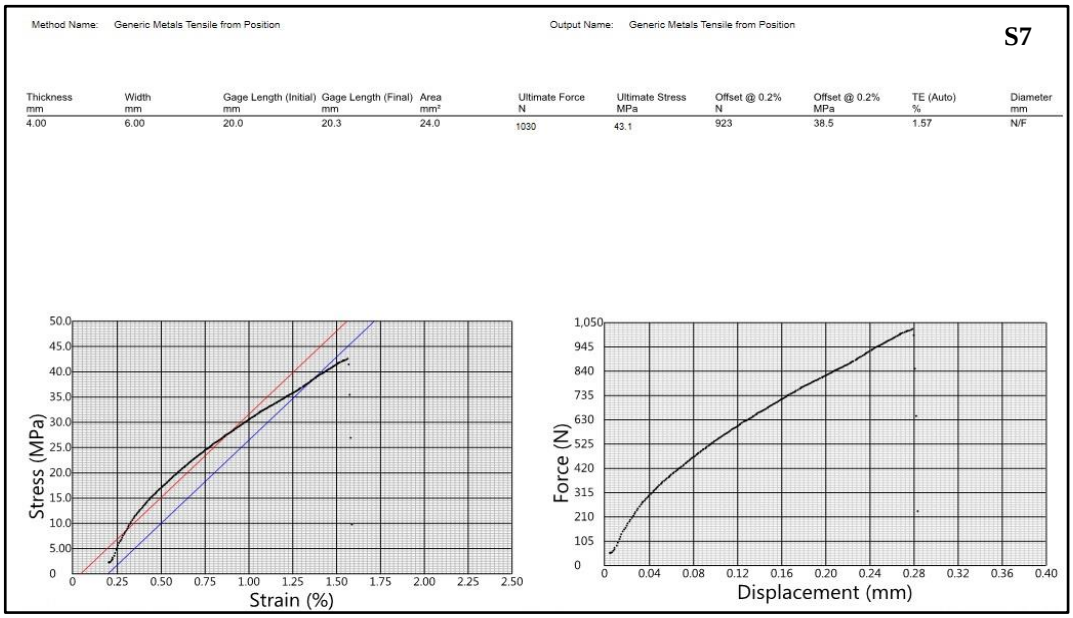

Figure 5.15: Tensile Strength Measurement of Specimen S7

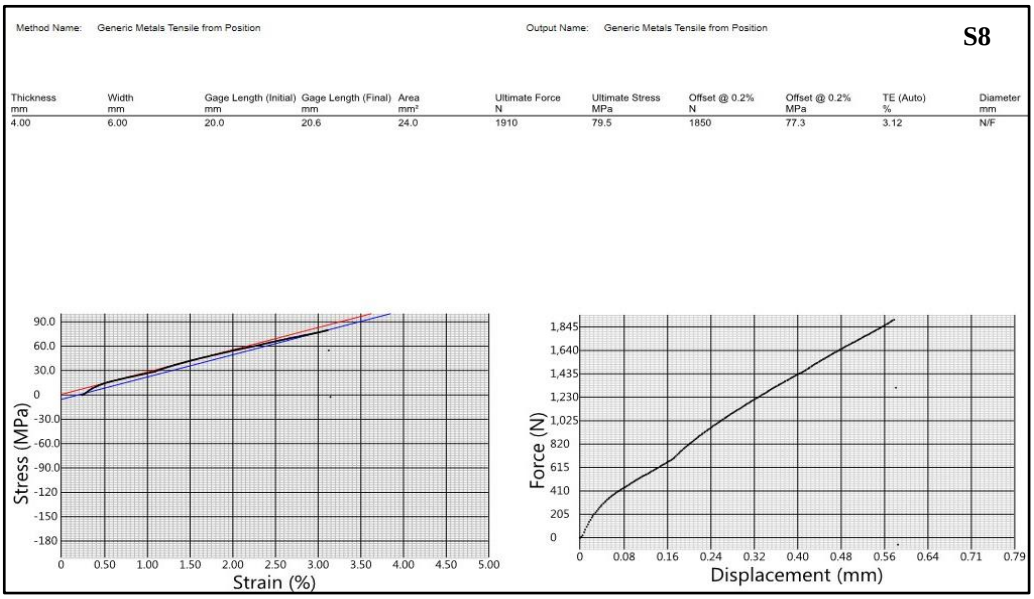

Figure 5.16: Tensile Strength Measurement of Specimen S8

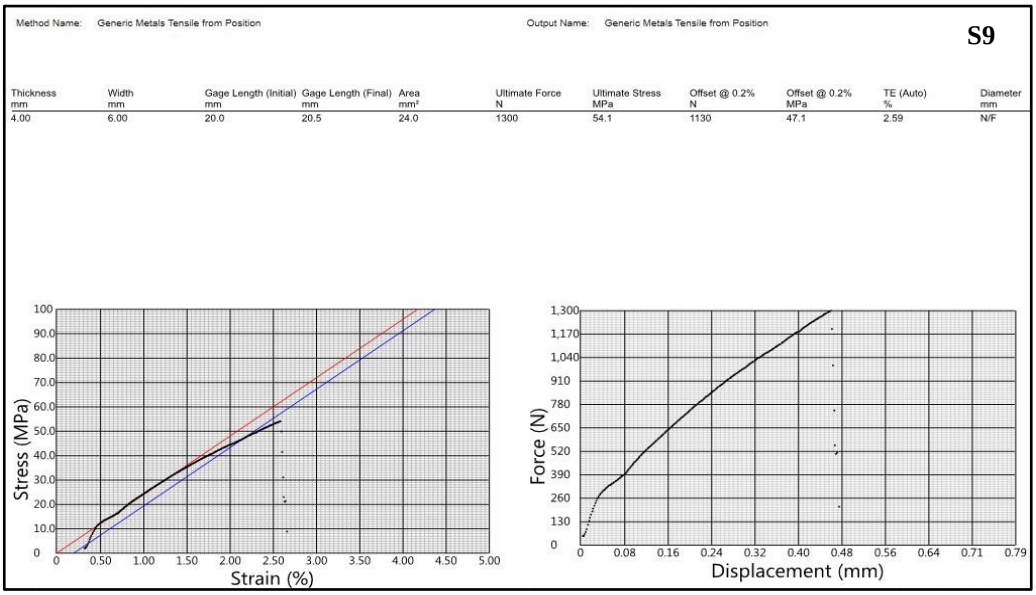

Figure 5.17: Tensile Strength Measurement of Specimen S9

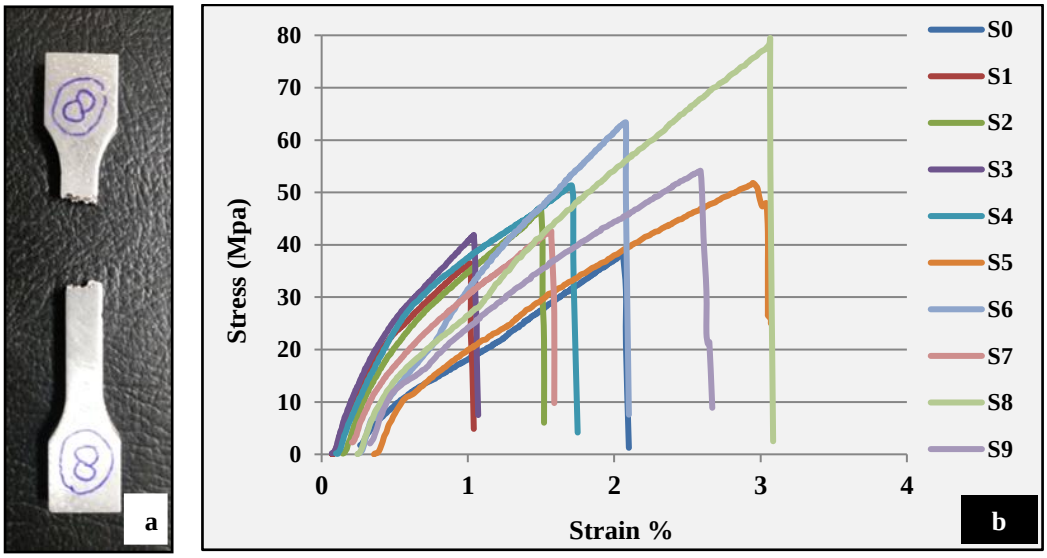

Figure 5.18: (a)Fractured Tensile Test Specimen (b) Stress-Strain Diagrams

Analysis of variance was performed to observe the impact of control factors on quality attribute. The effects of process parameters on tensile strength and S/N ratio have been plotted in Figure 5.19**.** Figures 5.19a, 5.19b and 5.19d display that on increasing wt.% of eggshell particles, wt.% of SiC particles and mechanical stirring time, tensile strength of composites was increased. Whereas plot in Figure 5.19c exhibits that composites tensile strength was decreased with increasing wt.% of Al_2O_3 particles. Table 5.24 represents average values of tensile strength and S/N ratio for each process parameter at all levels.

Table 5.24: Response Table: Tensile Strength

Process Parameter	**Level**	**Eggshell Particles wt.%**		**SiC Particles wt.%**		**Al_2O_3 Particles wt.%**		**Mechanical Stirring Time**	
Type of Data	-	Raw Data	S/N Ratio	Raw Data	S/N Ratio	Raw Data	S/N Ratio	Raw Data	S/N Ratio
Average Values	L1	41.6	30.6	43.6	30.9	59.9	33.3	47.6	31.6
	L2	55.6	33.0	59.1	33.4	50.0	32.2	51.1	32.1
	L3	58.6	33.2	53.2	32.6	45.9	31.3	57.1	33.0
Main Effects	L2-L1	14.1	2.4	15.5	2.5	-9.9	-1.1	3.4	0.5
	L3-L2	3.0	0.2	-5.9	-0.8	-4.2	-0.9	6.1	0.9
Difference (L3-L2) - (L2-L1)		-11.1	-2.2	-21.4	-3.3	5.7	0.3	2.6	0.4
L1, L2 and L3 display the process parameter levels. (L2-L1) represents main effect while corresponding process parameter changes from level 1 to level 2. (L3-L2) denotes main effect during process parameter change from level 2 to level 3.									

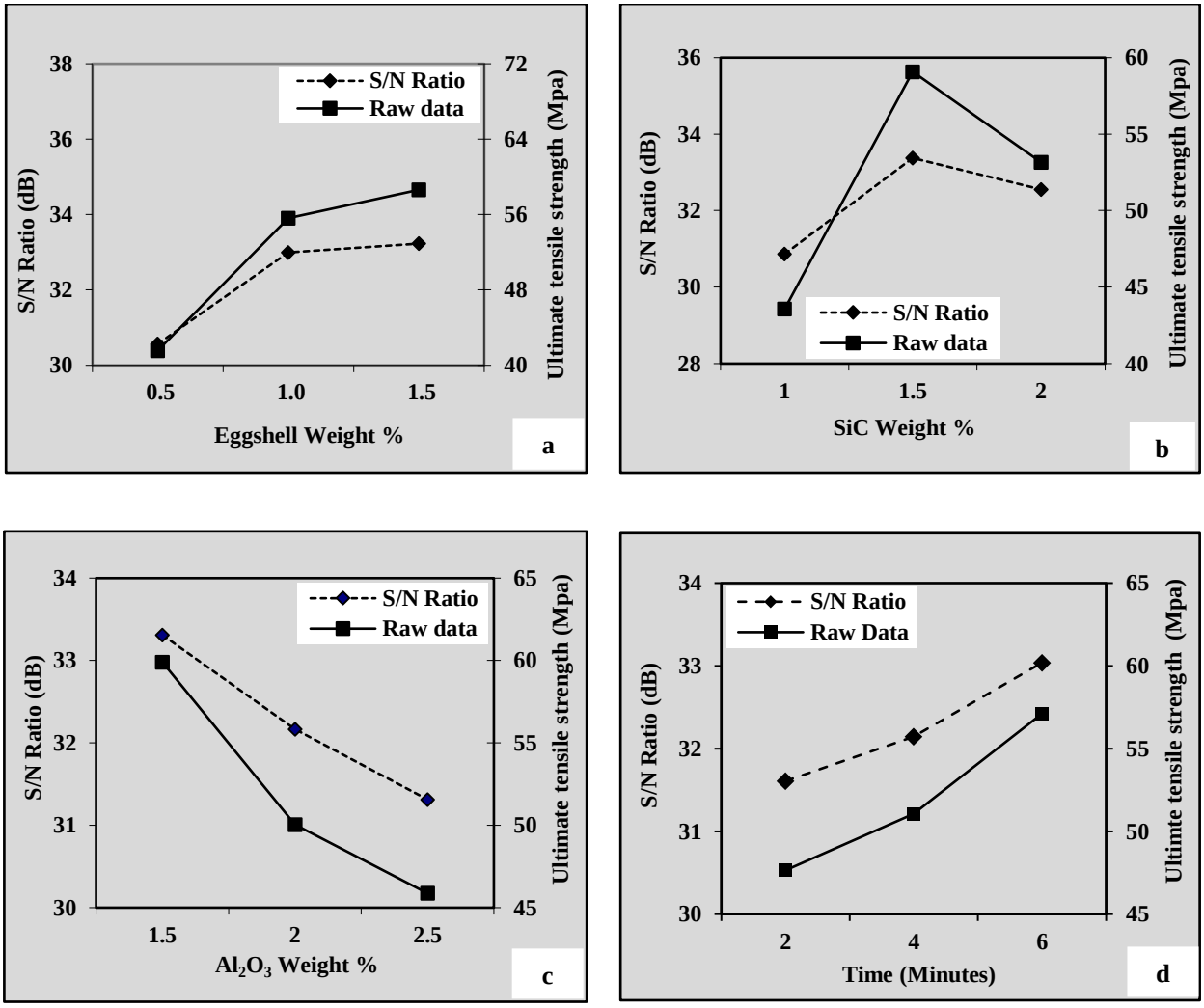

Figure 5.19: Effect of (a) Eggshell Particles wt.% (b) SiC Particles wt.% (c) Al_2O_3 Particles wt.% (d) Mechanical Stirring Time on Tensile Strength and S/N Ratio

Table 5.25 demonstrates ANOVA results at 95% confidence level in terms of F-ratio and percentage contribution of process parameters. Control factors eggshell content with percentage contribution P=34.22%, silicon carbide content with percentage contribution P=25.30%, aluminium oxide content with percentage contribution P=21.43% and mechanical stirring time with percentage contribution P=9.49% had perceptible influence on tensile strength of hybrid composites. By analysing S/N ratio and mean response characteristic, significant control value optimum levels were identified as A_3, B_2, C_1 and D_3.

Table 5.25: Analysis of Variance (ANOVA) for Tensile Strength

Factor	Sum of Squares (SS)	Degrees of Freedom	Variance (V)	Percentage Contribution (P)	F-Ratio
Eggshell Particles wt.%	1492.35	2	746.18	34.22	32.23*
SiC Particles wt.%	1103.09	2	551.54	25.30	23.82*
Al_2O_3 Particles wt.%	934.56	2	467.28	21.43	20.18*
Mechanical Stirring Time	413.77	2	206.88	9.49	8.94*
Others/Errors	416.73	18	23.15	9.56	-
Total	4360.50	26	-	100.00	-
***Significant factor at confidence level of 95%, F critical =3.55 (Value from table)**					

Table 5.26 presents ANOVA computation at 95% confidence level with F-ratio and percentage contribution for S/N ratio.

Table 5.26: Analysis of Variance (ANOVA) for S/N Ratio

Factor	Sum of Squares (SS)	Degrees of Freedom	Variance (V)	Percentage Contribution (P)	F-Ratio
Eggshell Particles wt.%	13.01	2	6.51	40.66	4.15
SiC Particles wt.%	9.83	2	4.91	30.70	3.13
Al_2O_3 Particles wt.%	6.03	2	3.02	18.84	1.92
Mechanical Stirring Time	3.14	-	-	-	-
Others/Errors	3.14	2	1.57	9.80	-
Total	32.01	8	-	100.00	-
No significant factor at confidence level of 95%, F critical =19 (Value from table)					

The pooled versions of ANOVA for tensile strength raw data and S/N ratio are demonstrated in Tables 5.27 and 5.28.

Table 5.27: Pooled ANOVA for Tensile Strength Raw Data

Factor	SS	Degrees of Freedom (Pooled)	V (Pooled)	SS'	P % (Modified)	F-Ratio
Eggshell Particles wt.%	1492.35	2	746.18	1446.05	33.16	32.23*
SiC Particles wt.%	1103.09	2	551.54	1056.78	24.24	23.82*
Al_2O_3 Particles wt.%	934.56	2	467.28	888.26	20.37	20.18*
Mechanical Stirring Time	413.77	2	206.88	367.47	8.43	8.94*
Others/Errors	416.73	18	23.15	601.95	13.80	-
Total	4360.50	26	-	4360.50	100	-
***Significant factor at confidence level of 95%, F critical =3.55 (Value from table)**						

Table 5.28: Pooled ANOVA for Tensile Strength S/N Ratio

Factor	SS	Degrees of Freedom (Pooled)	V (Pooled)	SS'	P % (Modified)	F-Ratio
Eggshell Particles wt.%	13.01	2	6.51	9.88	30.87	4.15
SiC Particles wt.%	9.83	2	4.91	6.69	20.90	3.13
Al_2O_3 Particles wt.%	6.03	2	3.02	2.89	9.04	1.92
Mechanical Stirring Time	-	-	-	-	-	-
Others/Errors	3.14	2	1.57	12.54	39.19	-
Total	32.01	8	-	32.01	100	-
No significant factor at confidence level of 95%, F critical =19 (Value from table)						

For estimation of predicted mean of tensile strength (X_{mp}), equation 5.10 is used after putting the values of following response average components from Table 5.23:

$\overline{G} = 51.94, \overline{A_3} = 58.6, \overline{B_2} = 59.1\ , \overline{C_1} = 59.9, \overline{D_3} = 57.1$

$$X_{mp} = \overline{G} + \left(\overline{A_3} - \overline{G}\right) + \left(\overline{B_2} - \overline{G}\right) + \left(\overline{C_1} - \overline{G}\right) + \left(\overline{D_3} - \overline{G}\right) \quad (5.10)$$

From equation 5.10, predicted mean optimum value of tensile strength X_{mp} was computed to be 78.9 Mpa. Table 5.25 shows error variance= 23.15 and DOF for error =18. For F-ratio evaluation at 95% confidence interval standard statistical table was used. The calculated confidence interval (CI) using equation 5.6, was ± 8.25. Hence the confidence interval with respect to 95% confidence level of predicted optimum tensile strength was 70.6 < Tensile Strength (TS in Mpa) < 87.2. It was followed by a confirmation experiment by running three more replications for tensile strength of developed hybrid composites at optimal levels of significant process parameters and it was observed that mean value of tensile strength 67.94 Mpa as reported in Table 5.29 was lying within the confidence interval 70.6 < TS (Mpa) < 87.2.

Table 5.29: Confirmation Experiment for Tensile Strength

Quality Characteristic	**Replications**			**Mean**
Tensile Strength of Composites (Mpa)	Replication 1	Replication 2	Replication 3	
	68.26	75.32	75.25	72.94 Mpa

SEM micrographs of fractured tensile test specimens are shown below, in Figure 5.20.

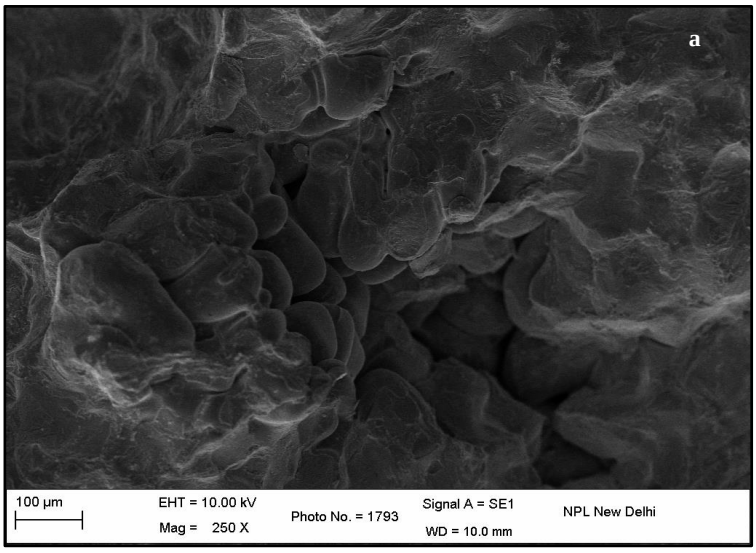

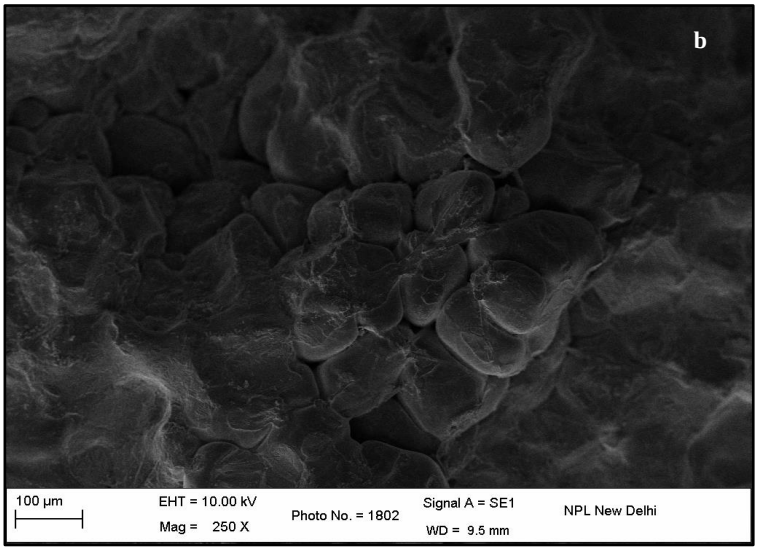
b
100 µm
EHT = 10.00 kV
Mag = 250 X
Photo No. = 1802
Signal A = SE1
WD = 9.5 mm
NPL New Delhi

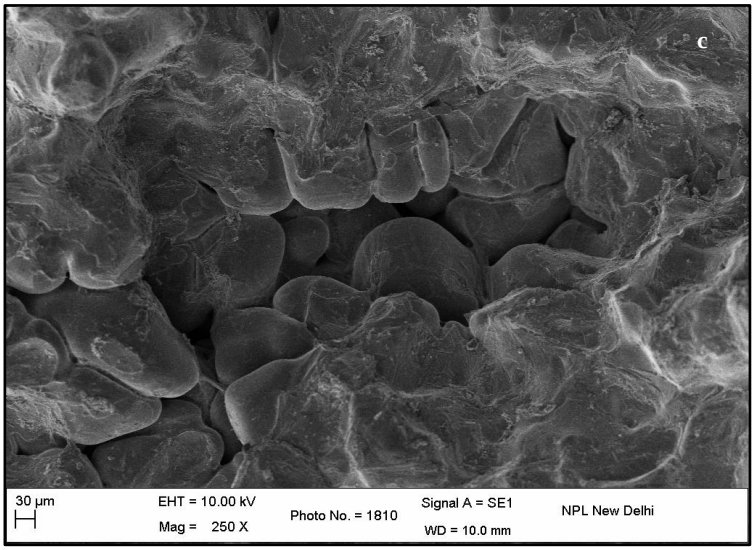
c
30 µm
EHT = 10.00 kV
Mag = 250 X
Photo No. = 1810
Signal A = SE1
WD = 10.0 mm
NPL New Delhi

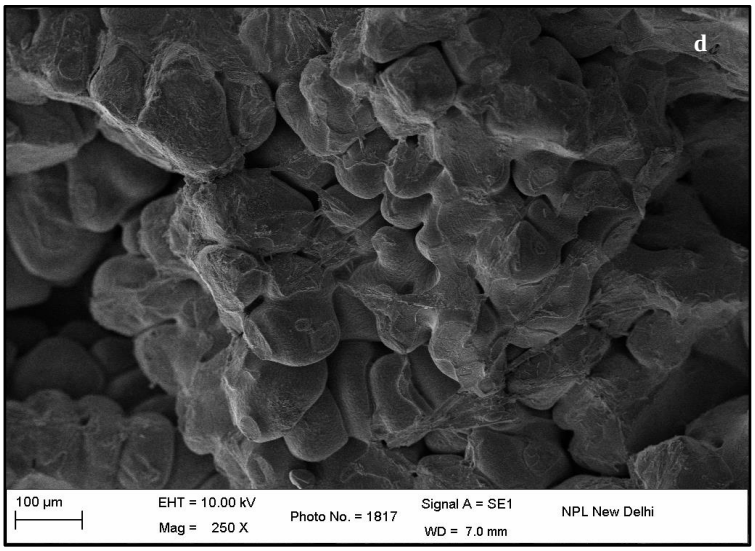
d
100 µm
EHT = 10.00 kV
Mag = 250 X
Photo No. = 1817
Signal A = SE1
WD = 7.0 mm
NPL New Delhi

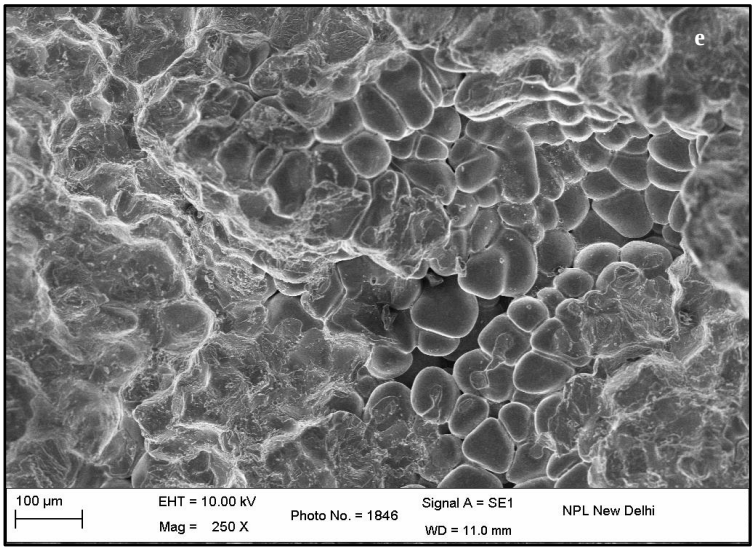
e
100 µm
EHT = 10.00 kV
Mag = 250 X
Photo No. = 1846
Signal A = SE1
WD = 11.0 mm
NPL New Delhi

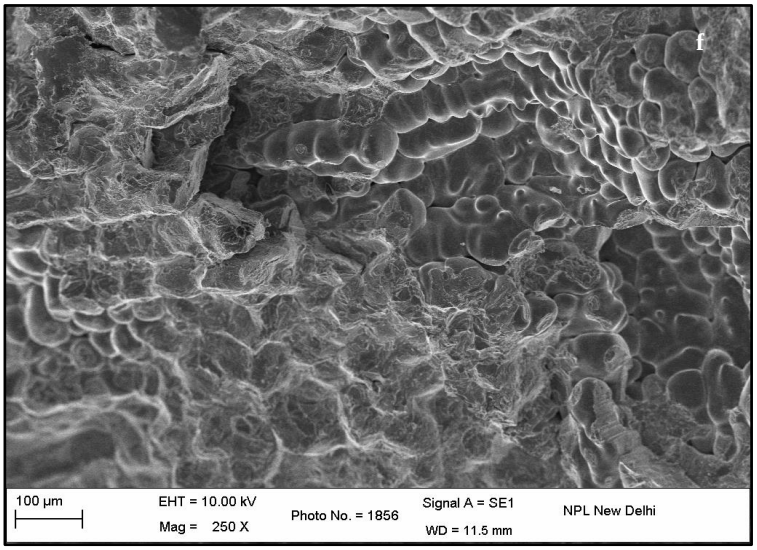
f
100 µm
EHT = 10.00 kV
Mag = 250 X
Photo No. = 1856
Signal A = SE1
WD = 11.5 mm
NPL New Delhi

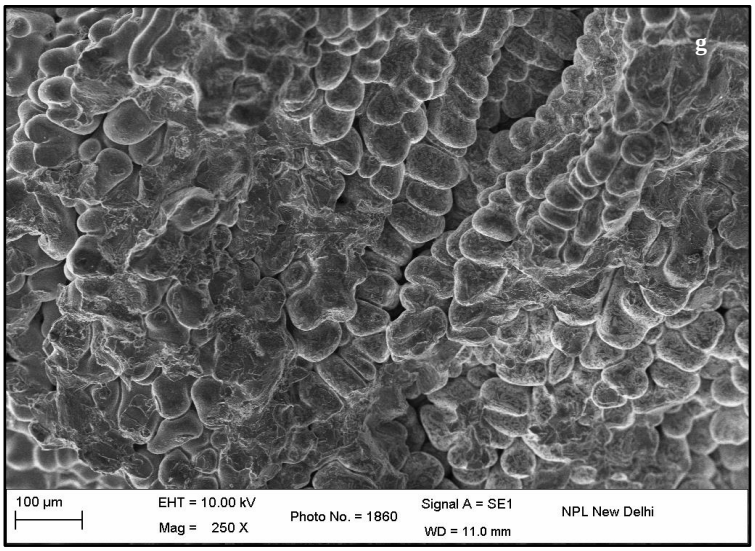
g
100 µm
EHT = 10.00 kV
Mag = 250 X
Photo No. = 1860
Signal A = SE1
WD = 11.0 mm
NPL New Delhi

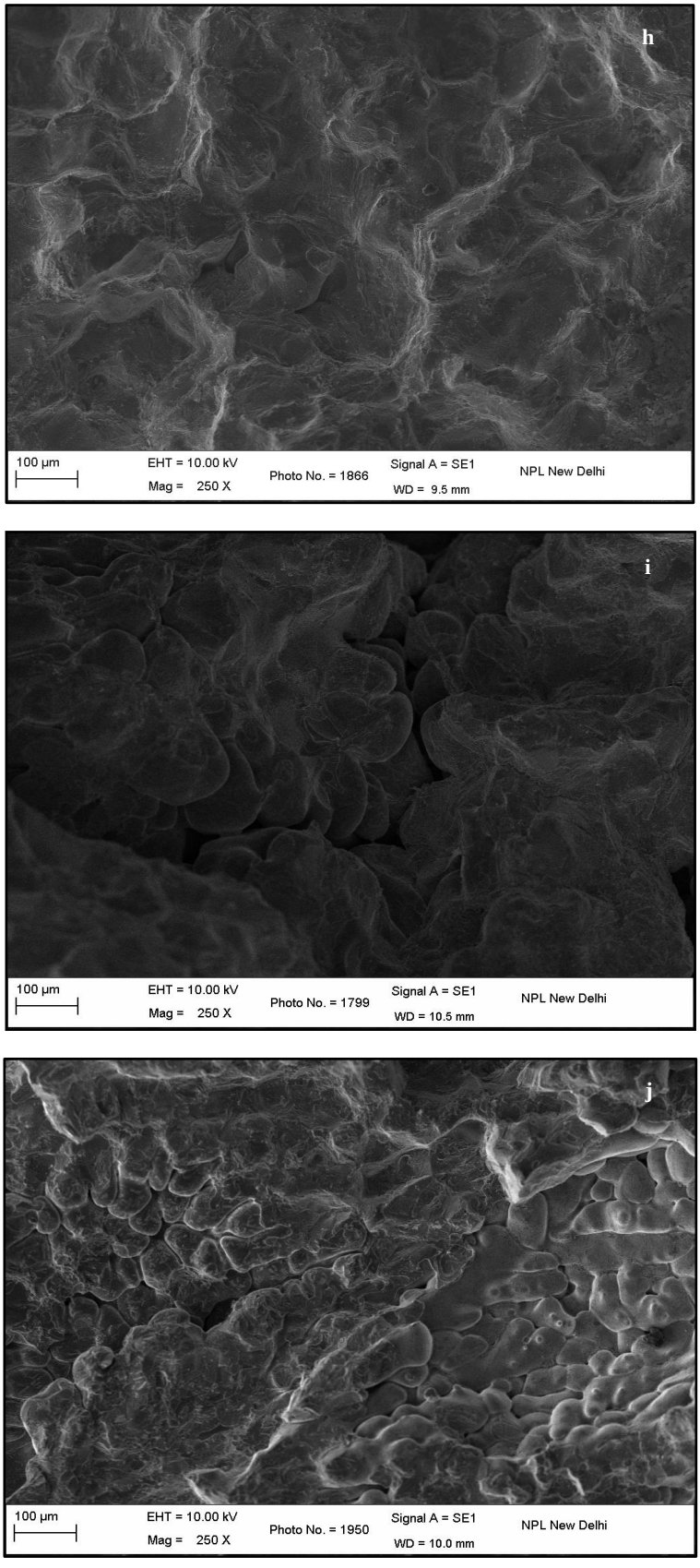

Figure 5.20: SEM Micrographs of Fractured Surfaces of Composite Specimens (a) S0 (b) S1 (c) S2 (d) S3 (e) S4 (f) S5 (g) S6 (h) S7 (i) S8 (j) S9 After Tensile Test

In synthesized hybrid aluminium metal matrix composites, there may be potential existence of grain boundary strengthening due to infusion of reinforcement particles. Grain boundaries in any material are indomitable borders for dislocations. The count of dislocations in a grain influences the stress on adjacent grain, activating the dislocation source and endorsing deformations in adjacent grain. In present investigation, by altering the grain size, number of dislocations accumulated on grain boundaries could be influenced significantly. The grain boundaries behaved as pinning points for dislocations, impeding their mobility in a continuous slip plane, hindering the plasticity and providing strength to material [176]. Formation of second phases during casting process and non-uniform distribution of reinforcement particles influenced the fracture mechanism significantly. Fracture behaviour of present hybrid aluminium composites was largely governed by different strain carrying capabilities of hard and brittle reinforcement particles and soft and ductile aluminium base alloy and the difference in thermal coefficient of expansion of the two phases. The difference in strain carrying capabilities caused stress concentrations near reinforcement particles and intermetallics etc. separating reinforcements from adjacent matrix material, resulting into decohesion. Additionally, degree of agglomeration, reinforcement particle sizes and local plastic constraints also contributed into material failure.

Dislocations at matrix-reinforcement interface were induced due to thermal mismatch between the two phases. These dislocations interacted with other dislocations, reinforcement particles and precipitates, causing dislocation movement resulting into formation of dimples on fracture surfaces. Evolution and coalescence of numerous micro-voids nucleated at various grain boundaries, dislocations and inclusions, also created these cup-shape depressions. In present investigation, the fractured surfaces were appeared dull and dimpled, exhibiting cup-cone mode of fracture which substantiated that the fracture occurred with a crack initiation.

The fracture was noticed to be predominantly ductile in nature (dimple rupture), indicating that necking of tensile test specimen under axial load eventuated before the metal matrix failure took place. The dimple sizes were observed to be proportional to strength and ductility, finer dimples led to higher

strength and ductility as in case of specimens S5 and S8. However, in case of hybrid composites specimen S7, reduced ductility may be due to infusion of hard eggshell, SiC and Al_2O_3 particles concentrating stress at metal matrix-reinforcement interface and localizing crack initiation resulting into brittleness. On applying load, the micro-voids grew till the activation of coalescence mechanism (due to elongation of voids), leading towards complete material failure. Ultimate fracture of test specimens was critically controlled through inclusion of hard reinforcement particles, restricting sources of micro-voids and dimples on various fractured surfaces [177]. On exerting external axial load on hybrid aluminium composite specimens, the reinforcement particles acted as load bearing agents, transferring reduced loads to metal matrix, hence increasing the strength of composites as compared to unreinforced base metal. Increase in tensile strength of composites may be attributed to precipitation during their synthesis. On exerting external load, the dislocations got entangled and interacted through orowan strengthening mechanism, increasing material's strength. Orowan strengthening mechanism is related to precipitation hardening, where the metal melt produced fine particles which impeded dislocation's movements. The precipitate particles made dislocations bow around them, restricting their passing and making material stronger.

Some of the micrographs of fractured surfaces also demonstrated de-cohesive rupture (in specimens S4, S5 and S6), caused due to rupture of protective layers surrounding reinforcement particles. Localized quasi-cleavage fracture modes, displaying properties of both plastic deformation and cleavage were observed in fractured surfaces of specimens S1, S2 and S3. Combination of de-cohesive and quasi-cleavage fracture modes was observed in micrograph of specimen S7 [178]. In exceptional case, ultimate tensile strength of a composite specimen S1 was observed to be lesser than that of base metal (specimen S0) and it may be as a result of formation of loosely bound reinforcement particle micro-clusters due to some agglomeration and porosity. Some detached reinforcement particles were also noticed due to the breakage of bonds between metal matrix and reinforcements. It was ascertained from present experimental data that as percentage porosity increased, hardness and tensile strength of fabricated hybrid

composites decreased due to failure inception from voids within composites. Here as- cast Al7075-T6 specimen S0 with maximum percentage porosity showed lower microhardness and tensile strength whereas hybrid composite specimen S8 with higher reinforcement contents, longer stirring time and lesser percentage porosity demonstrated higher microhardness and tensile strength.

5.6 Fatigue Life

Standard fatigue test specimens were fabricated as per ASTM E 468/606 (in three replications) for rotating beam fatigue test with a fixed load of 2 kg, constant speed of 500 rpms and various fatigue parameters as given in Table 5.30. As-cast Al7075-T6 standard fatigue specimen along with nine hybrid aluminium composite standard specimens, in three replications were investigated for fatigue life on rotating beam fatigue testing machine (as shown in Figure 5.21). Fatigue test observations corresponding to three replications of developed hybrid composite specimens with respective S/N ratios for "larger the better" type of quality characteristic are given in Table 5.31. Low cycle fatigue life of various specimens was enhanced significantly as compared to their unreinforced counterpart (specimen S0). Graphs in Figure 5.22 exhibit the influence of different control factors on S/N ratio and fatigue life of synthesized hybrid composites. For maximum fatigue life (in terms of reversible load cycles survived) and S/N ratio, optimum control factor levels are A_3, B_2, C_1 and D_3. Average number of load cycles survived and S/N ratios for each process parameter at all levels are displayed by Table 5.32.

Table 5.30: Fatigue Test Parameters

Load (kg)	2
Load (N)	19.6
Gauge Cross Sectional Area (mm^2)	45.58
Stress (N/mm^2)	0.43
Stress (Mpa)	0.43
Maximum Stress (Mpa)	0.43
Minimum Stress (Mpa)	-0.43
Mean Stress (Mpa)	0
Stress Range (Mpa)	0.86
Stress Amplitude (Mpa)	0.43
Stress Ratio	-1

Figure 5.21: Rotating Beam Fatigue Testing Machine and

Table 5.31: Observations for Reversible Load Cycles Survived and S/N Ratio

Load Cycles Survived					
Load Cycles Survived by as-cast Al7075-T6 Specimen S0: 94 Cycles					
Composite Specimen	**Observation 1 (Cycles)**	**Observation 2 (Cycles)**	**Observation 3 (Cycles)**	**Mean Value (Cycles)**	**S/N Ratio (dB)**
S1	234	240	236	236.67	45.72
S2	310	305	314	309.67	48.06
S3	360	359	342	353.67	49.20
S4	483	470	486	479.67	51.86
S5	522	520	525	522.33	52.60
S6	630	654	650	644.67	54.42
S7	2415	2398	2418	2410.33	65.88
S8	4556	4563	4569	4562.67	71.42
S9	1960	1969	1973	1967.33	64.12

Table 5.32: Response Table: Fatigue Life

Process Parameter	**Level**	**Eggshell Particles wt.%**		**SiC Particles wt.%**		**Al_2O_3 Particles wt.%**		**Mechanical Stirring Time**	
Type of Data	-	Raw Data	S/N Ratio	Raw Data	S/N Ratio	Raw Data	S/N Ratio	Raw Data	S/N Ratio
Average Values	L1	300	47.7	1042.2	54.5	1814.7	57.2	908.8	54.1
	L2	548.9	52.9	1798.2	57.4	918.9	54.7	1121.6	56.1
	L3	2980.1	67.1	988.6	55.9	1095.4	55.9	1798.7	57.5
Main Effects	L2-L1	248.9	5.3	756.0	2.9	-895.8	-2.5	212.8	2.0
	L3-L2	2431.2	14.2	-809.7	-1.4	176.6	1.2	677.1	1.4
Difference (L3-L2) - (L2-L1)		2182.3	8.9	-1566	-4.3	1072.3	3.7	464.3	-0.6
L1, L2 and L3 display the process parameter levels. (L2-L1) represents main effect while corresponding process parameter changes from level 1 to level 2. (L3-L2) denotes main effect during process parameter change from level 2 to level 3.									

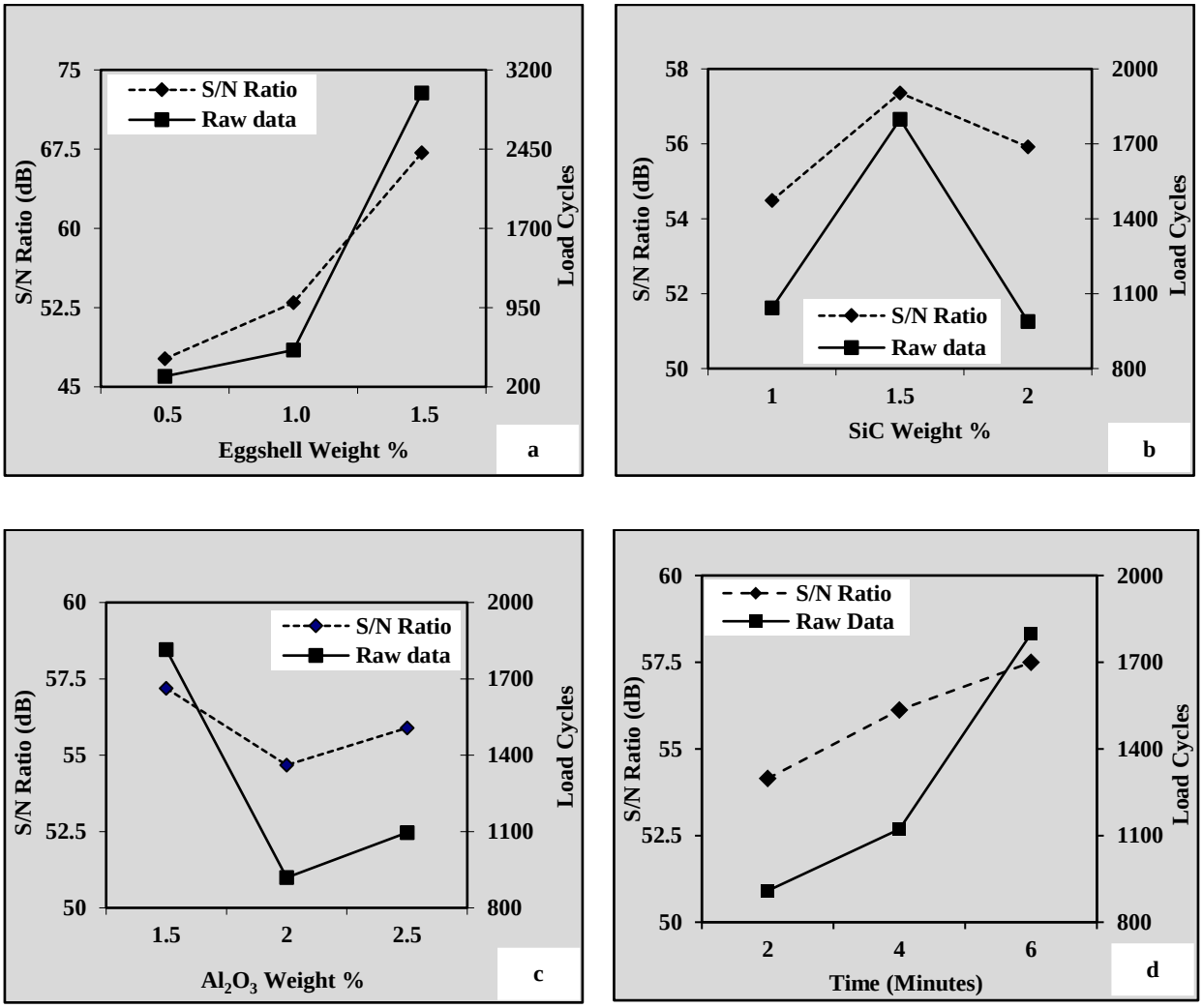

Figure 5.22: Effect of (a) Eggshell Particles wt.% (b) SiC Particles wt.% (c) Al_2O_3 Particles wt.% (d) Mechanical Stirring Time on Fatigue Life and S/N Ratio

ANOVA results in terms of F-ratio and percentage contribution of different process parameters, computed at a confidence level of 95% are given in Table 5.33. It can be interpreted that all the four process parameters eggshell particles wt.% with percentage contribution P=77.24%, SiC particles wt.% with percentage contribution P=7.22%, Al_2O_3 particles wt.% with percentage contribution P=7.93% and mechanical stirring time with percentage contribution P=7.61% had significant influence on low cycle fatigue life of synthesized hybrid composites.

Table 5.33: Analysis of variance (ANOVA) for Fatigue Life

Factor	Sum of Squares (SS)	Degrees of Freedom	Variance (V)	Percentage Contribution (P)	F-Ratio
Eggshell Particles wt.%	39467348.22	2	19733674.1	77.24	306741.05*
SiC Particles wt.%	3689928.67	2	1844964.33	7.22	28678.20*
Al_2O_3 Particles wt.%	4052610.89	2	2026305.44	7.93	31496.98*
Mechanical Stirring Time	3886968.22	2	1943484.11	7.61	30209.60*
Others/Errors	1158	18	64.33	0.002	-
Total	51098014	26	-	100	-
***Significant factor at confidence level of 95%, F critical =3.55 (Value from table)**					

Table 5.34 demonstrates AVONA results for S/N ratio established at 95% confidence level for F-ratio and percentage contribution.

Table 5.34: Analysis of variance (ANOVA) for S/N Ratio

Factor	Sum of Squares (SS)	Degrees of Freedom	Variance (V)	Percentage Contribution (P)	F-Ratio
Eggshell Particles wt.%	608.68	2	304.34	94.00	64.23*
SiC Particles wt.%	12.39	2	6.19	1.91	1.31
Al_2O_3 Particles wt.%	9.48	-	-	-	-
Mechanical Stirring Time	17.01	2	8.50	2.63	1.79
Others/Errors	9.48	2	4.74	1.46	-
Total	647.55	8	-	100.00	-
***Significant factor at confidence level of 95%, F critical =19 (Value from table)**					

Table 5.35 and 5.36 display pooled versions of ANOVA for fatigue life raw data and S/N ratio.

Table 5.35: Pooled ANOVA for Fatigue Life Raw Data

Factor	SS	Degrees of Freedom (Pooled)	V (Pooled)	SS'	P % (Modified)	F-Ratio
Eggshell Particles wt.%	39467348.2	2	19733674	39467219.6	77.24	306741.1*
SiC Particles wt.%	3689928.7	2	1844964.3	3689800.0	7.22	28678.2*
Al_2O_3 Particles wt.%	4052610.9	2	2026305.4	4052482.2	7.93	31496.9*
Mechanical Stirring Time	3886968.2	2	1943484.1	3886839.6	7.61	30209.6*
Others/ Errors	1158.0	18	64.33	1672.67	0.00	-
Total	51098014.0	26	-	51098014.0	100	-
***Significant factor at confidence level of 95%, F critical =3.55 (Value from table)**						

Table 5.36: Pooled ANOVA for Fatigue Life S/N Ratio

Factor	SS	Degrees of Freedom (Pooled)	V (Pooled)	SS'	P % (Modified)	F-Ratio
Eggshell Particles wt.%	608.68	2	304.34	599.2	92.53	64.23*
SiC Particles wt.%	12.39	2	6.19	2.91	0.45	1.31
Al_2O_3 Particles wt.%	-	-	-	-	-	-
Mechanical Stirring Time	17.01	2	8.50	7.53	1.16	1.79
Others/Errors	9.48	2	4.74	37.9	5.9	-
Total	647.55	8	-	647.55	100	-
***Significant factor at confidence level of 95%, F critical =19 (Value from table)**						

S/N ratio and mean response characteristics analysis was carried out using optimum levels of significant factors as A_3, B_2, C_1 and D_3 for prediction of load cycles survived (X_{mp}) using equation 5.11.

Following components were evaluated using experimental data from Table 5.31.

$\overline{G} = 1276.33$, $\overline{A_3} = 2980.11$, $\overline{B_2} = 1798.22$, $\overline{C_1} = 1814.67$ and $\overline{D_3} = 1798.67$

$$Z_{mp} = \overline{G} + \left(\overline{A_3} - \overline{G}\right) + \left(\overline{B_2} - \overline{G}\right) + \left(\overline{C_1} - \overline{G}\right) + \left(\overline{D_3} - \overline{G}\right) \quad (5.11)$$

Predicted mean optimum value of low cycle fatigue life in terms of number of load cycles survived by composites X_{mp} = 4562 was obtained using equation 5.11. From Table 5.33, error variance = 64.33 and DOF for error =18 were observed. At 95% confidence interval, F-ratio value was determined from standard statistical table and the confidence interval (CI) calculated from equation 5.6, was ± 14. Confidence interval for predicted optimum load cycles survived with respect to 95% confidence level was 4562 ±14, i.e. 4548 < load cycles survived (LCS) < 4576. Further a confirmation experiment was conducted by running three additional replications for fatigue life in synthesized composites at optimal levels of prevalent process parameters. Confirmation experiment observations are given in Table 5.37 and it was recorded that mean number of load cycles survived by composite were 4568, falling within the confidence interval i.e. 4548 < LCS < 4576, hence being in good agreement with Taguchi optimization technique.

Table 5.37: Confirmation Experiment for Fatigue Life

Quality Characteristic	**Replications**			**Mean**
Fatigue Life of Composites in (Load Cycles Survived)	Replication 1	Replication 2	Replication 3	
	4569	4597	4539	4568 (Load Cycles Survived)

The optical micrographs of fractured surfaces of fatigue test specimens are shown below, in Figure 5.23. In present investigation, the enhancement in fatigue life of developed hybrid composites as compared to unreinforced metal matrix, may be attributed to the load bearing performance of hard filler particles, strengthening of interfacial bonding, restricting the dislocation movement by pinning them down

through reinforcements and strain localization initiated at reinforcement-base metal interface.

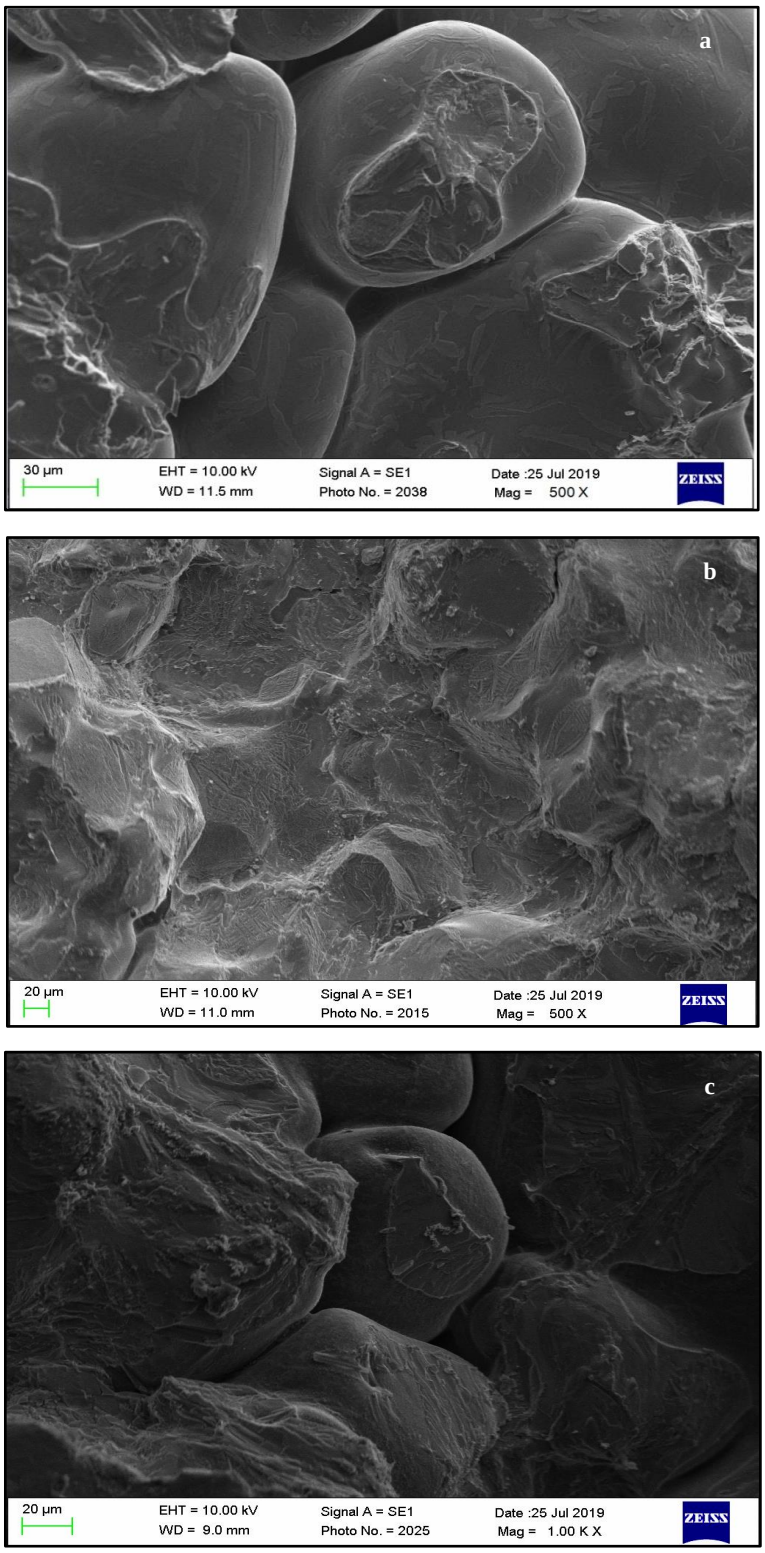

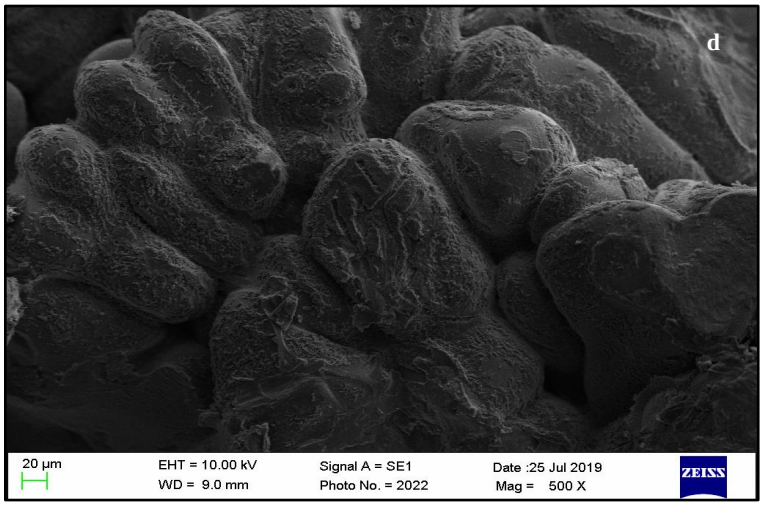
d
20 µm
EHT = 10.00 kV
WD = 9.0 mm
Signal A = SE1
Photo No. = 2022
Date :25 Jul 2019
Mag = 500 X
ZEISS

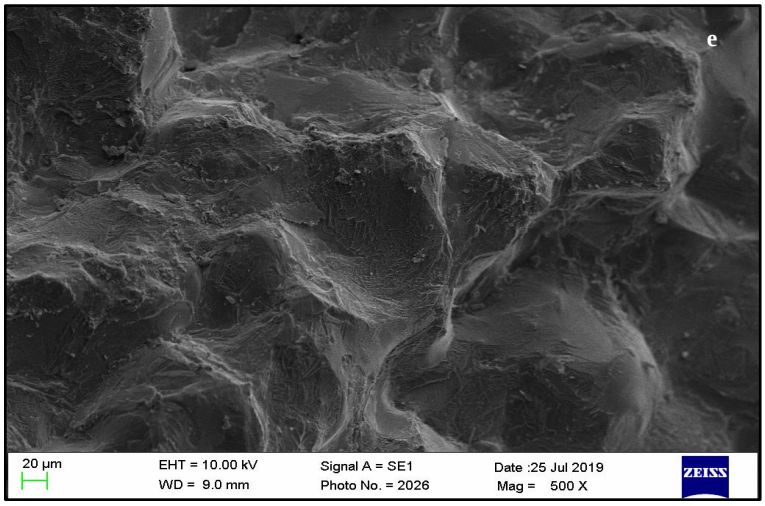
e
20 µm
EHT = 10.00 kV
WD = 9.0 mm
Signal A = SE1
Photo No. = 2026
Date :25 Jul 2019
Mag = 500 X
ZEISS

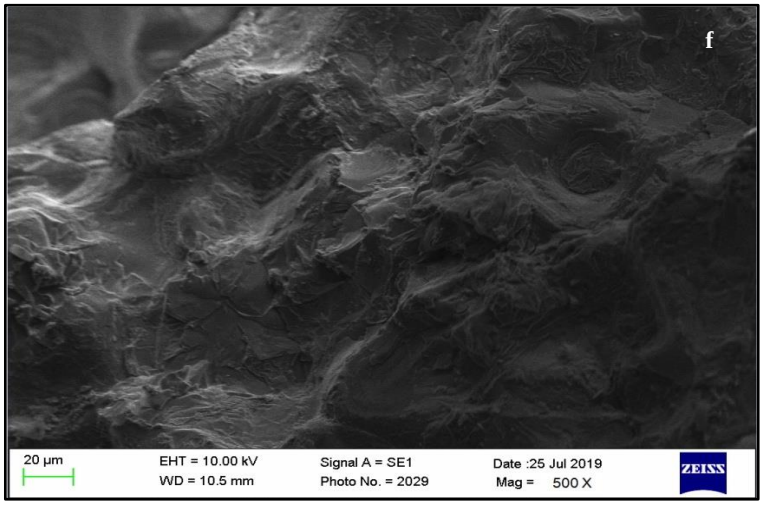
f
20 µm
EHT = 10.00 kV
WD = 10.5 mm
Signal A = SE1
Photo No. = 2029
Date :25 Jul 2019
Mag = 500 X
ZEISS

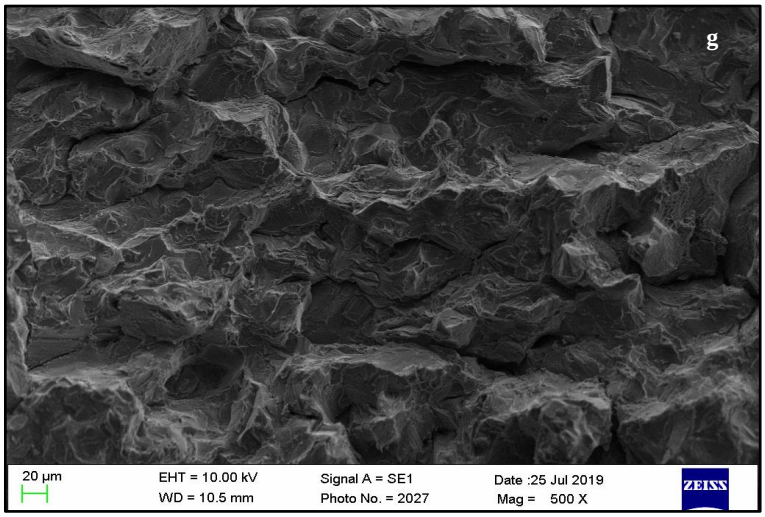
g
20 µm
EHT = 10.00 kV
WD = 10.5 mm
Signal A = SE1
Photo No. = 2027
Date :25 Jul 2019
Mag = 500 X
ZEISS

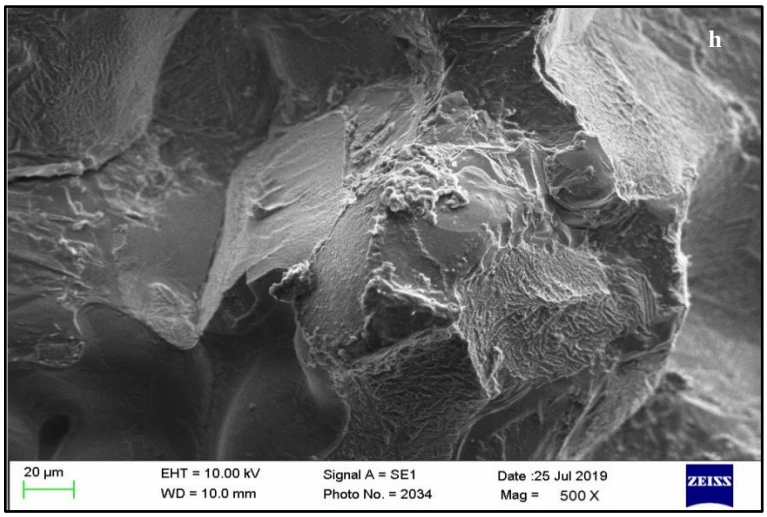
h
20 µm
EHT = 10.00 kV
WD = 10.0 mm
Signal A = SE1
Photo No. = 2034
Date :25 Jul 2019
Mag = 500 X
ZEISS

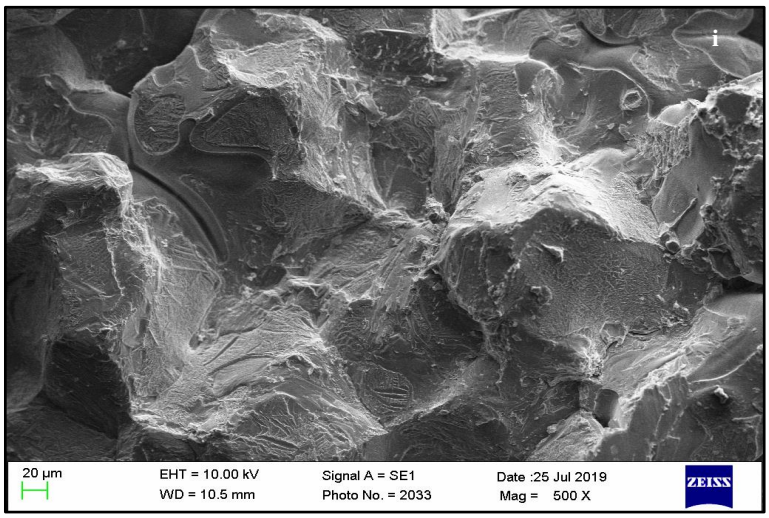
i
20 µm
EHT = 10.00 kV
WD = 10.5 mm
Signal A = SE1
Photo No. = 2033
Date :25 Jul 2019
Mag = 500 X
ZEISS

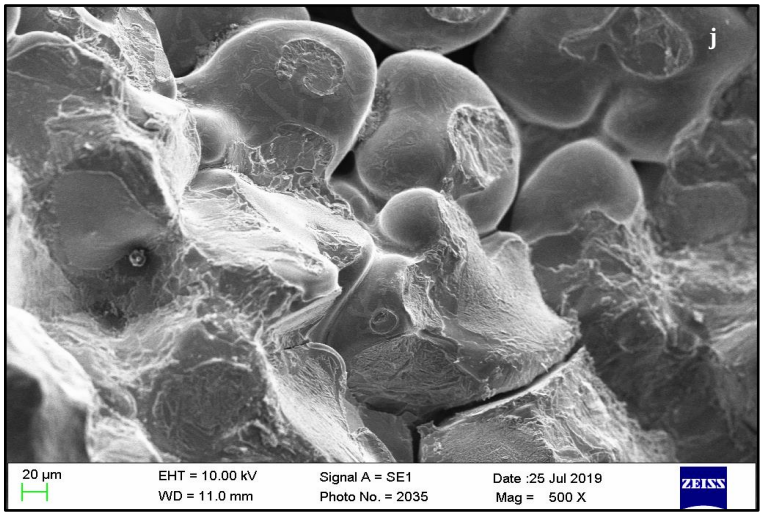

Figure 5.23: SEM Micrographs of Fractured Surfaces of Composite Specimens (a) S0 (b) S1 (c) S2 (d) S3 (e) S4 (f) S5 (g) S6 (h) S7 (i) S8 (j) S9 After Fatigue Test

Disruption of crack growth in composite materials can be attributed to various mechanisms of crack tip protection such as crack closure, deflection and crack bridging [179]. Hard reinforcement particulates inhibited the formation of voids and cracks in metal matrix, hence increased the fatigue life of synthesized composites. Additionally, homogeneous dispersion of particulate reinforcements in metal matrix acted as barrier to the development of slip bands due to reversible cyclic loading and decreased slip distance. This phenomenon resulted into enhanced resistance towards fatigue crack inception, hence impeding the surface crack initiation. The hard reinforcement particles also carried stresses redistributed by metal matrix, hence higher stresses were required to deform the composites translating into higher fatigue life [180]. Processing deformities in hybrid aluminium composites such as agglomerated reinforcement particles and external inclusion (producing stress concentration and increasing local stress intensity, resulting into fast free surface crack nucleation) significantly influenced their fatigue strength.

With lower reinforcement contents, the fatigue crack growth deflection and branching at interfaces was observed which retarded the fatigue crack growth as compared to unreinforced base metal, whereas beyond 4.5% combined reinforcement content, the formation of voids was increased resulting into brittleness and decrease in fatigue life (in case of composite specimen S9). Sometimes it was also observed that under strain controlled cyclic loading

conditions; composite specimens demonstrated inferior low cycle fatigue life due to high dislocation densities near interface and stress concentration close to reinforcement particles.

Fatigue failure is comprised of three stages (i) crack nucleation, (ii) crack growth and (iii) ultimate fracture. Crack progression marks or beach marks (displaying in change in position of fatigue crack front) and striations (representing microscopic fingerprint related to crack propagation) in propagation region of fractured specimen surfaces were observed. Micrographs of composites exhibiting limited dimple structure, indicated the presence of stronger interfacial bonding between metal matrix and reinforcement phases, within synthesized composites. Blunt edges in SEM images of fractured surfaces can be observed, designated the plastic deformation of specimen materials under reversible cyclic loading before permanent failure.

Cracks due to coalescence of micro-voids may also be witnessed in SEM micrographs along with occurrence of cup-cone fractures, exhibiting the ductile nature of fractured specimen materials (in specimens S1, S4, S5, S6, S7 and S8). Detection of some round dendrite structures in SEM images of specimens S0, S2, S3 and S9 may be attributed to the specimen fracture because of incipient melting, where the components with lower melting points melted early and resulted into brittle and low strength components. Possible delamination or cleavage surfaces were represented by step structures present in micrograph of specimen S6.

5.6.1 Effect of Surface Roughness on Fatigue life

Fatigue failure of engineering components depends on various factors such as surface quality (described by surface texture, residual stress and microstructure) material type and environment effect etc. Surface finish of a component manufactured through different machining processes, plays a major role in determining its fatigue behaviour. As-cast Al-7075-T6 specimen S0 and synthesized composite specimens were investigated on a stylus profiler (Make Zeiss, Model: SURFCOM FLEX 50, as shown in Figure 5.24) for their surface roughness in terms of average roughness (Ra) and mean roughness depth (Rz) as presented in Table 5.38.

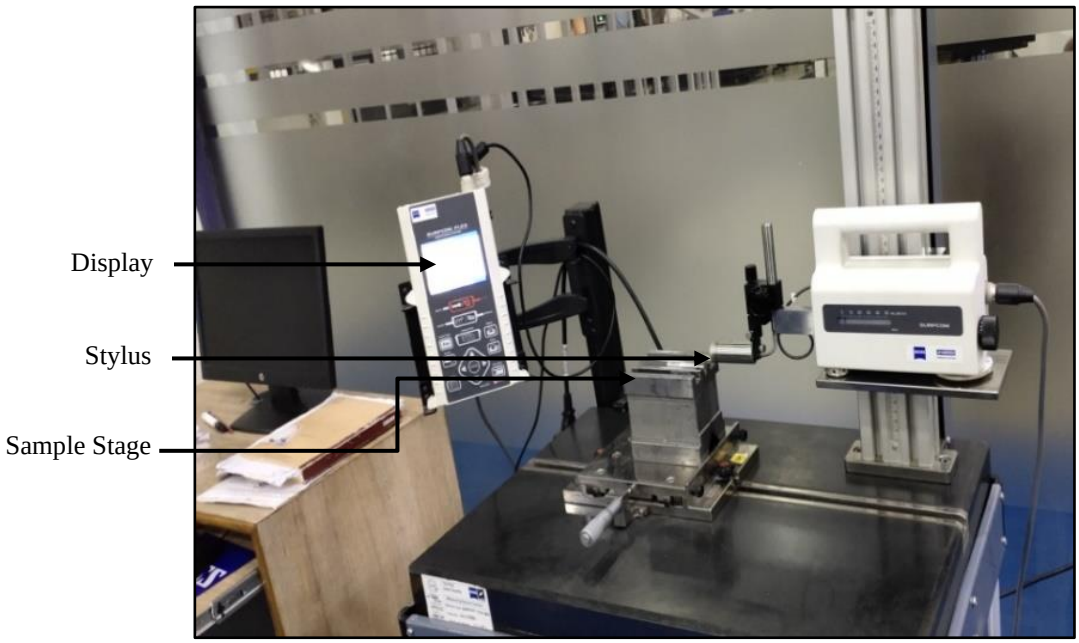

Figure 5.24: Stylus Profiler

Table 5.38: Surface Roughness

Specimen	Ra (µm)	Rz (µm)
S0	1.147	5.671
S1	1.377	9.296
S2	4.321	27.968
S3	1.283	12.295
S4	1.195	7.272
S5	1.191	7.912
S6	1.07	7.648
S7	0.811	4.968
S8	0.787	5.048
S9	0.788	4.704

Average surface roughness observations, mean values with respective S/N ratios for "smaller the better" type of quality characteristic are given in Table 5.39.

Variation in surface roughness of different specimens, may be attributed to different degrees of uniformity of dispersion of reinforcement particles into metal matrix. If the mixing of fillers in synthesized composites was not appropriate, peaks, valleys and micro pores might exist, providing inferior surface finish of machined component. Additionally, presence of hard reinforcement particles in produced hybrid aluminium metal matrix composites acted as small cutting edges resulting into poorer surface finish (as in case of specimen S2) as compared to base metal specimen S0. Improved surface finish in some composite specimens was due to

burnishing effect, produced by reinforcement particles trapped between flank tool face and machined surface of component.

Table 5.39: Observations for Average Surface Roughness and S/N Ratio

Average Surface Roughness					
Average Surface Roughness of as-cast Al7075-T6 Specimen S0: 1.14 µm					
Composite Specimen	**Observation 1 (µm)**	**Observation 2 (µm)**	**Observation 3 (µm)**	**Mean Value (µm)**	**S/N Ratio (dB)**
S1	1.35	1.42	1.37	1.38	-2.80
S2	4.38	4.84	3.76	4.33	-12.77
S3	1.24	1.32	1.28	1.28	-2.15
S4	1.25	1.21	1.15	1.20	-1.61
S5	1.21	1.17	1.19	1.19	-1.51
S6	0.98	1.13	1.09	1.07	-0.58
S7	0.76	0.85	0.82	0.81	1.82
S8	0.79	0.82	0.76	0.79	2.04
S9	0.82	0.84	0.71	0.79	2.02

Greater the surface roughness, lower the fatigue life, as stress concentration under cyclic loading in present study initiated from micro notches existing on surfaces with uneven geometric profiles.

Fatigue life of a mechanical component is divided into two components, (i) fatigue crack initiation life and (ii) crack growth life. In present experimental investigation, surface roughness may have majorly influenced the crack initiation stage, as the fatigue cracks usually were initiated from large intermetallic inclusions and reinforcement clusters near the surface, hence inferior the surface finish lower is the fatigue life [181], as shown in Figure 5.25.

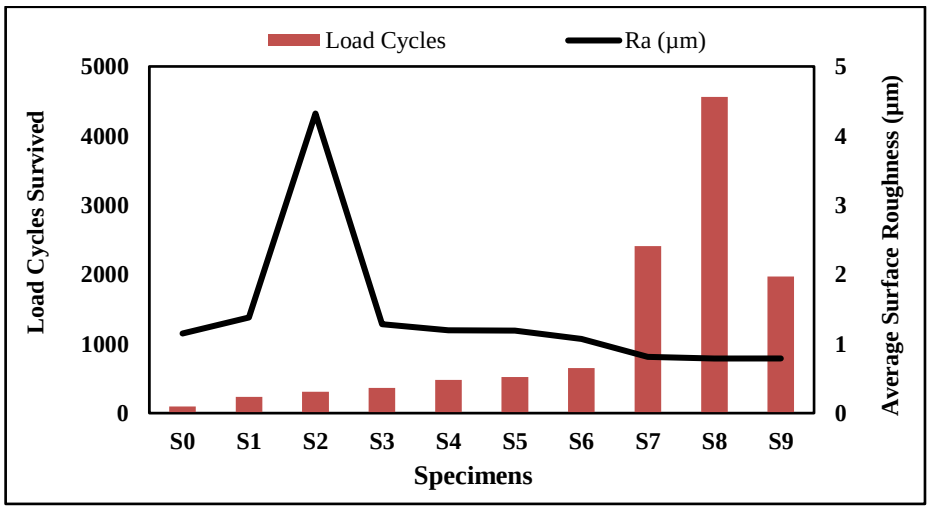

Figure 5.25: Roughness Vs Fatigue Life

Effects of all the prevalent process parameters during composite fabrication on S/N ratio and residual stress were studied and plotted as in Figure 5.26. Graphs in Figures 5.26a and 5.26d display that on increasing wt.% of eggshell particles and mechanical stirring time, average surface roughness in composites was decreased whereas from Figures 5.26b and 5.26c, it can be observed that on increasing SiC particles wt.%, and Al_2O_3 particles wt.% average surface roughness was increased. Various graphs from Figure 5.26 explain that for minimum surface roughness in synthesized hybrid aluminium composites and S/N ratio optimum process parameter levels were 3rd level of eggshell particles content (A_3), 1st level of SiC particles content (B_1), 2nd level of Al_2O_3 particles content (C_2) and 3rd level of mechanical stirring time (D_3). Average values of surface roughness and S/N ratios for each process parameter at all levels are displayed by Table 5.40.

Table 5.40: Response Table: Surface Roughness

Process Parameter	**Level**	**Eggshell Particles wt.%**		**SiC Particles wt.%**		**Al_2O_3 Particles wt.%**		**Mechanical Stirring Time**	
Type of Data	-	Raw Data	S/N Ratio	Raw Data	S/N Ratio	Raw Data	S/N Ratio	Raw Data	S/N Ratio
Average Values	L1	2.3	-5.9	0.7	-0.9	1.1	-0.4	1.1	-0.8
	L2	1.2	-1.2	2.1	-4.1	0.8	-4.1	2.1	-3.8
	L3	0.8	2.0	1.1	-0.2	2.1	-0.6	1.1	-0.6
Main Effects	L2-L1	-1.2	4.7	1.4	-3.2	-0.3	-3.7	0.9	-3.1
	L3-L2	-0.4	3.2	-1.0	3.8	1.0	3.5	-1.0	3.3
Difference (L3-L2) - (L2-L1)		0.8	-1.5	-2.4	7.1	1.3	7.2	-1.9	6.3
L1, L2 and L3 display the process parameter levels. (L2-L1) represents main effect while corresponding process parameter changes from level 1 to level 2. (L3-L2) denotes main effect during process parameter change from level 2 to level 3.									

ANOVA at 95% confidence level was carried out to study effect of process parameters on utility function. Table 5.41 shows percentage contribution and F-ratio of different factors affecting the surface roughness. Table 5.42 displays ANOVA results computed at 95% confidence level with F-ratio and percentage contribution of various factors for S/N ratio.

Table 5.41: Analysis of Variance (ANOVA) for Average Surface Roughness

Factor	Sum of Squares (SS)	Degrees of Freedom	Variance (V)	Percentage Contribution (P)	F-Ratio
Eggshell Particles wt.%	11.57	2	5.79	38.30	166.08*
SiC Particles wt.%	6.20	2	3.10	20.53	89.01*
Al_2O_3 Particles wt.%	6.25	2	3.13	20.69	89.71*
Mechanical Stirring Time	5.56	2	2.78	18.40	79.79*
Others/Errors	0.63	18	0.03	2.08	-
Total	30.21	26	-	100	-
***Significant factor at confidence level of 95%, F critical =3.55 (Value from table)**					

Table 5.42: Analysis of Variance (ANOVA) for S/N Ratio

Factor	Sum of Squares (SS)	Degrees of Freedom	Variance (V)	Percentage Contribution (P)	F-Ratio
Eggshell Particles wt.%	93.95	2	46.97	56.76	4.65
SiC Particles wt.%	25.53	2	12.76	15.43	1.26
Al_2O_3 Particles wt.%	25.83	2	12.91	15.60	1.28
Mechanical Stirring Time	20.20	-	-	-	-
Others/Errors	20.20	2	10.10	12.21	-
Total	165.50	8	-	100.00	-
No significant factor at confidence level of 95%, F critical =19 (Value from table)					

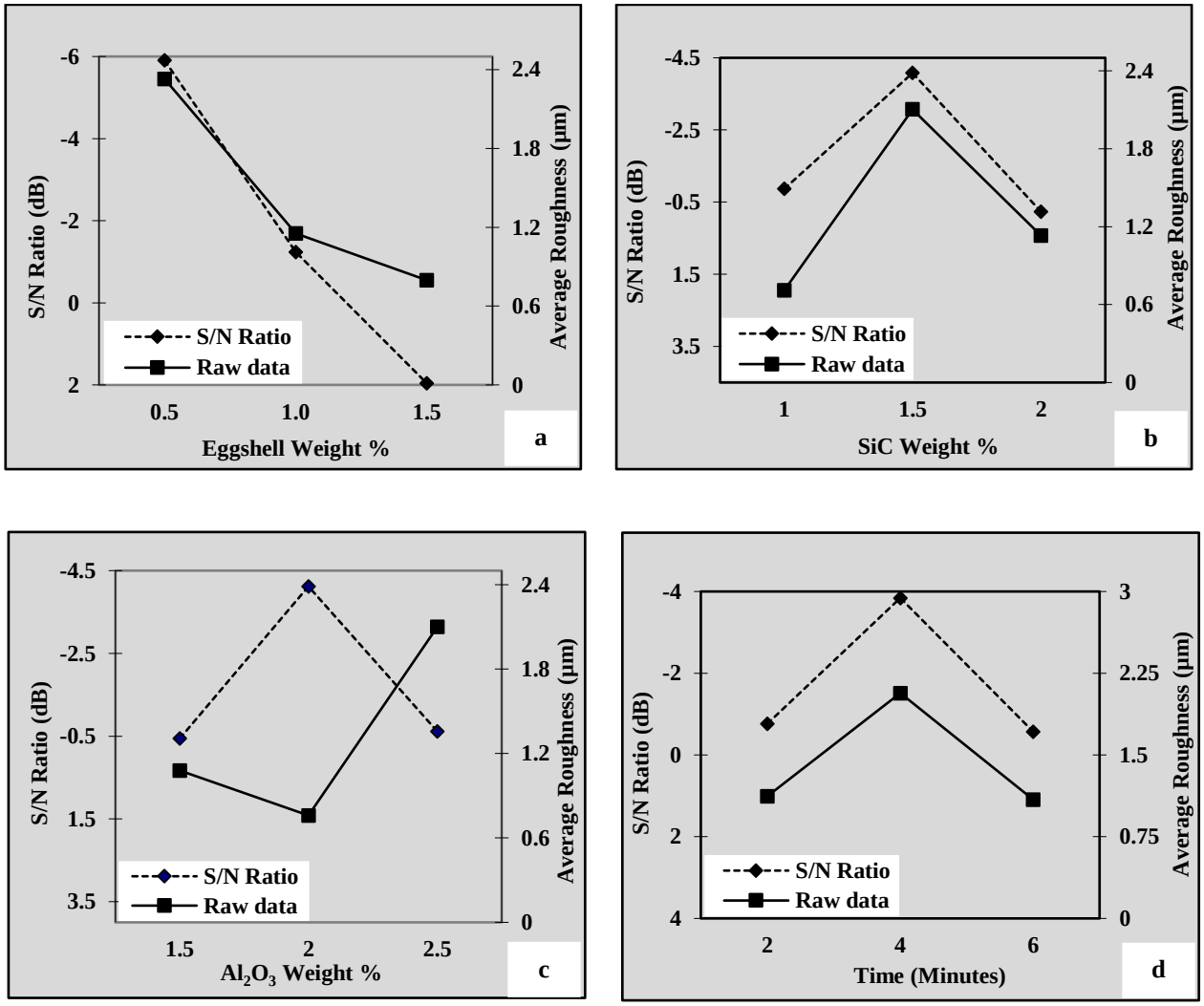

Figure 5.26: Effect of (a) Eggshell Particles wt.% (b) SiC Particles wt.% (c) Al_2O_3 Particles wt.% (d) Mechanical Stirring Time on Average Surface Roughness and S/N Ratio

It was realized from Table 5.41 that eggshell particles wt.% with percentage contribution P=38.30%, SiC particles wt.% with percentage contribution P=20.53%, Al_2O_3 particles wt.% with percentage contribution P=20.69% and mechanical stirring time with percentage contribution P=18.40% influenced the average surface roughness significantly. Table 5.43 and 5.44 display pooled versions of ANOVA for surface roughness raw data and S/N ratio. S/N ratio and mean response characteristics analysis was conducted and followed by realization of optimum levels of significant factors as A_3, B_1, C_2 and D_3 for prediction of mean surface roughness (X_{mp}).

Table 5.43: Pooled ANOVA for Roughness Raw Data

Factor	SS	Degrees of Freedom (Pooled)	V (Pooled)	SS'	P % (Modified)	F-Ratio
Eggshell Particles wt.%	11.57	2	5.79	11.50	38.07	166.08*
SiC Particles wt.%	6.20	2	3.10	6.13	20.30	89.01*
Al_2O_3 Particles wt.%	6.25	2	3.13	6.18	20.46	89.71*
Mechanical Stirring Time	5.56	2	2.78	5.49	18.17	79.79*
Others/Errors	0.63	18	0.03	0.91	2.99	-
Total	30.21	26	-	30.21	100	-
***Significant factor at confidence level of 95%, F critical =3.55 (Value from table)**						

Table 5.44: Pooled ANOVA for Roughness S/N Ratio

Factor	SS	Degrees of Freedom (Pooled)	V (Pooled)	SS'	P % (Modified)	F-Ratio
Eggshell Particles wt.%	93.95	2	46.97	73.74	44.56	4.65
SiC Particles wt.%	25.53	2	12.76	5.33	3.22	1.26
Al_2O_3 Particles wt.%	25.83	2	12.91	5.62	3.40	1.28
Mechanical Stirring Time	-	-	-	-	-	-
Others/Errors	20.20	2	10.10	80.80	48.82	-
Total	165.5	8	-	165.50	100	-
No significant factor at confidence level of 95%, F critical =19 (Value from table)						

Following response average components were evaluated using experimental data from Table 5.39.

$\overline{G} = 1.43,\ \overline{A_3} = 0.8, \overline{B_1} = 1.13\ , \overline{C_2} = 2.11$ and $\overline{D_3} = 1.09$

$$X_{mp} = \overline{G} + \left(\overline{A_3} - \overline{G}\right) + \left(\overline{B_1} - \overline{G}\right) + \left(\overline{C_2} - \overline{G}\right) + \left(\overline{D_3} - \overline{G}\right) \quad (5.12)$$

Predicted mean optimum value of residual stress X_{mp} = 0.85µm was calculated form equation 5.12. From Table 5.41, error variance = 0.03 and DOF for error =18 were obtained. F-ratio value at 95% confidence interval was determined from standard statistical table. The confidence interval (CI) calculated using equation 5.6, was ± 0.32. Confidence interval with respect to 95% confidence level of predicted optimum surface roughness was 0.53 < Ra (µm) < 1.17. Additionally, a confirmation experiment was carried out by running three more replications for roughness in developed hybrid composites at optimal levels of prevalent process parameters. Results of confirmation experiment were reported in Table 5.45 and it was realized that mean value of surface roughness 0.86µm fell within the confidence interval 0.53 < Ra < 1.17.

Table 5.45: Confirmation Experiment for Average Surface Roughness

Quality Characteristic	**Replications**			**Mean**
Average Surface Roughness in Composites (µm)	Replication 1	Replication 2	Replication 3	
	0.88	0.85	0.86	0.86 µm

A rough surface results into shorter fatigue life, as the fatigue crack commences more easily on rough surface. In machined components, residual stresses also caused faster fatigue crack growth. Also, higher roughness values induced increased stress concentrations at the root of surface profile, reducing fatigue life under same loading conditions. The upcoming section presents description of present chapter in a nutshell.

5.7 Summary

This chapter includes evaluation of synthesized composites for different mechanical and physical attributes such as density, porosity, residual stresses, microhardness, tensile strength and fatigue life, in order to conduct a comparative study with unreinforced base metal. Among produced composites in present experimental study, hybrid aluminium metal matrix composite specimen S8 was observed to acquire lowest porosity and residual stress combined with highest microhardness, tensile strength and fatigue life whereas the base metal as-cast Al7075-T6 specimen

was realized to possess inferior mechanical and physical characteristics. Prevalent process parameters eggshell particles weight %, silicon carbide particles weight %, aluminium oxide particles weight % and mechanical stirring time have been optimized for desired performance characteristics using analysis of variance. Optical micrographs of fractured specimens have been discussed in detail. Influence of surface roughness of machined components on their fatigue life has also been explained. Detailed tribological investigations for all the specimens (one as-cast Al7075 and nine hybrid aluminium composite specimens) at various specimen temperatures shall be discussed in forthcoming chapter.

CHAPTER 6

Tribological Characterization of Synthesized Hybrid Aluminium Composites

6.1 Introduction

Wear loss can be defined as progressive disintegration of material (expressed as mass loss, volume loss or linear dimension loss) from a solid surface due to action of another surface in contact. Wear phenomena can be classified into various main categories such as abrasive wear, adhesive wear, erosive wear, corrosive wear, diffusion wear, fretting, scuffing and surface fatigue. Aluminium alloys infused with various reinforcements have established themselves for numerous wear resistant engineering applications. In present chapter, tribological characteristics of Al7075-T6/Eggshell/SiC/Al_2O_3 hybrid composites synthesized through electromagnetic stir casting route were investigated at various specimen temperatures under dry and lubricated conditions. The forthcoming section discusses test procedure followed during wear analysis of produced aluminium composites.

6.2 Wear Test Procedure

In present experiment, the wear investigations were conducted on pin-on-disk rotary tribometer Make: Ducom, Atlas; TR-20L-PHM 800-DHM 850 with specimen temperature range upto 850^0C, frictional force range upto 210N and wear loss range upto 2100µm (as shown in Figure 6.1). The Ducom tribometer was an instrument, which complied with ASTM G99 for numerous real time measurements for tribological characterization of materials in form of pin and disk specimens in dry or lubricated conditions, with three crucial variables parameters; load, speed and temperature. It consisted of a spindle assembly, loading lever assembly, wear track adjustment system and wear and friction force sensors mounted on a base plate with a robust base structure to absorb force generated during test procedure and provided vibration free operation.

The wear disk was mounted over spindle assembly which was driven using a servo controlled motor. At spindle bottom, there was a proximity sensor enabled driven pulley, placed perpendicular to the rotating disk for rotation measurements. The specimen in form a pin was anchored on a fixture, mounted to the well balanced hanging loading lever. The loading lever assembly slid on base plate to fix wear track diameter and pneumatic loading unit applied load on specimen. Rotating disk and fixed pin specimen, as shown in Figure 6.2, generated friction force that was transferred to the friction load cell through loading lever. The wear at contact surface of specimen and disk, displaced the linear variable differential transformer wear sensor to conduct the real time friction and wear measurements.

Figure 6.1: Pin-on-disk Rotary Tribometer

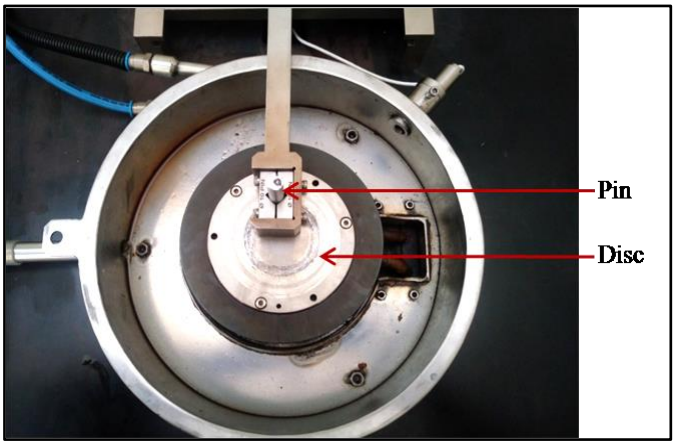

Figure 6.2: Pin Specimen on Rotating Disk

Ducom rotary tribometer operations were controlled by WinDucom 2010 software. This labview based software acquired and represented the linear wear, frictional force, coefficient of friction, speed, wear track diameter and specimen temperature etc., as shown in Figure 6.3. The acquired data could be exported to excel and can be presented in various ways.

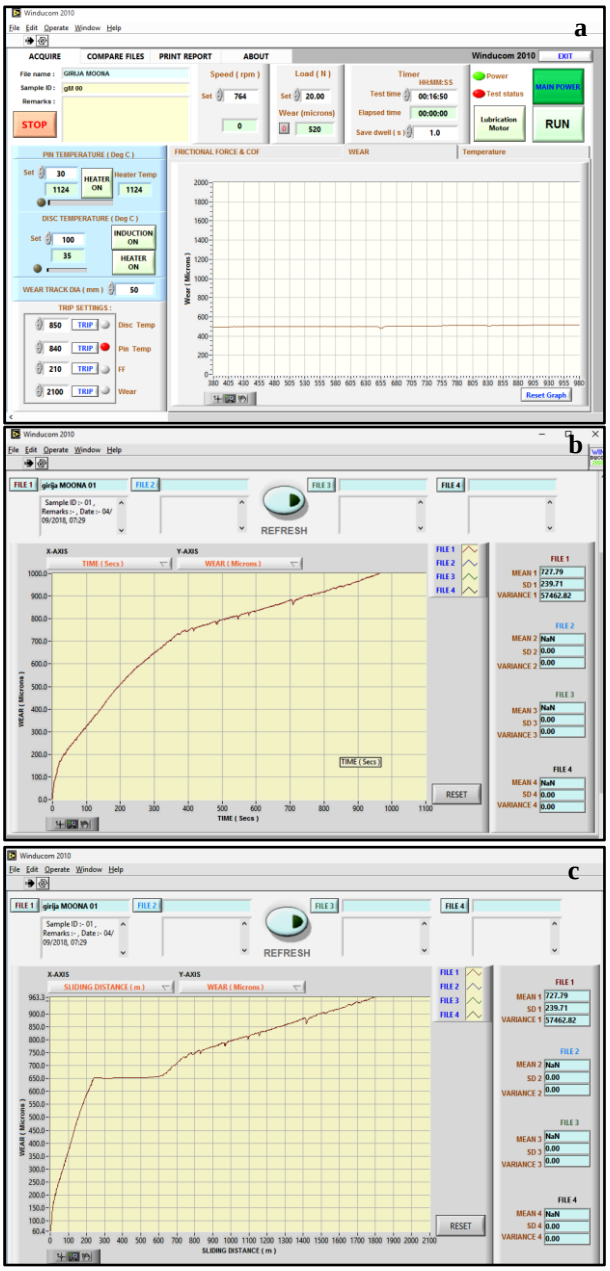

Figure 6.3: (a-c) Wear Data Display

Various wear characteristics of synthesized composites have been assessed and compared with base metal in following section.

6.3 Tribological Characterization

Ten wear test specimens (in three replications) were prepared as per ASTM G99-17 (length 50 mm, diameter 10 mm with polished hemispherical tip of diameter 10 mm, with specimen tip roughness ≈1.9µm and hardness HRC<35) to be tested for tribological characteristics against an EN 31 rotating disk (diameter: 100 mm, thickness: 8mm, surface roughness ≈1.0µm and hardness HRC 62), as shown in Figure 6.4.

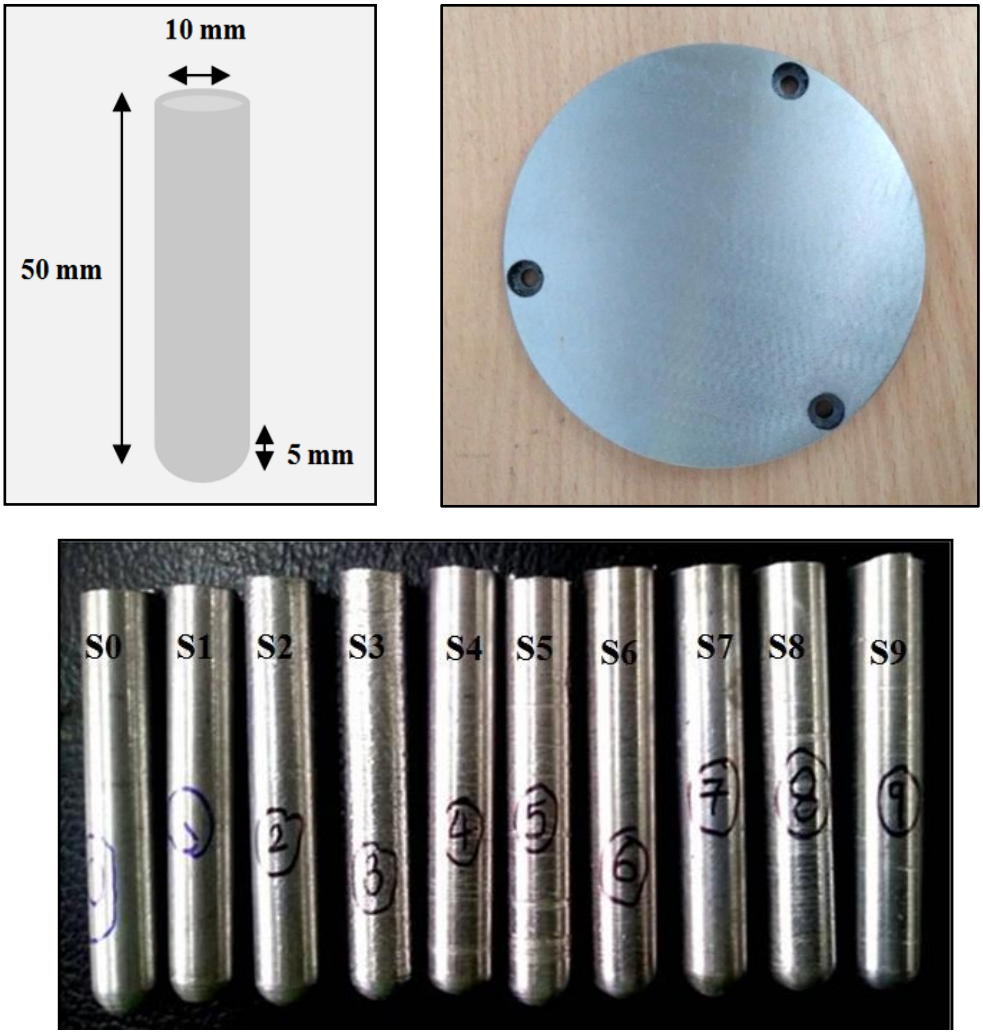

Figure 6.4: Wear Test Specimens and Disk

Wear investigations were conducted at a constant load of 20N for a sliding speed of 2m/s, sliding distance of 2 km, test duration 1000 seconds, disk rotation speed of 764 rpm and wear track diameter of 50 mm. All specimens (one as-cast Al7075-T6 and nine Al7075-T6/ eggshell/ SiC/ Al_2O_3 hybrid composites, in three replications)

were first tested at 30^0C specimen temperature under dry wear and lubricated condition (using SAE10W30 as lubricant) for wear loss, coefficient of friction and frictional force. Wear characteristics of as-cast Al7075-T6 specimen S0 and hybrid composite specimens (S1-S9) at specimen temperature 30^0C under dry experimental conditions are demonstrated in Table 6.1 and Figures 6.5 to 6.7.

At specimen temperature 30^0C, in dry test conditions, wear loss of synthesized aluminium hybrid composites was significantly reduced as compared to the unreinforced base alloy. On running the wear test for 1000 seconds, as-cast Al7075-T6 specimen S0 with coefficient of friction 0.83 and frictional force 17.2N exhibited highest wear loss of 1295 microns whereas hybrid composite specimen S8 with coefficient of friction 0.5 and frictional force 10N displayed lowest wear loss of 515 microns only.

Table 6.1: Wear Properties at 30^0C Specimen Temperature in Dry Test Condition

Specimen	Wear Loss (μm)	Average Coefficient of Friction	Average Frictional Force (N)
S0	1295	0.83	17.2
S1	1249	0.82	16.3
S2	1244	0.77	14.6
S3	1174	0.71	14.7
S4	917	0.71	14.2
S5	1029	0.77	15.2
S6	1098	0.67	13.1
S7	1039	0.61	12.2
S8	515	0.5	10.0
S9	630	0.63	12.4

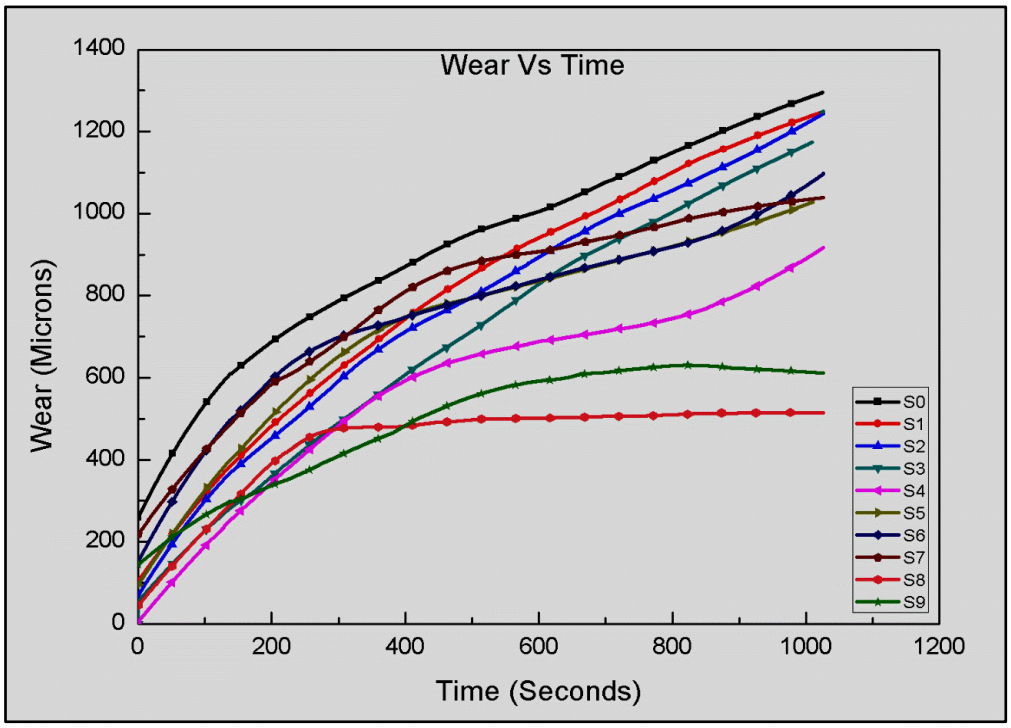

Figure 6.5: Wear Loss of Specimens at 30^0C Specimen Temperature During Dry Test Condition

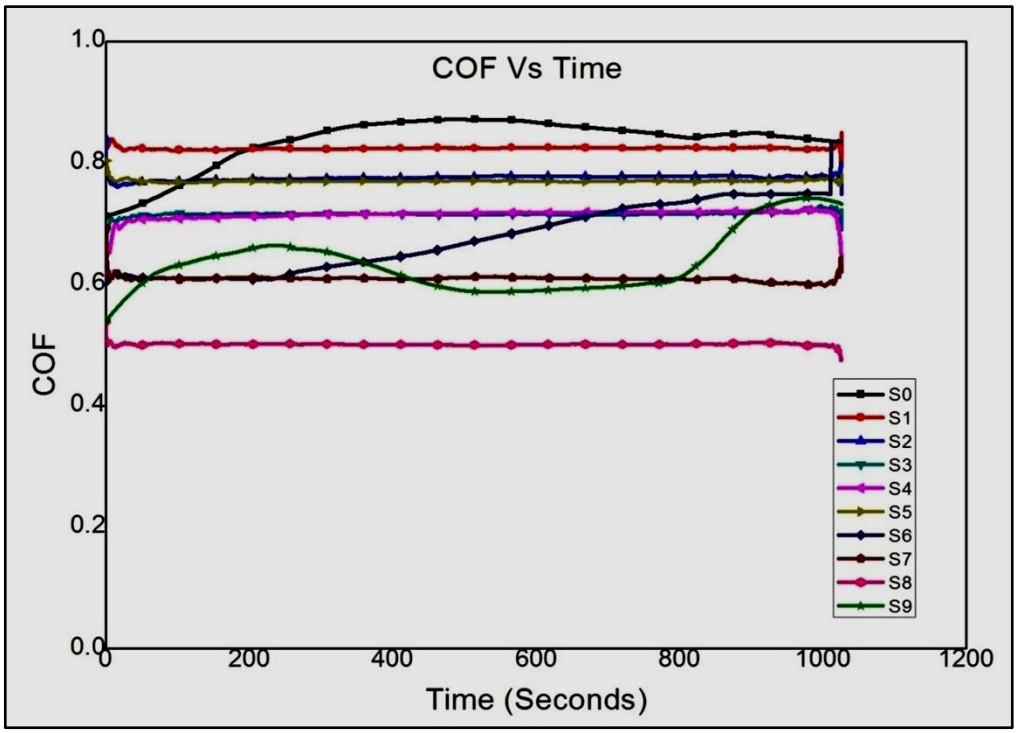

Figure 6.6: Coefficient of Friction of Specimens at 30^0C Specimen Temperature During Dry Test Condition

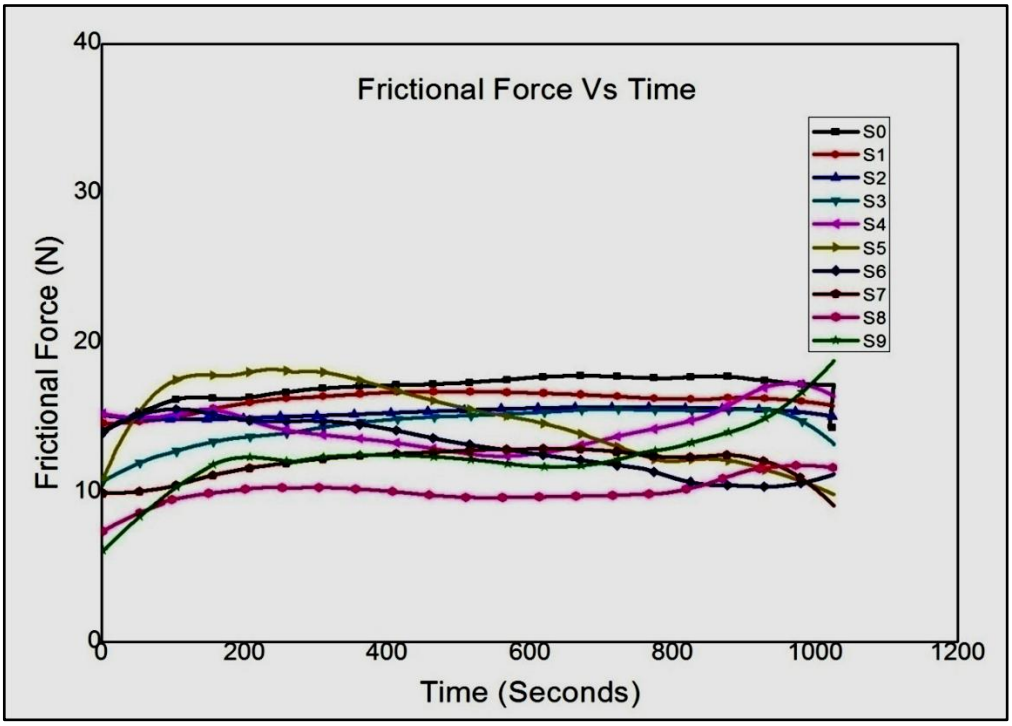

Figure 6.7: Frictional Force of Specimens at 30^0C Specimen Temperature During Dry Test Condition

In lubricated experimental conditions, wear attributes of as-cast Al7075-T6 specimen S0 and hybrid composite specimens (S1-S9) at specimen temperature 30^0C are demonstrated in Table 6.2 and Figures 6.8 to 6.10.

Table 6.2: Wear Properties at 30^0C Specimen Temperature in Lubricated Test Condition

Specimen	Wear Loss (µm)	Average Coefficient of Friction	Average Frictional Force (N)
S0	36	0.13	2.67
S1	33	0.13	2.54
S2	25	0.12	2.43
S3	19	0.08	1.64
S4	17	0.07	1.39
S5	13	0.06	1.25
S6	10	0.05	1.09
S7	14	0.04	1.02
S8	4	0.04	0.82
S9	12	0.05	0.88

Under the influence of lubricant, at specimen temperature 30^0C the as-cast Al7075-T6 specimen S0 with coefficient of friction 0.13 and frictional force 2.67N

demonstrated highest wear loss of 36 microns while the hybrid composite specimen S8 with coefficient of friction 0.04 and frictional force 0.82N was worn out only by 4 microns.

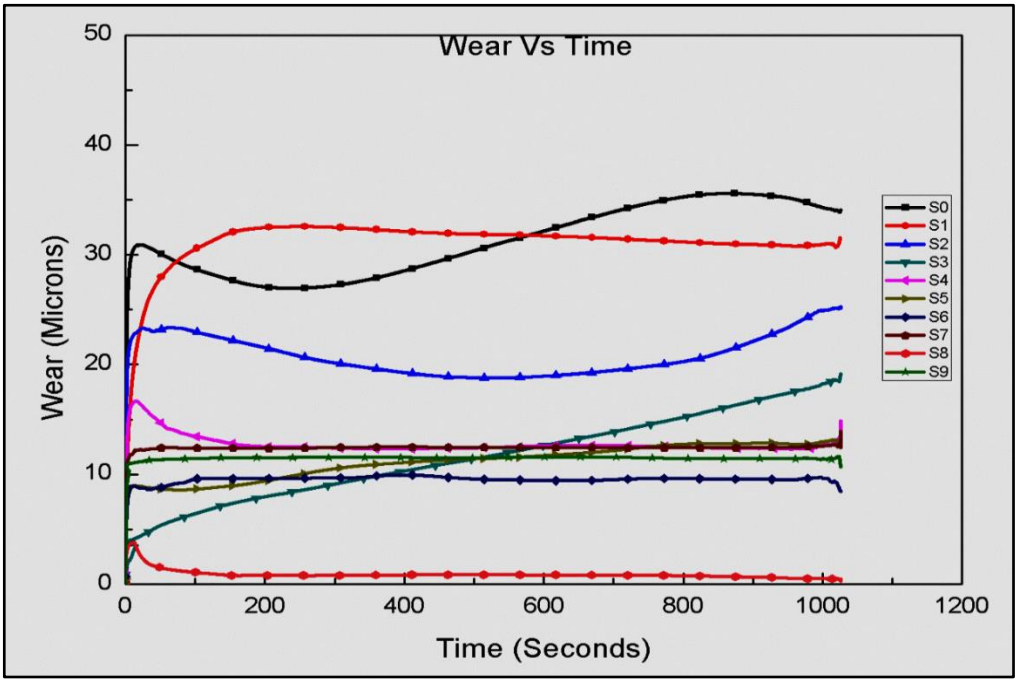

Figure 6.8: Wear Loss of Specimens at 30^0C Specimen Temperature During Lubricated Test Condition

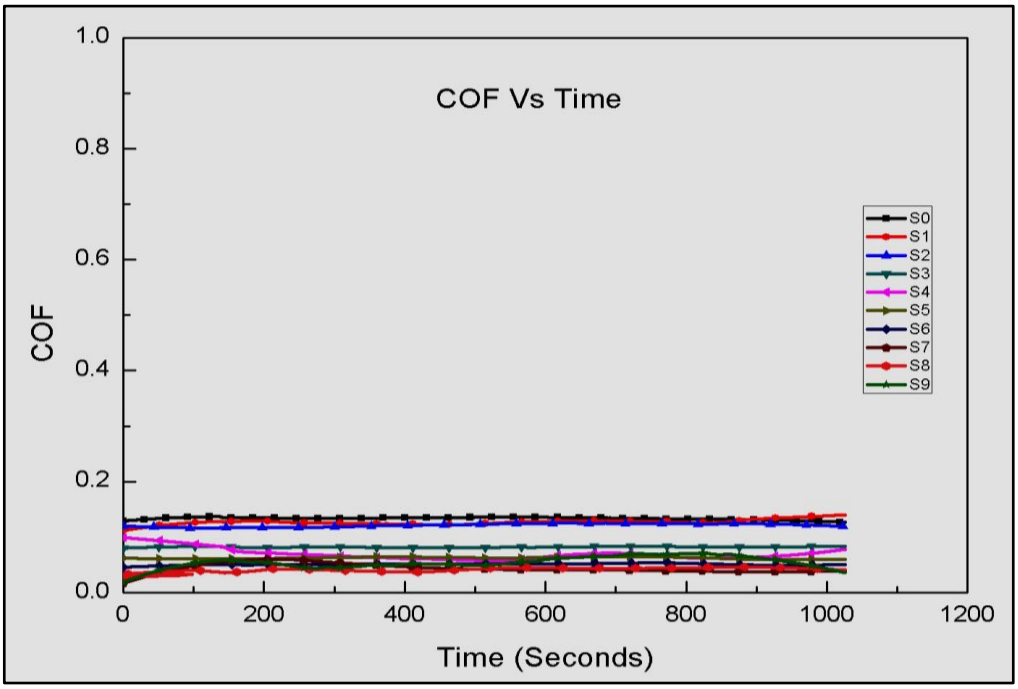

Figure 6.9: Coefficient of Friction of Specimens at 30^0C Specimen Temperature During Lubricated Test Condition

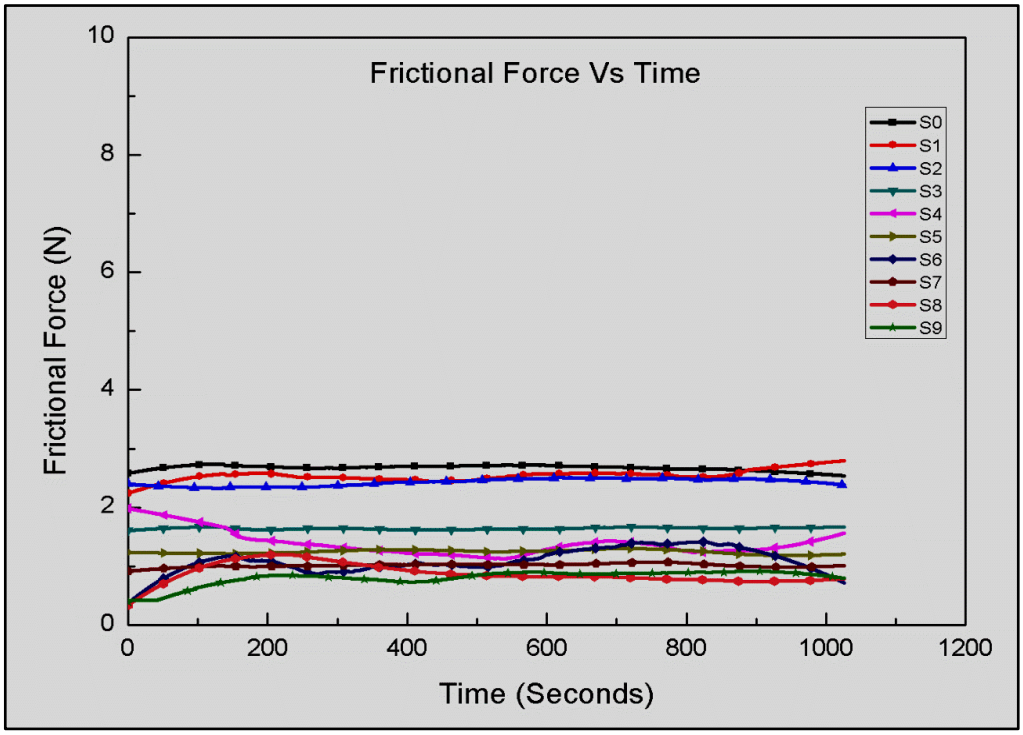

Figure 6.10: Frictional Force of Specimens at 30^{0}C Specimen Temperature During Lubricated Test Condition

At an elevated specimen temperature of 70^{0}C, wear properties of all the specimens in dry test condition are demonstrated in Table 6.3, and Figures 6.11 to 6.13.

Table 6.3: Wear Properties at 70^{0}C Specimen Temperature in Dry Test Condition

Specimen	Wear Loss (µm)	Average Coefficient of Friction	Average Frictional Force (N)
S0	1999	0.84	17.23
S1	1873	0.81	16.25
S2	1586	0.82	16.6
S3	1696	0.7	14.17
S4	1166	0.78	15.66
S5	1237	0.7	14.03
S6	923	0.74	16.52
S7	975	0.65	9.73
S8	354	0.25	4.93
S9	764	0.36	7.01

At 70^{0}C specimen temperature, in dry wear test condition the as-cast Al7075-T6 specimen S0 with coefficient of friction 0.84 and frictional force 17.2N showed highest wear loss of 1999 microns. The aluminium hybrid composite specimen S8

with coefficient of friction 0.25 and frictional force 4.9N exhibited lowest wear loss of 354 microns.

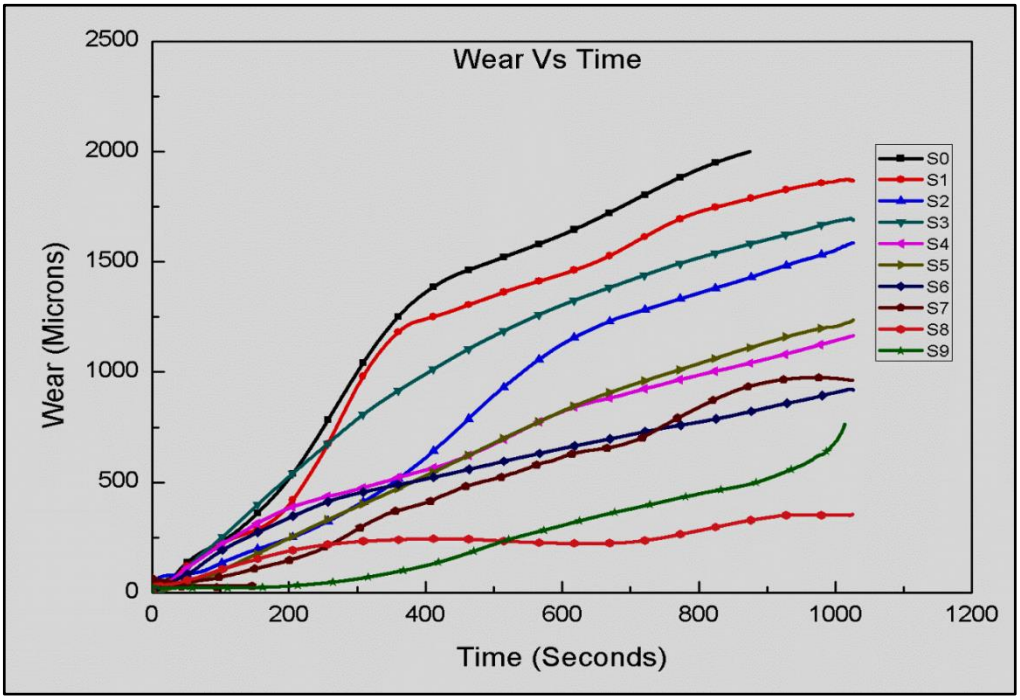

Figure 6.11: Wear Loss of Specimens at 70^{0}C Specimen Temperature During Dry Test Condition

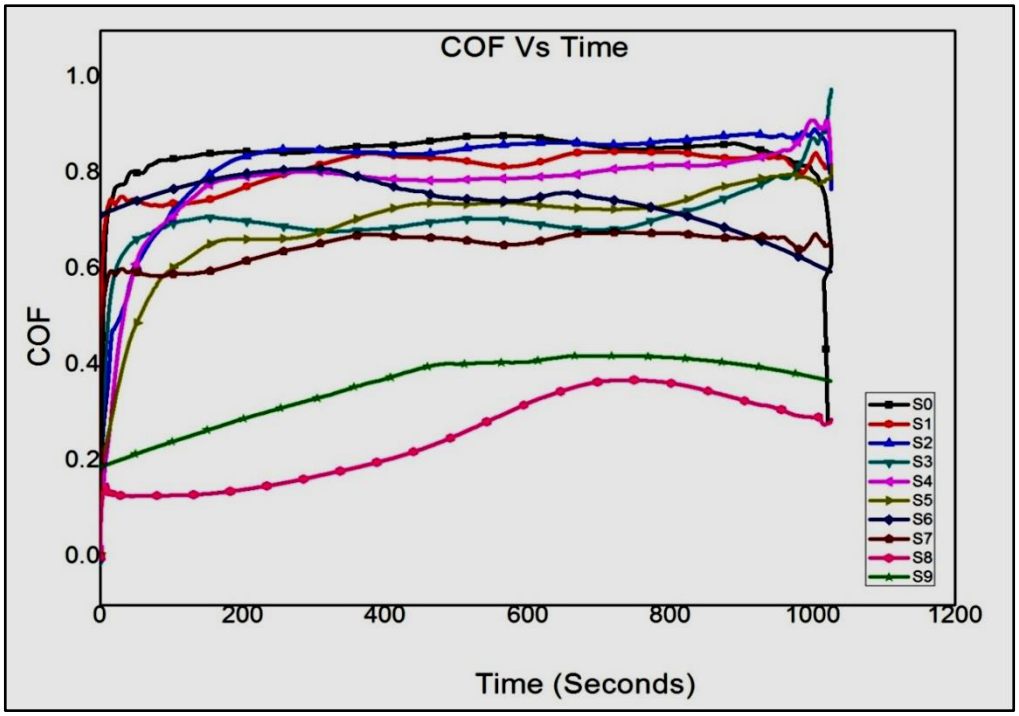

Figure 6.12: Coefficient of Friction of Specimens at 70^{0}C Specimen Temperature During Dry Test Condition

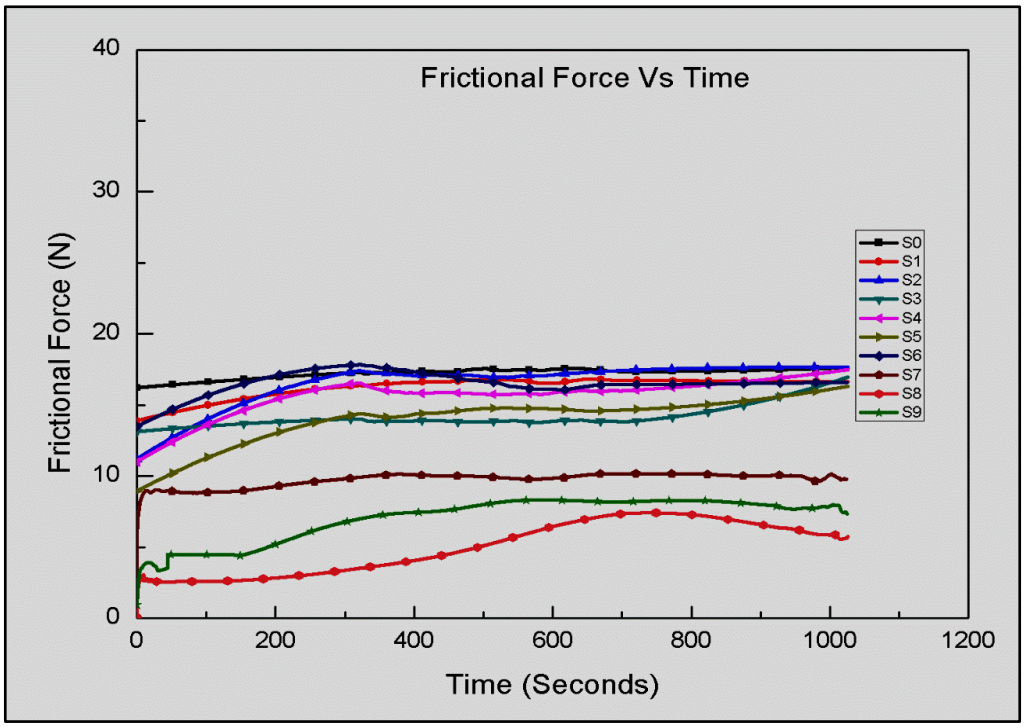

Figure 6.13: Frictional Force of Specimens at 70^{0}C Specimen Temperature During Dry Test Condition

In lubricated test conditions, wear characteristics of as-cast Al7075-T6 specimen S0 and hybrid composite specimens (S1-S9) at specimen temperature 70^{0}C are exhibited in Table 6.4 and Figures 6.14 to 6.16.

Table 6.4: Wear Properties at 70^{0}C Specimen Temperature in Lubricated Test Condition

Specimen	Wear Loss (µm)	Average Coefficient of Friction	Average Frictional Force (N)
S0	44	0.2	3.92
S1	43	0.18	3.52
S2	37	0.12	2.56
S3	32	0.12	2.31
S4	22	0.08	1.6
S5	15	0.1	2.04
S6	13	0.08	1.6
S7	17	0.06	1.2
S8	8	0.03	0.48
S9	16	0.04	0.85

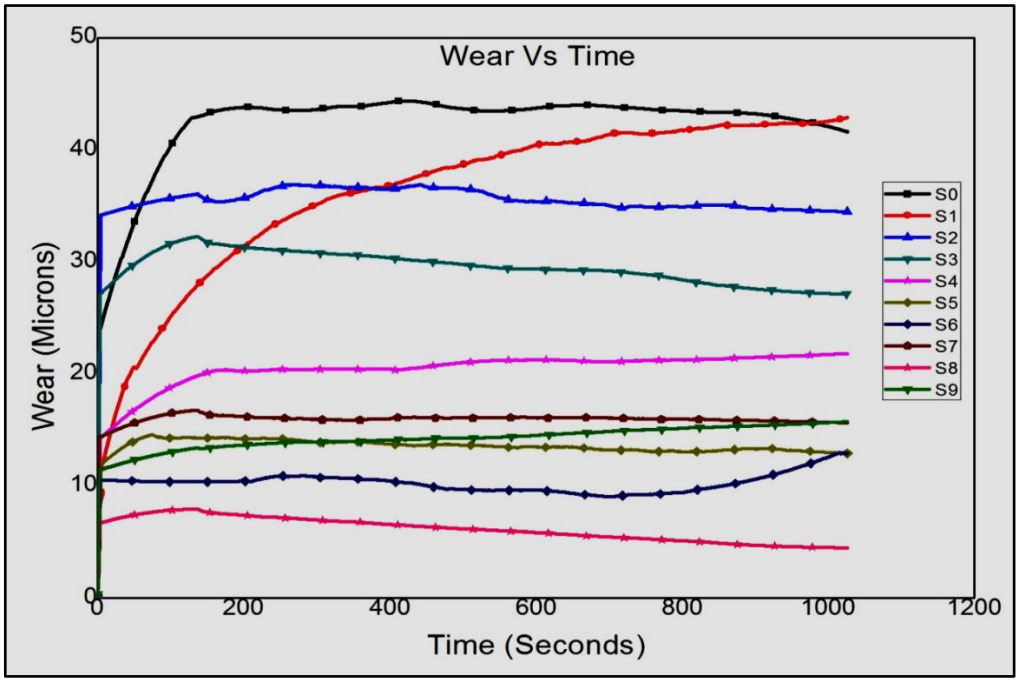

Figure 6.14: Wear Loss of Specimens at 70^{0}C Specimen Temperature During Lubricated Test Condition

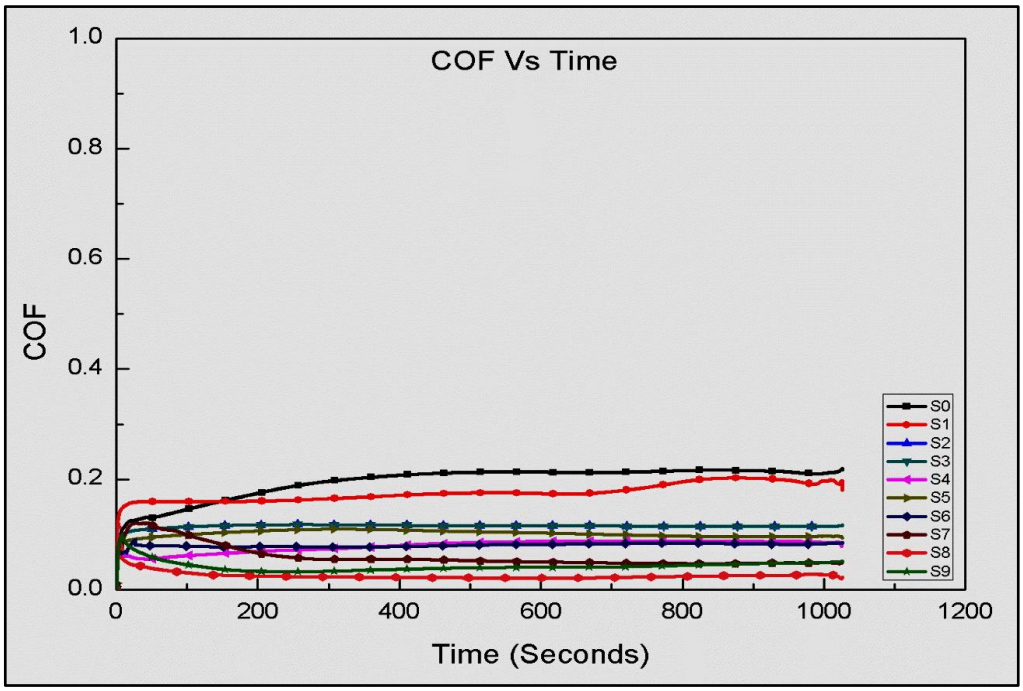

Figure 6.15: Coefficient of Friction of Specimens at 70^{0}C Specimen Temperature During Lubricated Test Condition

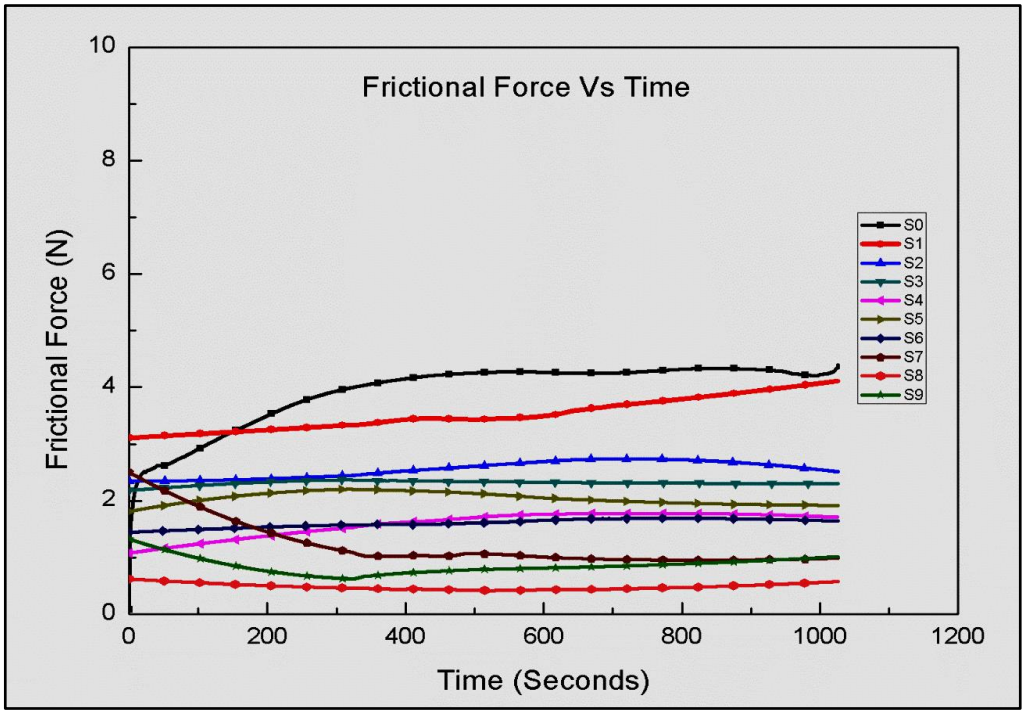

Figure 6.16: Frictional Force of Specimens at 70^0C Specimen Temperature During Lubricated Test Condition

Under lubricated wear condition, at 70^0C specimen temperature the as-cast specimen S0 with coefficient of friction 0.2 and frictional force 3.92N displayed highest wear loss of 44 microns while hybrid composite specimen S8 with coefficient of friction 0.03 and frictional force 0.48N was worn out by only 8 microns.

In composites, the hard reinforcement particles supported applied wear load before the metal asperities gets fractured hence restricting the surface delamination and plastic deformation, leading towards improved wear resistance in comparison of base metal. The strong interfacial bonding between filler and base metal played significant role in deporting applied load from base metal to hard reinforcement particles, restricting surface delamination and plastic deformations and maintaining structural integrity of metal matrix leading towards improved wear properties [182]. The reduction in coefficient of friction of composite specimens was also observed due to uniformly distributed filler particles acting as load bearing agents and diminishing the contact between specimens and rotating disk. As per Archard's law, the enhancement in tribological properties of synthesized aluminium hybrid composites as compared to their unreinforced counterpart may be attributed to the

hardness of infused reinforcements providing secondary harder phases into metal matrix.

In presence of lubricant, the developed hybrid composites exhibited superior wear characteristics because the thin lubricant film formed between specimen and disk reduced material loss due to relative movement. This film accommodated clusters of reinforcement particles, which were ruptured into smaller particles and these particles realigned themselves along the sliding plane hence lowering the wear loss and coefficient of friction. It was observed that on increasing the specimen pin temperature, its constituent material was transformed into softer one, leading towards increased material loss on rubbing against the rotating disk. At elevated temperatures, more frictional heating occurred between the contact surfaces due to less heat depletion and resulted into higher coefficients of friction and more wear. At higher specimen temperatures, the reinforcement particles in hybrid composites contributed to maintain their structural integrity and constrained the crack nucleation on reinforcement-metal interface as compared to the unreinforced alloy.

It was ascertained from the above tribological analysis, that the energy transformed due to frictional contact of specimen and rotating disk may be exhausted in terms of heat generation, vibrations and material deformation or may be stored in the wear system. This asymmetric segregation of energy between the specimen and disk material and within the specimen material may be attributed to the fact that specimen materials with same coefficients of friction could demonstrate different wear losses [183]. Also due to comparable thermal expansion coefficients of all the three reinforcements, the residual stresses were reduced in hybrid aluminium composites (specimen S1 to S9) while exposing them to thermal fluctuations during wear study, as shown in Figure 6.17 posing them as thermally stable and high temperature deformation resistant materials as compared to the unreinforced Al7075-T6 specimen S0 with highest residual stress -216MPa.

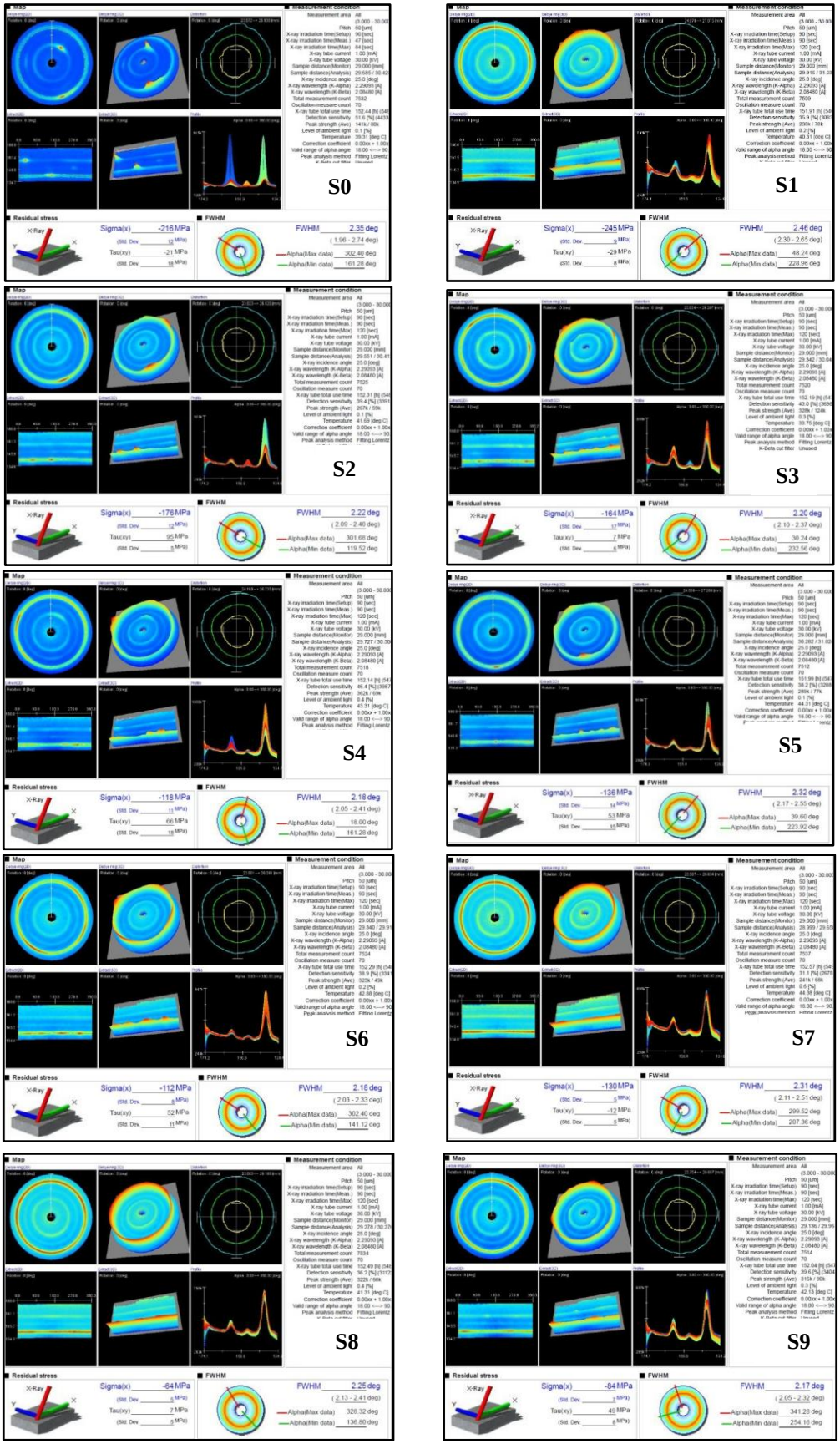

Figure 6.17: Residual Stresses in Worn Samples

Base metal specimen S0 and composite specimen S8 (exhibiting most superior wear characteristics among developed hybrid composite specimens) were further investigated for tribological characteristics at increased specimen temperatures of 150^0C and 250^0C under dry wear conditions only, due to explicit constraints because of the flash point and changed viscosity of lubricant used. At 150^0C pin temperature, the as-cast Al7075-T6 specimen S0 with coefficient of friction 0.72 and frictional force 14.4 N displayed maximum wear of 1693 microns whereas the composite specimen S8 with coefficient of friction 0.33 and frictional force 6.6 N exhibited maximum wear of 117 microns as shown in Figures 6.18-6.20.

At 250^0C specimen temperature, the as-cast Al7075-T6 specimen S0 with coefficient of friction 0.7 and frictional force 15.5 was worn out by 1760 microns and the composite specimen S8 with coefficient of friction 0.42 and frictional force 10.8 was worn out by 527 microns as shown in Figures 6.21 to 6.23.

When specimen temperature was further increased, the softer base metal surrounding reinforcement particles started getting fractured and the particle reinforcements near the contact surface started surrendering their load bearing capacity causing increased wear loss. At elevated temperatures, the wear mechanism in pin specimens gets converted from oxidation wear to delamination and finally to severe wear. At increased specimen temperatures, specimens with reasonably lower hardness underwent drastically increased material loss due to wear because of nonappearance of protective oxide layer attributed to softening and recrystallization of the metal matrix.

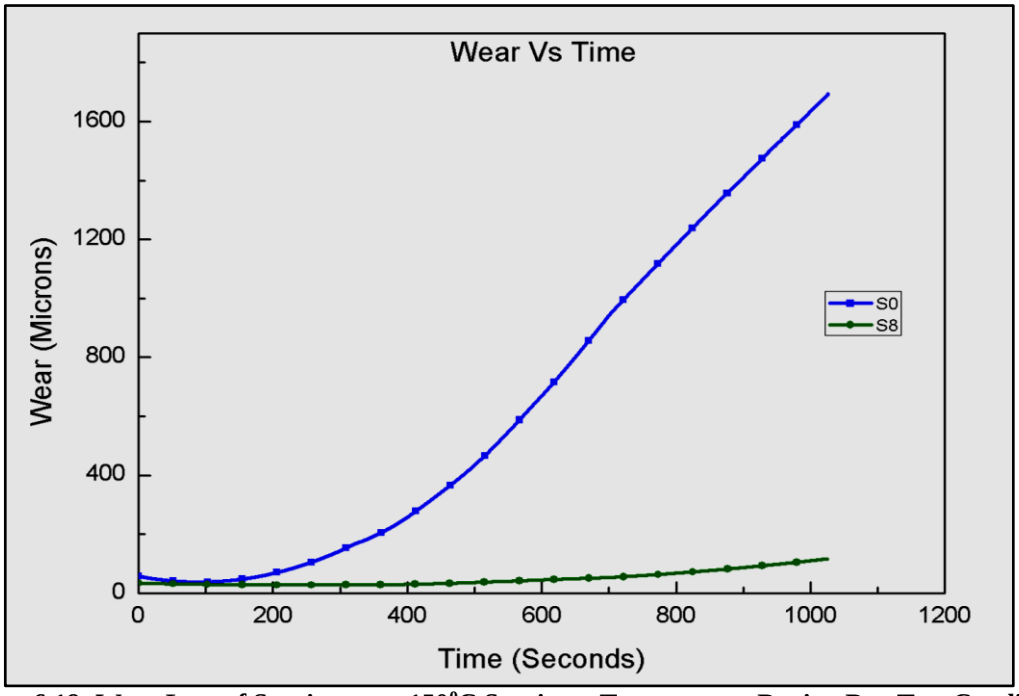

Figure 6.18: Wear Loss of Specimens at 150^{0}C Specimen Temperature During Dry Test Condition

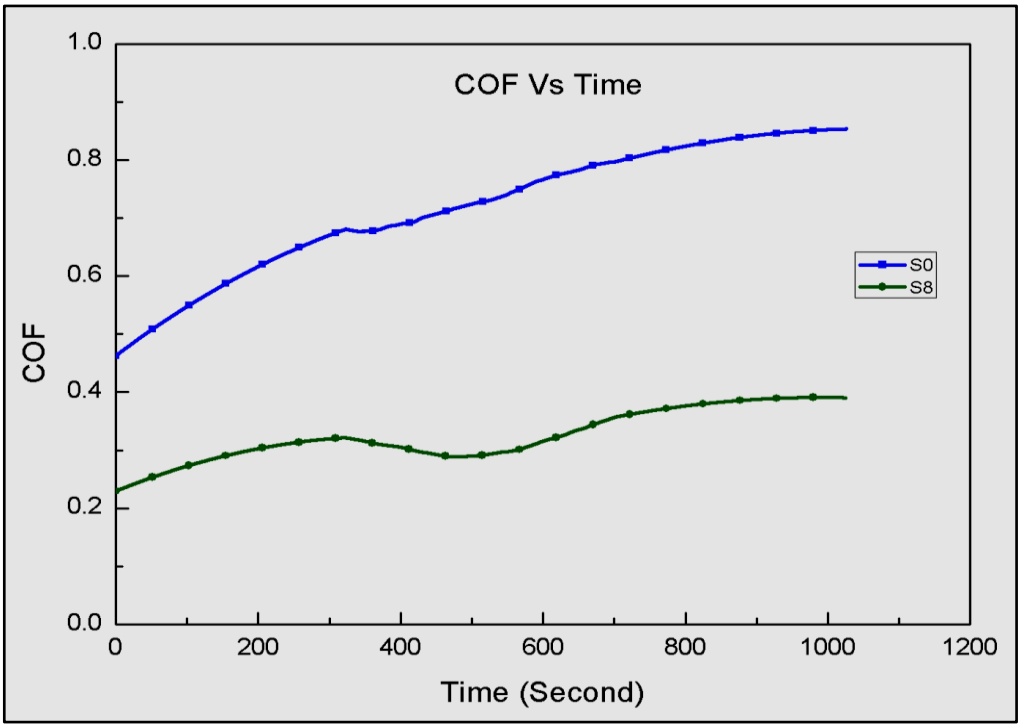

Figure 6.19: Coefficient of Friction of Specimens at 150^{0}C Specimen Temperature During Dry Test Condition

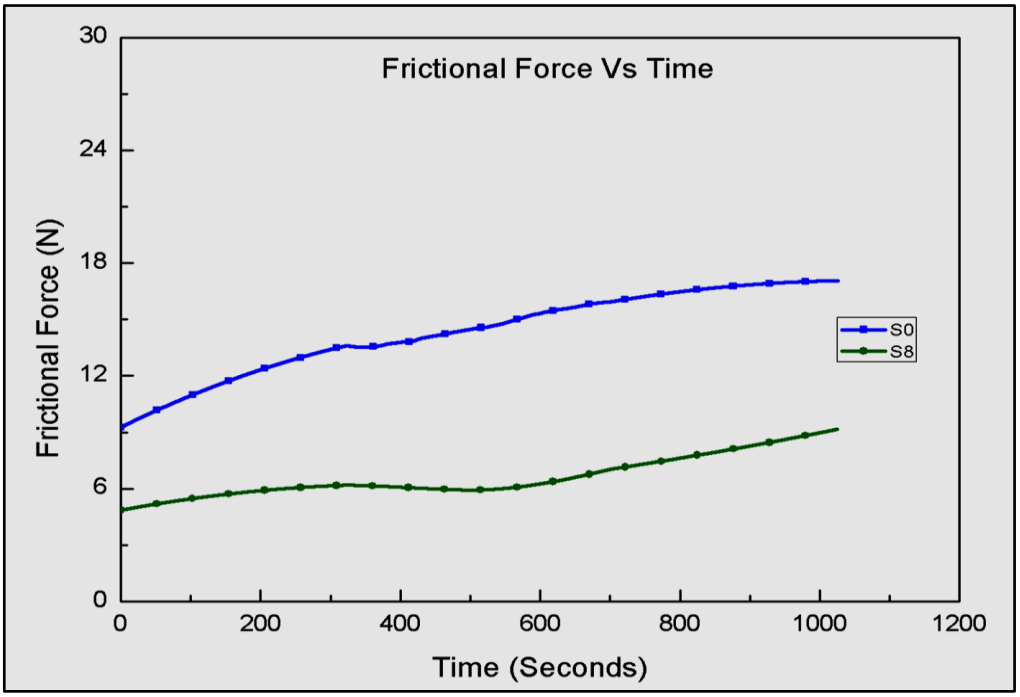

Figure 6.20: Frictional Force of Specimens at 150^{0}C Specimen Temperature During Dry Test Condition

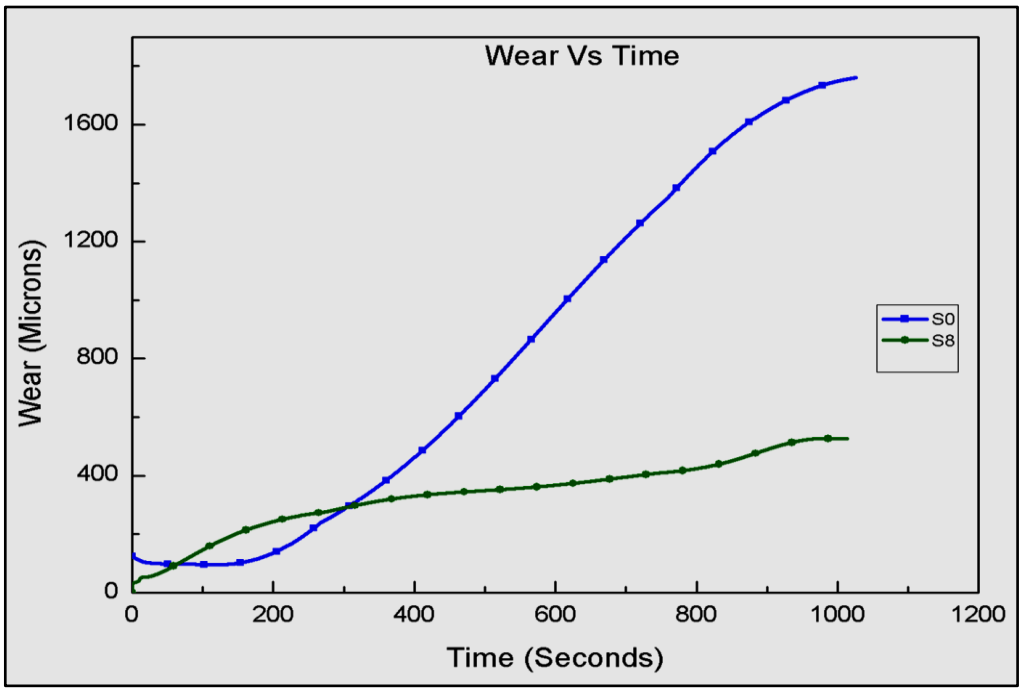

Figure 6.21: Wear Loss of Specimens at 250^{0}C Specimen Temperature During Dry Test Condition

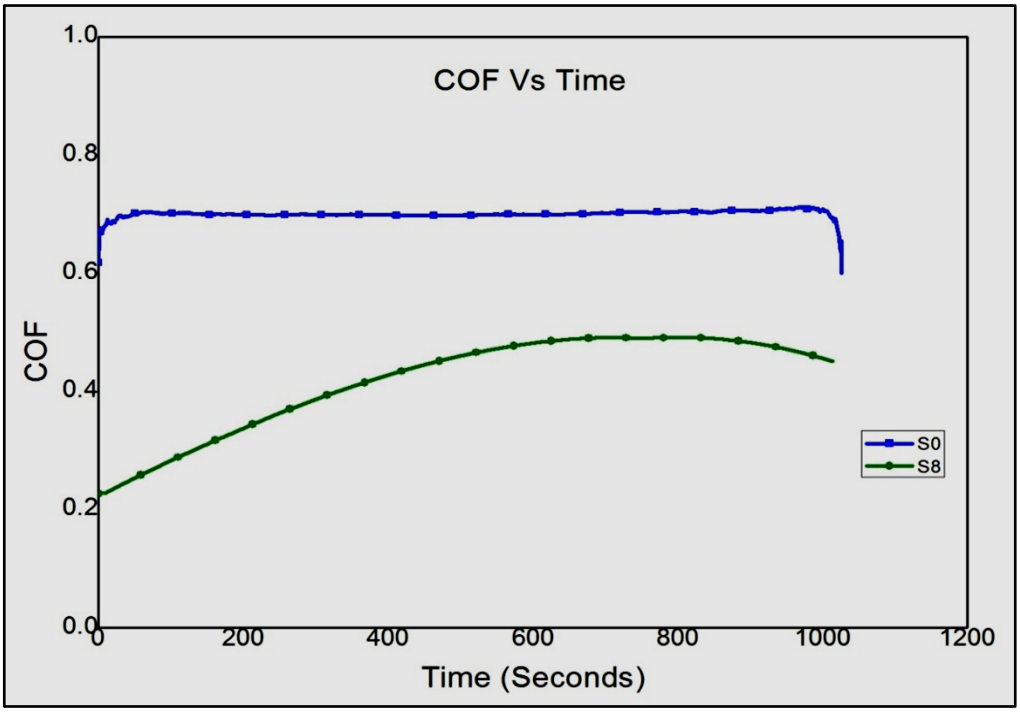

Figure 6.22: Coefficient of Friction of Specimens at 250^{0}C Specimen Temperature During Dry Test Condition

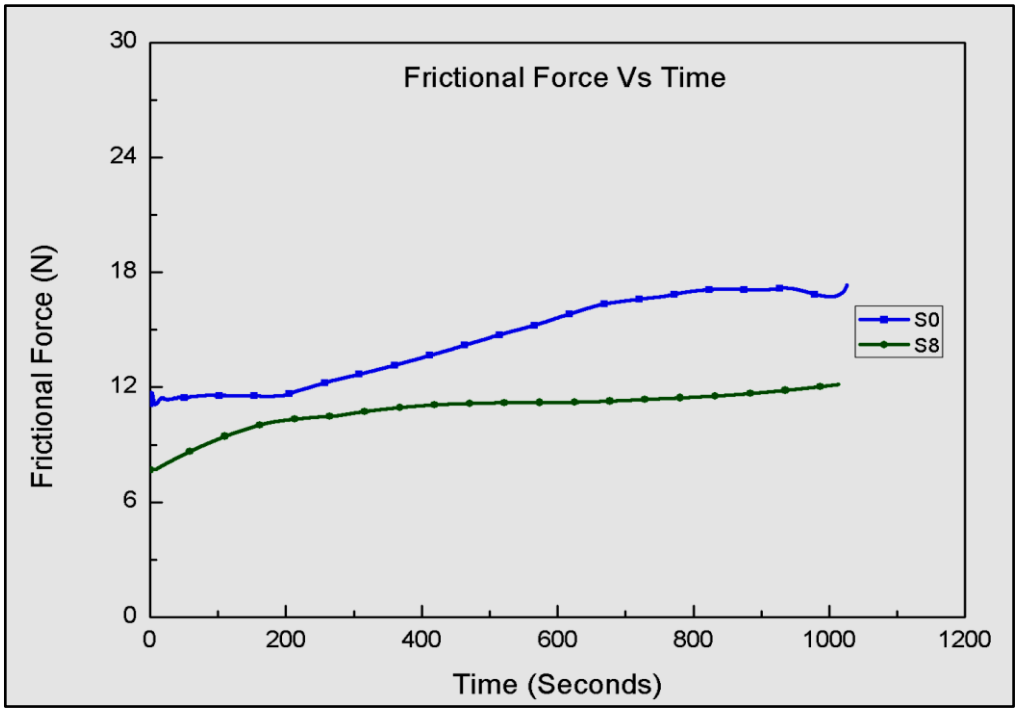

Figure 6.23: Frictional Force of Specimens at 250^{0}C Specimen Temperature During Dry Test Condition

The tribolayer (also known as mechanically mixed layer, composed of oxide layer, wear debris and Fe transferred from the counter face i.e. disk) kept appearing at the contact surface even at elevated specimen temperatures, until the wear became severe. As the temperature increased, the thickness of tribolayer was increased reducing wear but on increasing the temperature further, the mechanically mixed layer totally delaminated, hence increased the wear losses. Optical micrographs of original specimen surfaces are compared with worn specimen surfaces using Field Emission Scanning Electron Microscope, Make: Zeiss; Model: Supra 40VP in Figure 6.24 below.

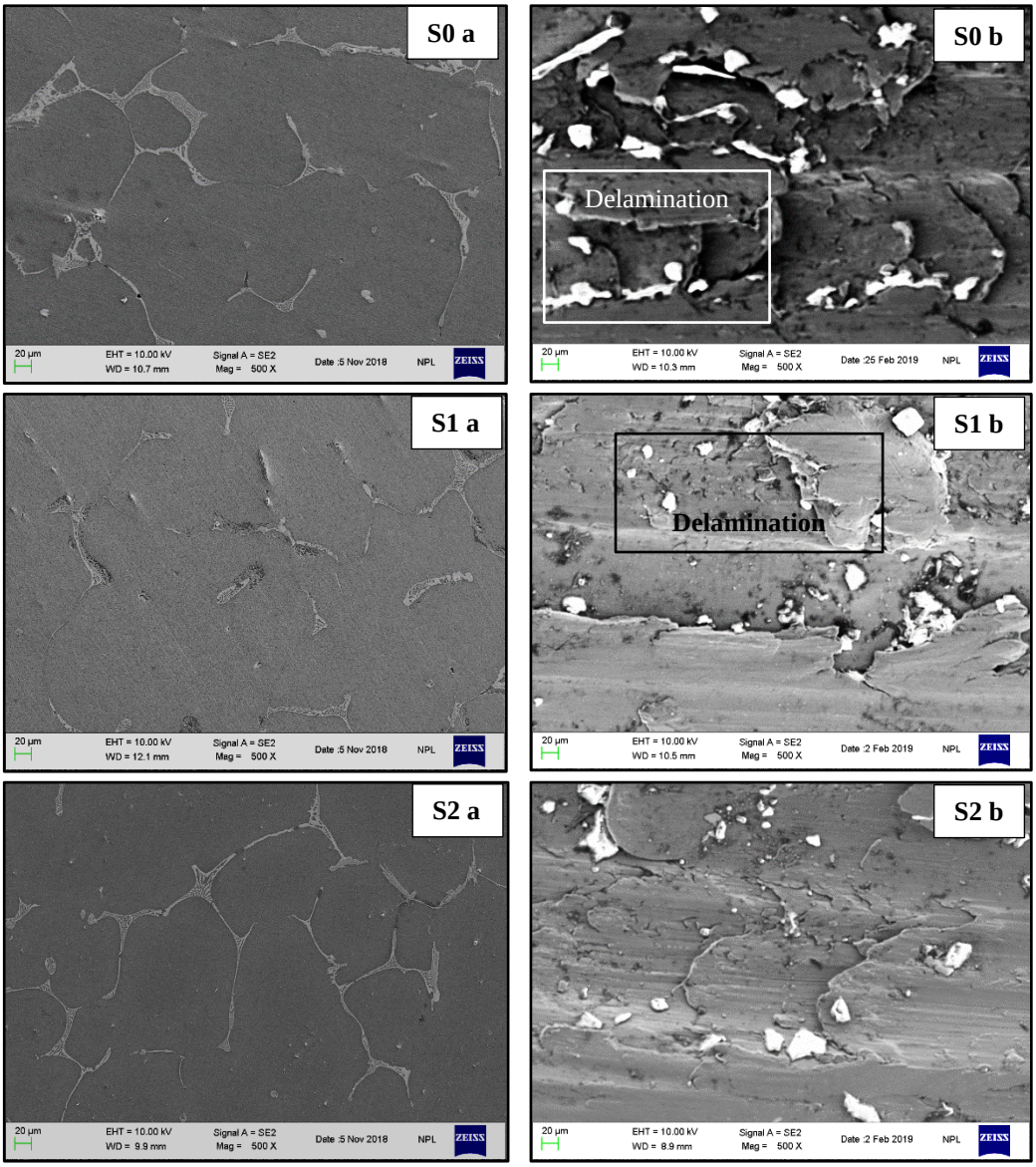

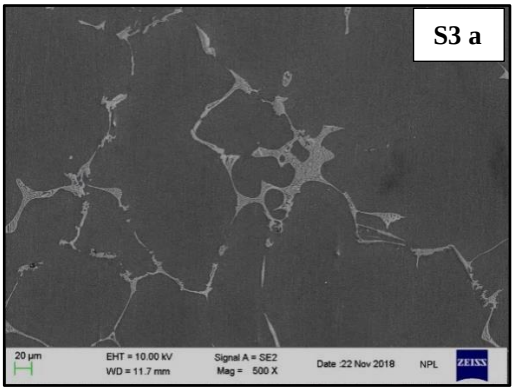
S3 a
20 µm
EHT = 10.00 kV
WD = 11.7 mm
Signal A = SE2
Mag = 500 X
Date :22 Nov 2018
NPL
ZEISS

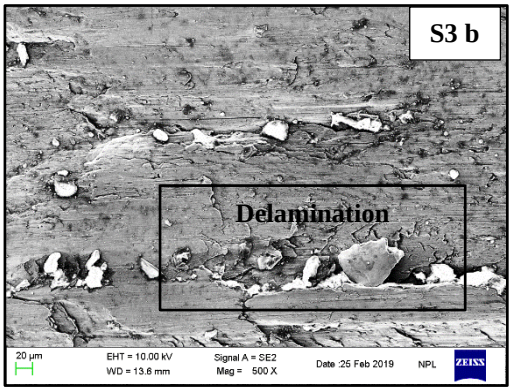
S3 b
Delamination
20 µm
EHT = 10.00 kV
WD = 13.6 mm
Signal A = SE2
Mag = 500 X
Date :25 Feb 2019
NPL
ZEISS

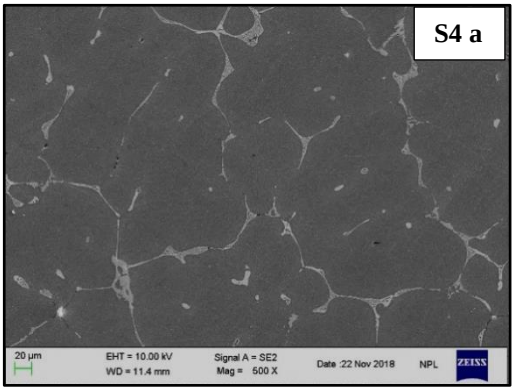
S4 a
20 µm
EHT = 10.00 kV
WD = 11.4 mm
Signal A = SE2
Mag = 500 X
Date :22 Nov 2018
NPL
ZEISS

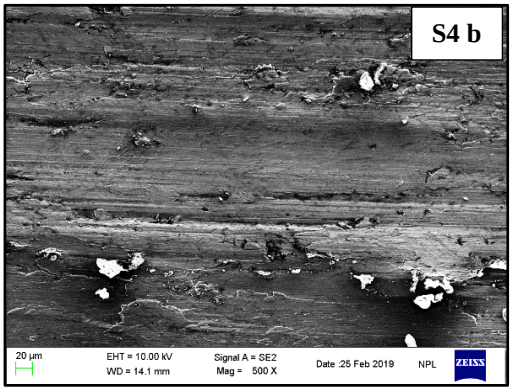
S4 b
20 µm
EHT = 10.00 kV
WD = 14.1 mm
Signal A = SE2
Mag = 500 X
Date :25 Feb 2019
NPL
ZEISS

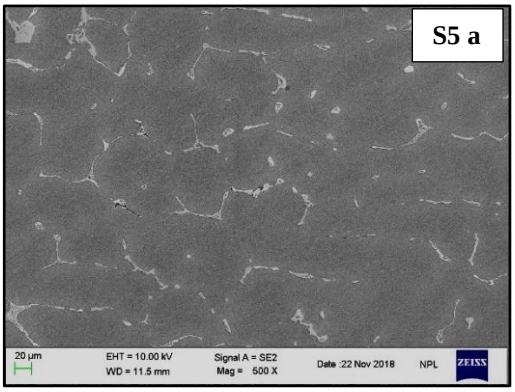
S5 a
20 µm
EHT = 10.00 kV
WD = 11.5 mm
Signal A = SE2
Mag = 500 X
Date :22 Nov 2018
NPL
ZEISS

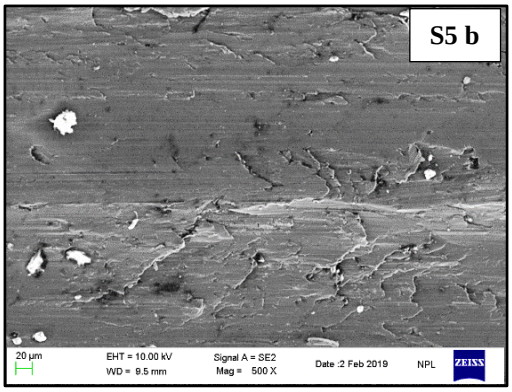
S5 b
20 µm
EHT = 10.00 kV
WD = 9.5 mm
Signal A = SE2
Mag = 500 X
Date :2 Feb 2019
NPL
ZEISS

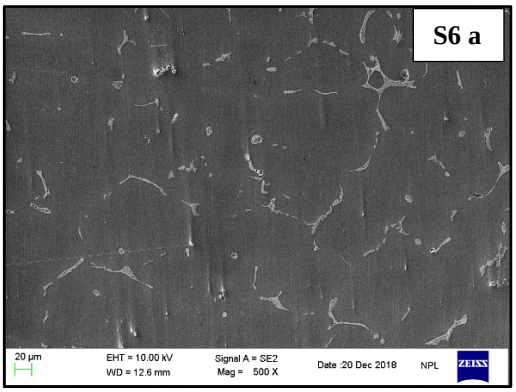
S6 a
20 µm
EHT = 10.00 kV
WD = 12.6 mm
Signal A = SE2
Mag = 500 X
Date :20 Dec 2018
NPL
ZEISS

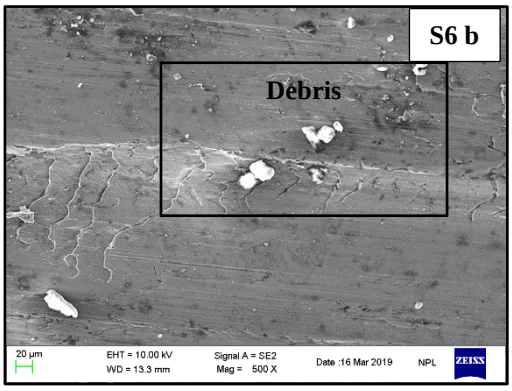
S6 b
Debris
20 µm
EHT = 10.00 kV
WD = 13.3 mm
Signal A = SE2
Mag = 500 X
Date :16 Mar 2019
NPL
ZEISS

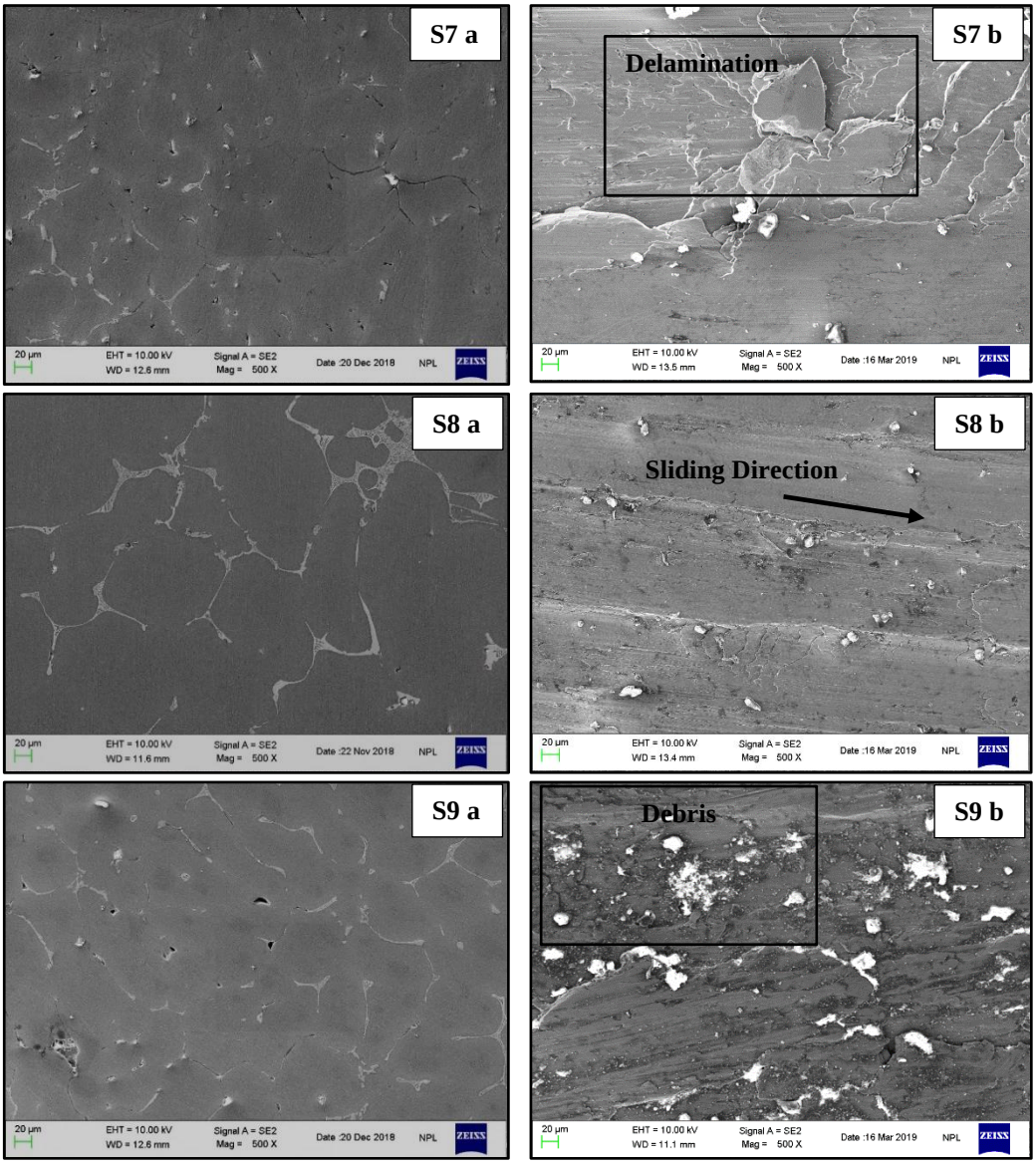

Figure 6.24: SEM Micrographs of (S0 a - S9 a) Original Specimens Surfaces (S0 b - S9 b) Worn Specimens Surfaces

SEM image of worn surface of as-cast Al7075-T6 specimen S0 emerged to be rough and corrugated with deeper voids and adhesive grooves as compared to the aluminium hybrid composite worn surfaces, demonstrating improved wear resistance because uniformly distributed hard reinforcement particles in synthesized composites increased their strength, hardness, thermal stability, load bearing capacity and resisted penetration [183]. These reinforcement particles in hybrid composites restrain crack nucleation due to strong metal matrix-reinforcement interfacial bonding, showing enhanced wear properties as compare to unreinforced base metal. In micrographs of different composite specimens,

severe wear marks on friction surfaces substantiate higher hardness of reinforcement particles as compared to the grinding material EN31.

Sometimes harder asperities penetrated the specimen surfaces and deep trenches occurred there, as in SEM images of specimen S1, S2, S6 and S9. SEM micrographs of investigated specimens such as S3, S4, S5 and S7, also displayed elongated craters laid parallel to sliding direction along with micro-ploughing marks, delamination and flaky wear sediments on wear surfaces indicating adhesive and abrasive wear mechanisms. On further analysing the morphological images, worn surface of aluminium hybrid composite specimen S8 was realized to be homogeneous and covered with smaller wear debris in comparison of other specimens. Smoothest appearance of wear surface of hybrid composite specimen S8 can be attributed to the uniform dispersion of load bearing reinforcement particles and presence of oxide tribolayer (XRD of original specimen is compared with XRD of worn specimen demonstrating presence of oxides, as shown in Figure 6.25) formed between pin specimens and rotating disk restricting metal-to-metal contact and chemical interactions with the counterface hence reducing coefficient of friction and wear loss. On increasing specimen temperature, the occurrence of propagating cracks along weak regions of investigated wear surfaces may be attributed to thickening of the oxide layer and making it brittle. This fragile oxide layer exacerbated gluing of specimen material lumps on rotating disk causing vigorous pull-out of reinforcement particles in form of fragmented and agglomerated powder from metal matrix due to weak bonding strength at higher temperatures.

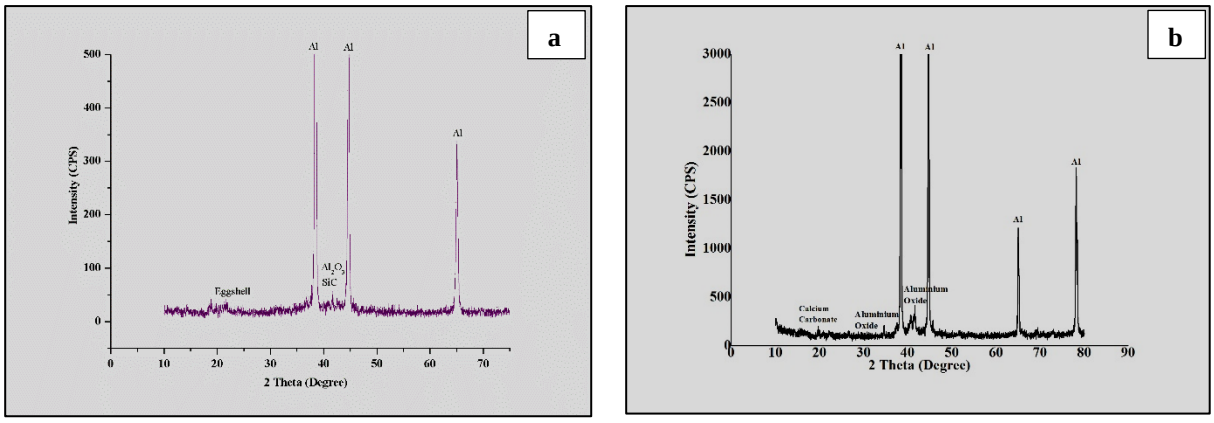

Figure 6.25: XRD of (a) Original Specimen (b) Worn Specimen

Next section deliberates process parameter optimization for wear loss of hybrid aluminium metal matrix composites.

6.4 Parametric Optimization for Wear Loss

Table 6.5 demonstrates three observations corresponding to three replications for wear loss of developed hybrid composite specimens, at 30^0C specimen temperature with dry wear test conditions, with respective S/N ratio for "smaller the better" type of quality characteristic.

Table 6.5: Observations for Wear Loss and S/N Ratio

Wear Loss					
Average Wear Loss of as-cast Al7075-T6 Specimen S0: 1295 µm					
Composite Specimen	**Observation 1 (µm)**	**Observation 2 (µm)**	**Observation 3 (µm)**	**Mean Value (µm)**	**S/N Ratio (dB)**
S1	1249	1265	1233	1249	-61.93
S2	1244	1240	1248	1244	-61.90
S3	1174	1173	1175	1174	-61.39
S4	917	920	915	917	-59.25
S5	1029	1030	1032	1030	-60.26
S6	1098	1100	1097	1098	-60.81
S7	1039	1029	1050	1039	-60.34
S8	515	525	504	515	-54.23
S9	630	634	626	630	-55.99
Constant Wear Test Parameters					
Load	20 N				
Sliding Speed	2 m/s				
Sliding Distance	2000 m				
Test Duration	1000 Sec				
Disk Rotation Speed	764 rpm				
Wear Track Diameter	5 mm				

Plots in Figure 6.26 demonstrate the influence of different process parameters wear loss and S/N ratio in synthesized composites. It is exhibited that with increased eggshell particles content (Figure 6.26a), reasonable silicon carbide and aluminium oxide particles contents (Figures 6.26b and 6.26c) and longer mechanical stirring time (Figure 6.26d) wear loss in developed hybrid aluminium metal matrix composites was decreased noticeably. It was inferred that for minimum wear loss and S/N ratio, 3rd level of eggshell content (A_3), 2nd level of SiC content (B_2), 2nd level of Al_2O_3 content (C_2) and 3rd level of mechanical stirring time (D_3) were optimum levels. Average value of wear loss and S/N ratio for each process parameter at all levels are displayed by Table 6.6.

Table 6.6: Response Table: Wear Loss

Process Parameter	**Level**	**Eggshell Particles wt.%**		**SiC Particles wt.%**		**Al_2O_3 Particles wt.%**		**Mechanical Stirring Time**	
Type of Data	-	Raw Data	S/N Ratio	Raw Data	S/N Ratio	Raw Data	S/N Ratio	Raw Data	S/N Ratio
Average Values	L1	1222.3	-61.7	1068.6	-60.5	954.0	-59.0	969.8	-59.4
	L2	1015.3	-60.1	929.7	-58.8	930.4	-59.0	1127.2	-61.0
	L3	728.0	-56.9	967.4	-59.4	1081.2	-60.7	868.7	-58.3
Main Effects	L2-L1	-207.0	1.6	-138.9	1.7	-23.6	-0.1	157.4	-1.6
	L3-L2	-287.3	3.3	37.8	-0.6	150.8	-1.6	-258.6	2.7
Difference (L3-L2) - (L2-L1)		-80.3	1.6	176.7	-2.3	174.3	-1.6	-416.0	4.3
L1, L2 and L3 display the process parameter levels. (L2-L1) represents main effect while corresponding process parameter changes from level 1 to level 2. (L3-L2) denotes main effect during process parameter change from level 2 to level 3.									

Table 6.7 shows ANOVA results computed at 95% confidence level, with demonstration of F-ratio and percentage contribution of various factors toward quality characteristic. It was observed that eggshell particles wt.% (P=68.17%), silicon carbide particle wt.% (P=5.70%), aluminium oxide particle wt.% (P=7.28%) and mechanical stirring time (P=18.78%) had significant effect on wear loss in synthesized hybrid composites. Table 6.8 demonstrates ANOVA results calculated at 95% confidence level, with display of F-ratio and percentage contribution for S/N ratio.

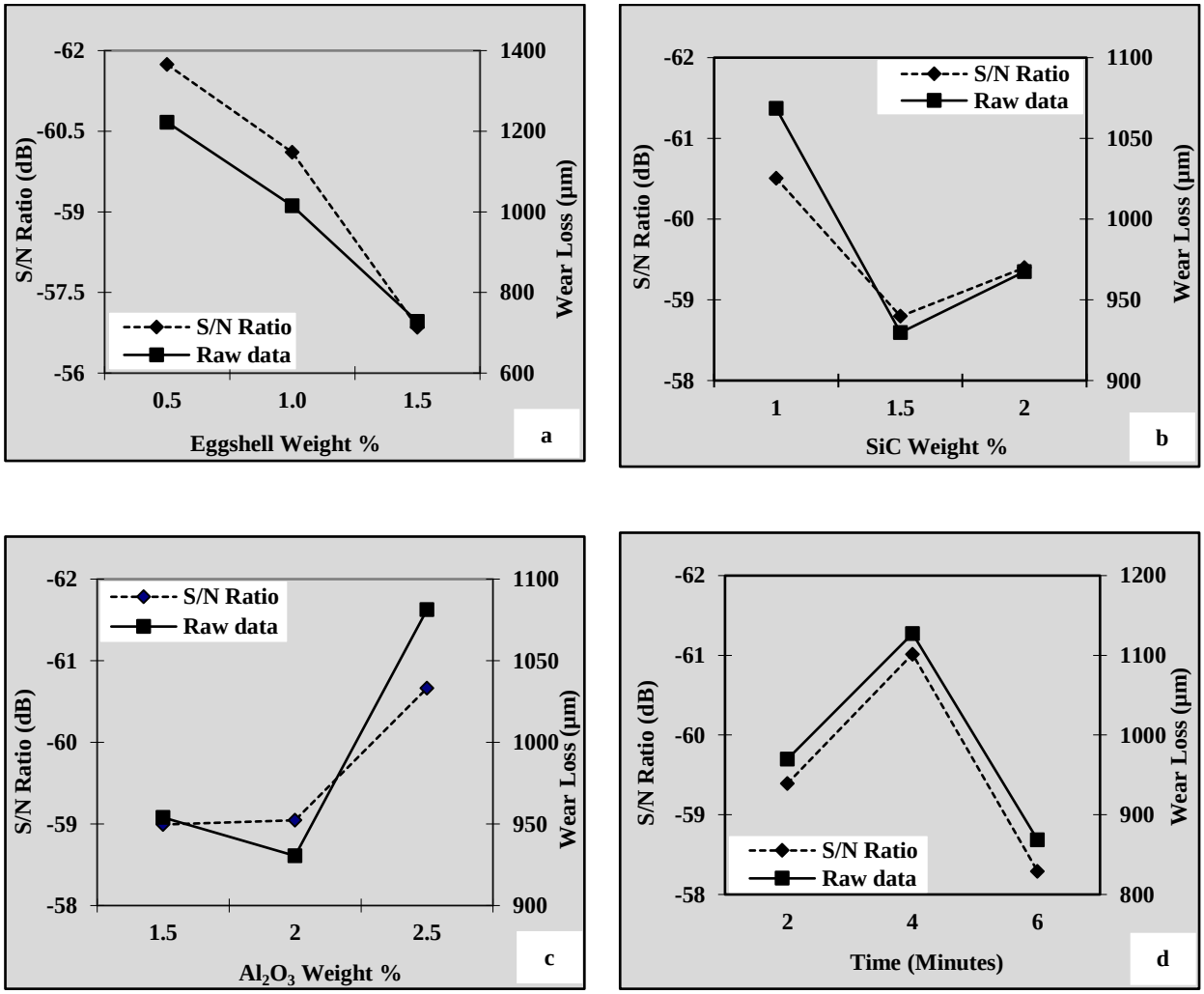

Figure 6.26: Effect of (a) Eggshell Particles wt.% (b) SiC Particles wt.% (c) Al_2O_3 Particles wt.% (d) Mechanical Stirring Time on Wear Loss and S/N Ratio

Table 6.7 Analysis of variance (ANOVA) for Wear Loss

Factor	Sum of Squares (SS)	Degrees of Freedom	Variance (V)	Percentage Contribution (P)	F-Ratio
Eggshell Particles wt.%	1109324.67	2	554662.33	68.17	9587.63*
SiC Particles wt.%	92822.22	2	46411.11	5.70	802.24*
Al_2O_3 Particles wt.%	118422.89	2	59211.44	7.28	1023.50*
Mechanical Stirring Time	305589.56	2	152794.78	18.78	2641.14*
Others/Errors	1041.33	18	57.85	0.06	-
Total	1627200.67	26	-	100	-
***Significant factor at confidence level of 95%, F critical =3.55 (Value from table)**					

Table 6.8 Analysis of variance (ANOVA) for S/N Ratio

Factor	Sum of Squares (SS)	Degrees of Freedom	Variance (V)	Percentage Contribution (P)	F-Ratio
Eggshell Particles wt.%	37.18	2	18.59	63.70	8.24
SiC Particles wt.%	4.51	-	-	-	-
Al_2O_3 Particles wt.%	5.41	2	2.71	9.27	1.2
Mechanical Stirring Time	11.26	2	5.63	19.30	2.50
Others/Errors	4.51	2	2.26	7.73	-
Total	58.36	8	-	100	-
No significant factor at confidence level of 95%, F critical =19 (Value from table)					

Table 6.9 and 6.10 demonstrate pooled versions of ANOVA for wear loss raw data and S/N ratio.

Table 6.9: Pooled ANOVA for Wear Loss Raw Data

Factor	SS	Degrees of Freedom (Pooled)	V (Pooled)	SS'	P % (Modified)	F-Ratio
Eggshell Particles wt.%	1109324.7	2	554662.3	1109208.96	68.17	9587.63*
SiC Particles wt.%	92822.22	2	46411.11	92706.52	5.70	802.24*
Al_2O_3 Particles wt.%	118422.89	2	59211.44	118307.19	7.27	1023.50*
Mechanical Stirring Time	305589.56	2	152794.8	305473.9	18.77	2641.14*
Others/ Errors	1041.33	18	57.85	1504.15	0.09	-
Total	1627200.67	26	-	1627200.67	100	-
***Significant factor at confidence level of 95%, F critical =3.55(Value from table)**						

Table 6.10: Pooled ANOVA for Wear Loss S/N Ratio

Factor	SS	Degrees of Freedom (Pooled)	V (Pooled)	SS'	P % (Modified)	F-Ratio
Eggshell Particles wt.%	37.18	2	18.59	32.66	55.96	8.23
SiC Particles wt.%	-	-	-	-	-	-
Al_2O_3 Particles wt.%	5.41	2	2.71	0.9	1.53	1.20
Mechanical Stirring Time	11.26	2	5.63	6.75	11.56	2.49
Others/ Errors	4.51	2	2.26	18.05	30.94	-
Total	58.36	8	-	58.36	100	-
No significant factor at confidence level of 95%, F critical =19 (Value from table)						

After analysing S/N ratio and mean response characteristic, optimum levels of physically and statistically significant factors were determined to be A_3, B_2, C_2 and D_3. The predicted mean of wear loss at optimal level of process parameters was enumerated using equation 6.1.

$$X_{mp} = \overline{G} + \left(\overline{A_3} - \overline{G}\right) + \left(\overline{B_2} - \overline{G}\right) + \left(\overline{C_2} - \overline{G}\right) + \left(\overline{D_3} - \overline{G}\right) \quad (6.1)$$

Here X_{mp} denoted the predicted mean of wear loss at optimum condition and $\overline{G}$ was the grand average of all 27 observations of utility characteristics from Table 6.5. $\overline{A_3}$, $\overline{B_2}$, $\overline{C_2}$ and $\overline{D_3}$ represented the average values of wear loss at optimal level of significant process parameters. On submitting estimated values of various response averages as $\overline{G} = 988.56$, $\overline{A_3} = 728$, $\overline{B_2} = 929.67$, $\overline{C_2} = 930.44$ and $\overline{D_3} = 868.67$ in equation 6.1, predicted mean optimum value of wear loss was realized to be 491 µm. From Table 6.7 the values were obtained for error variance (57.85) and degree of freedom (DOF) for error (18) whereas F-ratio value at 95% confidence interval was determined from standard statistical table.

Further, confidence interval (CI) calculated using equation 5.6, was ± 13.0. Hence confidence interval with respect to 95% confidence level of predicted optimum wear loss was 478 < Wear loss (µm) < 504. In accordance with Taguchi's optimization approach, a confirmation experiment was conducted by running three more replications for wear loss of produced hybrid aluminium composites at optimal levels of prevalent process parameters as given in Table 6.11 in order to authenticate the predicted results. It is realized from Table 6.11 that confirmation experiment result obtained for wear loss in composites was covered within the predicted confidence interval 478 < Wear loss (µm) < 504.

Table 6.11: Confirmation Experiment for Wear Loss

Quality Characteristic	**Replications**			**Mean**
Wear Loss of Composites (µm)	Replication 1	Replication 2	Replication 3	
	492	496	5610	499 µm

Consolidated tribological characteristics of synthesized hybrid aluminium composite specimen S8 (eggshell wt.%: 1.5, SiC wt.%: 1.5, Al_2O_3 wt.%: 1.5 and mechanical stirring time: 6 minutes), acquiring outstanding wear attributes are compared with unreinforced as-cast Al7075-T6 specimen S0, in Table 6.12.

Table 6.12: Tribological Attributes Comparison of Specimens S8 and S0

Wear Attributes	**Hybrid Aluminium Metal Matrix Composite Specimen S8**	**As-cast Al7075-T6 Specimen S0**
Wear Loss at 30^0C Specimen Temperature in Dry Test Condition	515 µm	1295 µm
Coefficient of Friction at 30^0C Specimen Temperature in Dry Test Condition	0.5	0.83
Frictional Force at 30^0C Specimen Temperature in Dry Test Condition	10.0 N	17.2 N
Wear Loss at 30^0C Specimen Temperature in Lubricated Test Condition	4 µm	36 µm
Coefficient of Friction at 30^0C Specimen Temperature in Lubricated Test Condition	0.04	0.13
Frictional Force at 30^0C Specimen Temperature in Lubricated Test Condition	0.82 N	2.67 N

Wear Loss at 70^0C Specimen Temperature in Dry Test Condition	354 µm	1999 µm
Coefficient of Friction at 70^0C Specimen Temperature in Dry Test Condition	0.25	0.84
Frictional Force at 70^0C Specimen Temperature in Dry Test Condition	4.93 N	17.23 N
Wear Loss at 70^0C Specimen Temperature in Lubricated Test Condition	8 µm	44 µm
Coefficient of Friction at 70^0C Specimen Temperature in Lubricated Test Condition	0.03	0.2
Frictional Force at 70^0C Specimen Temperature in Lubricated Test Condition	0.48 N	3.92 N
Wear Loss at 150^0C Specimen Temperature in Dry Test Condition	117 µm	1693 µm
Coefficient of Friction at 150^0C Specimen Temperature in Dry Test Condition	0.33	0.72
Frictional Force at 150^0C Specimen Temperature in Dry Test Condition	6.6 N	14.4 N
Wear Loss at 250^0C Specimen Temperature in Dry Test Condition	527 µm	1760 µm
Coefficient of Friction at 250^0C Specimen Temperature in Dry Test Condition	0.42	0.7
Frictional Force at 250^0C Specimen Temperature in Dry Test Condition	10.8 N	15.5 N

The following section presents terse outline of present chapter.

6.5 Summary

Bare aluminium alloys are not considered as much acclaimed materials for high performance wear resistant applications because of lower hardness. Hard particulate reinforcements infused into aluminium alloys, during synthesis of aluminium metal matrix composites, enhance wear resistance by restricting the plastic deformations, hence advocating their applications in automobile and aerospace sectors. This chapter includes evaluation of synthesized composites and base metal for tribological attributes such as wear loss, coefficient of friction and frictional force through pin-on disk wear test at fixed load of 20N, speed of 2 m/s and sliding distance of 2 km. Standard wear test specimens (as-cast Al7075-T6 and

produced hybrid composite specimens) were investigated at different specimen temperatures; 30^0C, 70^0C, 150^0C and 250^0C for dry/lubricated wear test conditions.

Momentous enhancement was observed in wear characteristics of hybrid composite specimens as compared to the unreinforced base metal specimen. Optical micrographs of worn specimens have been discussed in detail for wear mechanism analysis. Process parameter optimization was carried out through ANOVA analysis. Machinability investigations for all the specimens (one as-cast Al7075 and nine hybrid aluminium composite specimens) shall be discussed in next chapter.

CHAPTER 7

Machinability of Synthesized Hybrid Aluminium Composites

7.1 Introduction

Augmented characteristics of advance engineering materials can be of utmost utilization, when amalgamated with reasonable machinability. Though aluminium metal matrix composites are recognized as state-of-the-art functional materials with enhanced mechanical attributes depending upon base metal composition, reinforcements and various process parameters, yet sometimes the non-homogeneous nature combined with abrasive reinforcement materials, contribute significantly in their arduous machining, restricting their widespread applications in industry.

In present research work, after synthesis hybrid aluminium composites were converted into useful engineering components though various machining processes and were observed to be difficult to machine by the virtue of the hard reinforcement particles infused into metal matrix (without comprising of any chemical reaction) as compared to the conventional materials. This chapter includes machinability analysis of hybrid aluminium composites (Al7075-T6 as base metal with reinforcements eggshell particles wt.% 0.5, 1and 1.5, average particle size ≈ 60 µm, SiC particles wt.% 1, 1.5 and 2, average particle size ≈ 65 µm and Al_2O_3 particles wt.% 1.5, 2 and 2.5, average particle size ≈ 90 µm), mechanically stirred for variable time durations and further synthesized through electromagnetic stir casting route. Discussions on machinability study of composites have been included in upcoming section.

7.2 Machinability Study

Machinability is defined as the degree of ease with which a material is machined with gratifying surface finish. Broadly, hard to machine materials are classified in to three categories:

(i) Hard materials

(ii) Ductile materials

(iii) Non-homogeneous materials, reducing material removal rate and producing inferior surface finish.

In aluminium metal matrix composites, infused reinforcements enhanced numerous mechanical and physical attributes, but at the cost of their machinability. Past investigations on aluminium composites exhibited inferior machinability due to irregular material removal rate, abrasive tool wear (hard reinforcement particles such as titanium boride, boron carbide and silicon carbide cause intense tool wear) and deteriorated quality of the machined surface. In extreme cases, during machining of aluminium based composites, plucking effect of tool on hard reinforcement particles eventuated into poor surface quality and damage of workpiece. On exploring various machining parameters, it has been experienced that surface finish and tool wear contribute the most towards making composite machining uneconomical. During machining operation, the tool interacts with aluminium matrix and reinforcement particles alternatively, responding in absolutely different manner, resulting into increased abrasive tool wear (created by impacts at cutting edge and by sliding movement of reinforcement particles relative to the rake and clearance face of machining tool), poor surface quality, discordant material removal and costly production process.

Hence, major complications confronted during machining of aluminium composites were substandard surface finish, inconsistent material removal rate and rapid tool wear. Machining parameters optimization of aluminium composites using artificial neural network and analysis of variance, demonstrated that surface finish of machined workpiece was primarily influenced by feed rate followed by cutting speed and depth of cut (increased depth of cut and feed rate reduced surface quality). Though various alternative processes such as net shape forming and modified casting have been explored to sidestep machining operations, yet they have their own restraints projecting machining as an indispensable part of manufacturing process [184].

The degree of accomplishment of aluminium metal matrix composites depends on their appositeness for various machining operations. Additional demanding factor pertinent to machining of particulate reinforced aluminium composites was realized to be destruction and/or pull-out of reinforcement

materials at sub surface zone, generating micro-cracks, pits, and voids hence diminishing the mechanical and physical characteristics of machine component [185]. Machining of aluminium composites infused with silicon carbide fibers/particles and aluminium oxide demonstrated poor machinability in terms of irregular materials removal rate and deteriorated surface finish [186]. It was also observed that increased volume fraction of SiC in aluminium composites reduced tool life whereas reduction in SiC particle size increased tool life significantly [187, 188]. Machinability investigations of boron carbide (5-20 wt.%) reinforced Al 6061 composite using uncoated carbide insert showed improved surface finish with elevated B_4C content. On machining Al/SiC_p composite with reinforcement volume fraction of 16% and particle size of 30, 45 and 110 μm using carbide tool, it was realized that reinforcement quantity and its size significantly influenced the surface finish of machined components [189]. Machined aluminium 6061/10 wt.% alumina particles composites with variable reinforcement particle sizes displayed high tool wear and poor surface finish [190]. TiB_2/Al composite machined using polycrystalline diamond cutting tools required higher machining forces and exhibited better surface finish as compared to unreinforced alloy [191]. Infusion of mica in Al 356/SiC/rice husk ash hybrid composites resulted into reduced flank wear due to lubricating attributes of mica. [192]. Reduced tool life was noticed during machining of glass reinforced aluminium composites using coated carbide cutting tool, however polycrystalline cubic boron nitride tool outperformed it in terms of surface finish, material removal rate and tool wear [193]. Al/ SiC_p (5, 10 and 15 wt.%) composites machined on conventional lathe machine under dry cutting operation, using hard carbide coated cutting TiN tool demonstrated uneven surface [194].

Though, during machining of aluminium composites, metal removal rate (MRR) and surface finish depends on various parameters such as feed rate, cutting speed, depth of cut, work material hardness and tool angles etc., however the most significant parameters are cutting speed, depth of cut and feed rate. On increasing feed rate, friction grows between the composite material workpiece and cutting edge, increasing cutting forces and causing heat generation, which adversely affects the machining environment. To overcome this issue, lubricants and cutting fluids

were used during machining of aluminium composites to provide tighter dimensional tolerances of the workpiece and to enhance machinability, pertaining to superior surface finish, consistent material removal rate and longer tool life. Researchers have investigated the repercussions of cutting parameters on surface finish of Al7075/SiC/graphite composites using polycrystalline diamond cutting tool. Machining evaluation of Al/5% SiC particle composites exhibited that feed rate and cutting speed are the predominant influencing parameters for surface finish, material removal rate and too wear [195]. It was observed by researchers that on turning of A359/SiC/20p composites at higher feed rate, larger volume of material was removed before reaching to wear limit [196]. Influence of various machining parameters on Al/fly ash composites were investigated and it was observed that notch wear, occurring at the intersection of rake and flank surface and at the end radial depth of was the main reason of tool failure [197]. On turning Al2024/Al_2O_3 composite specimens using TiN (K10) coated and uncoated tool, it has been observed that the tool life decreased at higher cutting speed. Turning of Al-5Mg alloys reinforced with 5 Vol% of saffil and 15 Vol. % of silicon carbide using conventional ceramics and polycrystalline diamond cutting tools led towards longer tool life and improved surface finish at high feed rate and low cutting speed, whereas depth of cut appeared to be insignificant [198] Milling of Al-4%Cu/B_4Cp composites using uncoated and coated tools at different feed rates resulted into variable tool wear [199].

In aluminium composites, reinforcement particles fracture and their debonding during machining procedure may be attributed to the distribution and magnitude of stresses and strains in composites and cutting tool interaction with reinforcement particles. Improved machining attributes of aluminium composites surmount excessive chatter, surface irregularities, enormous tool wear and limit the usage of metal cutting fluids, addressing environmental concerns and health issues. Critical machining parameters and their effects on machined aluminium metal matrix composite components are succinctly discussed below:

- **Reinforcement**

  Hard reinforcement particles infused in aluminium matrix substantially influence the machinability of composites (due to anisotropic and non-homogeneous nature) in form of irregular material removal and increased surface roughness. The content, size and distribution of reinforcement materials significantly affect the surface finish of machined surfaces of aluminium metal matrix composite components. Increased reinforcement contents and larger reinforcement sizes extensively restrict the machinability of composites.

- **Feed Rate**

  Surface finish is considered to be the most critical cutting attribute for evaluation of machinability of aluminium metal matrix composites. Feed negatively influences the surface finish of machined aluminium composite components. It predominantly affects the subsurface damage and cutting forces. High feeds originate higher cutting forces, generating voids around reinforcement particles which combine and form micro-cracks and initiate composite failure along the shear band. Apparently feed has insignificant impact on tool wear in comparison of other machining parameters, as higher feed increases heat conduction from cutting zone to workpiece, thus reduce tool wear rate. Feed rate marginally increases the flank wear in comparison of cutting speed, hence is considered as the second influential machining parameter after cutting speed [200].

- **Depth of Cut**

  During machining of aluminium metal matrix composites, depth of cut adversely influences surface finish, subsurface damage and tool wear. Though depth of cut affects the tool wear inappreciably, it has a substantial effect on tool life as compared to the feed during machining [200].

- **Cutting Speed**

  Cutting speed is the most prominent parameter for tool life. Higher cutting speeds develop rapid increase in flank wear, leading towards catastrophic tool failure. During machining of aluminium composites, low cutting speeds create built-up edges, these built-up edges increase the actual rake angle of

cutting tool, hence reducing the cutting forces and providing longer tool life. Cutting forces during machining of aluminium composites depend on fracture of reinforcement particles, chip formation and ploughing due to friction between tool and workpiece surface. The reinforcement particles present in aluminium matrix offer resistance against particle fracture and ploughing etc., resulting into challenging machining of composites. For aluminium composites in lubricated machining conditions, higher cutting speeds provide longer tool life with disintegrated surface finish with increased gaps and voids [201].

- **Tooling**

  Adequate machining of aluminium metal matrix composites requires cutting tool materials to be harder and stiffer than the work piece materials. Commonly used tool materials are tungsten carbide, polycrystalline diamond, cubic boron nitride and Chemical vapour deposition diamond (CVD). Selection of appropriate cutting tool material results into enhanced surface finish, reduced sub-surface damage, reduced tool wear and reduced power consumption due to decreased friction at tool and workpiece interface [201]. During machining of aluminium composite materials, heat generation takes place in primary shear zone (conversion of major part of energy into heat), secondary deformation zone (heat generation due to rubbing between tool chip interface) and flank wear zone (heat produced due to rubbing between tool and machined surface). The increased temperature caused plastic deformation and fracture of cutting edge, inconsistent material removal and surface damage followed by dimensional inaccuracy of machined workpiece. On performing machining on aluminium metal matrix composites, temperature is elevated at cutting tool workpiece interface resulting into poor surface finish. For ameliorated machinability of aluminium composites, referring to consistent material removal rate and superior surface finish, is it essential to optimize assorted machining parameters, tool geometry and machining conditions [201].

In present experimental investigation, as-cast Al7075-T6 specimen (S0) and synthesized hybrid aluminium metal matrix composite specimens (S1-S9), as

shown in Figure 7.1 were evaluated for their machinability in terms of material removal rate, surface roughness and types of chips formed with machining parameters as given below:

- Cutting speed: 6 m/min
- Depth of cut: 1mm
- Feed rate: 0.3 mm/second
- Test duration: 30 seconds

Machinability studies were carried out on a convention lathe machine (Model No. SG: 2, Electric motor: 2HP, Speed 50-1200 rpm, Distance between centres: 125 mm) with tungsten carbide cutting tool as shown in Figure 7.2. Composite machinability attributes; material removal rate, surface roughness and chip formation are deliberated in forthcoming sections.

Figure 7.1: Machinability Study Specimens

7.2.1 Material Removal Rate and Surface Roughness

Generally, poor machinability of aluminium metal matrix composites results into increased product cost and restrained applications despite of their excellent mechanical and physical properties. Machining of aluminium composites has been somewhat challenging in comparison of the parent alloy, due to considerable hardness of infused reinforcement particles. The abrasive action of these reinforcement particles results into arbitrary material removal and inferior

surface finish, hence influencing some critical mechanical attributes of the machined component. Material removal rate of synthesized aluminium composite specimens during turning operation on a conventional lathe machine with tungsten carbide cutting tool is represented in Table 7.1. In case of aluminium composites machinability evaluation, acceptable performance was ascertained only when the cutting tool material (in present study, tungsten carbide) was harder than reinforcements. It was observed from Table 7.1, that the material removal rate decreased just marginally in synthesized hybrid aluminium metal matrix composites as compared to their unreinforced counterpart (base metal), due to remarkable uniform dispersion of reinforcement particles into matrix material.

Table 7.2 demonstrates surface roughness parameters of as-cast Al7075 specimen and nine aluminium composite specimens after machining. A combined representation of material removal rate and roughness for each specimen is demonstrated in Figure 7.3. During machining of developed hybrid aluminium composites, when the cutting tool interacted with reinforcement particles and the particle were sheared, better surface finish was obtained. Whereas when reinforcement particles were pulled out by the cutting tool, cracks and pits were formed on the machined surface, conceiving deteriorated surface finish as compared to the unreinforced metal matrix.

Figure 7.2: Machinability Investigations

Table 7.1: Material Removal Rate of Specimens

Specimen	Speed in RPM	Initial Weight (g)	Final Weight (g)	Material Removed (g)	Material Removal Rate (MRR in g/sec)
S0	195	18.87	18.74	0.13	0.0043
S1	195	16.53	16.44	0.09	0.0030
S2	195	18.62	18.51	0.11	0.0037
S3	195	18.91	18.81	0.10	0.0033
S4	195	18.05	17.95	0.10	0.0033
S5	195	17.47	17.35	0.12	0.0040
S6	195	16.18	16.08	0.10	0.0033
S7	195	17.95	17.85	0.10	0.0033
S8	195	17.22	17.10	0.12	0.0040
S9	195	17.04	16.93	0.11	0.0037

Table 7.2: Surface Roughness of Specimens

Specimen	Ra (µm)	Rz (µm)
S0	1.15	5.69
S1	1.47	9.92
S2	1.35	8.74
S3	1.23	11.79
S4	1.11	6.75
S5	1.14	7.57
S6	1.27	9.08
S7	1.12	6.86
S8	1.02	6.54
S9	1.13	6.75

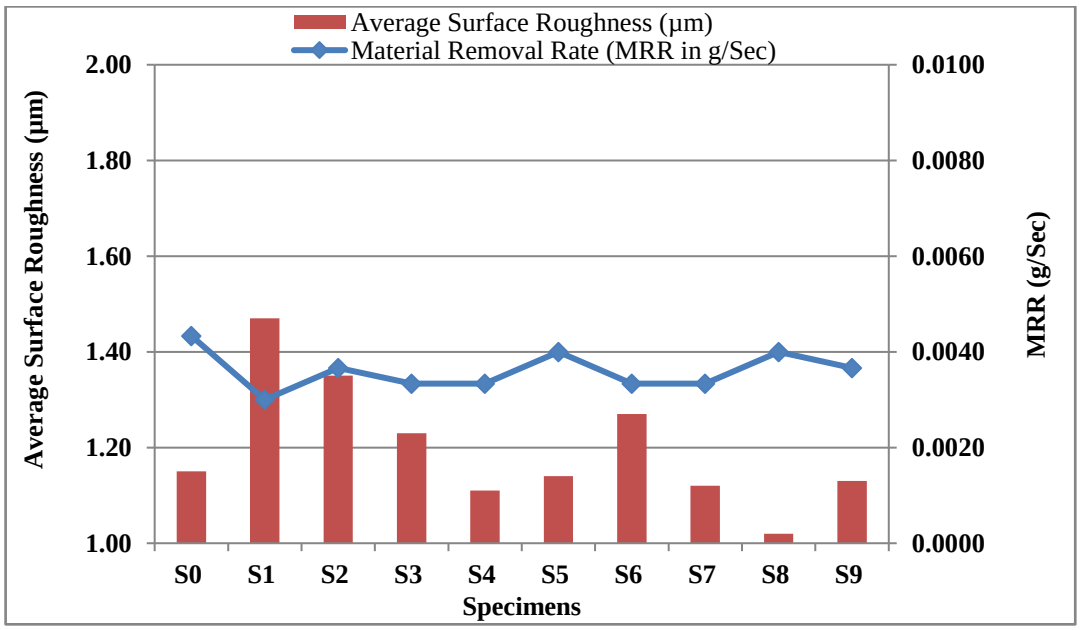

Figure 7.3: Material Removal Rate and Roughness

7.2.2 Chip Formation

Machining characteristics of any material is appreciated effectively through chip formation investigations. To enhance the machinability of aluminium composites and their relevance in different industrial applications, generation of discontinuous chips with no chip breaker is required for stable machining process. The chip size in aluminium metal matrix composites significantly depends upon reinforcement particles content, various cutting parameters and tool geometry. Addition of hard reinforcement particles into aluminium matrix reduced ductility causing production of semi continuous chips during machining and the composite chips exhibited a systematic breaking trend depending on reinforcement content. It was also observed that a chip breaking criterion related the chip breaking mechanism with composite mechanical attributes [202].

Chip formation is primarily accompanied by shear zone plastic deformation and depends on microstructure, ductility and thermal conductivity etc. of the composite materials. During investigation of chip formation mechanism in machining of aluminium metal matrix composites, it has been observed that at lower cutting speed thin, flaky and segmented chips were produced whereas semi continuous and continues chips were generated at higher cutting speed. Also, on machining aluminium composites at fixed depth of cut, fixed cutting speed and increased feed rate, chips with increased length and a greater number of curls were obtained. It was observed that during machining of aluminium composites at lower cutting speed needle like segmented chips were formed whereas at higher cutting speed continuous, semi-continuous chips were produced [202].

In present experiment, after machining of unreinforced Al7075-T6 alloy, longer chips were obtained due to its ductile nature, as demonstrated by Figure 7.4 a. During machining of aluminium composites, semi continuous (saw toothed segmental) chip formation took place in shear zone along with micro-ploughing and reinforcement particle fracture, as shown in figure 7.4 b. During machining, long chips were broken into smaller pieces due to side-curling and upward action of chips, accelerating the crack propagation. Additionally, some small clusters of reinforcement particles present within aluminium composites, increased stresses to accelerate crack propagation and material fractured in form of segmented chips.

Figure 7.4: Chips Formed During Machining of (a) As-cast Al7075-T6 (b) Aluminium Composites

During chip formation, shear stresses were enforced by the rake surface of machining tool, causing crack initiation from the outside chip free surface. Due to stress concentration at particle edges, de-cohesion and separation of reinforcement particles from aluminium matrix within the chip resulted into generation of small voids. On further shearing of aluminium composites, crack growth was accelerated, and they propagated along the shear plane due to coalescence of these voids, followed by fracture and sliding of composite material generating segmented chips. The crack formation in deformation zone occurred due to cutting edge advances into the work piece, generating plastic deformation. As the cutting tool advanced further, the crack started propagating and material lump moved up the rake face. The force and motion constraints acting on material lump caused crack propagation towards the surface, detaching small chip fragments [203]. During machining of synthesized composites, presence of hard reinforcement particles also exhibited enhanced chip disposability.

In general, machining cost of any manufactured component enhances the total cost approximately by 20%, hence in addition to augmented mechanical attributes of aluminium composites, optimal machinability is immensely desired. Evidently, machining of aluminium composites is not effortless due to the abrasive nature of infused reinforcement particles, resulting into degraded surface finish, unstable material removal rate and reduced tool life. However, in some specific cases, reasonable machinability of composites may be attributed to their uniform microstructures and selection of appropriate cutting parameters, providing sturdy

dimensional tolerances and desired surface finish to the machined component, endorsing their wide industrial applications. Next section includes summarized review of present chapter.

7.3 Summary

This chapter includes discussions on machinability of aluminium composites along with various critical complications confronted. Reasons for limited machinability, inconsistent material removal rate and inferior surface finish have also been deliberated. Critical machining parameters and their influences on machinability of aluminium composites have been discussed briefly. A comparative representation of material removal rate and average surface roughness of all the specimens (S0-S9) have been included in this chapter. The next chapter shall attempt to enlist major research findings of present experimental investigation, limitations of research work and future scopes.

CHAPTER 8

Conclusion and Future Scopes

8.1 Research Findings

Constitutional motivation for present research work was to produce and extensively characterize ecodesigned and cost-effective hybrid aluminium metal matrix composites with conspicuously augmented physical and mechanical attributes. This is in line to accentuate the utilization of agricultural waste for composite production. Eggshell waste is an inordinately serious menace to our environment, generating odour and disadvantageous microbial growth. Eggshells were processed and used for synthesis of Al7075-T6/ Eggshell/SiC/Al_2O_3 hybrid composites as per the design matrix through electromagnetic stir casting technique, followed by assessment of composites and process parameter optimization. Fabricated hybrid aluminium composites with remarkably upgraded characteristics may be endorsed for automotive applications due to better tribological and fatigue properties, high strength structural applications and light weight aerospace applications.

Synthesized composites were evaluated for microstructure, elemental composition and distinctive traits.

- ***Microstructure and Elemental Composition***
  - In this thesis, optical micrographs of synthesized composites exhibited their stable microstructure with finer grain sizes due to heterogeneous nucleation caused by infusion of particle reinforcements. They also exhibited some traces of porosity and detrimental pores due to various process induced effects, with presence of noticeable amounts of various element in XRD and EDS spectrograms.
- ***Porosity***
  - A maximum relative enhancement of only 2.2% was observed in density of composites, whereas maximum relative decrease in

percentage porosity of synthesized hybrid composites was upto 76% as compared to as-cast Al7075-T6.

- ANOVA computation demonstrated that only eggshell particles wt.% (P=66.82%) had significant effect on percentage porosity of synthesized hybrid composites, whereas other process parameters SiC particles wt.% (P=4.75%), Al_2O_3 wt.% (P=3.63%) and mechanical stirring time (P=4.21%) remained insignificant. Predicted optimum value of percentage porosity through Taguchi parameter design approach was (0.35±0.23), which was confirmed experimentally.

➢ ***Residual Stress***

- Maximum relative decrease in residual stress in composites has been observed to be 76% as compared to as-cast Al7075-T6 specimen.
- ANOVA results demonstrated that eggshell particles wt.% (P=66.65%), SiC particles wt.% (P=12.09%) and Al_2O_3 particles wt.% (P=5.32%) influenced the residual stresses significantly, whereas mechanical stirring time (P=2.91%) had infinitesimal influence. Predicted optimum value of residual stress through Taguchi approach was (25.63±40.9) Mpa and this was verified experimentally.

➢ ***Microhardness***

- Maximum relative enhancement of 83% in microhardness of hybrid composites has been witnessed as compared to their unreinforced counterpart.
- Microhardness of synthesized hybrid composites was influenced significantly by all the process parameters. Eggshell particles wt.% (P=54.06%) appeared to be the most significant process parameter followed by SiC particles wt.% (P=28.96%), Al_2O_3 particles wt.% (P=15.85%) and mechanical stirring time (P=0.64%). Predicted optimum value of microhardness through Taguchi parameter design approach was (320.01±5.54) HV, which was confirmed experimentally.

- ***Tensile Strength***
  - There has been a maximum relative increase of 106% in tensile strength of fabricated hybrid composites as compared to the as-cast Al7075-T6 specimen.
  - Eggshell particles content (P=34.22%) had the highest perceptible influence on tensile strength of hybrid composites, followed by other significant process parameters i.e. SiC particles content (P=25.30%), Al_2O_3 particles content (P=21.43%) and mechanical stirring time (P=9.49%). Predicted optimum value of tensile strength obtained using Taguchi approach was (78.9±8.25) Mpa and this was experimentally verified through confirmation experiment.
- ***Fatigue Life***
  - Number of reversible load cycles survived by synthesized composites were increased upto many folds in comparison to their unreinforced counterparts.
  - Eggshell particles wt.% (P=77.24%) appeared to be the most predominant process parameter affecting low cycle fatigue life of synthesized hybrid composites, followed by other significant process parameters i.e. SiC particles wt.% (P=7.22%), Al_2O_3 particles wt.% (P=7.93%) and mechanical stirring time (P=7.61%). Predicted optimum number of load cycles survived through Taguchi parameter design approach was (4562±14), which was confirmed experimentally.
- ***Surface Roughness***
  - Maximum relative decrease of 30% in average surface roughness of fabricated hybrid composites was noticed as compared to the base alloy.
  - Eggshell particles wt.% (P=38.30%) was the most significant process parameter to influence average surface roughness of aluminium composites, followed by other significant process parameters i.e. SiC particles wt.% (P=20.53%), Al_2O_3 particles wt.% (P=20.69%) and mechanical stirring time (P=18.40%). Predicted optimum value of

surface roughness obtained using Taguchi approach was (0.85±0.32) μm and this was experimentally verified.

This thesis encapsulates a comprehensive tribological behaviour analysis of developed composites at various specimen temperatures for dry and lubricated wear test conditions. This analysis has been conducted in order to advocate the produced composites for various wear resistant applications.

- ***Tribological Investigations***
  - **Dry Sliding Behaviour at 30^0C Specimen Temperature**
    Hybrid composites displayed maximum relative decrease of 60% in wear loss, decrease of 40% in coefficient of friction and decrease of 42% in frictional force as compared to unreinforced aluminium alloy.
  - **Lubricated Sliding Behaviour at 30^0C Specimen Temperature**
    Hybrid composites demonstrated maximum relative decrease of 89% in wear loss, decrease of 69% in coefficient of friction and decrease of 69% in frictional force with respect to base metal.
  - **Dry Sliding Behaviour at 70^0C Specimen Temperature**
    Hybrid composites exhibited maximum relative reduction of 82% in wear loss, reduction of 70% in coefficient of friction and reduction of 71% in frictional force in comparison of their unreinforced counterpart.
  - **Lubricated Sliding Behaviour at 70^0C Specimen Temperature**
    Synthesized hybrid composites showed maximum relative abatement of 82% in wear loss, abatement of 85% in coefficient of friction and decrease of 88% in frictional force as compared to base alloy.
  - **Dry Sliding Behaviour at 150^0C Specimen Temperature**
    Hybrid composite specimen S8 represented a relative reduction of 93% in wear loss, 54% in coefficient of friction and 54% in frictional force in comparison of as-cast Al7075-T6 specimen S0.
  - **Dry Sliding Behaviour at 250^0C Specimen Temperature**
    Synthesized hybrid composite specimen S8 affirmed a relative reduction of 70% in wear loss, 40% in coefficient of friction and 30% in frictional force in comparison of specimen S0.
  - ANOVA results demonstrated that wear loss of synthesized hybrid

composites was influenced significantly by all the process parameters. Eggshell particles wt.% (P=68.17%) appeared to be the most significant process parameter followed by SiC particles wt.% (P=5.70%), Al_2O_3 particles wt.% (P=7.28%) and mechanical stirring time (P=18.78%). Predicted optimum value of wear loss obtained using Taguchi approach was (491±13) µm and this was experimentally verified.

The thesis includes exhaustive machinability investigation of synthesized composites in terms of material removal rate and surface roughness.

- ***Machinability***

  On infusion of reinforcement particles, machinability of hybrid composites was witnessed to remain unblemished in terms of proportionate material removal rate (material removal rate of specimen S8: 0.0040g/sec and of specimen S0: 0.0043g/sec) and comparable surface roughness (average surface roughness of specimen S8: 1.02µm and of specimen S0: 1.15µm). Additionally, the chips formed during machining of composite were curled and semi-continuous.

Present research work provides an all-inclusive framework for synthesis, characterization and process parameter optimization of environment friendly aluminium hybrid composites. ANOVA analysis demonstrated that among all the process parameters, eggshell content evolved to be predominant in influencing numerous composite characteristics extensively. Produced hybrid composites were realized to be excessively economical with maximum total reinforcement content of 5.5% only. With outstandingly augmented mechanical and physical attributes such as low density, decreased porosity, reduced residual stresses, enhanced hardness, high strength, improved fatigue life, justifiable machinability and sustainable tribological characteristics over an expanded range of temperatures etc. synthesized hybrid aluminium composite have momentous potential for advance engineering applications, superseding various conventional materials in a blazing way. Limitations of present research work have been summarized in upcoming section.

8.2 Limitation of Research Work

Complications confronted during present experimental investigation include the following concerns.

- Stirring speed is a critical process parameter, significantly influencing the composite attributes. Mechanical stirrer of stir casting setup used for present experiment, rotated at a fixed speed of 150 rpm, hence nowhere in present research work variable stirring speed was not taken into account for evaluation of hybrid aluminium composite characteristics.
- Due to practical constrains, during solidification of various castings after electromagnetic stir casting process, no specific procedure was adopted to release trapped air, resulting to various defects and causing noticeable material loss.
- Hybrid composites have not been evaluated for other critical attributes such as isotropy, stiffness, toughness, corrosion resistance and thermal expansion etc. due limited availability of synthesized materials.

The next section includes future research scopes in extension of present investigation.

8.3 Recommendations for Future Research

Present research subject matter has been extremely impactful pertaining to the novel advancements in metal matrix composites. Though, it provides a comprehensive blend of fabrication, characteristics evaluation and parameter optimization of ecodesigned and cost-effective hybrid aluminium composites with remarkably enhanced traits, however there is plausible scope for future research, which may lead to better interpretation of unconsidered scientific aspects related to hybrid aluminium composites in detail. The scope of diversified future works in perpetuation with present study has been discussed below.

- The present work can further be extended to a revolutionary and extremely interesting study to investigate the influence of various reinforcement sizes on different characteristics of hybrid aluminium metal matrix composites.
- Limited research work has been carried out to study the effects of other dominating process parameters such as preheat temperature, stirring

temperature, stirring speed and stirrer's position on hybrid composite attributes. Present experimental investigation has a persuasive extension scope in this direction.

- Present experimental investigations may be extended for exhaustive corrosion resistance assessment of synthesized hybrid aluminium composites, by designating appropriate processing conditions, as processing conditions may cause rapid corrosion in composites as compared to monolithic alloys. Other critical characteristics such as toughness, creep and machinability etc. can also be explored extensively in order to upsurge the industrial applications of produced hybrid aluminium composites.
- Attempts may be carried out to produce low cost reinforcements and to develop aluminium composites from nonstandard low cost aluminium alloys with desired properties in extreme working conditions. Only non-conventional reinforcements may be used with different matrix materials for production of hybrid composites.
- A separation technique may be applied to separate reinforcements from composite waste and reuse them as fresh fillers.
- In order to evaluate the industrial competence of developed hybrid aluminium composites, manufacturing and evaluation of real components may be conducted.

BIBLIOGRAPHY

1. Lloyd D J (1999) Particle reinforced aluminium and magnesium matrix composites. *Int. Mater. Rev*. 39: 1–23
2. Moona G, Sharma R, and Sindhu N et al. (2015) Effect of filler size on properties of Linear Low-Density Polyethylene-Silica nanocomposites. *J. Polym. Mater.* 32(3):251-264
3. Ozden S, Ekici R and Nair F (2007) Investigation of impact behaviour of aluminium based SiC particle reinforced metal matrix composites. *Compos. Part A.* 38 (2):484-494
4. Murayama B (1999) Progress and promise in aluminium composites. *Metal. prog.* 155(6) : 47-50
5. Choi S M and Awaji H (2005) Nano composite – a new material design concept. *Sci. Technol. Adv. Mater.* 6:2–10
6. Ozcataslbas Y (2003) Investigation of the machinability behaviour Al_4C_3 reinforced Al based composite produced by mechanical alloying technique. *Compos. Sci. Technol*. 63 (1):53-61
7. Kok M (2005) Production and mechanical properties of Al_2O_3 particle-reinforced 2024 aluminium alloy composites. *J. Mater. Process. Technol*. 161: 381–387
8. Clyne T W (2001) Metal matrix composites: Matrices and processing. *Encyclopedia of materials science and technology* (ed.) A Mortensen (Elsevier)
9. Surappa M K (2003) Aluminium matrix composites: challenges and opportunities. *Sadhana*. 28(1–2) : 319–334
10. Yanming Q and Zehua Z (2000) Tool wear and its mechanism for cutting SiC particle reinforced aluminium matrix composites. *J. Mater. Process. Technol*. 100 (1-3): 194-199
11. Ronald G F (2010) A review of recent research on mechanics of multifunctional composite materials and structures. *Compos. Struct*. 92: 2793–2810
12. Rao Rama S and Padmanabhan G (2012) Fabrication and mechanical properties of aluminium-boron carbide composites. *Int. J. Mater. Biomater. Appl.* 2: 15-18
13. Rohatgi P K, Kim J K and Gupta N et al. (2006) Compressive characteristics of A356/fly ash cenosphere composites synthesized by pressure infiltration technique. *Compos.: Part A Appl. Sci Manuf.* 37: 430-437
14. Park B G, Crosky A G and Hellier A K (2008) High cycle fatigue behaviour of microsphere Al_2O_3–Al particulate metal matrix composites. *Compos.: Part B Engg.* 39: 1257-1269.
15. Ding H Z, Biermann H and Hartmann O (2002) A low cycle fatigue model of a short-fiber reinforced 6061 aluminium alloy metal matrix composites. *Compos. Sci. Technol.* 62: 2189–2199
16. Cerit A A, Karamiş M B and Fehmi N et al. (2008) Effect of reinforcement particle size and volume fraction on wear behaviour of metal matrix composites. *Tribol. Ind.* 30 (3): 31–36

17. Kala H, Mer K K S and Kumar S (2014) A review on mechanical and tribological behaviours of stir cast aluminium matrix composites. *Proc. Mater. Sci.* 6: 1951 – 1960

18. Anantha Prasad M G and Bandekar N (2015) Study of microstructure and mechanical behaviour of aluminium/garnet/carbon hybrid metal matrix composites (hmmcs) fabricated by chill casting method. *J Mater. Sci. Chem. Eng.* 3: 1-8

19. Caron S and Masounave J (1990) A literature review on fabrication techniques of particulates reinforced metal matrix composites. *Proceeding of International Conference: Fabrication of Particulate Reinforced Metal Matrix Composites*, Montreal, Canada, 79-85

20. Woo K D and Zhang D L (2004) Fabrication of Al-7 wt.% Si-.04 wt.% Mg/SiC nano-composite powder and bulk nano composite by high energy ball milling and powder metallurgy. *Curr. Appl. Phys.* 4: 175–178

21. George H S (2007) Introduction to composite materials. (https://doi.org/10.1016/B978-075067124-8/50001-1)

22. Tsutsui T (2012) Recent technology of powder metallurgy and applications. *Hitachi Chemical Technical Report* No. 54: 12-20

23. Basem E T, Heba L and Ahmed E et al. (2017) Weight reduction and strengthening of marine hatch covers by using composite materials. *IJNAOE*. 9 (2): 185-198

24. Koli D, Agnihotri G and Purohit R (2014) A Review on properties, behavior and processing methods for Al- nano Al_2O_3 composites. *Proc Mater. Sci*. 6: 567 – 589

25. Alaneme K K, Akintunde I B and Olubambi P A et al. (2013) Fabrication characteristics and mechanical behavior of rice husk ash–alumina reinforced Al-Mg-Si alloy matrix hybrid composites. *J. Mater. Res. Technol.* 2(1): 60–67

26. Anish R, Robert G and Shivapragash M (2012) Techniques for processing metal matrix composites; A survey. *Proc. Eng*. 38: 3846-3854

27. Jain V K S, Muhammed P M and Muthukumaran S et al. (2018) Microstructure, mechanical and sliding wear behavior of AA5083–B4C/SiC/TiC surface composites fabricated using friction stir processing. *Trans. Indian Inst. Met*. 71(6): 1519–1529

28. Zohoor M, Besharati Givi M K and Salami P (2012) Effect of processing parameters on fabrication of Al-Mg/Cu composites via friction stir processing. *Mater. Des.* 39: 358–365

29. Gokhan A and Bilge Y (2019) Wear response of glass fiber and ceramic tile-reinforced hybrid epoxy matrix composites. *Iranian Polymer Journal*. 28: 21-29

30. Das S, Chandrasekaran M G and Samanta S et al. (2019) Fabrication and tribological study of AA6061 hybrid metal matrix composites reinforced with SiC/B_4C nanoparticles. *Ind. Lubr. Tribol.* 71 (1): 83 – 93

31. Ercenk E, Sen U, Bayrak G and Yilmaz S (2014) Glass and glass ceramics produced from fly ash and boron waste. *Acta. Phys. Pol. A.* 125: 626–628

32. Shen Q, Wu C and Luo G et al. (2014) Microstructure and mechanical properties of Al-7075/B_4C composites fabricated by plasma activated sintering . *J Alloys Compd.* 588: 265-270

33. Maleki A, Meratian and Gupta M (2008) Synthesis of in-situ aluminium matrix composite, using a new activated powder injection method. *Metall. Mat. Trans. A.* 39: 3034-3039

34. Raei M, Panjepour M and Meratian M (2016) Pseudo-in-situ stir casting: a new method for production of aluminium matrix composites with bimodal-sized B_4C reinforcement. *Int. J Min. Metall. Mater.* 23: 981-990

35. Matsumuro M and Kitsudo T (2006) Fabrication of *in-situ* intermetallic compound dispersed aluminium matrix composites by addition of metal powders. *Mater. Trans.* 47: 2972-2979

36. Hai S, Wenli G and Zhaohui F et al. (2012) Processing, microstructure and tensile properties of nano sized Al_2O_3 particle reinforced aluminium matrix composites. *Mater. Des*. 36: 590-596

37. Yilmaz S O and Buytoz S (2007) Relationship between thermal and sliding wear behaviour of Al6061/Al_2O_3 metal matrix composites. *J Mater. Sci*. 42: 4485-4493

38. https://sg.inflibnet.ac.in/bitstream/10603/17747/8/08_chapter%203.pdf

39. Asif M, Chandra K and Misra P S (2011) Development of aluminium based hybrid metal matrix composites for heavy duty applications. *J Min. Mater. Charact. Eng*. 10: 1337-1338

40. Sharma P (2012) Determination of mechanical properties of aluminium based composites. *IJET*. 3: 157-152.

41. Iacoba G, Ghicaa V G and Buzatua M et al. (2014) Studies on wear rate and micro-hardness of the Al/Al_2O_3/Gr hybrid composites produced via powder metallurgy. *Compos. Part B*. 69: 603–611

42. Babalola P O, Bolu C A and Inegbenebor A O et al. (2014) Development of aluminium matrix composites: A review. *Online Int. J Eng. Technol. Res*. 2: 1-11

43. Zhanga X P, Yea L and Y.-W. Maia et al. (1999) Investigation on diffusion bonding characteristics of SiC particulate reinforced aluminium metal matrix composites (Al/SiCp-MMC), *Compos. Part A*. 30: 1415–1421

44. Woo K and Lee H B (2007) Fabrication of Al alloy matrix composites reinforced with sub sieve- sized Al_2O_3 particles by the in-situ displacement reaction using high energy ball-milled powder. *Mater. Sci. Eng. A*. 449: 829-832

45. Vishwanathan V, Laha T and Balani K et al. (2006) Challenges and advances in nanocomposite processing techniques. *Mater. Sci. Eng. R.* 54: 121-285

46. Mishra R S, Ma Z Y and Charit I (2003) Friction stir processing: a novel technique for fabrication of surface composite. *Mater. Sci. Eng. A.* 341:307-310

47. Torralba J M, Costa C E and Velasco F (2003) P/M aluminium matrix composites: An overview. *J Mater. Process. Technol*. 133: 203-206

48. Mazahery, Abdizadeh H and Baharvandi H R (2009) Development of high-performance A356/nano- Al_2O_3 composites. *Mater. Sci. Eng. A*. 518: 61–64

49. Manu K M S, Ajay Raag L and Rajan T P D (2016) Liquid metal infiltration processing of metallic composites: a critical review. *Metall. Mater. Trans. B*. 47B: 2799-2819

50. Miranda R M, Santos T G and Gandra J et al. (2013) Reinforcement strategies for producing functionally graded materials by friction stir processing in aluminium alloys. *J. Mater. Process. Technol.* 213 (9): 1609–1615

51. Poovazhagan L, Kalaichelvan K and Rajadurai A et al. (2013) Characterization of hybrid silicon carbide and boron carbide nanoparticles-reinforced aluminum alloy composites. *Proc Eng.* 64:681–689

52. Surappa M K and Rohatgi P K (1981) Preparation and properties of cast aluminium-ceramic particle composites. *J Mater. Sci.* 16: 983-993
53. Dhanashekar M and Senthil K V S (2014) Squeeze casting of aluminium metal matrix composites: An overview. *Proc. Eng*. 97: 412-420
54. Han Q, Setchi R and Evan L S (2016) Synthesis and characterization of advanced ball-milled Al-Al_2O_3 nanocomposites for selective laser melting. *Powder Technol*. 297:183-192
55. Saberi Y, Zebarjad, S M and Akbari G H (2009) On the role of nano-size SiC on lattice strain and grain size of Al/SiC nanocomposite. *J Alloy Comd*. 484:637-640
56. Moona G, Walia R S and Rastogi V et al. (2018) Aluminium metal matrix composites: A retrospective investigation. *IJPAP*. 56: 164-175
57. Schultz B F, Ferguson J B and Rohatgi P K (2011) Microstructure and hardness of Al_2O_3 nanoparticle reinforced Al–Mg composites fabricated by reactive wetting and stir mixing. *Mater. Sci. Eng. A*. 530:87-97
58. Martin B, Cecilia P and Frantisek S (2011) The effect of native Al_2O_3 skin disruption on properties of fine Al powder compacts. *J Alloy Compd*. 509: S235-S238
59. Dora S P, Shobha C and Ramanaiah N (2014) Investigations on mechanical properties of hybrid aluminium composites. *J Mater. Res. Technol.* 3(1):79-85
60. Alaneme K K, Ademilua B O and Bodunrin M O (2013) Mechanical properties and corrosion behaviour of aluminium hybrid composites reinforced with silicon carbide and bamboo leaf ash. *Tribol. Ind*. 35 (1):25-35
61. Singh J (2016) Fabrication characteristics and tribological behaviour of Al/SiC/Gr hybrid aluminium matrix composites: A review. *Friction*.4 (3):191-207
62. Rajmohan T, Ranganathan S and Suryakumari T S A (2014) Experimental Study on fabrication of hybrid (Al+TiO_2+Gr) metal matrix composites. *IJAEA.* 7 (2):11-24
63. Veeresh K G B, Rao C S P and Selvaraj N et al (2010) Studies on Al6061-SiC and Al7075-Al_2O_3 metal matrix composites. *J Miner. Mater. Charact. Eng*. 9 (1):43-55
64. Devaraju A, Kumar A and Kotiveerachari B (2013) Influence of addition of Grp/Al_2O_3p with SiCp on wear properties of aluminium alloy 6061-T6 hybrid composites via friction stir processing. *T Nonferr. Metal. Soc*. 23 (5):1275-1280
65. Zhang F, Kacmarek W A and Lu L (2000) Formation of Al-TiN metal matrix composite via mechanochemical route. *Scripta Mater*. 43 (12):1097-1102
66. Baradeswaran A and Perumal E A (2013) Influence of B_4C on the tribological and mechanical properties of Al7075–B_4C composites. *Compos. Part B.* 54:146-152
67. Stojanović B, Babić M and Veličkovic S et al. (2016) Tribological behaviour of aluminum hybrid composites studied by application of factorial techniques. *Tribol. T*. 59:522-529
68. Gupta M, Lai M O and Soo C Y (1996) Effect of type of processing on the microstructural features and mechanical properties of Al-Cu/SiC metal matrix composites. *Mater. Sci. Eng A*. 210:114-122
69. Kumar C A V, Rajadurai J S and Sundararajan S (2016) Performance enrichment on tribological characteristics of powder metallurgy processed aluminium

particulate composites by inclusion of rutile (TiO_2). *J Mater. Res*. 31(16):2445-2456

70. Lu L, Lai M O and Su Y et al (2001) In situ TiB_2 reinforced Al alloy composite. *Scripta Mater*. 45(9):1017-1023

71. Slipenyuk A, Kuprin V and Milman Y et al. (2006) Properties of P/M processed particle reinforced metal matrix composites specified by reinforcement concentration and matrix-to-reinforcement particle size ratio. *Acta Mater.* 54(1):157-166

72. Prasad D S and Krishna A R (2011) Production and mechanical properties of A356.2/RHA composites. *Int. J Adv. Sci Technol*. 33:51-57

73. Bauri R and Surappa M K (2009) Processing and compressive strength of Al–Li–SiCp composites fabricated by a compound billet technique. *J Mater. Process. Technol.* 209(4):2077-2084

74. Bharath V, Nagaral M and Auradi V et al. (2014) Preparation of 6061Al-Al_2O_3 MMC's by stir casting and evaluation of mechanical and wear properties. *Proc. Mater. Sci*. 6:1658-1667

75. Ronald B A, Vijayaraghavan L and Krishnamurthy R (2007) Studies on grooving of dispersion strengthened metal matrix composites. *Mater. Forum.* 31:102-109

76. Durai, T G, Das K and Das S (2007) Wear behaviour of nano structured Al (Zn)/Al_2O_3 and Al (Zn)–4Cu/Al_2O_3 composite materials synthesized by mechanical and thermal process. *Mater. Sci. Eng. A.* 471:88-94

77. Tousi S S, Yazdani R R and Salahi E (2009) Production of Al–20 wt.% Al_2O_3 composite powder using high energy milling. *Powder Technol*. 192:346-351

78. Tavoosi M, Karimzadeh F and Enayati M H (2009) Bulk Al–Zn/Al_2O_3 nanocomposite prepared by reactive milling and hot-pressing methods. *J Alloy Compd*. 475:198-201

79. Shafiei-Zarghani A, Kashani-Bozorg S F and Zarei- Hanzaki A (2011) Wear assessment of Al/Al_2O_3 nano-composite surface layer produced using friction stir processing. *Wear*. 270:403-412

80. Ramesh C S, Keshavamurthy R and Channabasappa B H (2010) Friction and wear behaviour of Ni–P coated Si 3N 4 reinforced Al6061 composites. *Tribol. Int.* 43(3):623-634

81. Bienias J, Walczak M and Surowska B (2003) Microstructure and corrosion behaviour of aluminium fly ash composites. *J Optoelectron. Adv. Mater*. 5(2):493-502

82. Anilkumar H C, Hebbar H S and Ravishankar (2011) Mechanical properties of fly ash reinforced aluminium alloy (Al6061) composites. *Int. J Mech. Miner. Eng*. 6(1):41-45

83. Rino J, Sivalingappa D and Koti H (2013) Properties of Al6063 MMC reinforced with zircon sand and alumina. *IOSR-JMCE.* 5(5):72-77

84. Ravichandran M and Dinesh K S, *SSRG* (2014) Synthesis of Al-TiO_2 composites through liquid powder metallurgy route. *SSRG-IJME*. 1(1):12-15

85. Keshavamurthy R and Sadananda M (2013) Microstructure and mechanical properties of Al7075-TiB_2 in-situ composite. *Res. J Mater. Sci.* 1(10):6-10

86. Kumar A, Mahapatra M M and Jha P K (2012) Fabrication and characterizations of mechanical properties of Al-4.5%Cu/10TiC composite by in-situ method. *J Min. Mater. Char. Eng.*11:1075-1080

87. Umanath K, Palanikumar K and Selvamani S T (2013) Analysis of dry sliding wear behaviour of Al6061/SiC/Al_2O_3 hybrid metal matrix composites. *Compos. B Eng.* 53:159-168

88. Rao R N, Das S and Mondal D P (2010) Effect of heat treatment on the sliding wear behaviour of aluminium alloy (Al–Zn–Mg) hard particle composite. *Tribol. Int*. 43:330-339

89. Suresha S and Sridhara B K (2012) Friction characteristics of aluminium silicon carbide graphite hybrid composites. *Mater. Des*. 34:576-583

90. Alaneme K K and Aluko A O (2012) Fracture toughness (K1C) and tensile properties of as-cast and age-hardened aluminium (6063)–silicon carbide particulate composites. *Scientia Iranica.* 19(4):992-996

91. Yar A A, Montazerianb M and Abdizadeh H et al. (2009) Microstructure and mechanical properties of aluminium alloy matrix composite reinforced with nanoparticle MgO. *J Alloys Compd.* 484:400-404

92. Kumar A, Lal S and Kumar S (2013) Fabrication and characterization of A359/Al_2O_3 metal matrix composite using electromagnetic stir casting method. *J Mater. Res. Technol*. 2(3):250-254

93. James J S, Venkatesan K and Kuppan P et al. (2014) Hybrid aluminium metal matrix composite reinforced with SiC and TiB_2. *Proc. Eng.* 97:1018-1026

94. Veeresh Kumar G and Rao CSP and Selvaraj N (2011) Mechanical and tribological behavior of particulate reinforced aluminium metal matrix composites – a review. *J Min. Mater. Charact. Eng*. 10(1):59-91

95. Xu W, Wu X and Honma T et al. (2009) Nanostructured Al–Al_2O_3 composite formed in situ during consolidation of ultrafine Al particles by back pressure equal channel angular pressing. *Acta Mater*. 57:4321-4330

96. Deng C F, Wang D Z and Zhang X X et al. (2007) Damping characteristics of carbon nanotube reinforced aluminium composite. *Mater. Lett.* 61:3229-3231

97. Carreño-Gallardo C, Estrada-Guel I and Romero-Romo M et al. (2012) Characterization of Al_2O_3NP–Al2024 and AgCNP–Al2024 composites prepared by mechanical processing in a high energy ball mill. *J Alloys Compd*. 536: S26-S30

98. Ahamed H and Senthilkumar V (2011) Consolidation behaviour of mechanically alloyed aluminium based nanocomposites reinforced with nanoscale Y_2O_3/Al_2O_3 particles. *Mater. Charact.* 62:1235-1249

99. Nayak S S, Pabi S K and Kim D H et al. (2010) Microstructure-hardness relationship of Al–(L12) Al_3Ti nanocomposites prepared by rapid solidification processing. *Intermetallics*. 18:487-492

100. Liu Y Q, Cong H T and Wang W et al. (2009) AlN nanoparticle-reinforced nanocrystalline Al matrix composites: Fabrication and mechanical properties. *Mater. Sci. Eng. A.* 505:151-156

101. Ozben T, Kilickap E and Cakir O (2008) Investigation of mechanical and machinability properties of SiC particle reinforced Al-MMC. *J Mater. Process. Technol*. 198:220-225

102. Reddy M S, Chetty S V and Premkumar S et al. (2014) Influence of reinforcements and heat treatment on mechanical and wear properties of Al7075 based hybrid composites. *Proc. Mater. Sci*. 5:508-516

103. Alaneme K K and Sanusi O K (2015) Microstructural characteristics, mechanical and wear behaviour of aluminium matrix hybrid composites reinforced with alumina, rice husk ash and graphite. *Eng. Sci. Technol. Int J* 18:416-423

104. Bodunrin M O, Oladijo O P and Daramola O O et al (2016) Porosity measurement and wear performance of aluminium hybrid composites reinforced with silica sand and bamboo leaf ash. *Int. J Eng*. XIV:231-238

105. Mahendra K V and Radhakrishna K (2010) Characterization of stir cast Al—Cu—(fly ash + SiC) hybrid metal matrix composites. *J Compos. Mater*. 44:989-1005

106. Rawal S (2001) Metal-matrix composites for space applications. *JOM*. 53:14-17

107. Yan C, Lifeng W and Jianyue R (2008) Multi-functional SiC/Al composites for aerospace applications. *Chinese J Aeronaut*. 21:578-584

108. Devaraju A, Kumar A and Kumaraswamy A et al (2013) Wear and mechanical properties of 6061-T6 aluminium alloy surface hybrid composites [(SiC + Gr) and (SiC + Al_2O_3)] fabricated by friction stir processing. *J Mater. Res. Technol.* 2: 362–369

109. Dinaharan I and Murugan N (2012) Dry sliding wear behaviour of AA6061/ZrB_2 in-situ composite, *T. Nonferr. Metal. Soc.* 22: 810-818

110. Rebba B and Ramanaiah N (2014) Studies on mechanical properties of 2024 Al – B_4C composites. *Adv. Mater. Manuf. Charact.* 4: 42-46

111. Balasivanandhaprabu S, Karunamoorthy I and Kathiresan S et al. (2006) Influence of stirring speed and stirring time on distribution of particles in cast metal matrix composite. *J Mater. Proc. Technol.* 171: 268-273

112. Ramakoteswara V, Ramanaiah N and Sarcar M M M (2014) Fabrication and investigation on Properties of TiC reinforced Al7075 metal matrix composites. *Appl. Mech. Mater.* 592: 349-353

113. Boopathi M M, Arulshri K P and Iyandurai N (2013) Evaluation of mechanical properties of aluminium alloy 2024 reinforced with silicon carbide and fly ash metal matrix composites. *Am. J Appl. Sci.* 10: 219-229

114. Nai S M L and Gupta M (2002) Influence of stirring speed in the synthesis of Al/SiC based functionally gradient materials. *Compos. Struct.*57:227-233

115. Ramakoteswara V, Ramanaiah N and Sarcar M M M (2015) Dry sliding wear behaviour of Al7075 reinforced with titanium carbide (TiC) particulate composites. *Proceedings of International Conference on Advances in Materials, Manufacturing and Applications (AMMA 2015).* 2: 9-11

116. Radhika N, Subramanian R and Venkat Prasat S (2011) Tribological behaviour of aluminium /alumina/graphite hybrid metal matrix composite using Taguchi's techniques. *J Min. Mater. Charact. Eng.* 10: 427-443

117. Bhaskar H B and Sharief A (2012) Tribological properties of Aluminium 2024 alloy-Beryl particulate MMC's. *Bonfring Int J Ind. Eng. Mgmt. Sci.* 4: 143-147

118. Casati R and Vedani M (2014) Metal matrix composites reinforced by nano-particles—A review. *Metals (Basel).* 4(1): 65– 83, 2014.

119. Deng C, Wang, D and Zhang X (2007) Processing and properties of carbon nanotubes reinforced aluminium composites. *Mater. Sci. Eng. A*. 444: 138- 145
120. Esawi A M K and Morsi K (2007) Dispersion of carbon nanotubes (CNT) in aluminium powder. *Compos. Part A.* 3: 646-650
121. Lokesh G N, Ramachandra M and Mahendra K V et al. (2013) Characterization of Al-Cu alloy reinforced fly ash metal matrix composites by squeeze casting method. *Int. J Eng. Sci. Technol.* 5: 71-79
122. Hashim J, Looney L and. Hashmi M S J (1999) Metal matrix composites: production by the stir casting method. *J. Mater. Process. Technol.* 92/93:1–7
123. Kashyap K T and Chandrashekar T (2001) Effects and mechanisms of grain refinement in aluminium alloys. *Bull. Mater. Sci*. 24: 345–353
124. Das S, Das S and Das K (2007) Abrasive wear of zircon sand and alumina reinforced Al–4.5 wt.% Cu alloy matrix composites–A comparative study. *Compos. Sci. Technol.* 67: 746–751
125. Deng C F, Zhang X X and Wang D et al. (2007) Preparation and characterization of carbon nanotubes/aluminium matrix composites. *Mater. Lett.* 61:1725-1728
126. Moses J J, Dinaharan I and Sekhar J S (2016) Prediction of influence of process parameters on tensile strength of AA6061/Tic aluminium matrix composites produced using stir casting, *T Nonferr. Metal. Soc*.26: 1498−1511
127. Muruganandan P, Easwaramoorthi M and Kannakumar K (2015) Aluminium fly ash composite- an experimental study with mechanical properties perspective. *Int. J Eng. Res.* 3: 78-83
128. Rajmohan T, Palanikumar K, and Ranganathan S (2013) Evaluation of mechanical and wear properties of hybrid aluminium matrix composites. *T Nonferr. Metal. Soc.* 23(9): 2509-2517
129. Zhu Y, Zhou A and Ji, Y et al (2015) Tribological properties of Ti_3SiC_2 coupled with different counterfaces. *Ceram. Int.* 41(5): 6950-6955
130. Yong Y, Jie L and Xiaochun L (2004) Study on bulk aluminium matrix nano-composite fabricated by ultrasonic dispersion of nano-sized SiC particles in molten aluminium alloy. *Mater. Sci. Eng. A.* 380: 378-383
131. Auradi V, Rajesh G L and Kori S A (2014) Processing of B_4C particulate reinforced 6061 Al metal matrix composites by melt steering involving two step addition. *Proc. Mater. Sci.* 6: 1068-1076
133. Christy T V (2010) A Comparative study on the microstructures and mechanical properties of Al 6061 alloy and the MMC Al 6061/TiB_2/12P. *J Min. Mater. Charact. Eng.* 9 (1):57-65
134. Kainer K U (2006) Metal Matrix Composites: Custom-made materials for automotive and aerospace engineering. *Wiley-VCH, Weinheim,* ISBN: 978-3-527-31360-0
135. Stojanovic B and Ivanovic L (2015) Application of aluminium hybrid composites in automotive industry. *Technical Gazette*. 22:247-251
136. Rohatgi P K, Ray S and Liu Y (1992) Tribological properties of metal matrix-graphite particle composites. *Int. Mater. Rev*. 37:129-152
137. Nidhish B N and Sijo M T (2014) Effect of silicon carbide percentage on fracture toughness of aluminium silicon carbide metal matrix composites. *Int. J Res. Eng. Tech*. 3:412-415

138. Fatchurrohman N, Iskandar I and & Suraya S et al (2015) Sustainable analysis in the product development of Al-metal matrix composites automotive component. *Appl. Mech. Mater*. 695:32-35

139. Szumigala M and Polus l (2015) Applications of aluminium and concrete composite structures. *Proc. Eng*. 108:544-549

140. Purcek G, Saray O, and Kul O (2010) Microstructural evolution and mechanical properties of severely deformed Al-12Si casting alloy by equal-channel angular extrusion. *Met. Mate. Int.* 16:145–154.

141. Ruch P W, Beffort O and Kleiner S et al (2006) Selective interfacial bonding in Al (Si)–diamond composites and its effect on thermal conductivity. *Compos. Sci. Technol*. 66:2677-2685

142. Kawata H and Maki K (2007) Recent trends in heat resistant/wear resistant sintered alloys. *Hitachi powdered metals technical report*. No 6

143. Nturanabo F, Masu L and Kirabira J B (2019) Novel applications of aluminium metal matrix composites (DOI: http://dx.doi.org/10.5772/intechopen.86225)

144. Mavhungu S T, Akinlabi E T and Onitiri M A et al (2017) Aluminium matrix composites for industrial use: Advances and trends. *Proc. Manuf.* 7:178-182

145. Smith C A (2001) Discontinuous reinforcements for metal matrix composites. *DWA Aluminium Composites. ASTM Handbook*. 21

146. Pawar P B and Abhay A (2014) Development of aluminium based silicon carbide particulate metal matrix composite for spur gear. *Proc. Mater. Sci*. 6:1150-1156

147. Müller S, Schubert T and Fiedler F et al (2011) Properties of sintered P/M aluminium composites. *Proceedings of the Euro international powder metallurgy congress and Exhibition.* Barcelona

148. Mandal A, Murthy B S and Chakraborty M (2009) Sliding wear behaviour of T6 treated A356-TiB_2 in-situ composites. *Wear*. 66:865–72.

149. Siva P D and Shoba C (2014) Hybrid composites – a better choice for high wear resistant materials. *J Mater. Res. Technol*. 3:172-178

150. Singh J and Chauhan A (2016) Characterization of hybrid aluminium matrix composites for advanced applications – A review. *J Mater. Res. Technol*. 5:159-169

151. Garg D and Dyer P N (1993) Erosive wear behaviour of chemical vapor deposited multilayer tungsten carbide coating. *Wear*. 162–164: 552–557

152. Mirsalimov V M and Akhundova P E (2018) Minimization of stress state of a hub of friction pair. *Adv. Math. Phys.* 2018: 1–10

153. Kato K (2000) Wear in relation to friction - A review. *Wear.* 241: 151–157

154. Akbari M K, Baharvandi H R and Mirzaee O (2013) Nano-sized aluminium oxide reinforced commercial casting A356 alloy matrix: Evaluation of hardness, wear resistance and compressive strength focusing on particle distribution in aluminium matrix. *Compos. Part B Eng*. 52: 262–268

155. Sawla S and Das S (2004) Combined effect of reinforcement and heat treatment on the two-body abrasive wear of aluminium alloy and aluminium particle composites. *Wear.* 257: 555–561

156. Ted Guo M L and Tsao C Y A (2002) Tribological behaviour of aluminium/SiC/nickel-coated graphite hybrid composites. *Mater. Sci. Eng. A.* 333: 134–145

157. Paramsothy M, Hassan S F and Srikanth N et al (2009) Enhancing tensile/compressive response of magnesium alloy AZ31 by integrating with Al_2O_3 nanoparticles. *Mater. Sci. Eng. A.* 527: 162–168

158. Al-Qutub A M, Allam I M and Abdul Samad M A (2008) Wear and friction of Al-Al_2O_3 composites at various sliding speeds. *J Mater. Sci*. 43: 5797–5803

159. Ghandvar H, Farahany S and Idris M H (2018) Effect of wettability enhancement of sic particles on impact toughness and dry sliding wear behaviour of compocasted A356/20SiCp composites. *Tribol. Trans*. 61: 88–99

160. Ambigai R and Prabhu S (2019) Experimental and ANOVA analysis on tribological behaviour of Al/B 4 C micro and nanocomposite. *Aust. J Mech. Eng*. 17: 53–63

162. Daoud A, Abou El-Khair M T and Abdel-Azim A N (2004) Effect of Al_2O_3 particles on the microstructure and sliding wear of 7075 Al alloy manufactured by squeeze casting method. *J Mater. Eng. Perfor.* 13: 135–143

163. Clark Jr R, Coughran B and Traina I et al (2009) On the correlation of mechanical and physical properties of 7075-T6 Al alloy. *Eng. Fail Anal.* 12(4):520-526

164. Moona G, Walia R S and Rastogi V et al. (2019) Parameter optimization and characterization of environmental friendly aluminium hybrid metal matrix composites. *Mater. Res. Express*. 6: 1165d5

165. Ekka K K, Chauhan S R and Varun (2015) Dry sliding wear characteristics of SiC and Al_2O_3 nanoparticulate aluminium matrix composite using taguchi technique. *Arab J Sci. Eng.* 40: 571–581.

166. Selvakumar N and Narayanasamy P (2016) Optimization and effect of weight fraction of MoS_2 on the tribological behaviour of Mg-TiC-MoS_2 hybrid composites. *Tribol. T.* 59(4):733-747

167. Brar B S, Walia R S and Singh V P (2015) Electrochemical-aided abrasive flow machining (ECA2FM) process: a hybrid machining process. *Int. J Adv. Manuf. Tech.* 79(1-4):329-342

168. Narayanasamy P and Selvakumar N (2017) Effect of hybridizing and optimization of TiC on the tribological behaviour of Mg–MoS_2 Composites. *J Tribol-ASME.* 139(5):051301-0513011

169. Ravindran P, Manisekar K and Narayanasamy R et al (2013) Tribological behaviour of powder metallurgy-processed aluminium hybrid composites with the addition of graphite solid lubricant. *Ceram. Int.* 39(2):1169-1182

170. Singh H and Kumar P (2004) Tool wear optimization in turning operation by Taguchi method. *IJEMS.* 11(1):19-24

171. Goyal T, Walia R S and Sidhu T S (2013) Multi-response optimization of low-pressure cold-sprayed coatings through Taguchi method and utility concept. *Int. J Adv. Manuf. Tech.* 64(5-8):903-914

172. Withers P J and Bhadeshia H K D H (2000) Residual stress. Part 1 – Measurement techniques. *Mater. Sci. Tech.* 17 :355-366

173. Centea T and Hubert P (2012) Modelling the effect of material properties and process parameters on tow impregnation in out-of-autoclave prepregs. *Compos. Part A.* 43:1505-1503

174. Guzmán R E and Hernández Arroyo E (2016) Influence of thermal residual stress on behaviour of metal matrix composites reinforced with particles. *J Phys: Conference Series.* 687:012060
175. Liu H T and Sun L Z (2004) Effects of thermal residual stresses on effective elastoplastic behaviour of metal matrix composites. *Int. J Solids. Struct.* 41:2189-2203
176. Suresh K R, Niranjan H B and Martin Jabraj P et al (2003) Tensile and Wear Properties of Aluminium Composites. *Wear*. 255:638-642
177. Wong W L E, Gupta M and Lim C Y H (2006) Enhancing the mechanical properties of pure aluminium using hybrid reinforcement methodology. *Mater. Sci. Eng. A.* 423:148-152
178. Huang H, Tsutsumi S and Wang J et al (2017) High performance computation of residual stress and distortion in laser welded 301L stainless sheets. *Finite Elem. Anal. Des.* 135:1-10
179. Su H, Gao W and Feng Z et al (2012) Processing, microstructure and tensile properties of nano sized Al_2O_3 particle reinforced aluminium matrix composites. *Mater. Des.* 36:590-596
180. Moona G, Walia R S and Rastogi V et al. (2019) Parametric optimization of fatigue behaviour of hybrid aluminium metal matrix composites. *Mater. Today*. 21:1441-1445
181. K Walat and T Lagoda T (2014) Lifetime of semi-ductile materials through the critical plane approach. *Int. J Fatigue*. 67:73-77
182. Moona G, Walia R S and Rastogi V et al. (2020) Tribological characterization of eco-designed aluminium hybrid metal matrix composites. *IJEMS.* 27 (1): 47-57
183. Sahin Y and Kilicli V (2011) Abrasive wear behaviour of SiCp/Al alloy composite in comparison with ausferritic ductile iron. *Wear.* 271:2766-2774
184. Manna A and Bhattacharyya B (2003) A study on machinability of Al/SiC-MMC. *J Mater. Process. Technol.* 140:711-716
185. Lane C T (1990) Machining characteristics of particle reinforced aluminium. *Proceedings of the Conference Fabrication of Particulate Reinforced Metal Composites.* Montreal, Canada.
186. Muthukrishnan N and Davim J P (2009) Optimization of machining parameters of Al/SiC-MMC with ANOVA and ANN analysis. *J. Mater. Process. Technol*. (209):225-232
187. Tomac N, Tannessen K and Rasch FO (1992) Machinability of particulate aluminium matrix composites. *CIRP Ann. Manuf. Technol.* (41):55–58
188. Ciftci I, Turker M and Seker U (2004) Evaluation of tool wear when machining SiCp-reinforced Al-2014 alloy matrix composites. *Mater Des.* 25(3):251–255
189. Kannan S and Kishawy H A (2006) Surface characteristics of machined aluminium metal matrix composites. *Int. J. Mach. Tools. Manuf.* (46): 2017–2025
190. Debnath S, Reddy M M and Yi Q S (2016) Influence of cutting fluid conditions and cutting parameters on surface roughness and tool wear in turning process using Taguchi method. *Measurement*. (78):111–119.
191. Rui-song J, Wen-hu W and Guo-dong S et al. (2016) Experimental investigation on machinability of in situ formed TiB_2 particles reinforced Al MMCs. *J. Manuf. Process.* (23):249-257.

192. Gladston J A K, Dinaharan I and Sheriff N M et al. (2017) Dry sliding wear behavior of AA6061 aluminum alloy composites reinforced rice husk ash particulates produced using compocasting. *J. Asian Ceram. Soc.* 5(2):127-135.

193. Varadarajan Y S, Vijayaraghavan L and Krishnamurthy R (2002) The machinability characteristics of aluminosilicate fibre reinforced Al alloy composite. *Mater. Manuf. Process. (*17): 811-824

194. Kilickap E, Cakir O and Aksoy M et al. (2005) Study of tool wear and surface roughness in machining of homogenized SiC-p reinforced aluminium metal matrix composite. *J. Mater. Process. Technol.* (164–165):862–867

195. Lin J T, Bhattacharyya D and Lane C (1995) Case Study-Machinability of a silicon carbide reinforced aluminium metal matrix composite. *Wear*. (181–183): 883-888

196. Prakash Rao C R, Chandra P and Kiran R et al. (2016) Influence of machining parameters on cutting tool life while machining aluminium alloy fly ash composite. *IOP Conf. Ser.: Mater. Sci. Eng*. 149 012157

197. Chambers A R and Stephens S E (1991) Machining of Al 5Mg reinforced with 5 vol.% Saffil and 15 vol.% SiC. *Mat. Sci. Eng. A.* (135):287-290

198. Ubeyl M, Acir A and Karakas M S et al. (2008) Effect of feed rate on tool wear in milling of Al-4%Cu/B4Cp composite. *Mater. Manuf. Process.* (23): 865-870

199. Reddy S K and Kwang-Sup N S (2007) Experimental study of surface integrity during end milling of Al/SiC particulate metal-matrix composites. *J Mater. Process. Technol.* 201: 574-579

200. Davim J P, Silva J and Baptista A M (2007) Experimental cutting model of metal matrix composites (MMCs). *J Mater. Process. Technol.* 183:358–362

201. Kohli A, Bains H S and Jain S et al (2017) Machinability and wear of aluminium based metal matrix composites by MQL - A Review. *Mat. Sci. Res. India.* 14(2): 194-203

202. Lin J T, Bhattacharya D and Fergusod W G (1998) Chip formation in the machining of sic-particle reinforced aluminium-matrix composites. *Compos Sci Technol.* 58: 285-291

203. Radhika N, Subramanian R and Sajith A (2014) Analysis of chip formation in machining aluminium hybrid composites. *E3 J. Sci. Res*. 2(1): 009-015